



**BRAINPOWER**  
CONGRESS 2023

ร่วมกับสร้างและขับเคลื่อนงานวิจัยข้ามหน่วยงาน  
สู่อุตสาหกรรมแห่งอนาคต

# Surface Functionalized Metal-Organic Frameworks for Enhanced Carbon Dioxide

Chatphorn Theppitak,<sup>1</sup> Weerasak Homkrajai,<sup>2</sup> Sakchai Laksee,<sup>3</sup>  
Bunyarat Rungtaweeworanit,<sup>4</sup> Kittipong Chainok<sup>1\*</sup>

Thammasat University Research Unit in Multifunctional Crystalline Materials and Applications (TU-MCMA),  
Faculty of Science and Technology, Thammasat University, Pathum Thani 12121, Thailand



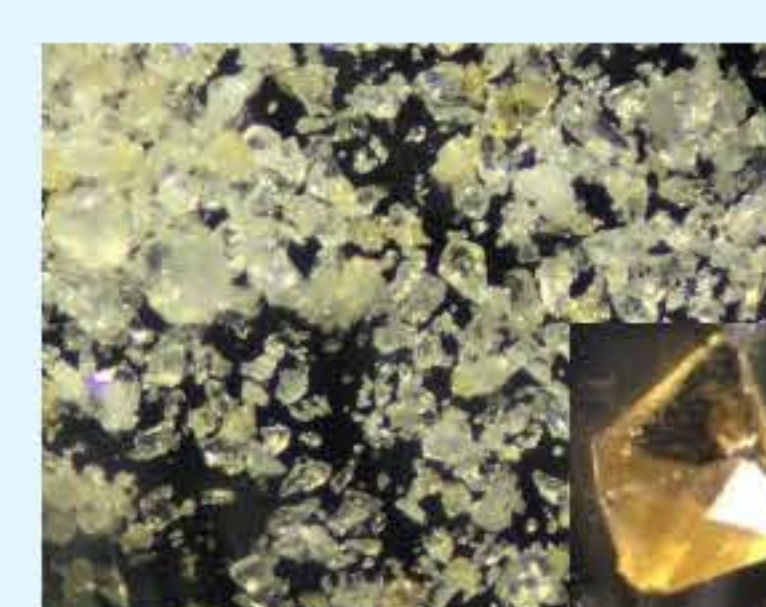
**TU-MCMA**  
"The Materials Chemistry & Chemical Crystallography of LOVE"



## Problem statement

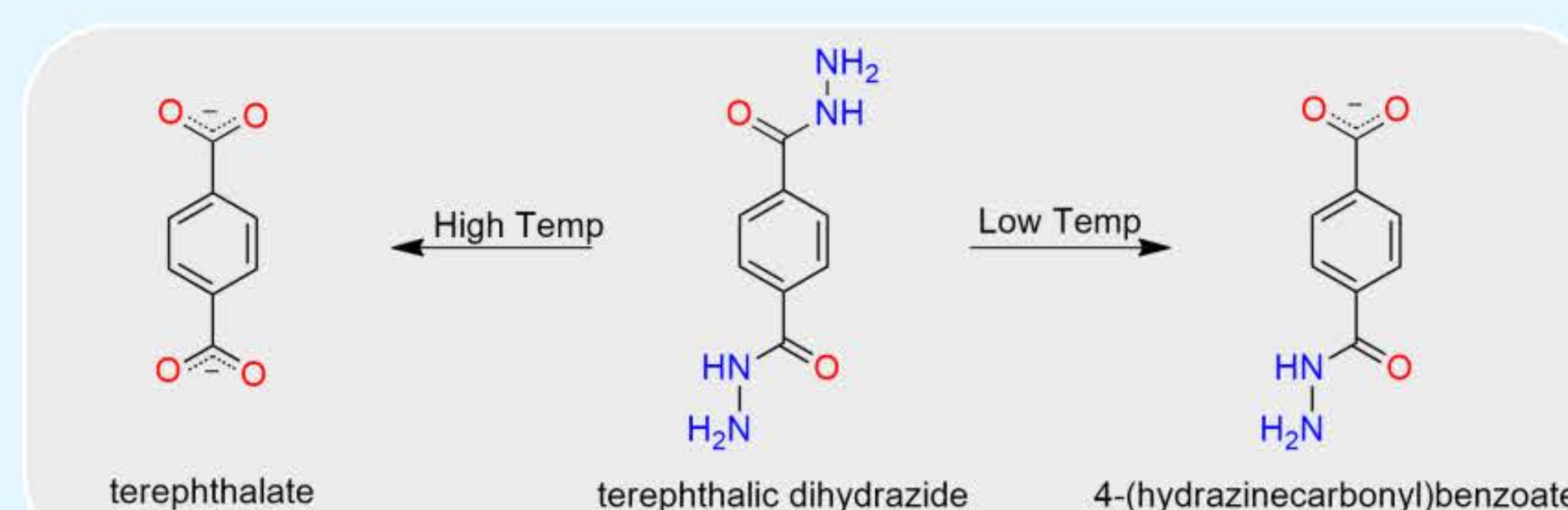
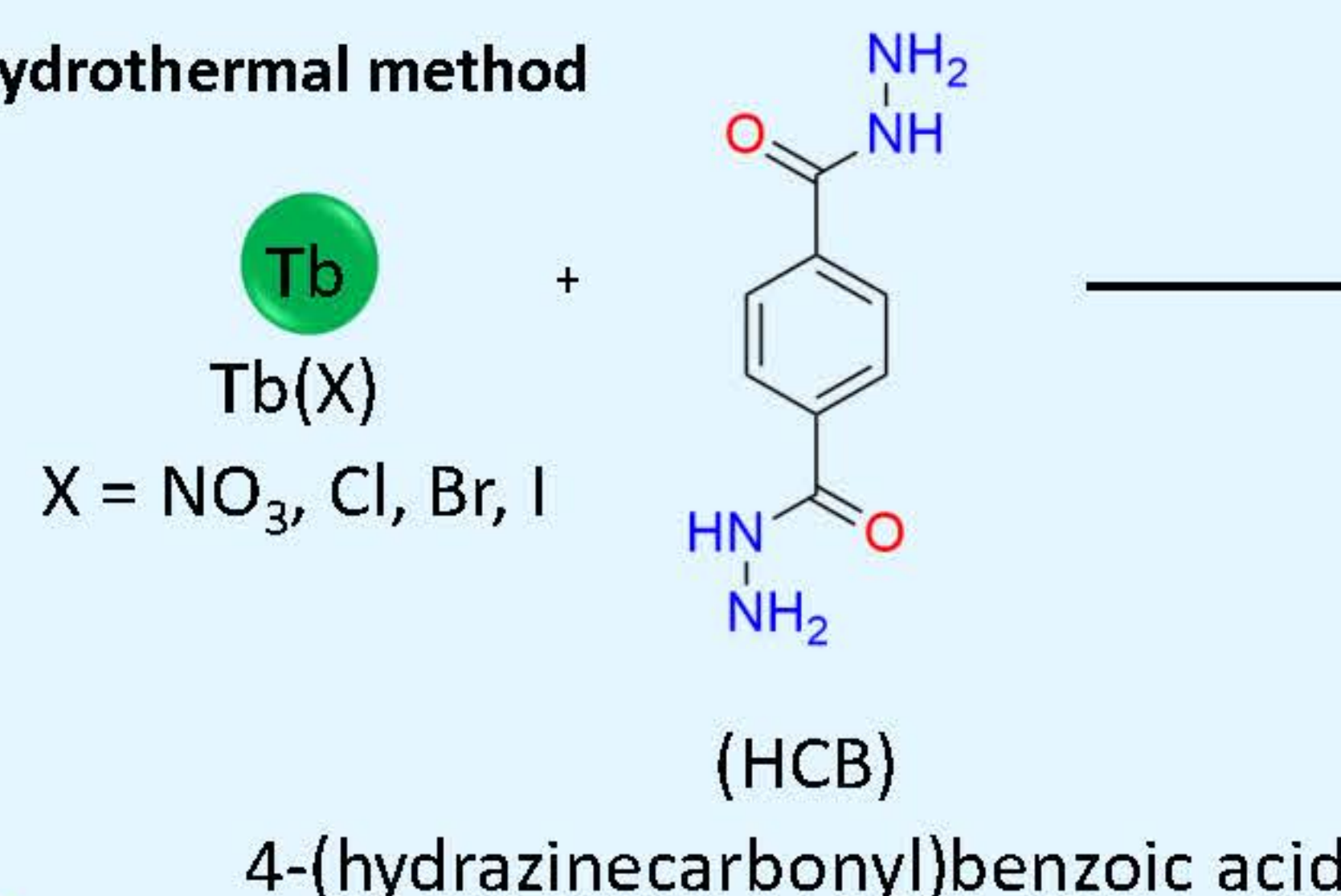
- EGAT agency has prepared the electricity and energy business for carbon neutrality that is in line with the goals of the world and Thailand. Leading to raising the goal of carbon neutrality in 2050 and net zero emissions in 2065 by using science research and innovation application of advanced technology for trapping Carbon Capture, Utilization and Storage (CCUS)
- Carbon Capture, Utilization, and Storage (CCUS) is a set of technologies and processes designed to capture carbon dioxide (CO<sub>2</sub>) emissions produced from the use of fossil fuels in electricity generation and industrial processes. CCUS aims to prevent CO<sub>2</sub> from being released into the atmosphere, where it contributes to climate change.
- Metal-Organic Frameworks, MOFs will be developed for CO<sub>2</sub> gas capture
- There is an emphasis on developing research personnel in various fields. To support production that uses advanced technology and to have more innovations and highly skilled scientists as the country needs

## Methods



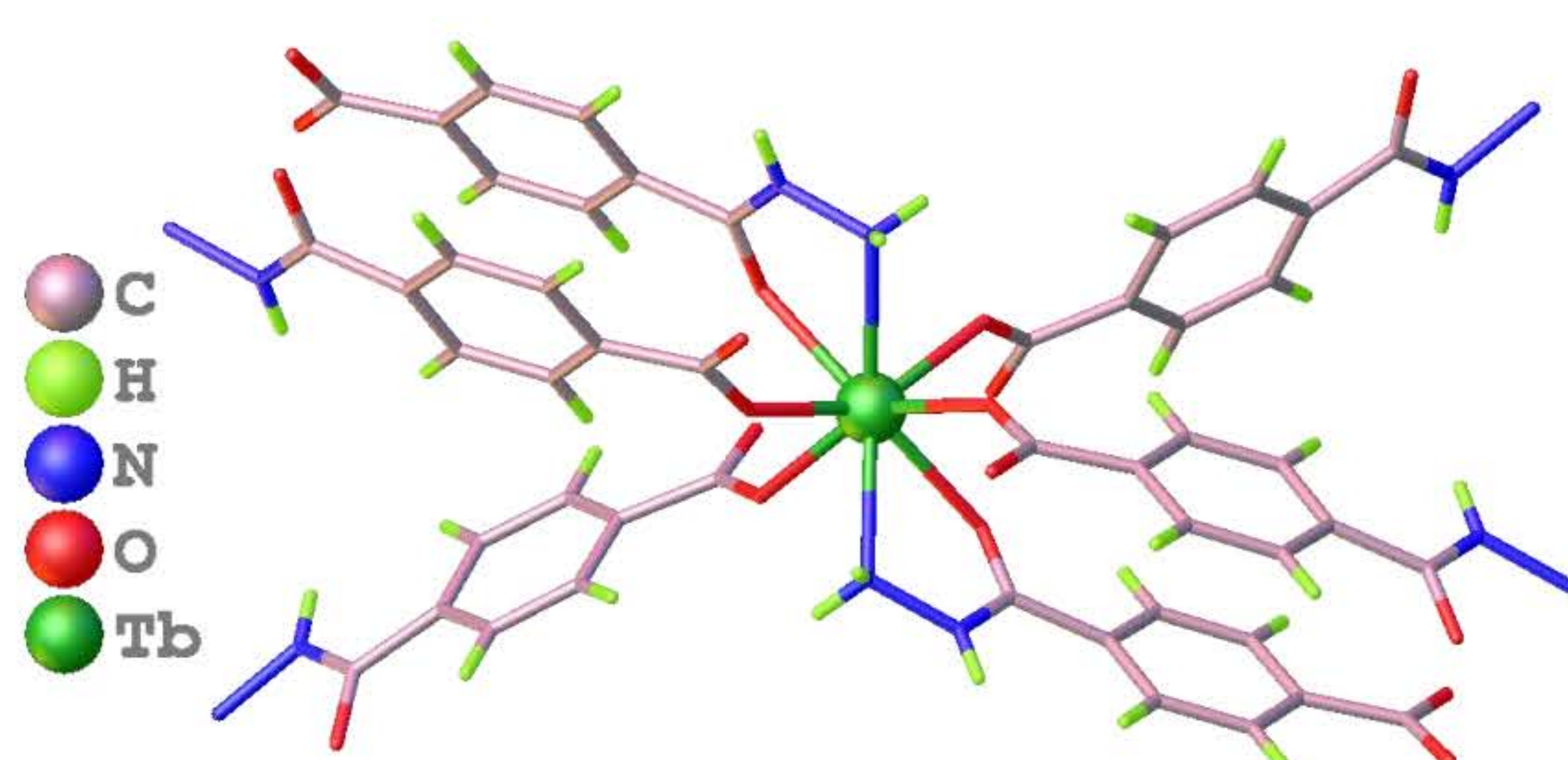
Crystal bipyramid shape

### Hydrothermal method

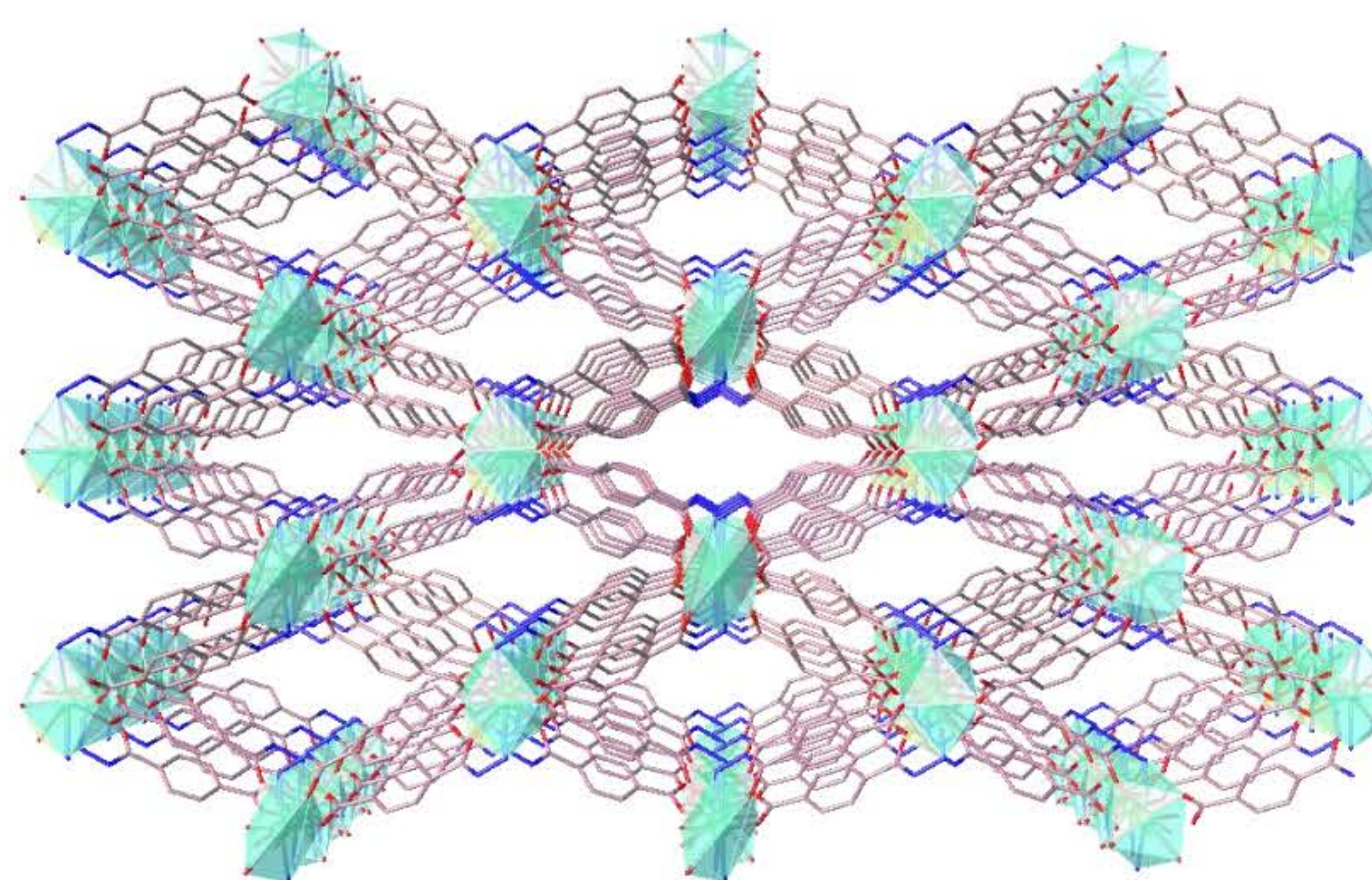


## Results & Discussion

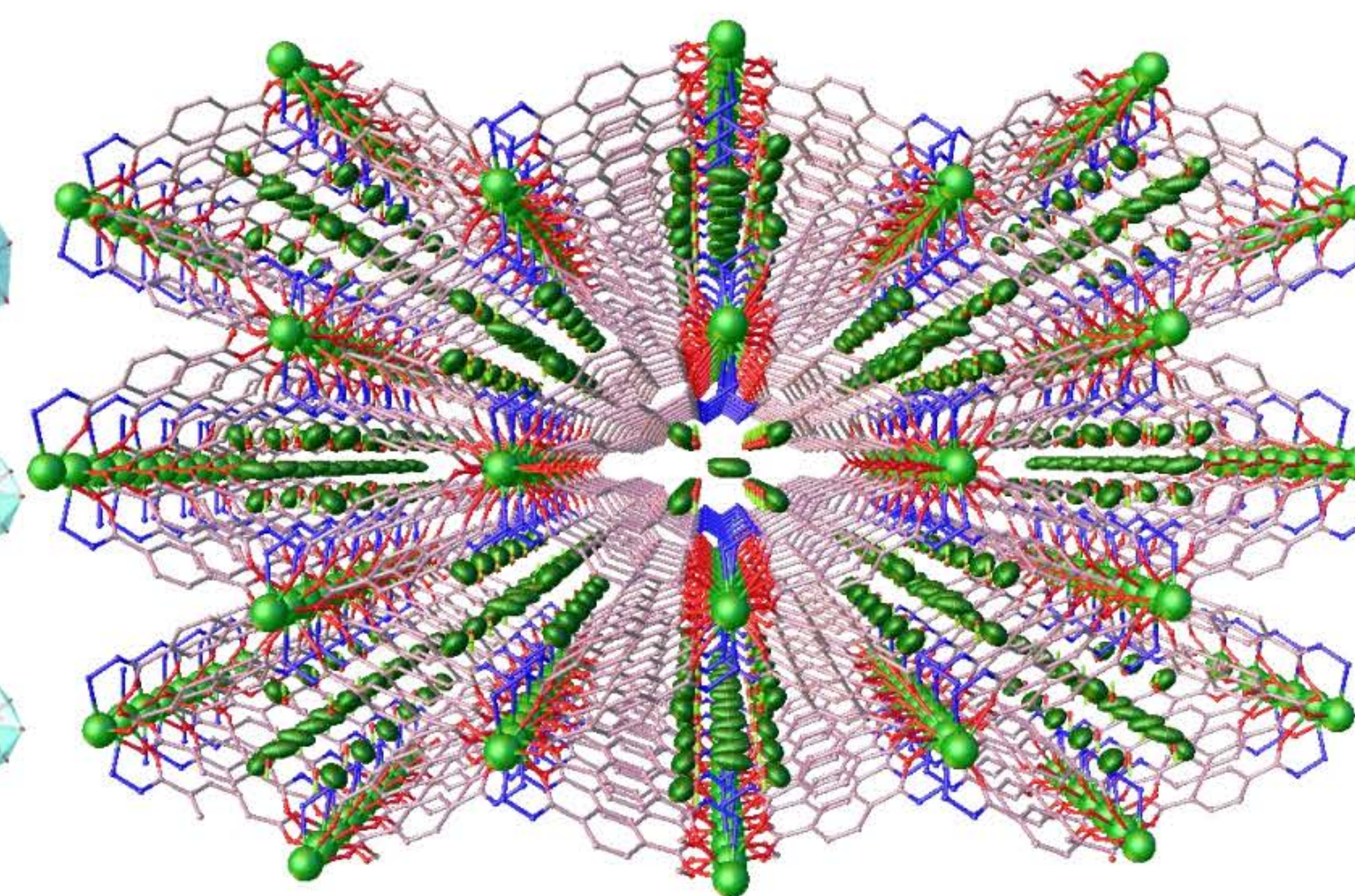
### Crystal structure



Coordination environment of [Tb(HCB)<sub>2</sub>]·X  
(X = NO<sub>3</sub>, Cl, Br, I, )  
Orthorhombic, *Pccn*

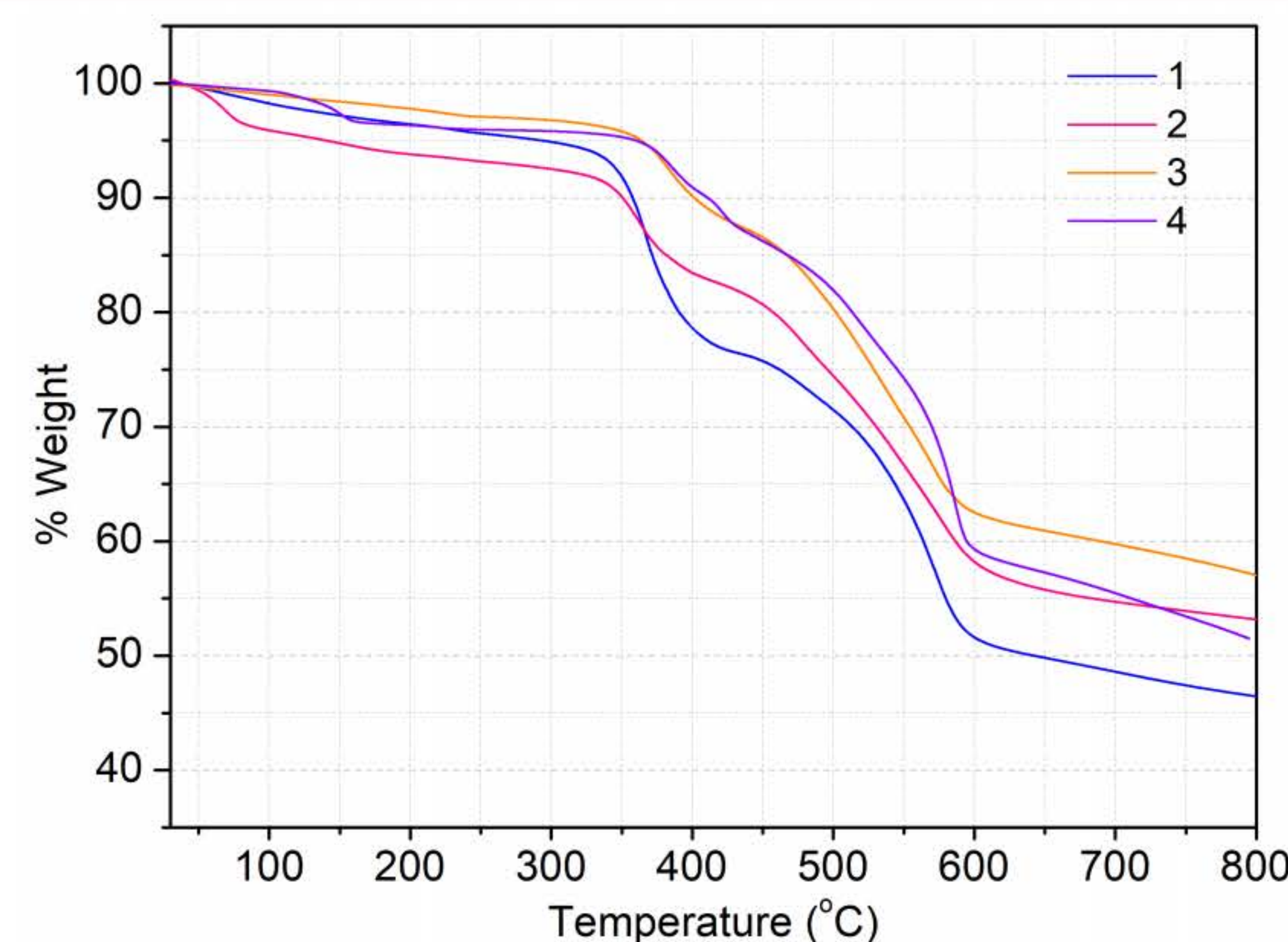
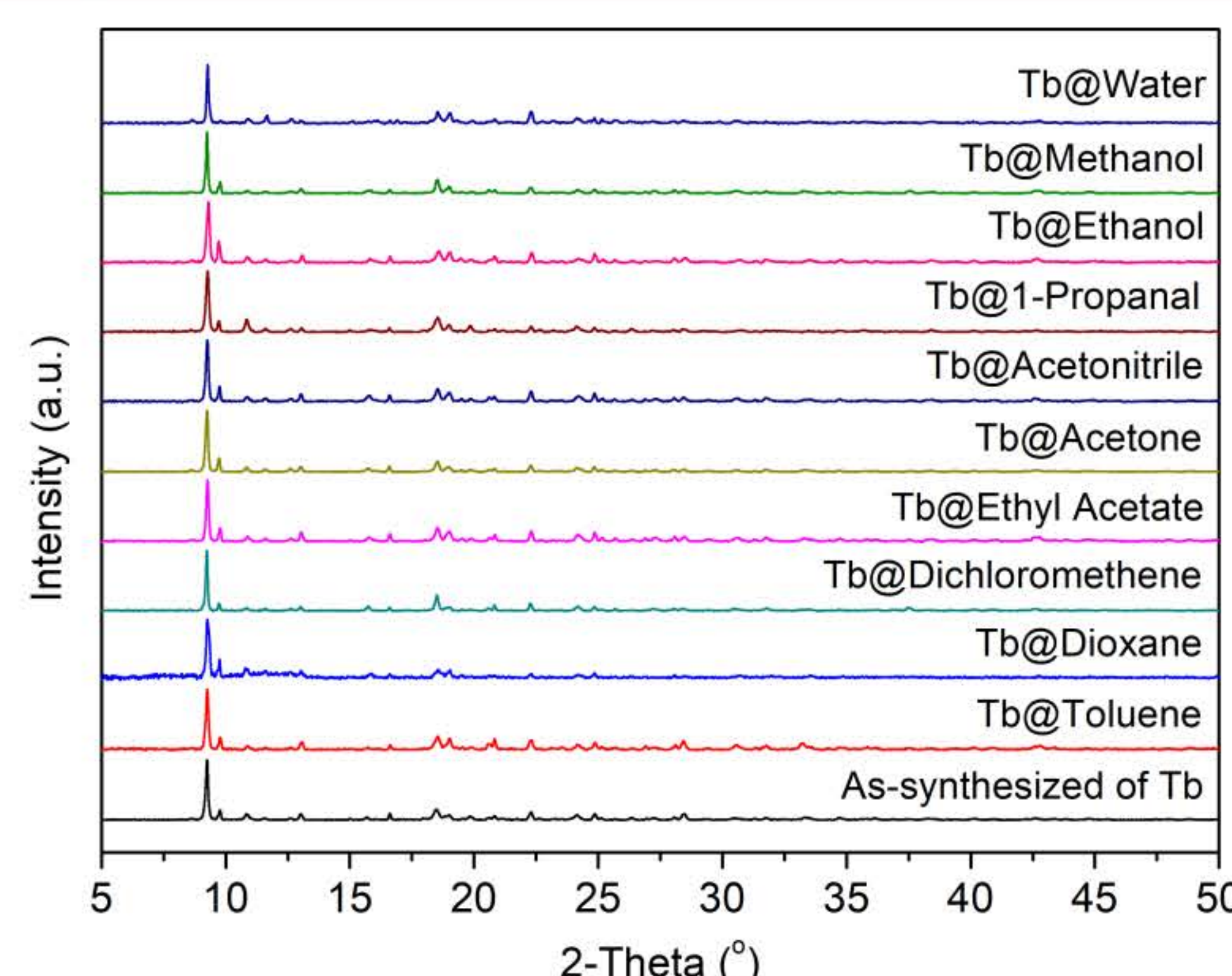
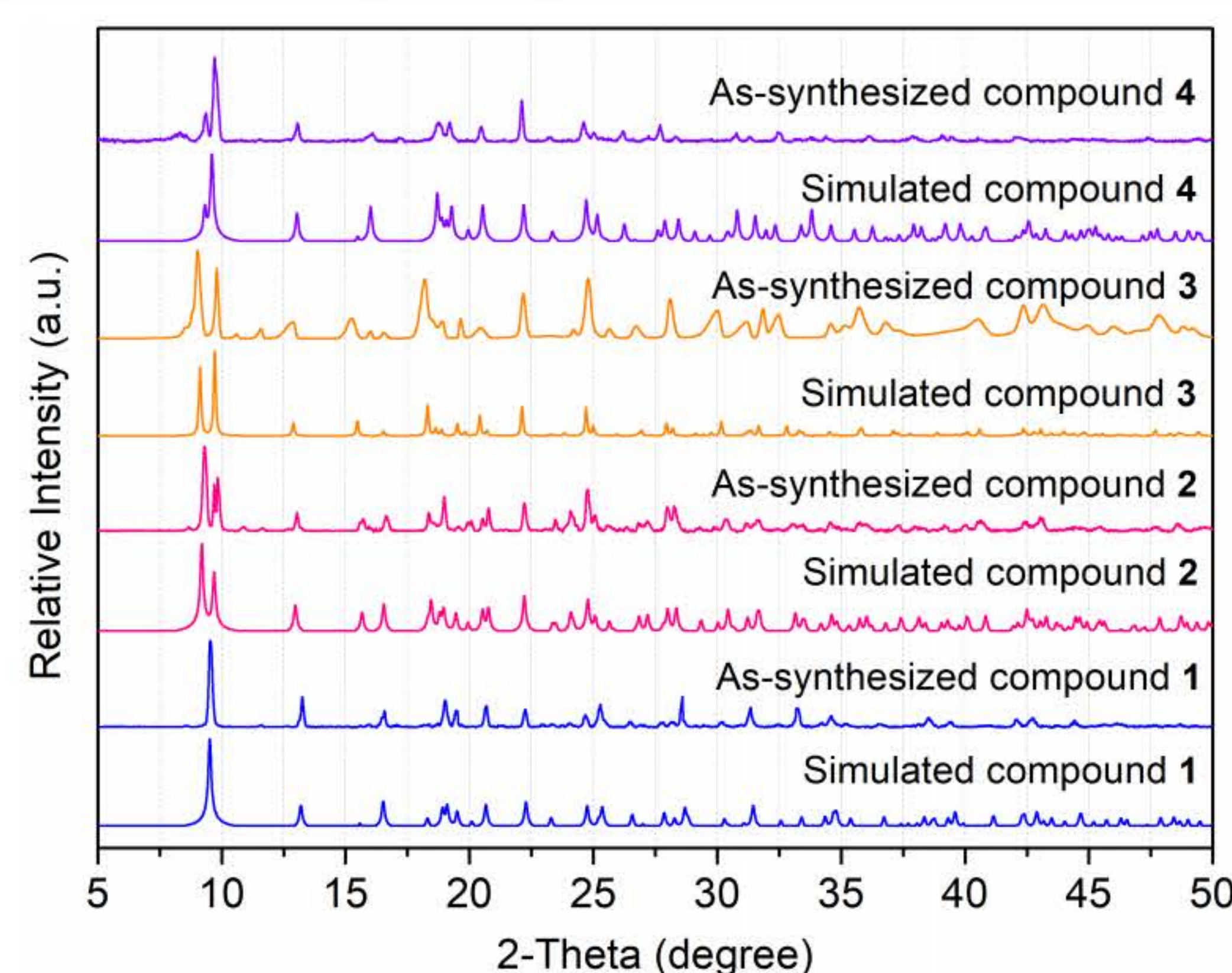


Perspective view of 3D frameworks  
along the c axis without the guest molecules  
reside in channels



3D frameworks with the guest (chloride  
anion) molecules reside in channels

### Phase purity and Thermal stability



Powder X-ray diffraction patterns of simulated, as-synthesized (left), in various solvent (middle) and thermogravimetric analysis curves (right) for compound 1, 2, 3, and 4

### Conclusion & Future prospects

- Four novel porous metal-organic framework (MOF) materials incorporating bifunctional ligands were effectively synthesized and thoroughly characterized using spectroscopic and diffraction techniques.
- After optimizing the synthesis in milligrams, the next step is to scale up production to grammes. Moving from lab-scale synthesis to industrial-scale output requires scaling up.
- Good chemical (wide range of solvents) and thermal stabilities (up to 330 °C) make these materials acceptable for industrial usage.
- High-pressure CO<sub>2</sub> adsorption isotherms for activated samples of these materials will be studied.
- Developing a prototype of a carbon dioxide (CO<sub>2</sub>) absorbent technology for use in EGAT's power plants is a complex task that involves multiple engineering and scientific considerations.



## Acknowledgements

This research has received funding support from the NSRF via the Program Management Unit for Human Resources & Institutional Development, Research and Innovation [grant number B13F660058]. The authors thank Thammasat University Research Unit in Multifunctional Crystalline Materials and Applications (TU-MCMA) and Electricity Generating Authority of Thailand (EGAT).



# APPLICATION OF METAL-ORGANIC FRAMEWORKS FOR CARBON DIOXIDE CONVERSION INTO CHEMICALS

Chana Panyanon,<sup>1</sup> Chatphorn Theppitak,<sup>1</sup> Suwadee Jiajaroen,<sup>1</sup> Issaraporn Rakngam,<sup>1</sup>  
Weerasak Homkrajai,<sup>2</sup> Sakchai Laksee,<sup>3</sup> Bunyarat Rungtaweeworanit,<sup>4</sup> and Kittipong Chainok,<sup>1\*</sup>

<sup>1</sup>Thammasat University Research Unit in Multifunctional Crystalline Materials and Applications (TU-MCMA)  
Faculty of Science and Technology, Thammasat University, Thailand

<sup>2</sup>Electricity Generating Authority of Thailand (EGAT), Thailand

<sup>3</sup>Nuclear Technology Research and Development Center, Thailand Institute of Nuclear Technology, Thailand

<sup>4</sup>National Nanotechnology Center, National Science and Technology Development Agency, Thailand

Corresponding Author: kc@tu.ac.th

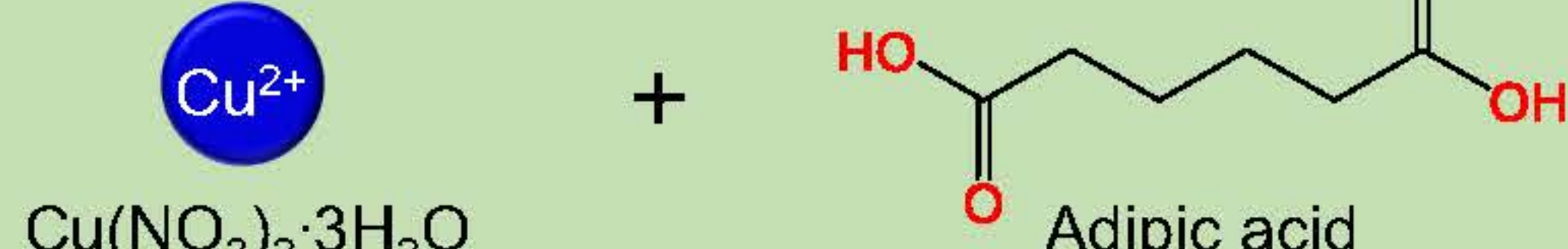


## Research Objectives

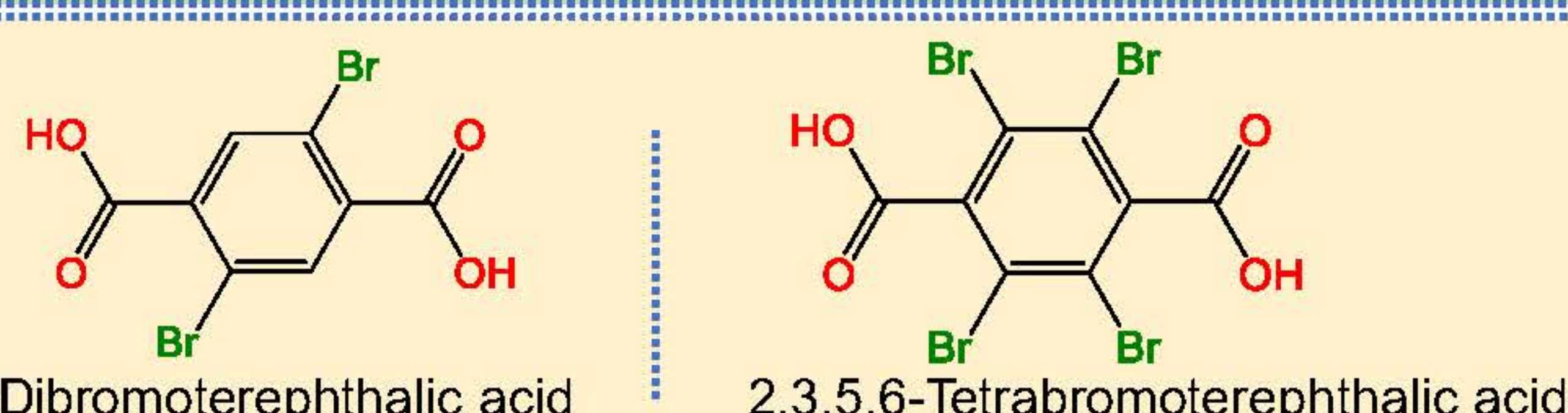
- To synthesize and physical characterize of new porous metal-organic frameworks (MOFs) under solvothermal conditions.
- To study the CO<sub>2</sub> adsorption-desorption of new porous MOFs at different temperatures under pressure 1 bar.
- To investigate the catalytic activity of new MOFs based heterogeneous catalyst for CO<sub>2</sub> conversion into value-added chemicals

## Synthesis Methods

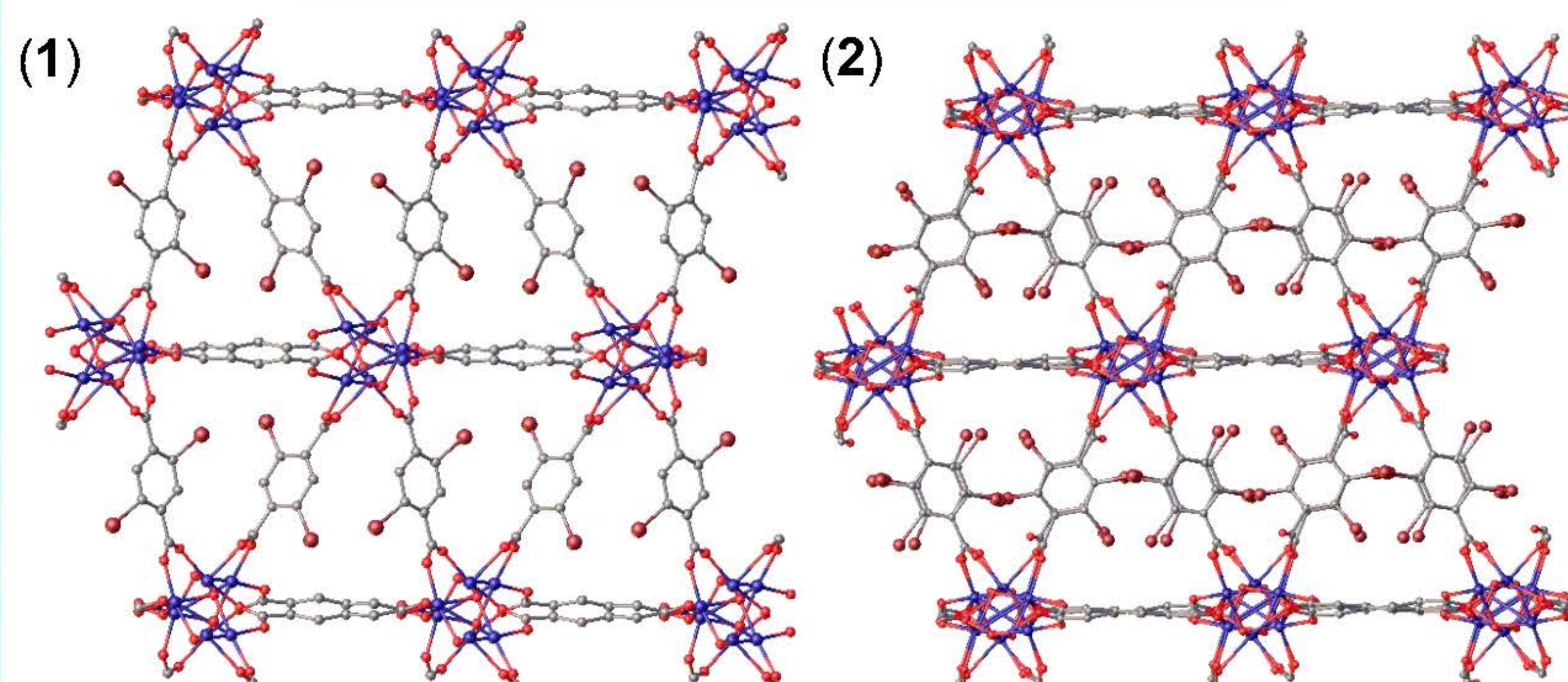
### Step 1



### Step 2



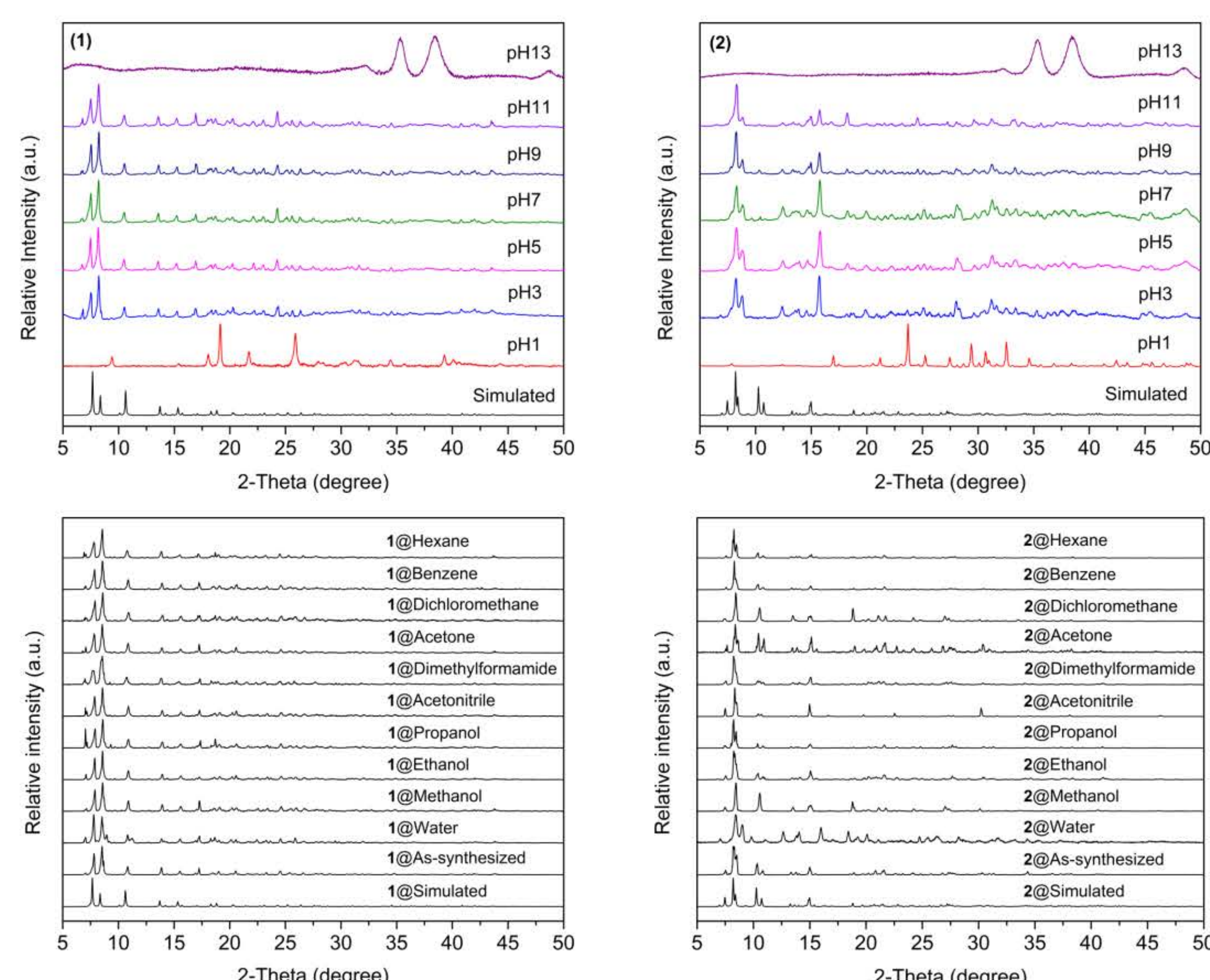
## Crystal Structures



The crystal packing of compounds 1 and 2

Compounds	1	2
System	monoclinic	triclinic
Space group	$P2_1/c$	$P-1$
a (Å)	12.5458(5)	13.2524(9)
b (Å)	23.0626(9)	13.4544(9)
c (Å)	9.9841(4)	17.4104(13)
$\alpha$ (°)	90	107.189(2)
$\beta$ (°)	108.693(1)	92.644(3)
$\gamma$ (°)	90	105.680(2)
V (Å <sup>3</sup> )	2736.40(19)	2828.4(4)

## pH and Solvent Stabilities



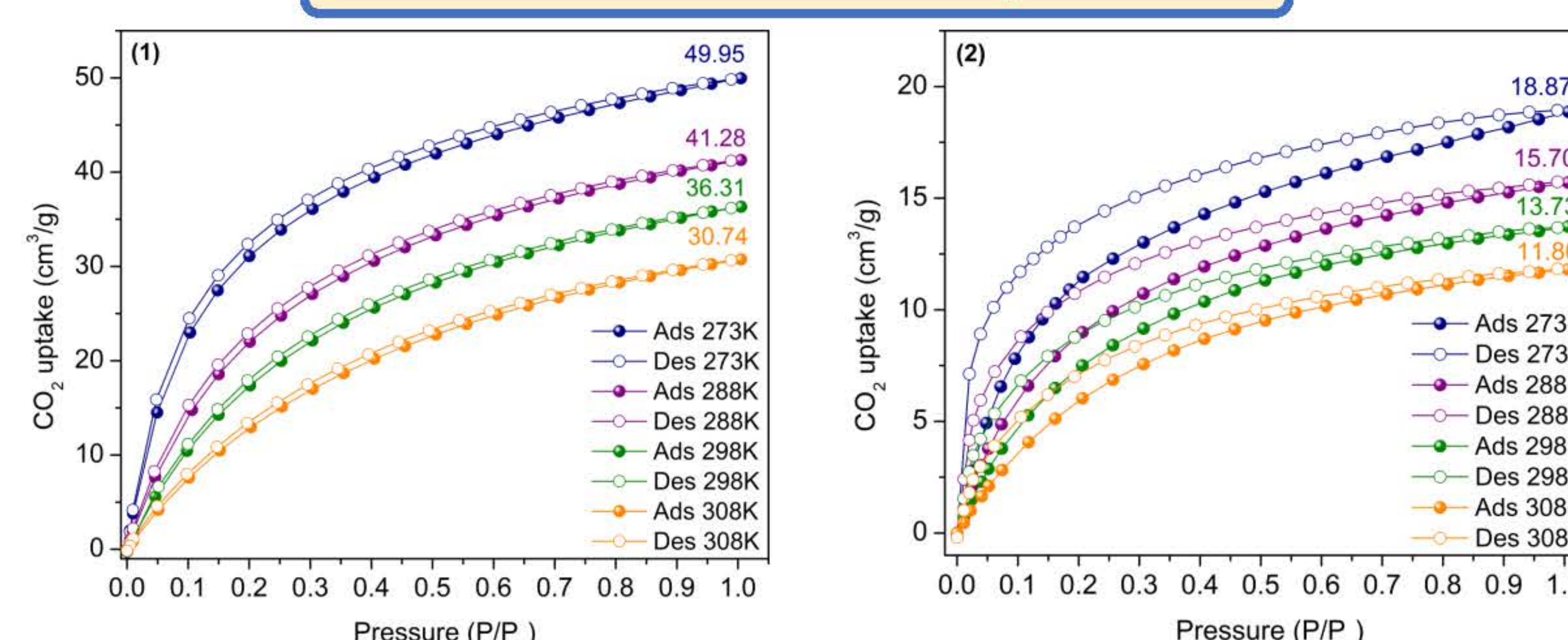
**Acknowledgements** :This research has received funding support from the NSRF via the Program Management Unit for Human Resources & Institutional Development, Research and Innovation [grant number B13F660058]. The author gratefully acknowledge TU-MCMA and EGAT.

## Carbon Dioxide Capture and Utilization

"Carbon dioxide is not a waste product but it will be a valuable substrate in the future"

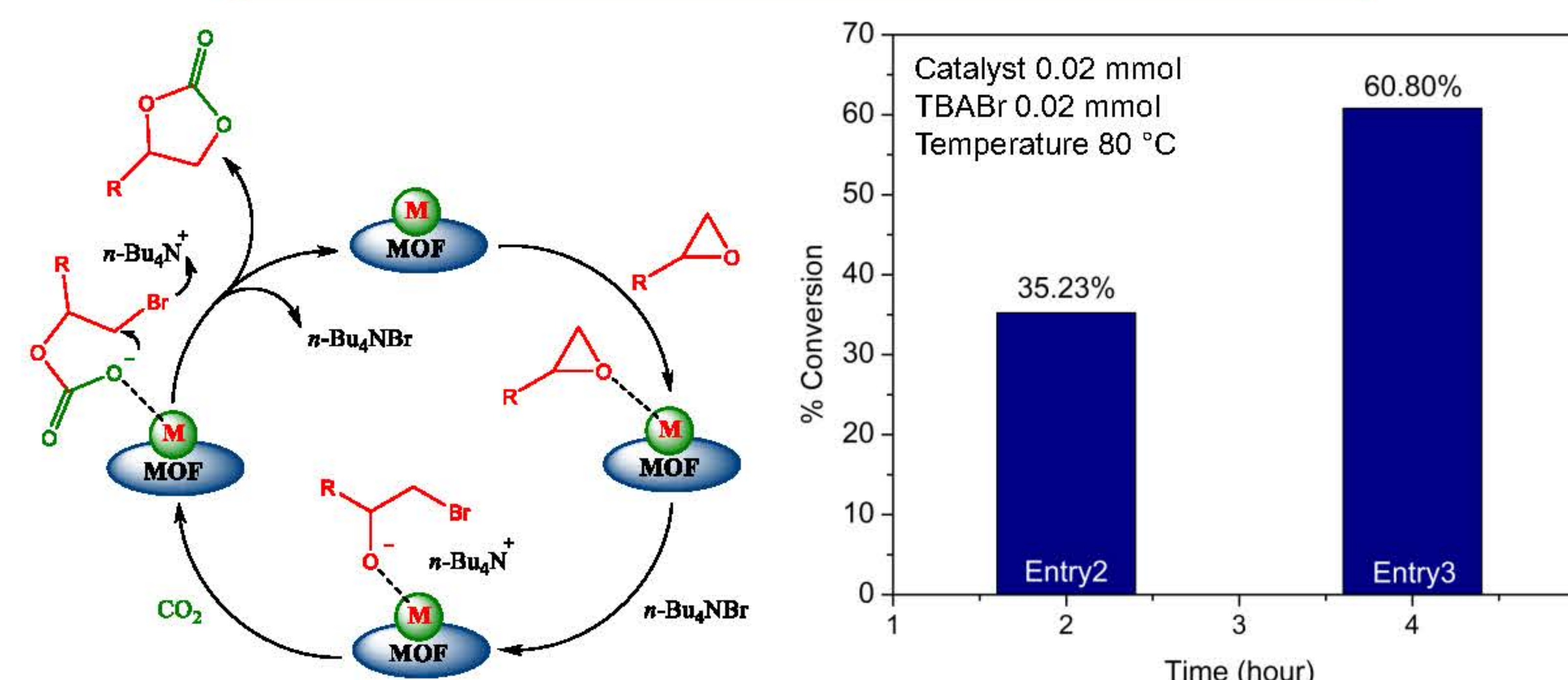
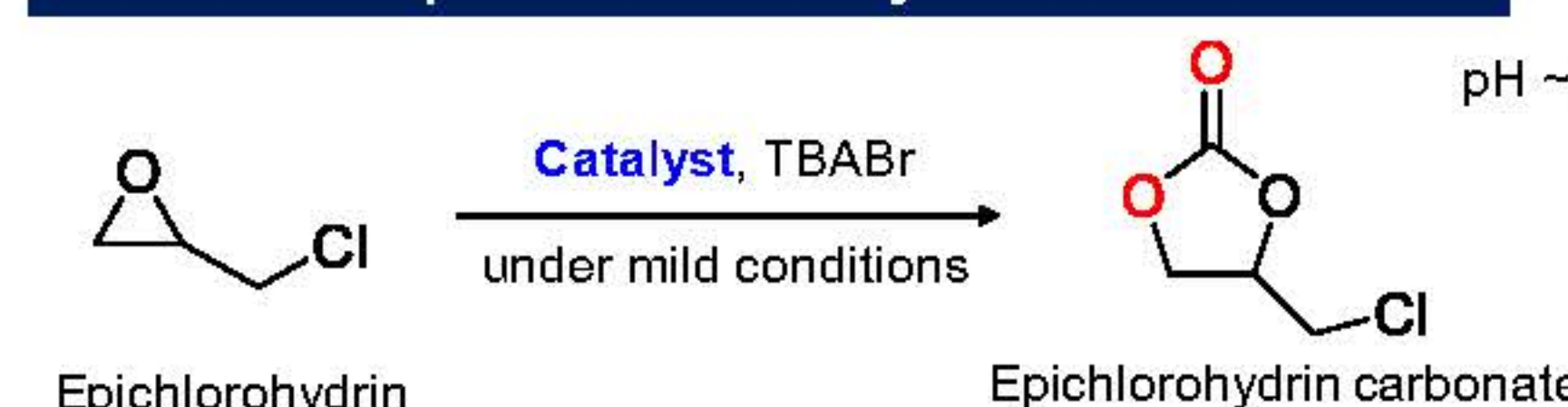


## Carbon Dioxide Adsorption



## Investigation of Catalytic Property

### Schematic representation of cycloaddition reaction



The mechanism path of the cycloaddition reaction of CO<sub>2</sub> with epichlorohydrin

## Conclusions

- Two new MOFs have been successfully synthesized from the same starting materials using different bromo-substituted benzenedicarboxylic ligands by solvothermal conditions and fully characterized.
- The activated 1 and 2 exhibited good thermal stabilities. These compounds showed good solvents and pH stabilities in the range of pH3-pH11.
- Interestingly, the maximum CO<sub>2</sub> uptake capacities of activated 1 and 2 were 49.95 and 18.87 cm<sup>3</sup>/g at 273 K under pressure 1 bar.
- Furthermore, 1 can also act as a heterogeneous catalyst for the cycloaddition reaction of CO<sub>2</sub> and epichlorohydrin under mild conditions to produce epichlorohydrin carbonate as starting substrate for chemical industries.
- Overall, the present study demonstrated that MOFs can readily be used as an alternative materials for value-added products to promote the net zero CO<sub>2</sub> emissions.

## Future Prospects

- Measurement of high-pressure CO<sub>2</sub> adsorption-desorption of activated MOFs based adsorbents at different temperatures.
- Investigation of the catalytic activity of MOFs based heterogeneous catalysts for CO<sub>2</sub> conversion and convert to value-added chemicals.
- Scale-up and formation of MOFs production to industrial scale.



Development of dye sensitizers applicable in photodynamic cancer therapy: A theoretical study

Parichart Suwannakham, Pannipa Panajapo, Phorntep Promma, Tunyawat Khrootkaew, Anyanee Kamkaew and Kritsana Sagarik\*

School of Chemistry, Institute of Science, Suranaree University of Technology, Nakhon Ratchasima 30000, Thailand.

Email: [kritsana@sut.ac.th](mailto:kritsana@sut.ac.th)

### Introduction

Photodynamic therapy (PDT) is a promising modality for a noninvasive cancer treatment. PDT uses an external chemical (photosensitizer, PS) that absorbs light and generates appropriate energy for  $^3\text{O}_2$  ( $^3\Sigma_g^-$ )  $\rightarrow$   $^1\text{O}_2$  ( $^1\Delta_g$ ); the cellular oxygen  $^3\text{O}_2$  absorbs the energy released from the excited PS through the relaxation between triplet excited state ( $T_n$ ) and ground state ( $S_0$ ) to generate  $^1\text{O}_2$ . Therefore, PS turns on therapeutic effects in the presence of  $^1\text{O}_2$ , and its toxicity leads to cell death as shown in Figure 1a.

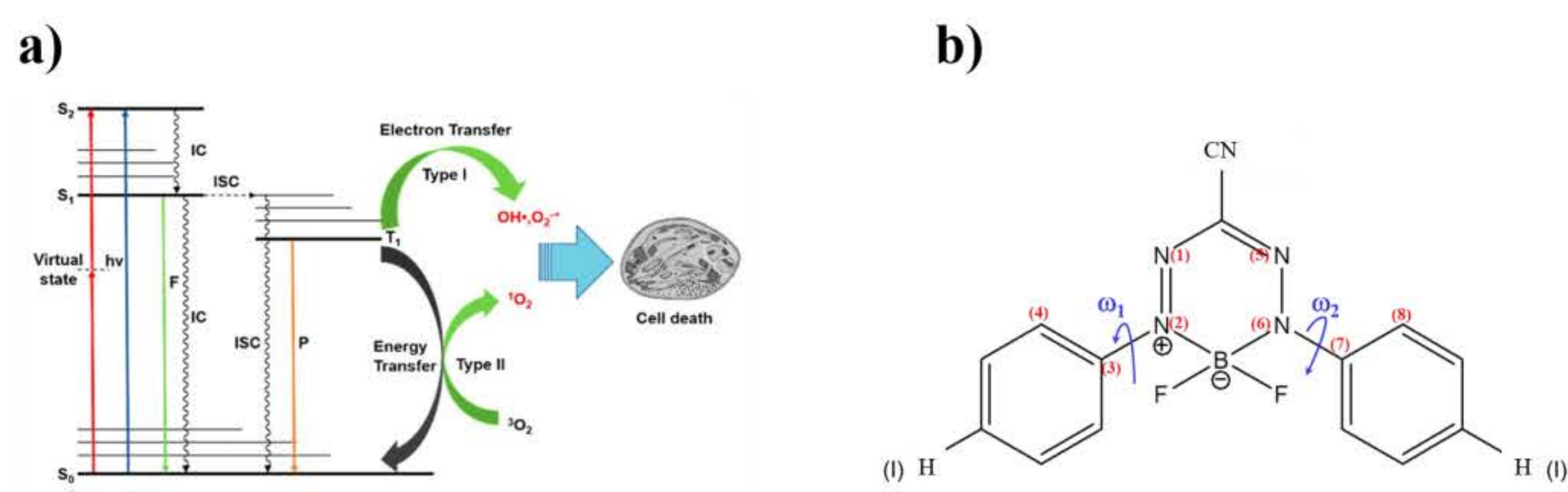


Figure 1 a) Jablonski diagram and pathway of photodynamic therapy (PDT).<sup>[1]</sup> b) Structure of BF<sub>2</sub>-FORM and BF<sub>2</sub>-FORM-D.

Boron difluoride formazanate dyes (BF<sub>2</sub>-FORM in Figure 1b) are fluorescent dyes with several applications in microscopy. Because BF<sub>2</sub>-FORM dyes exhibit outstanding photophysical properties, such as large molar extinction coefficients and high fluorescence quantum yield (in the far-red or near-infrared range), they have a high potential in cell imaging and photodynamic therapy applications. In this work, to improve the efficiency of PDT, theoretical methods were applied to study the mechanisms for photoluminescence of BF<sub>2</sub>-FORM dyes and its derivatives (BF<sub>2</sub>-FORM-D). The emphases were on the probabilities for interconversion (IC) and intersystem crossing (ISC), as well as the effect of the iodine substitutions (the heavy atom effect) on photophysical properties.

### Computational Methods

The computational methods used in this work are shown in Figure 2.

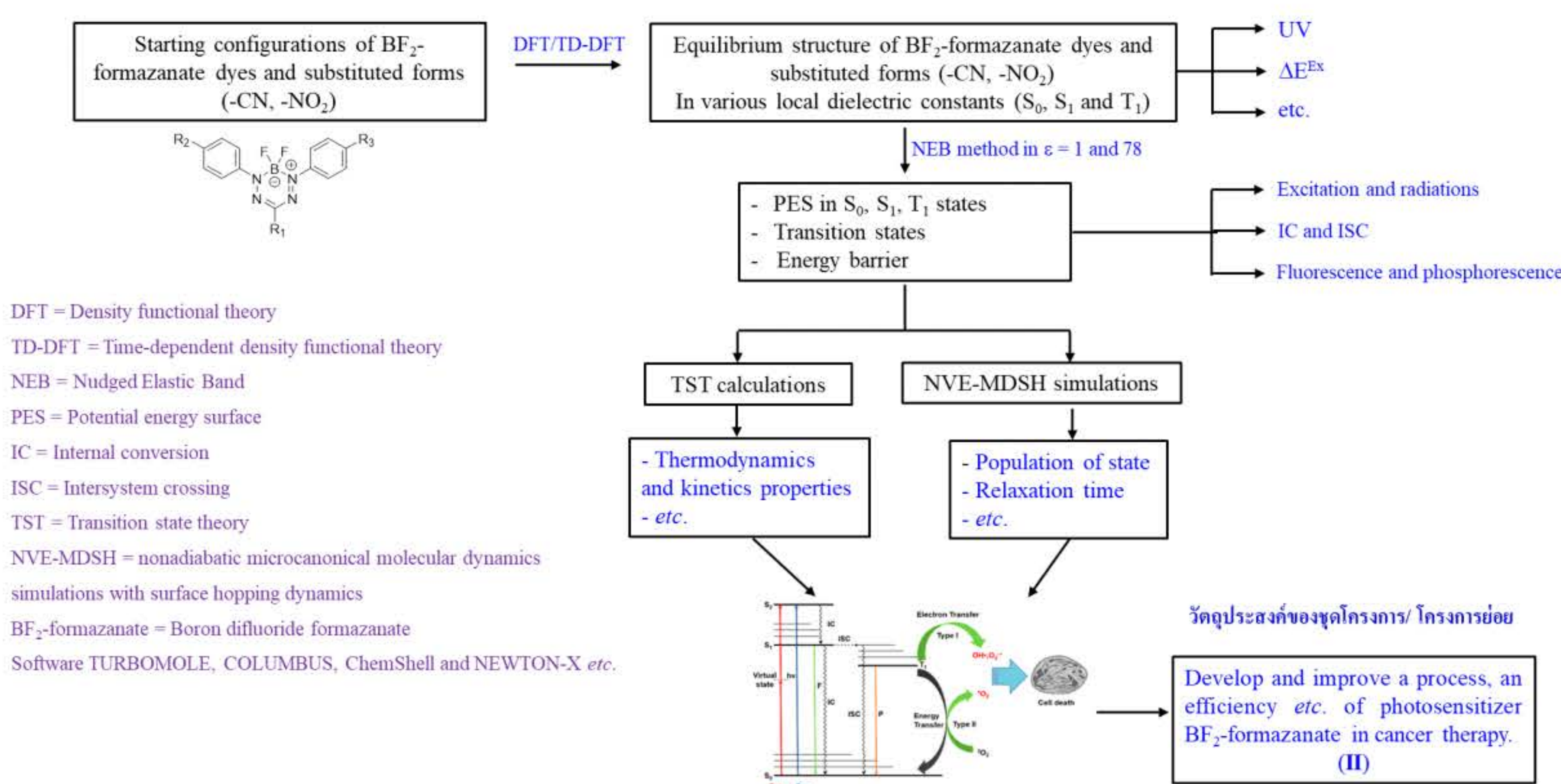
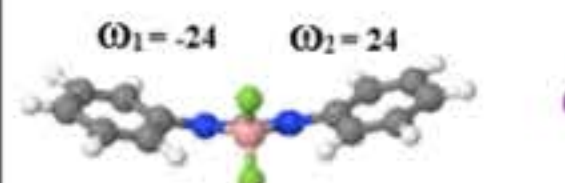
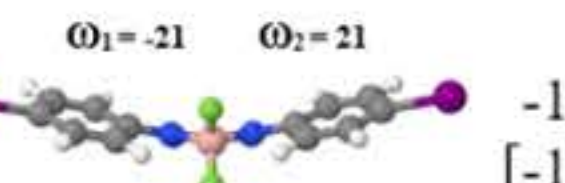
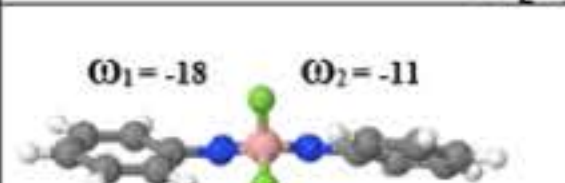
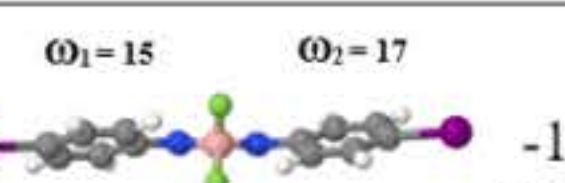
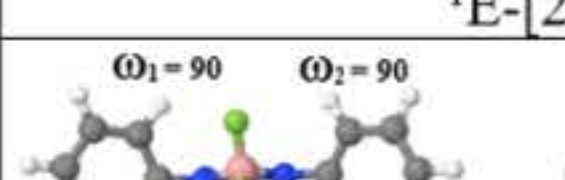
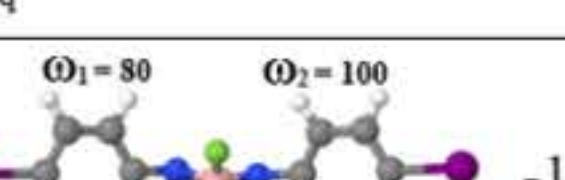
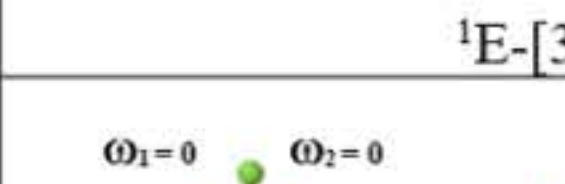
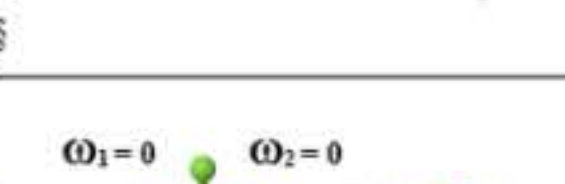


Figure 2 The theoretical methods used in this work.

### Results

**Equilibrium structures:** In the  $S_0$  state, the equilibrium structures of BF<sub>2</sub>-FORM and BF<sub>2</sub>-FORM-D are characterized by bent structure (G-[1]<sup>eq</sup>), whereas the propeller (<sup>1</sup>E-[2]<sup>eq</sup>) and perfect planar (<sup>3</sup>E-[4]<sup>eq</sup>) structures represent the structures in the  $S_1$  and  $T_1$  states, respectively. The photoexcitation energy of BF<sub>2</sub>-FORM is higher than BF<sub>2</sub>-FORM-D, ( $\Delta E_{S_0 \rightarrow S_1}^{TD-RHF} = 2.88$  and 2.42 eV or 431 and 513 nm, respectively).

Table 1. Structures and energies of BF<sub>2</sub>-FORM in the  $S_0$ ,  $S_1$  and  $T_1$  states, obtained from DFT and TD-DFT/B3LYP/6-311G calculations. [...] = values for BF<sub>2</sub>-FORM-D.

[BF <sub>2</sub> -FORM]	[BF <sub>2</sub> -FORM-D]	$E^{Tot}$	$\Delta E_{S_0 \rightarrow S_1}^{TD-RHF}$	$\Delta E_{S_0 \rightarrow S_1}^{TD-RHF}$	$\Delta E_{S_1 \rightarrow T_1}^{TD-RHF,PES}$	$\Delta E_{T_1 \rightarrow S_0}^{TD-RHF}$
 G-[1] <sup>eq</sup>	 G-[1] <sup>eq</sup>	-1037.31086 [-1058.87541]	2.88 [2.42]	-	-	1.45 [1.35]
 <sup>1</sup> E-[2] <sup>eq</sup>	 <sup>1</sup> E-[2] <sup>eq</sup>	-1037.21702 [-1058.79022]	-	2.13 [2.25]	-	1.13 [1.12]
 <sup>1</sup> E-[3] <sup>f</sup>	 <sup>1</sup> E-[3] <sup>f</sup>	-1037.20770 [-1058.78779]	-	1.82 [1.48]	0.30 [0.04]	1.52 [1.43]
 <sup>3</sup> E-[4] <sup>eq</sup>	 <sup>3</sup> E-[4] <sup>eq</sup>	-1037.26944 [-1058.83644]	-	0.91 [0.88]	-	0.91 [0.87]

### Results

**Electron density distribution and UV spectra:** The HOMOs in Figure 3a are characterized by strong  $\pi$  character at the formazanate heterocyclic and phenyl rings, whereas LUMOs are localized. The HOMOs and LUMOs suggest that BF<sub>2</sub>-FORM possesses a significantly lower  $\pi$  character than BF<sub>2</sub>-FORM-D. The UV spectra in Figure 3b show that BF<sub>2</sub>-FORM and BF<sub>2</sub>-FORM-D absorb light at  $\lambda_{max} = 446$  and 534 nm, respectively, which are in good agreement with the experimental absorption spectra,  $\lambda_{max} = 531$  nm<sup>[2]</sup>.

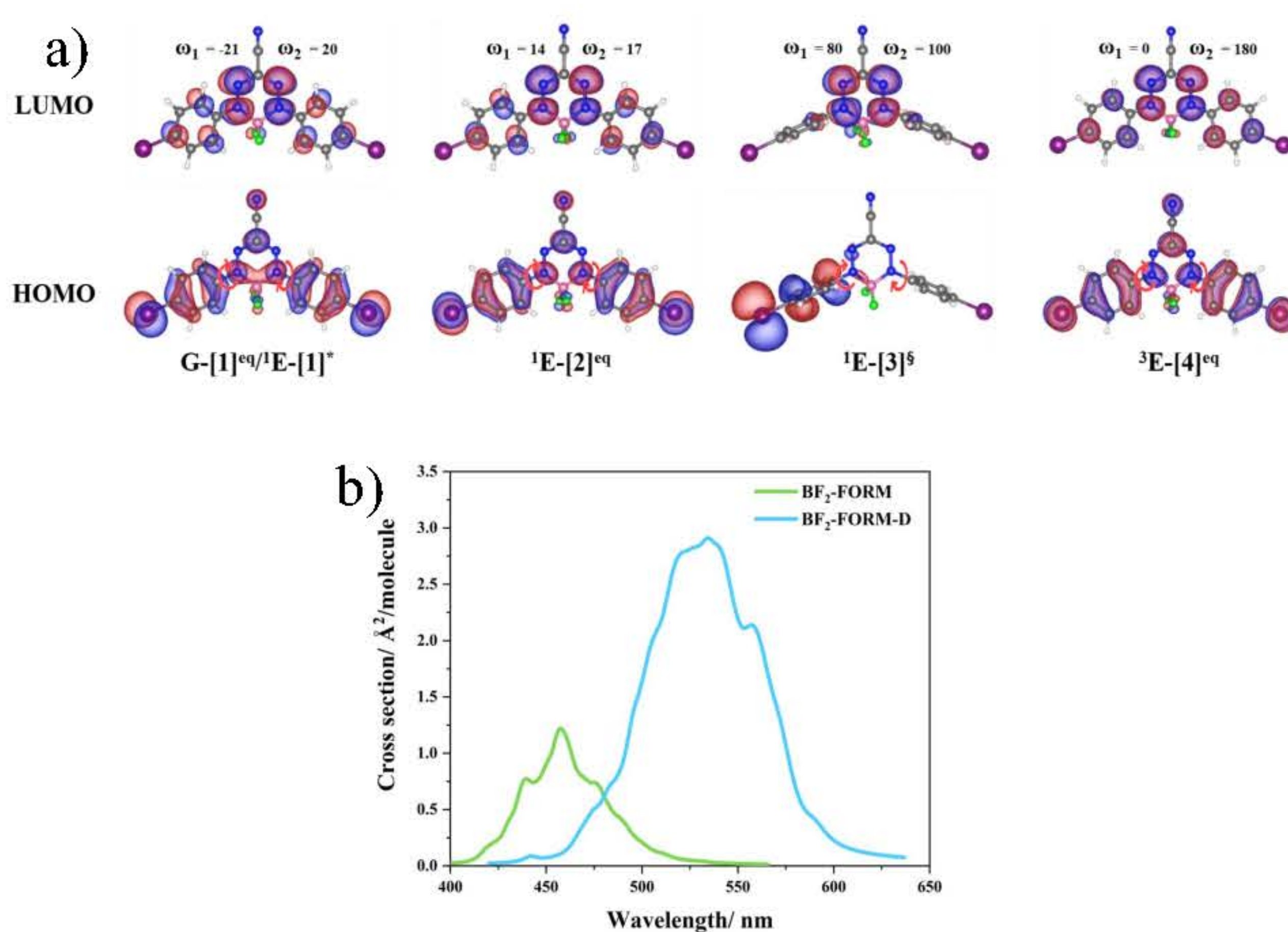


Figure 3 a) HOMO and LUMO of BF<sub>2</sub>-FORM-D in the  $S_0$  and  $S_1$  state, b) UV absorption spectra of BF<sub>2</sub>-FORM and BF<sub>2</sub>-FORM-D.

**Potential energy surface:** The  $S_1 \rightarrow S_0$  fluorescence ( $F$ ) of BF<sub>2</sub>-FORM and BF<sub>2</sub>-FORM-D (<sup>1</sup>E-[2]<sup>eq</sup>  $\rightarrow$  G-[2]) occur at 581 and 552 nm, respectively. The PES suggested two possibility for phosphorescence; (1)  $P_1$  occurs right after the  $S_1 \rightarrow T_1$  intersystem crossing (ISC at 814 and 864 nm, respectively); (2)  $P_2$  takes place after the ISC and structure relaxation to the equilibrium structure in the  $T_1$  state (<sup>3</sup>E-[3]<sup>f</sup>  $\rightarrow$  <sup>3</sup>E-[4]<sup>eq</sup>) (1365 and 1430, respectively). The latter ( $P_2$ ) are close to the energy for  $^3\text{O}_2$  ( $^3\Sigma_g^-$ )  $\rightarrow$   $^1\text{O}_2$  ( $^1\Delta_g$ ), 1378 nm (0.90 eV)<sup>[3]</sup>.

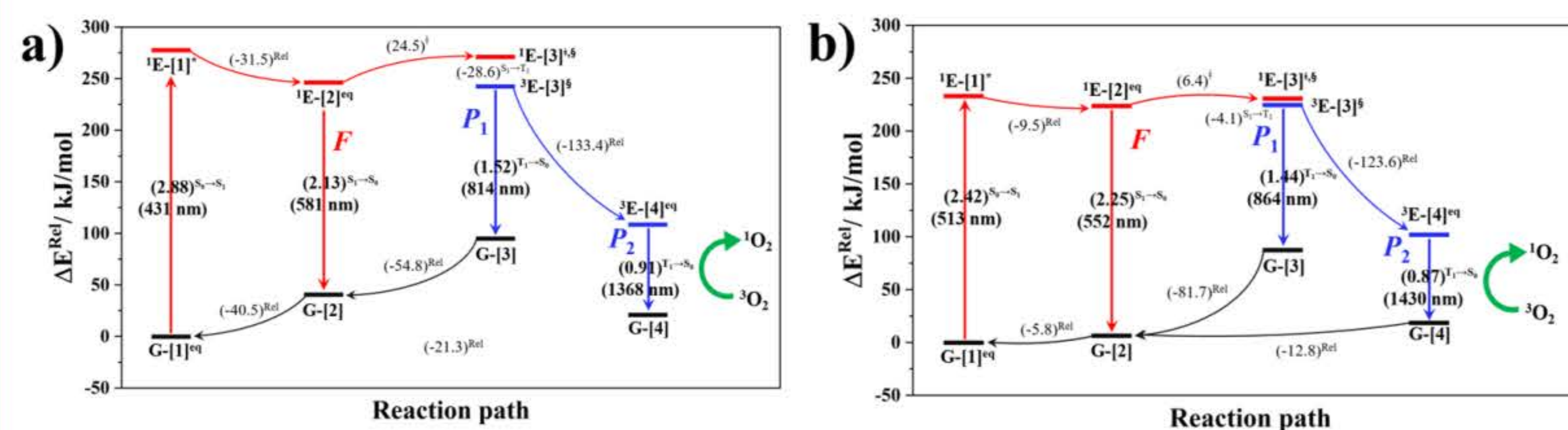


Figure 4 a)–b) Mechanisms of fluorescence and phosphorescence for BF<sub>2</sub>-FORM and BF<sub>2</sub>-FORM-D, respectively.

### Conclusions

- Equilibrium structures of BF<sub>2</sub>-FORM and BF<sub>2</sub>-FORM-D in the  $S_0$ ,  $S_1$  and  $T_1$  states are the same, characterized by bent, propeller and perfect planar structures, respectively.
- The HOMO and LUMO show lower  $\pi$  character in BF<sub>2</sub>-FORM than BF<sub>2</sub>-FORM-D.
- The UV spectra suggest that BF<sub>2</sub>-FORM and BF<sub>2</sub>-FORM-D absorb light at  $\lambda_{max} = 446$  and 534 nm, respectively.
- Fluorescence of BF<sub>2</sub>-FORM and BF<sub>2</sub>-FORM-D occur at 581 and 552 nm respectively.
- Two possibilities for the phosphorescence are:
  - $P_1$  occurs after the  $S_1 \rightarrow T_1$  ISC at 814 nm and 864 nm for BF<sub>2</sub>-FORM and BF<sub>2</sub>-FORM-D, respectively.
  - $P_2$  takes place after the <sup>3</sup>E-[3]<sup>f</sup>  $\rightarrow$  <sup>3</sup>E-[4]<sup>eq</sup> structure relaxation with 1365 nm (BF<sub>2</sub>-FORM) and 1430 nm (BF<sub>2</sub>-FORM-D) which close to the absorption energy for the  $^3\text{O}_2 \rightarrow ^1\text{O}_2$  transformation, 1378 nm, leading to cell death.

#### Acknowledgement:

This research has received funding support from (i) Suranaree University of Technology (SUT) (ii) NSRF via the Program Management Unit for Human Resources & Institutional Development, Research and Innovation [grant number B13F660060].

#### References

- Feng, G.; Zhang, G.-Q.; Ding, D., Design of superior phototheranostic agents guided by Jablonski diagrams. *Chemical Society Reviews*, 2020, 49, 8179–8234.
- Khrootkaew, T et al., The Heavy atom effect on intersystem crossing of boron difluoride formazanate complex-based photosensitizer: Experimental and theoretical studies. *Chemistry – An Asian Journal*, 2023, e202300808.
- Davies, M. J., Singlet oxygen-mediated damage to proteins and its consequences. *Biochemical and biophysical research communications*, 2003, 305(3), 761–770.





BRAINPOWER  
CONGRESS 2023

ร่วมกับสร้างและขับเคลื่อนงานวิจัยข้ามแนวหน้า  
สู่อุตสาหกรรมแห่งอนาคต

UW  
สร้างคน  
ข้ามพรมแดน

# Photocatalysis of enzymatic decarboxylation of unsaturated acid: catalytic process improvement

Pannipa Panajapo, Phorntep Promma, Parichart Suwannakham, Kritsana Sagarik\*

School of Chemistry, Institute of Science, Suranaree University of Technology, Nakhon Ratchasima 30000, Thailand.

## Introduction

Enzymatic decarboxylation of  $\alpha,\beta$ -unsaturated acid has been of interest [1-4] because the reaction has been anticipated to be a promising, environmentally friendly industrial process for producing styrene from natural resources. Payne et al. [1] suggested that styrene could be produced directly from cinnamic acid using ferulic acid decarboxylase (Fdc1) enzyme and prenylated flavin mononucleotide (prFMN) as the cofactor (Figure 1a). Because two forms of prFMN, namely, the iminium (im) and ketimine (ket), possess different catalytic activity, and the photoisomerization of prFMN<sup>im</sup> to prFMN<sup>ket</sup> reduces the efficiency of styrene production,

In this work, the photoisomerization of prFMN<sup>im</sup>→prFMN<sup>ket</sup> hypothesized by Bailey, et al. [5] was studied in detail using quantum chemical methods, transition state theory (TST) and molecular dynamic (MD) simulations. The theoretical results could be used as guidelines for the improvement of styrene production by inhibition of the prFMN<sup>im</sup>→prFMN<sup>ket</sup> isomerization.

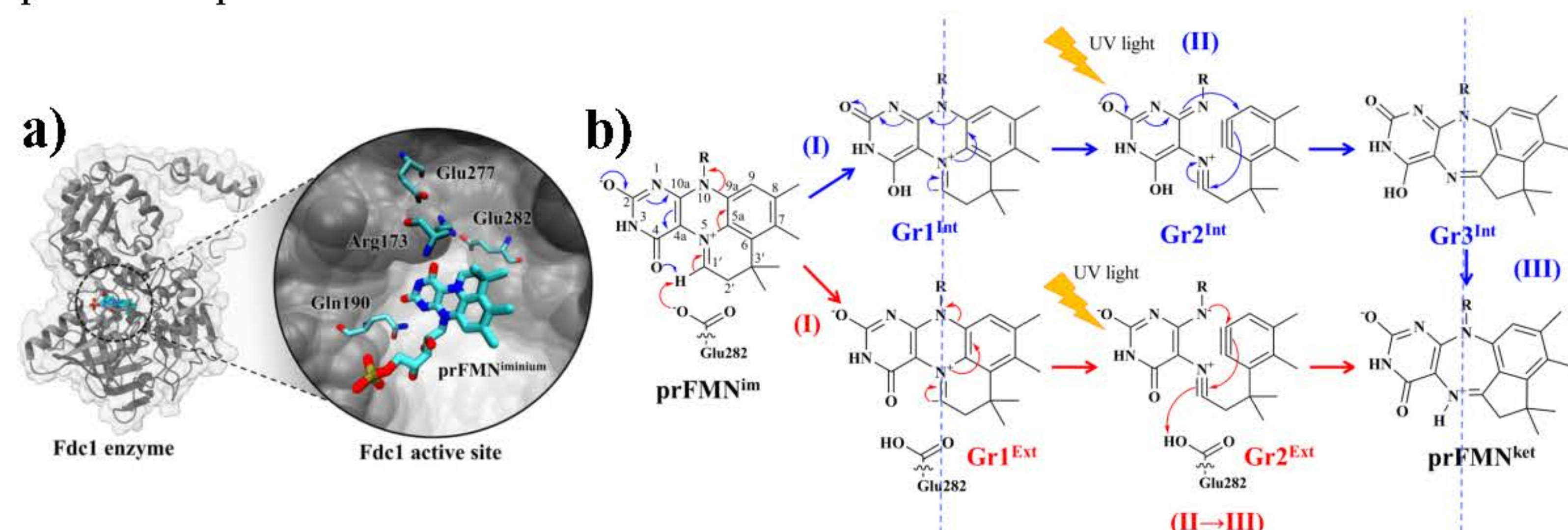


Figure 1 a) PrFMN<sup>im</sup> in the active site of Fdc1. b) Proposed mechanisms for the photoisomerization of prFMN<sup>im</sup>→prFMN<sup>ket</sup> [5].

## Computational methods

The active site of Fdc1 consisting of prFMN<sup>im</sup> and Arg173, Gln190, Glu277 and Glu282 were used as a model system. Based on the results obtained from geometry and reaction path optimizations, the photoisomerization mechanisms for prFMN<sup>im</sup>→prFMN<sup>ket</sup> were conducted in the  $S_0$  and  $S_1$  states using the DFT/B3LYP/DZP, TD-DFT/B3LYP/DZP and NEB methods.

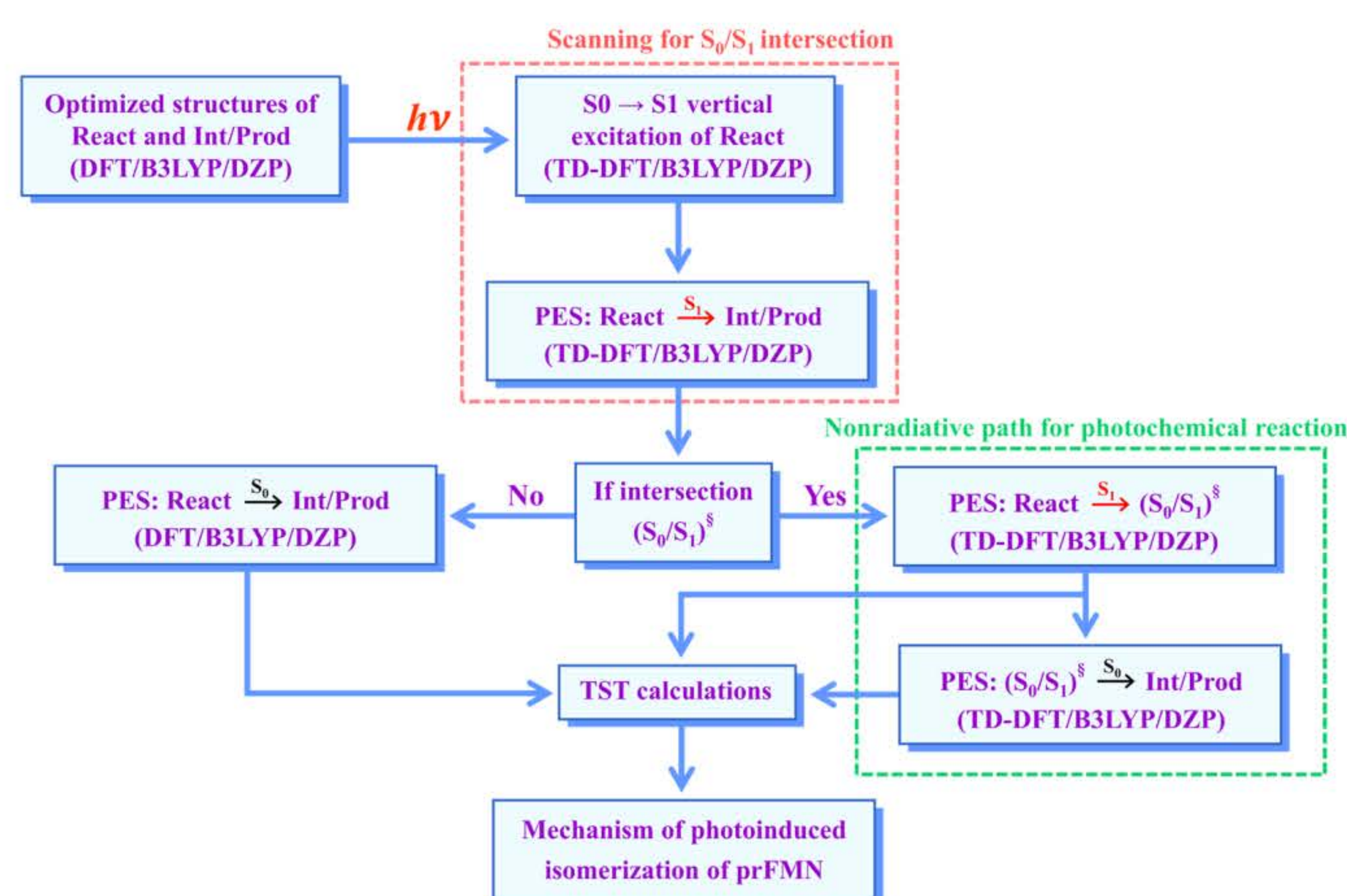


Figure 2 Computational methods used in this study.

## References

- [1] K. A. Payne, M. D. White, K. Fisher, B. Khara, S. S. Bailey, D. Parker, N. J. Rattray, D. K. Trivedi, R. Goodacre and R. Beveridge, Nature, 2015, 522, 497-501.
- [2] K. L. Ferguson, N. Arunrattanamook and E. N. G. Marsh, Biochemistry, 2016, 55, 2857-2863.
- [3] K. L. Ferguson, J. D. Eschweiler, B. T. Ruotolo and E. N. G. Marsh, J. Am. Chem. Soc., 2017, 139, 10972-10975.
- [4] C.-L. Lan and S.-L. Chen, J. Org. Chem., 2016, 81, 9289-9295.
- [5] S. S. Bailey, K. A. P. Payne, A. Saaret, S. A. Marshall, I. Gostinskaya, I. Kosov, K. Fisher, S. Hay and D. Leys, Nat. Chem., 2019, 11, 1049-1057.

## Results and discussion

Analysis of the proposed mechanisms in Figure 1b revealed two types of consecutive elementary reactions involving: (I) Intramolecular proton transfer in prFMN<sup>im</sup> (Type A) or intermolecular proton transfer from prFMN<sup>im</sup> to Glu282 (Type B); (II) heterocyclic ring expansion (isomerization) and; (III) reverse protonation. The theoretical results suggested that both pathways are not favorable due to high energy barriers. After several reaction path optimizations, the calculated PES suggested two low energy barrier paths.

For Type B in Figure 3, the photoisomerization could proceed through the  $S_0$ → $S_1$  vertically excited prFMN<sup>im,eq</sup>, which relaxes to the  $S_0$ / $S_1$  intersection, and followed by intermolecular proton transfer from prFMN<sup>im</sup> to Glu282 (I) and heterocyclic ring expansion (II) to form Gr3<sup>Ext,eq</sup>. The reverse protonation and generation of prFMN<sup>ket</sup> could occur in both  $S_0$  and  $S_1$  states, with a low energy barrier (III) and barrierless energy (III)\*, respectively.

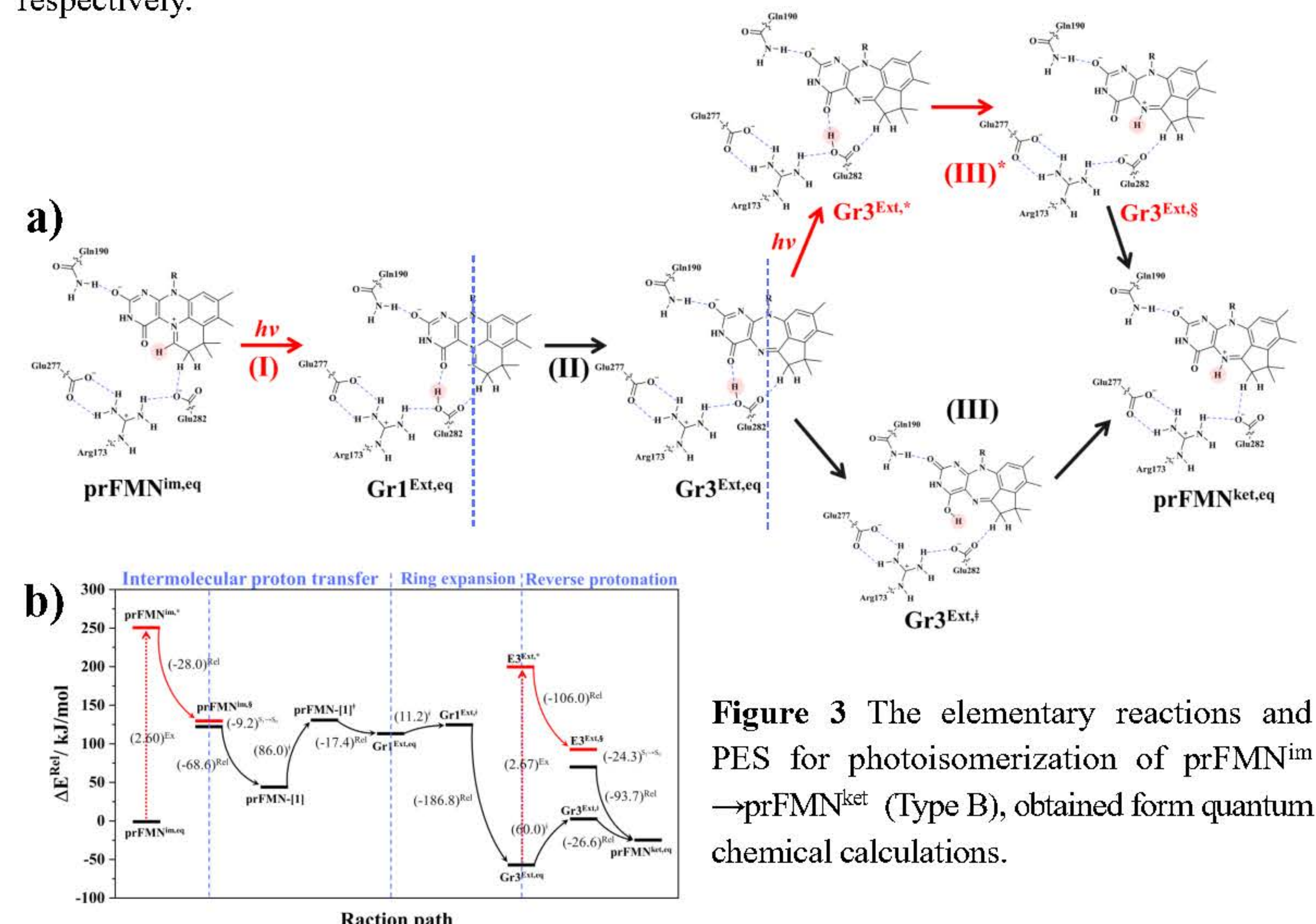


Figure 3 The elementary reactions and PES for photoisomerization of prFMN<sup>im</sup>→prFMN<sup>ket</sup> (Type B), obtained from quantum chemical calculations.

The photoisomerization Type A, which involves  $S_0$ → $S_1$  vertical excitation, concerted intramolecular proton transfer and ring expansion (I→II) to produce prFMN<sup>ket</sup> also possesses a low energy barrier.

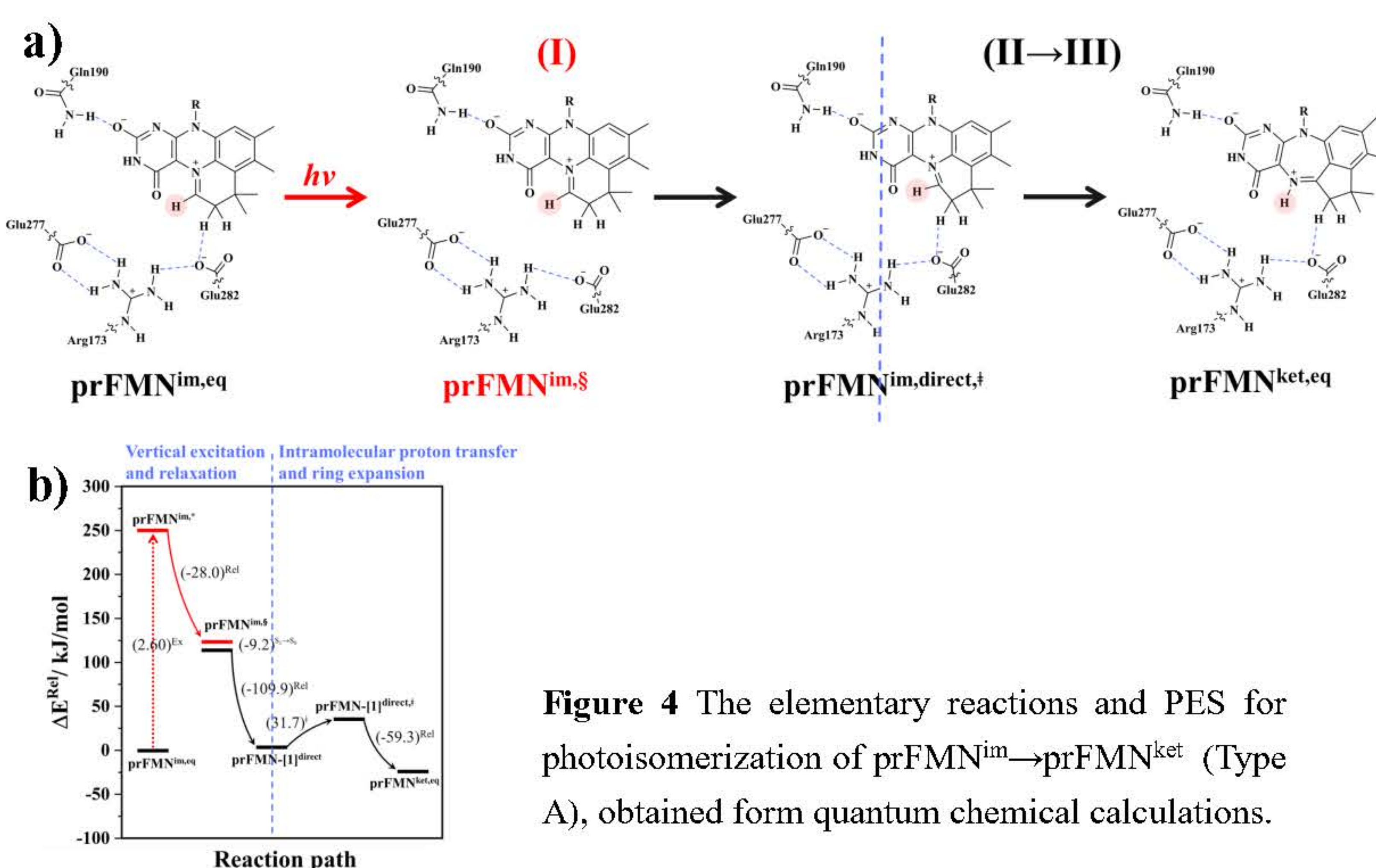


Figure 4 The elementary reactions and PES for photoisomerization of prFMN<sup>im</sup>→prFMN<sup>ket</sup> (Type A), obtained from quantum chemical calculations.

## Acknowledgement

This research has received funding support from (i) Suranaree University of Technology (SUT) (ii) NSRF via the Program Management Unit for Human Resources & Institutional Development, Research and Innovation [grant number B13F660060]



# Conversion of Oil Palm Empty Fruit Bunch to Value-Added Biochemical

Laksamee Jeanmard, Wichitpan Rongwong,\* Wanna Choorit

Biomass and Oil Palm Center of Excellence, Walailak University, Nakhon Si Thammarat 80161, Thailand

## Introduction

Oil palm is a major industrial crop in tropical countries.<sup>1</sup> Until now, palm oil manufacturing processes have utilized only 10% of biomass products from palm oil and palm kernel oil, while the remaining 90% of biomass is defined as waste. Oil palm empty fruit bunch (OPEFB) is one of the daily leftover solid residues from oil palm manufacturing, weighing many tonnes per day (Figure 1).<sup>2</sup> The accumulation of OPEFB might be harmful to the environment due to waste mismanagement.



Figure 1. The palm oil production process

However, OPEFB literally represents a huge supply of cellulose, which can be used to yield several high-value chemical feedstocks.<sup>3</sup> One of those is levulinic acid (LA), which is an ideal building block to produce value-added chemicals. Examples are 2-methyltetrahydrofuran (2-MeTHF), and  $\gamma$ -valerolactone (GVL) as fuels, tetrahydrofuran (THF) and 2-MTHF as solvents, succinic acid as a chemical intermediate, 5-amino levulinic acid (5-ALA) as an agrochemical,  $\alpha$ -angelica lactone, levulinate ester, and valeric acid as fragrances and food additives, 1,4-butanediol, and 1,4-pentanediol as plasticisers, as well as nylon 6,6 (polyamide) as a chemical used in polymer synthesis (Figure 2).

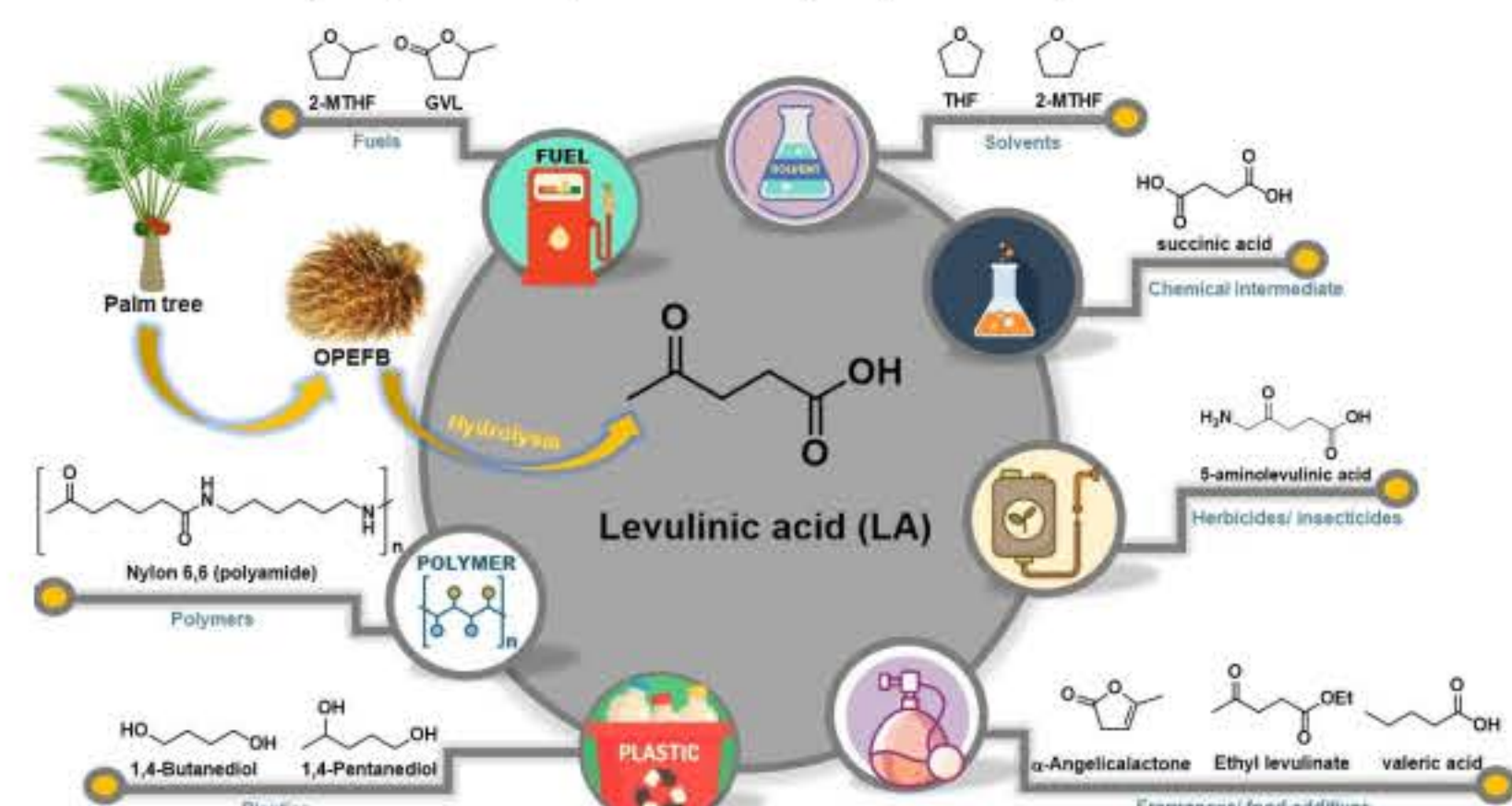


Figure 2. Application of levulinic acid (LA)

Agriculture is a key economic sector in Thailand, where it is a major food and agricultural product exporter. However, the increased import and use of herbicides over the past decade raises concerns about potential risks to the health of farmers, their families, the general population, especially children, and the environment. Glyphosate, an active substance in commercial herbicides, is commonly used to control non-selective weeds. However, Thailand has imposed some restrictions on its use due to its potential to cause cancer and other harm to people and the environment.<sup>4</sup>

## Methods

5-Aminolevulinic acid (5-ALA) is a non-proteinogenic five-carbon amino acid. It is an essential precursor for the biosynthesis of natural tetrapyrrole compounds, including porphyrin, chlorophyll, heme, and vitamin B12. 5-ALA has been widely used in a broad range of applications (Figure 3).

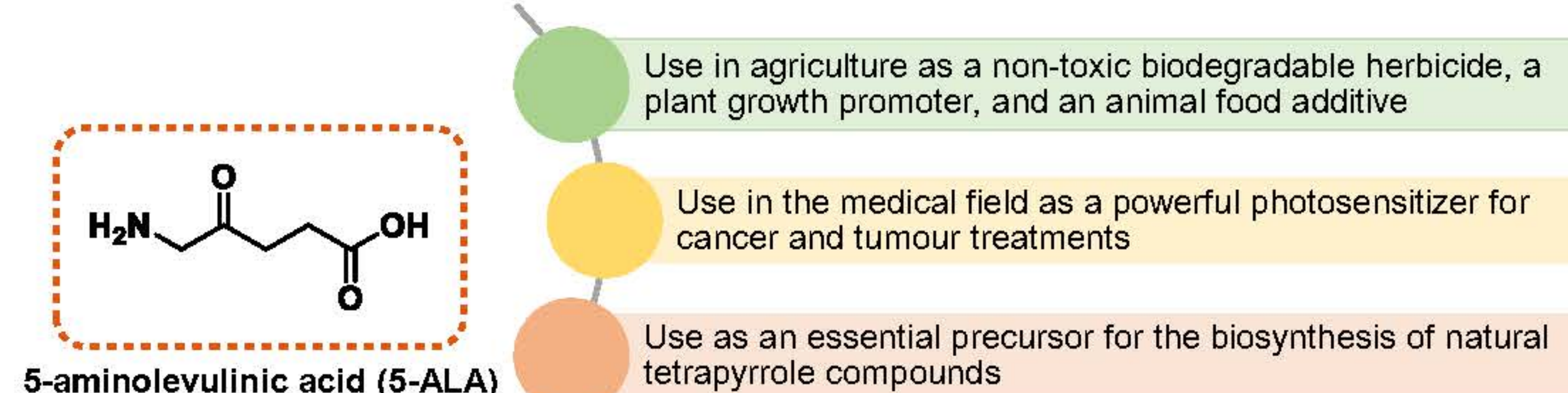


Figure 3. Applications of 5-aminolevulinic acid (5-ALA)

Owing to its high-valued applications and being non-toxic to humans and animals, 5-ALA has received a lot of interest in being used as a natural herbicide in place of the restricted glyphosate. Our research focuses on repurposing OPEFB, a solid waste byproduct of palm oil production, as a chemical feedstock LA and converting bio-LA into value-added 5-ALA (Figure 4). The initial step is to produce bio-LA from cellulose using hydrolysis reaction, while cellulose can be obtained by pre-treating OPEFB. The first stage has been mentioned in numerous reports. The second stage is the conversion of bio-LA into 5-ALA, which is the main focus of this work.

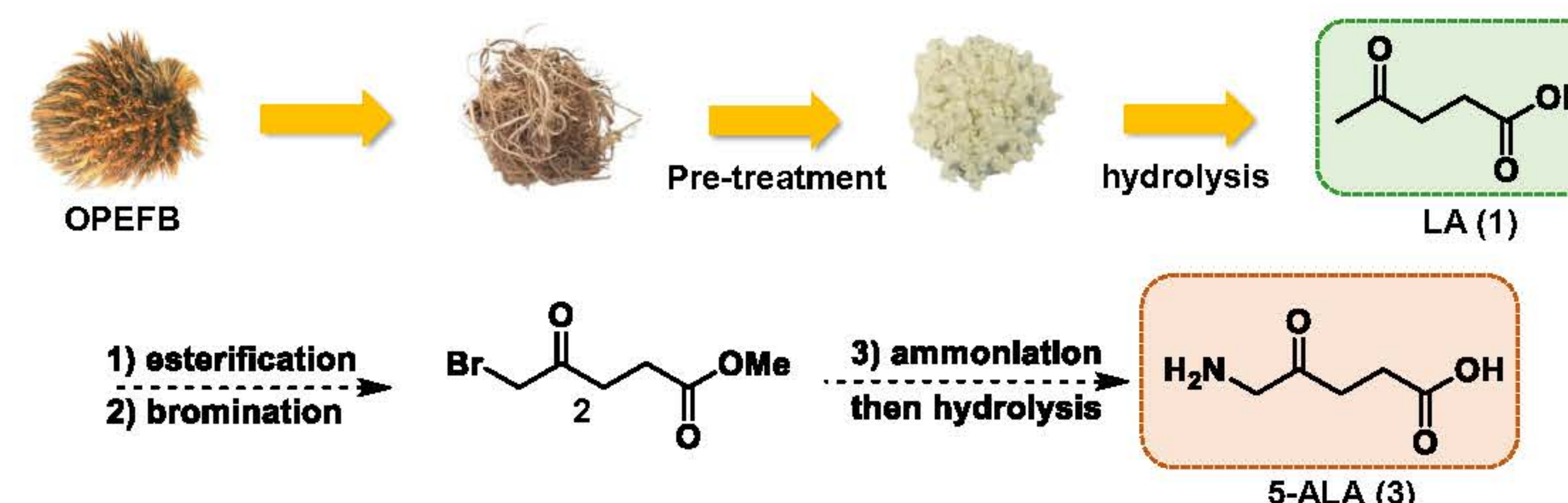


Figure 4. The proposed synthetic pathway of 5-ALA from bio-LA through the chemical method

We envisaged that the transformation of LA into 5-ALA would be set up via a three-step synthesis including esterification, bromination,<sup>5</sup> and one-pot ammoniation/hydrolysis (Figure 4).<sup>6</sup> A more sustainable and cost-effective synthesis approach with fewer steps is being studied, requiring the use of non-hazardous chemicals and mild reaction conditions. The short-synthesis method would minimise production costs, paving the way for the industrial process.

## Results and Discussion

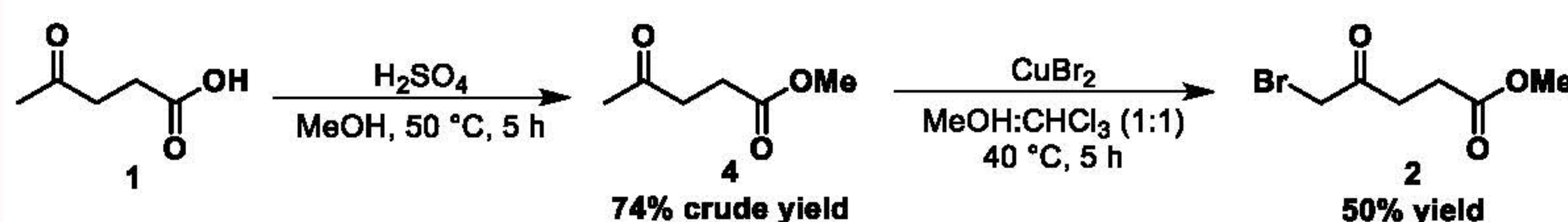
To study the synthesis of 5-ALA from a commercially available LA

To optimize reaction conditions to obtain the best yield in each step

To apply optimized conditions for the synthesis of 5-ALA from bio-LA

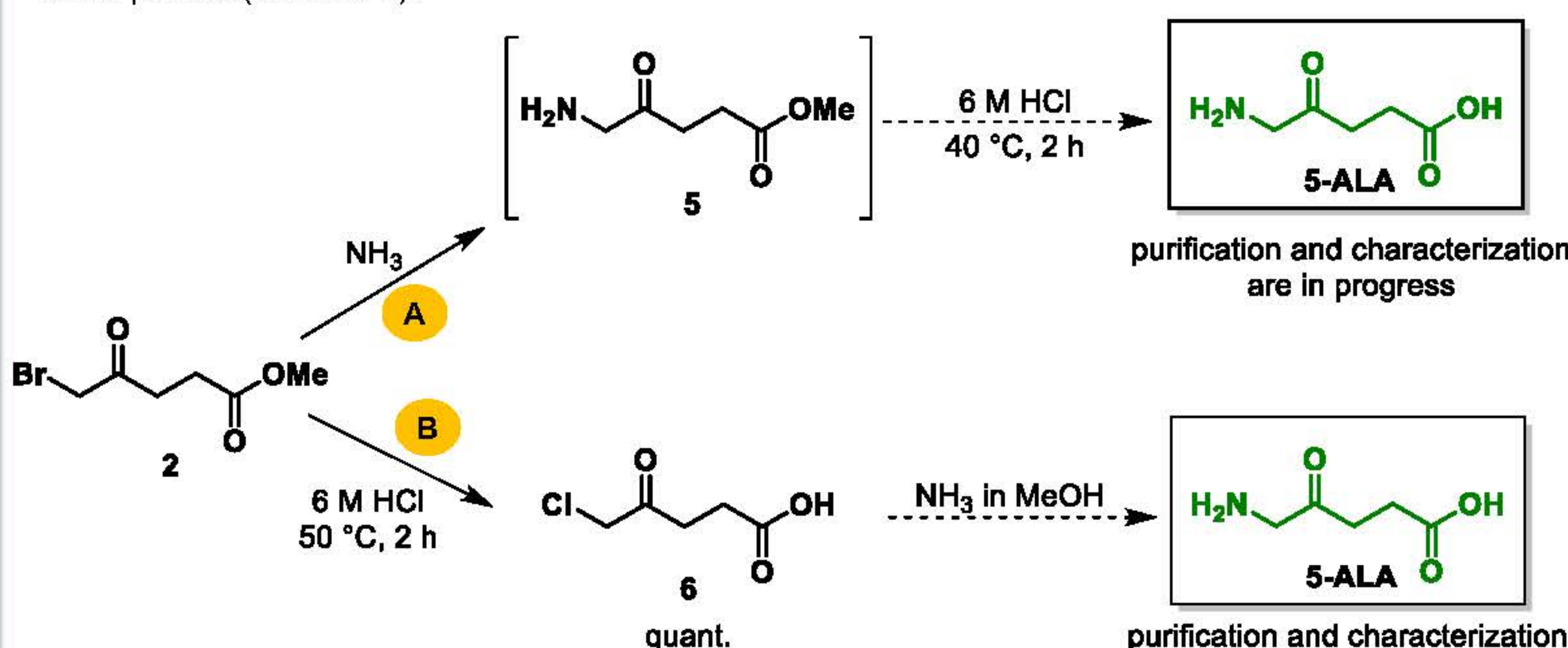
### The synthesis of 5-ALA from a commercially available LA

The transformation of LA (1) into 5-ALA (3) was proposed in three steps (Scheme 1). LA was initially esterified with MeOH under acidic conditions to provide methyl levulinate 4 in 74% crude yield. Bromination of 4 was carried out in the presence of CuBr<sub>2</sub> at 40 °C to afford 5-bromo levulinate 2 in 50% yield. 3-Bromo levulinate and 3,5-dibromo levulinate were also obtained as byproducts. To improve the yield and selectivity of 2, the amount of CuBr<sub>2</sub> and reaction temperature would be optimized.



Scheme 1. The synthesis of 5-bromo levulinate 2

With 5-bromo levulinate 2 in hand, the one-pot synthesis would be set as a final step. First, ammoniation of 2 was performed under the conditions of NH<sub>3</sub> in MeOH. 5-Aminolevulinic acid 5 was expected to form. After the removal of MeOH, the intermediate 5 was treated with 6 M HCl at 40 °C for 2 hours to give the unknown crude product (Scheme 2).



Scheme 2. Attempted synthesis of 5-aminolevulinic acid (5-ALA)

## Results and Discussion

Another synthetic pathway of 5-ALA was also studied. We converted levulinate 2 into carboxylic acid 6 by hydrolysis reaction. Then, ammoniation of 6 using NH<sub>3</sub> in MeOH furnished the unknown product. The ammoniation of 5-chlorolevulinic acid 6 was tricky due to the presence of a reactive carboxylic acid functional group in the same molecule. As with when we concentrated the crude product from pathway A, the temperature was set at 40 °C to avoid polymerization at high temperatures. Crude products from both pathways were characterized by <sup>1</sup>H-NMR spectroscopy compared to commercial 5-ALA. The <sup>1</sup>H-NMR analysis results of the crude product from pathway A are in accordance with the <sup>1</sup>H-NMR data of commercial 5-ALA (Figure 5). The crude product from pathway A is required to be purified by crystallization to obtain good NMR data.

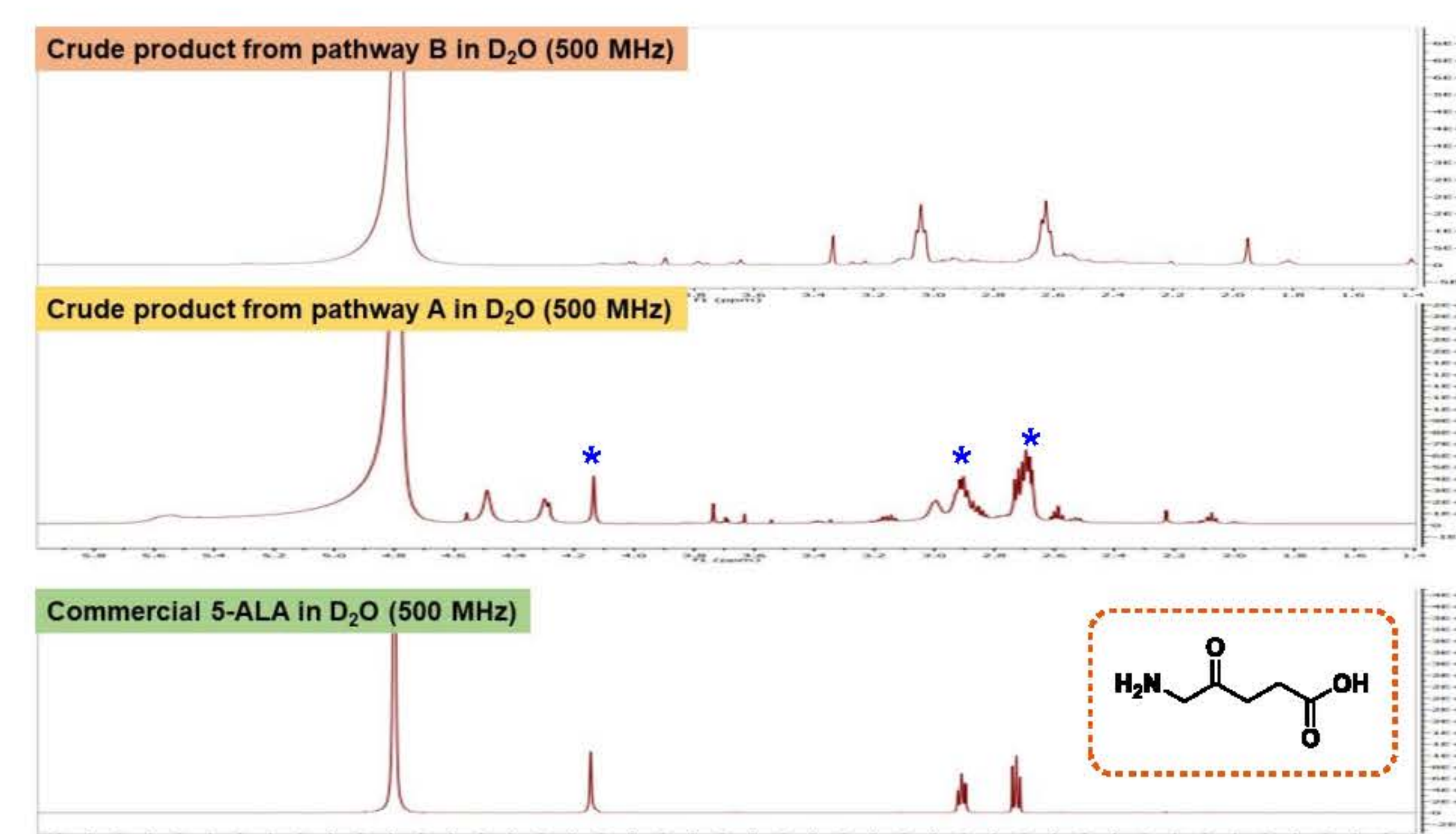


Figure 5. Comparison of <sup>1</sup>H-NMR results of crude products to <sup>1</sup>H-NMR data of commercial 5-ALA

## Conclusion

The synthesis of 5-ALA from commercial LA is ongoing. The crude product from the synthetic pathway A is required to be purified by crystallization. Once the <sup>1</sup>H-NMR results of the pure product are similar to the reference's, this method will be applied to the bio-LA. The bromination method using a non-toxic bromine donor is needed to develop for high yield and selectivity. As we are concerned about laboratory safety, bubbling ammonia gas from the cylinder into cold MeOH should be avoided. The freshly generated ammonia gas from the ammonia solution is suitable to prepare a saturated solution of NH<sub>3</sub> in MeOH on a laboratory scale. However, the ammoniation reaction using NH<sub>3</sub> in MeOH would be able to perform in the industrial process as it is easy to set up and work on.

## Acknowledgements

This research has received funding support from the NSRF via the Program Management Unit for Human Resources & Institutional Development, Research and Innovation [grant number B13F660062], and Southern Palm (1978) Co., Ltd.

[1] S. H. Chang, *Biomass and Bioenergy*, 2014, **62**, 174–181. [2] N. Mohammad, Md. Z. Alam, N. A. Kabbashi and A. Ahsan, *Resources, Conservation and Recycling*, 2012, **58**, 69–78. [3] D. U. C. Rahayu, J. E. Hutauruk, Y. K. Krisnandi and E. Saepudin, *IOP Conf. Ser.: Mater. Sci. Eng.*, 2020, **763**, 012034. [4] W. Laohadomchok, N. Nankongnab, S. Sirirattanapruk, P. Klaimala, W. Lianchamroon, P. Ousap, M. Jatiket, P. Kajitvichyanukul, N. Kitana, W. Siriwong, T. Hemachudhah, J. Satayavivad, M. Robson, L. Jaacks, D. B. Barr, P. Kongtip and S. Woskie, *Human and Ecological Risk Assessment: An International Journal*, 2021, **27**, 1147–1169. [5] Y. Zai, Y. Feng, X. Zeng, X. Tang, Y. Sun and L. Lin, *RSC Adv.*, 2019, **9**, 10091–10093. [6] N. K. Garg, R. Sarpong and B. M. Stoltz, *J. Am. Chem. Soc.*, 2002, **124**, 13179–13184.





BRainPOWER  
CONGRESS 2023

ร่วมกับสร้างและขับเคลื่อนงานวิจัยข้ามสาขา  
สู่อุตสาหกรรมแห่งอนาคต



สร้างคน  
บ้านพระมอแดน

WALAILAK UNIVERSITY



บริษัท ไบโอดีแก๊ส (ประเทศไทย) จำกัด BIO4GAS (THAILAND) CO., LTD.

# Enhancing Bio-hydrogen and Bio-methane Production of Concentrated Latex Wastewater (CLW) by Co-digesting with Palm Oil Mill Effluent (POME) : Batch and Continuous Performance Test and ADM-1 modeling

Marisa Raketh<sup>1</sup>, Rattana Jariyaboon<sup>1,2,\*</sup> Wanna Choorit<sup>3</sup>, Chonticha Mamimin<sup>4</sup>, Prawit Kongjan<sup>1,2</sup>

<sup>1</sup> Bio-Mass Conversion to Energy and Chemicals (Bio-MEC) Research Unit, Faculty of Science and Technology, Prince of Songkla University (PSU), Pattani, 94000, Thailand

<sup>2</sup> Department of Science, Faculty of Science and Technology, Prince of Songkla University (PSU), Pattani, 94000, Thailand

<sup>3</sup> Biomass and Oil Palm Research Center of Excellence, Walailak University, Tasala, Nakhon Si Thammarat 80161, Thailand

<sup>4</sup> Department of Biotechnology, Faculty of Technology, Khon Kaen University, Khon Kaen 40002, Thailand

\*Corresponding author: rattana.sa@psu.ac.th

## Introduction

In concentrated latex factories, a large amount of ammonia and sulfuric acid are used for the pretreatment of concentrated latex, resulting in a massive volume of concentrated latex wastewater (CLW) containing a high concentration of nitrogen (816–1,970 mg/L) and sulfate 1,889–4,210 mg/L, as well as chemical oxygen demand (COD) of 3,350–5,430 mg/L with 5.1 of C/N ratio is discharged<sup>1,2</sup>. Consequently, CLW has resulted in various environmental problems. Currently, some factories treat CLW using an anaerobic digestion (AD) process as a wastewater treatment system. However, low biogas production yield has been reported in previous studies<sup>3,4</sup>. This observation is due to the sulfate concentration in CLW that can be transformed to hydrogen sulfide (H<sub>2</sub>S) under anaerobic conditions<sup>5</sup>, which can later inhibit methanogens, resulting in uncertain AD process with possibly low biogas yield. Moreover, high nitrogen contents in CLW may also lead to AD process failure, since the inhibiting microbial growth in AD can be occurred. To overcome the limitations of CLW treatment by the AD process mentioned previously, the sulfate and nitrogen concentrations should be diluted in order to reduce the inhibitory level and enhance biogas production. Palm oil mill effluent (POME), namely the wastewater from palm oil mill, an important industry in the south of Thailand is one of the attractive choices to deal with the problem. POME has low total nitrogen (820–970 mg/L) and very low sulfur compound with quite high organic matter of 78,290–96,300 mg/L of COD, high C/N ratio (21.97–27.59)<sup>6</sup>. Hence, using CLW and POME as co-substrate is one wise way of diluting the potential produced inhibitor (H<sub>2</sub>S, ammonia, long chain fatty acid) balancing the macro and micronutrients, as well as the C/N ratio of the AD process, and consequently increased gases production yield compared with single substrates of CLW digestion and maintaining system stability. Moreover, the co-digestion of CLW as nitrogen-rich substrate with carbon-rich POME was suggested as the potential method to increase significant gaseous biofuel production under the control conditions of qualified co-substrates.

A promising system is represented by a two-stage AD process combining hydrogen (H<sub>2</sub>) and methane productions (CH<sub>4</sub>). This two-stage AD is an interesting process to treat sulfate-rich wastewater. The process is optimized by employing two separate reactors in series, operated at different conditions to have two different communities of microorganisms in each reactor by adjusting the pH and microbial growth, shorter detention time, and a higher energy recovery rate<sup>7</sup>. Additionally, the continuous stir tank reactor (CSTR) and up-flow anaerobic sludge blanket (UASB) reactor have various advantages and are attractive to be used for two-stage AD process of CLW and POME as co-substrate. Recently, researchers have applied more complex models, such as modified versions of the IWA Anaerobic Digestion Model No.1 (ADM-1)<sup>8</sup>. The ADM-1 model was developed to explain the AD process. Therefore, the model has been widely used, investigated, and enlarged to predict a large plurality of anaerobic wastewater systems until now. To our knowledge, there are lacked studies on the co-digestion of POME with CLW for H<sub>2</sub> and CH<sub>4</sub> production potential using a two-stage AD process which is the novelty of co-digestion substrates. This is to increase the capacity of the process through synergism, and the biodegradability of feedstocks could be improved by optimizing their complementary interaction. Therefore, this research aimed at investigating the possibility of co-digesting POME with CLW for H<sub>2</sub> and CH<sub>4</sub> production by employing the two-stage AD process. The POME:CLW mixing ratio effect was studied in batch mode, and the optimum POME:CLW mixing ratio was subsequently performed in a series of CSTR and UASB reactors. The modified ADM-1 implementation for the two-stage AD process of POME and CLW was also further examined in this research.

## Methods

### Co-substrate

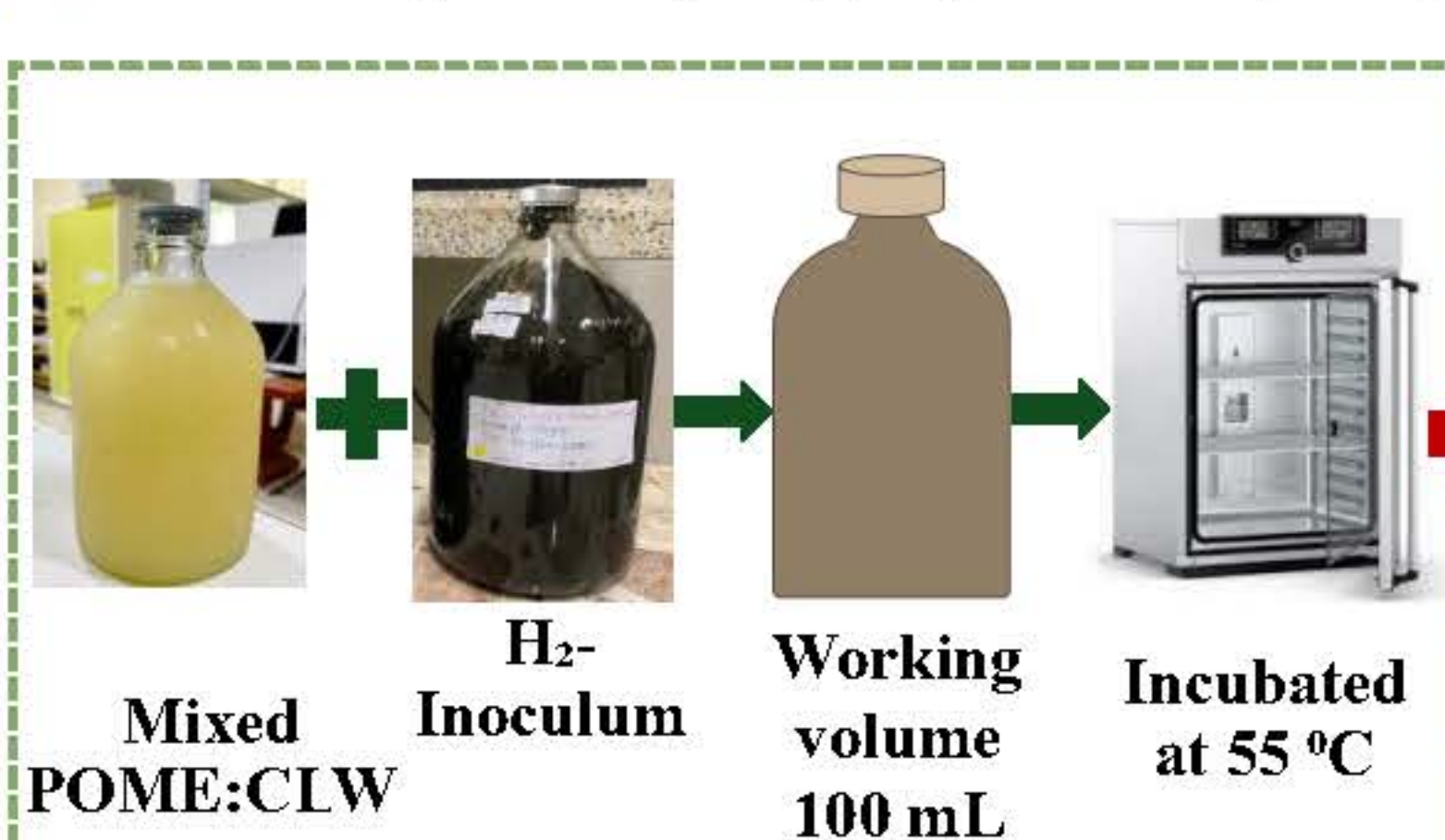


From Palm Pattana Southern Border Co., Ltd., Nong Chik, Pattani  
From ST Latex Co. Ltd., Sadao, Songkhla

### Analyze characteristics

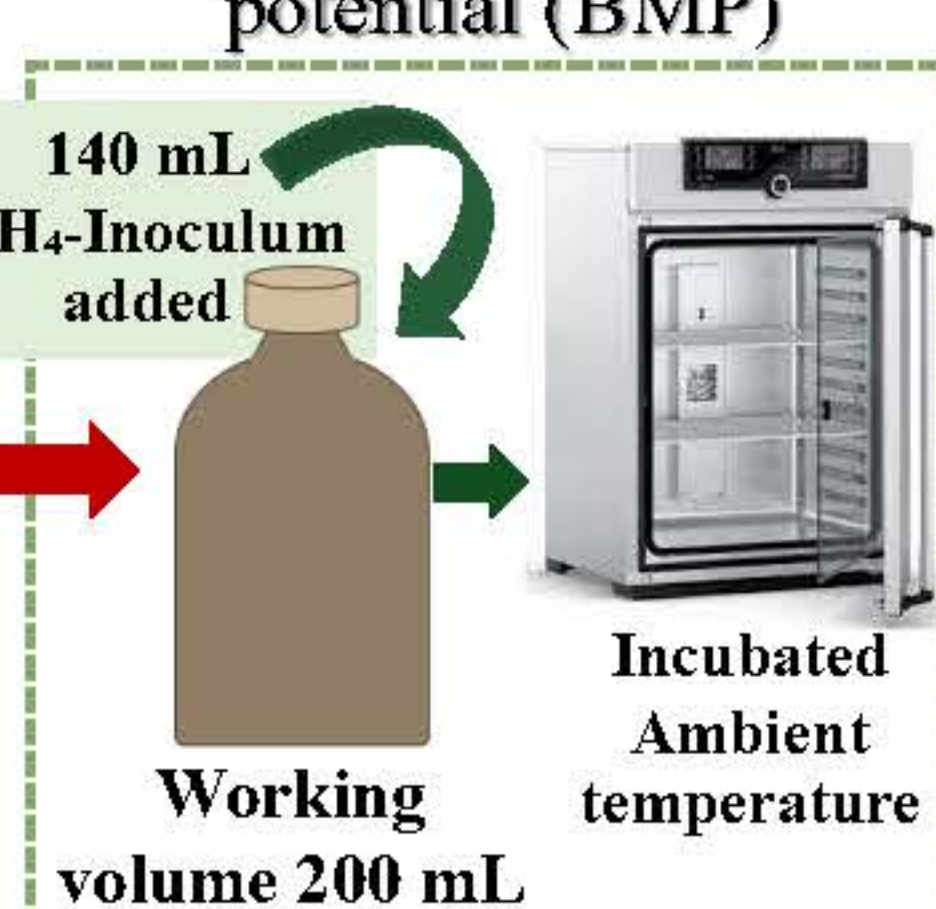
### Batch Performance

#### First stage: Biohydrogen potential (BHP)



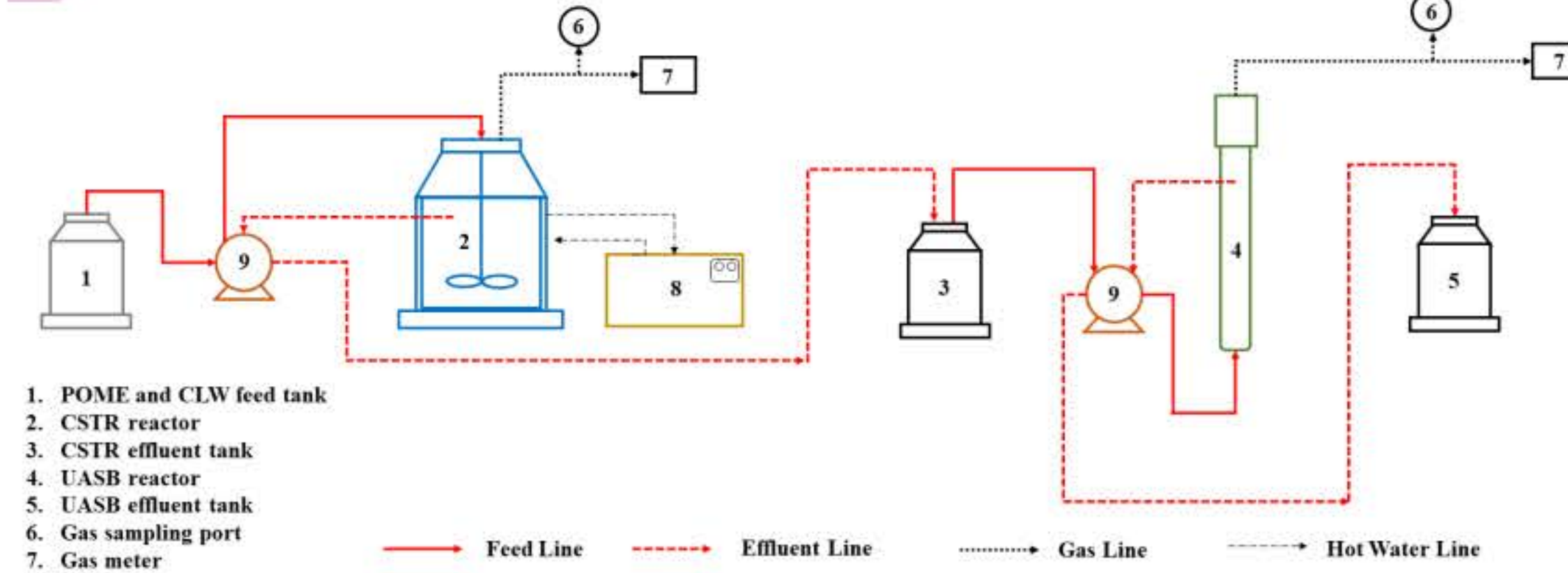
Conditions  
- POME:CLW mixing ratio of 100:0, 70:30, 50:50, 30:70 and 0:100  
- The initial organic concentration was 10 g-VS/L

#### Second stage: Biomethane potential (BMP)



### Continuous Performance

The schematic diagram for continuous system reactor set up and operation



Conditions: CSTR

- Total volume; 10 L (Working volume 7 L)  
- Temperature; Thermophilic (55±3°C)  
- HRT (days) for POME; 7, 5, 3, 2.5 and 2  
- HRT (days) for POME:CLW (70:30); 7 and 5

Conditions: UASB

- Total volume; 1.3 L (Working volume 1.2 L)  
- Temperature; Ambient (30±3°C)  
- HRT (days) for POME; 25, 20, 15 and 10  
- HRT (days) for POME:CLW (70:30); 15

## Results & Discussion

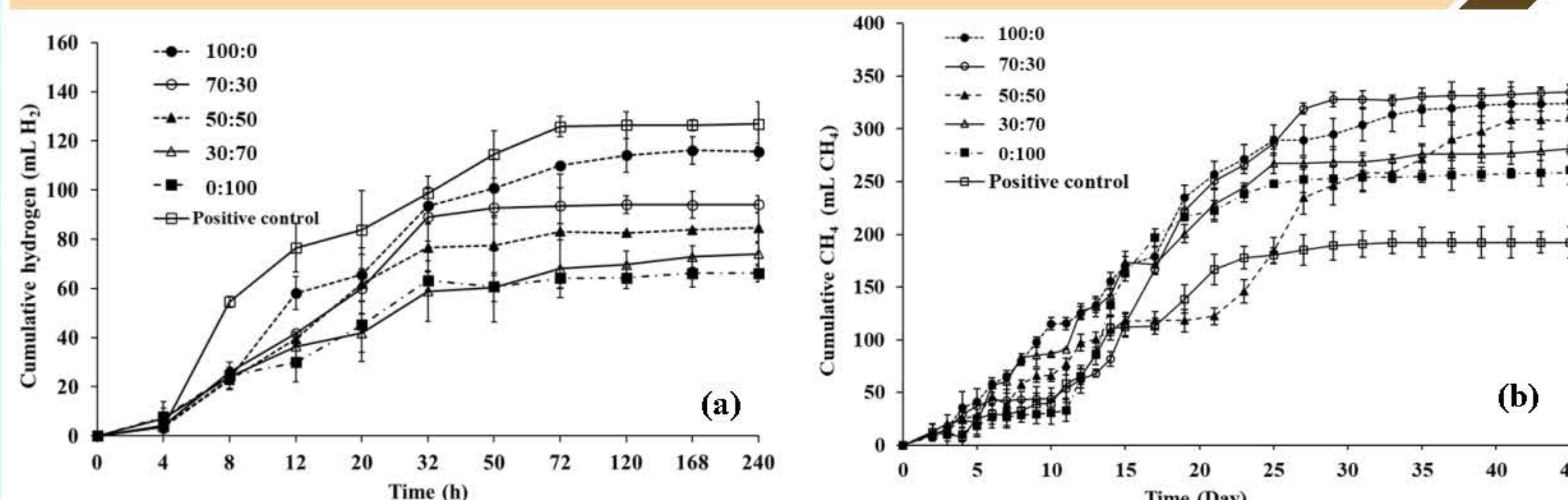


Fig. 1 Cumulative gas of batch two-stage AD process at various POME:CLW mixing ratios; (a) H<sub>2</sub> from first stage and (b) CH<sub>4</sub> from second stage

Table 1 potential of producing H<sub>2</sub> and CH<sub>4</sub> from batch two-stage AD process of POME:CLW at various mixing ratios

POME:CLW	Concentration in assay (100 mL working volume)					H <sub>2</sub> Stage		CH <sub>4</sub> stage		Total Energy (kJ/gVS)
	C/N Ratio	COD (g/L)	TKN (g/L)	Sulfate (mg/L)*	Alkalinity (mg/L)**	Yield (mL/gVS)	Energy (kJ/gVS)	Yield (mL/gVS)	Energy (kJ/gVS)	
100:0	29.00	19.19	0.18	0.00	3,175.00	115.57 <sup>a</sup>	1.22 <sup>a</sup>	543.25 <sup>a</sup>	18.21 <sup>a</sup>	19.43 <sup>a</sup>
70:30	21.80	18.06	0.51	8.87	3,355.00	94.16 <sup>b</sup>	1.00 <sup>b</sup>	558.01 <sup>a</sup>	18.70 <sup>a</sup>	19.70 <sup>a</sup>
50:50	17.00	17.30	0.73	14.78	3,475.00	84.65 <sup>c</sup>	0.90 <sup>c</sup>	520.74 <sup>b</sup>	17.46 <sup>b</sup>	18.35 <sup>b</sup>
30:70	12.30	16.55	0.95	20.69	3,595.00	73.99 <sup>d</sup>	0.78 <sup>d</sup>	468.52 <sup>c</sup>	15.70 <sup>c</sup>	16.49 <sup>b</sup>
0:100	5.10	15.42	1.28	29.56	3,775.00	66.20 <sup>d</sup>	0.70 <sup>d</sup>	435.60 <sup>c</sup>	14.60 <sup>c</sup>	15.30 <sup>c</sup>

\*\* are the statistically significant difference (p < 0.05); \* Sulfate concentration was calculated based on CLW because sulfate in POME was not analyzed; \*\* Alkalinity concentration was measured after mixing of POME and CLW in each ratio

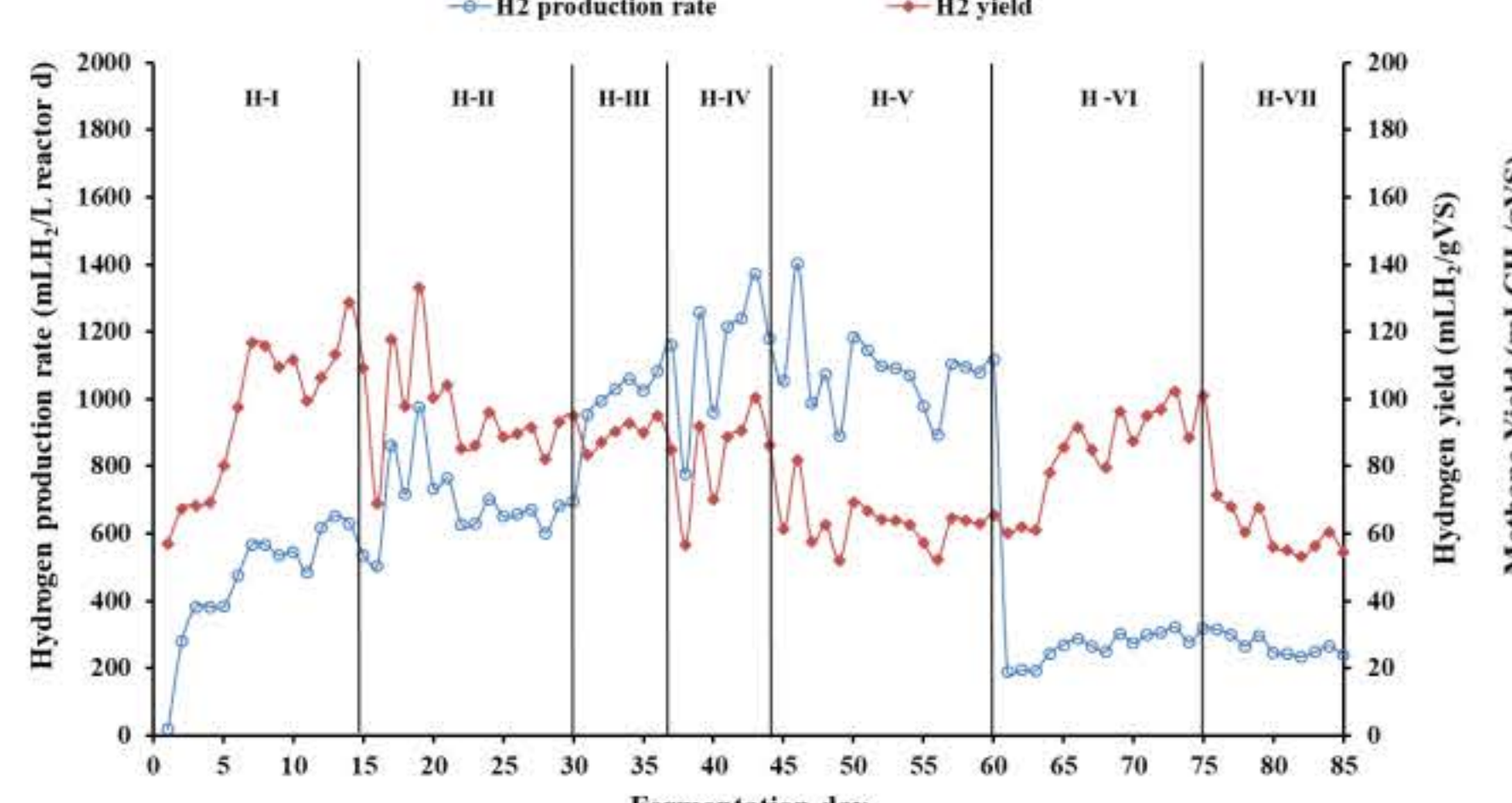


Fig. 2 H<sub>2</sub> yield and H<sub>2</sub> production rate in the CSTR reactor, for various levels of HRT (H-I= 7 days, H-II= 5 days, H-III= 3 days, H-IV= 2.5 days, H-V= 2 days, H-VI= 7 days, H-VII= 5 days)

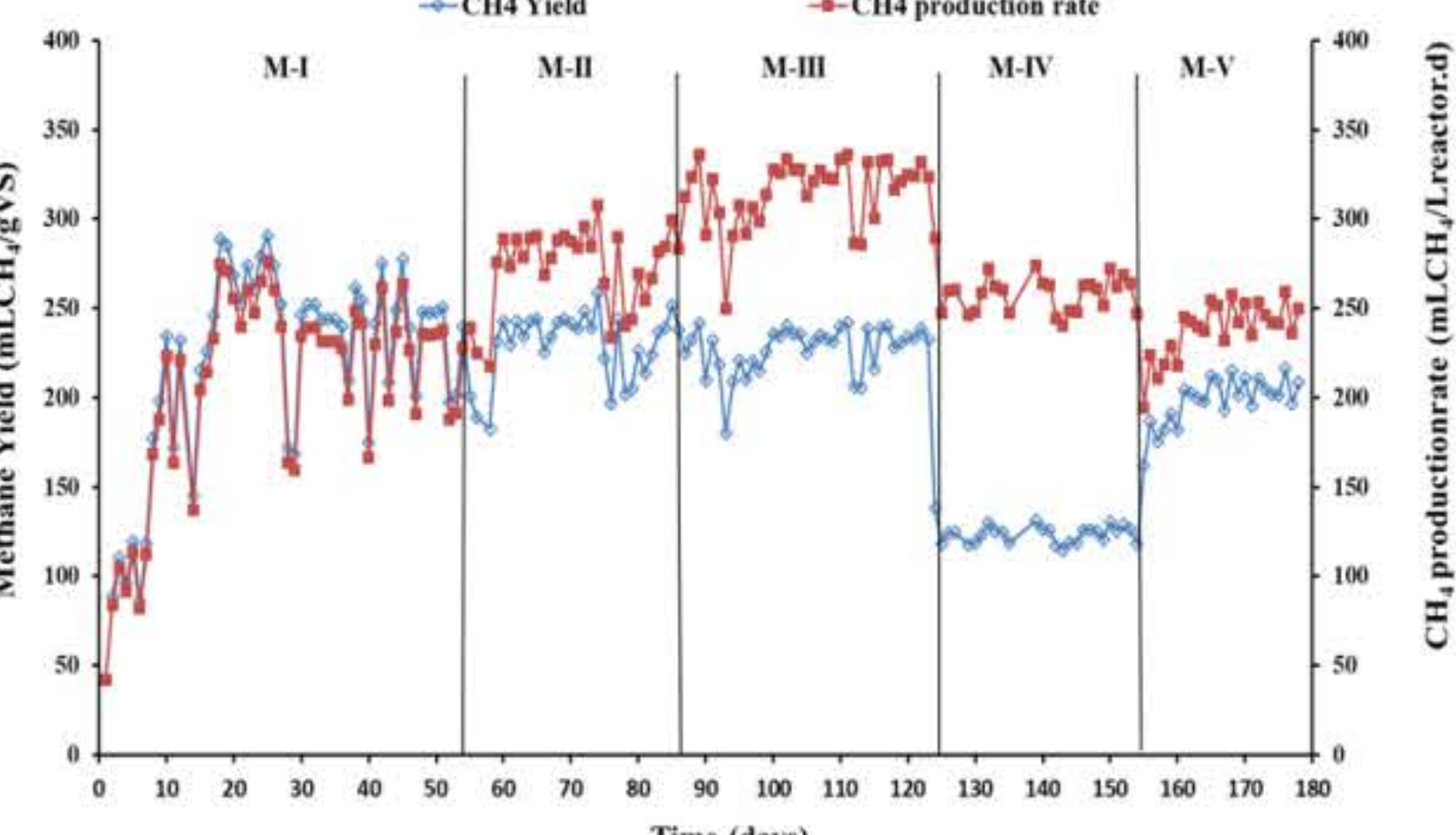


Fig. 3 CH<sub>4</sub> yield and CH<sub>4</sub> production rate in the UASB reactor, for various levels of HRT (M-I= 25 days, M-II= 20 days, M-III= 15 days, M-IV= 10 days, M-V= 15 days)

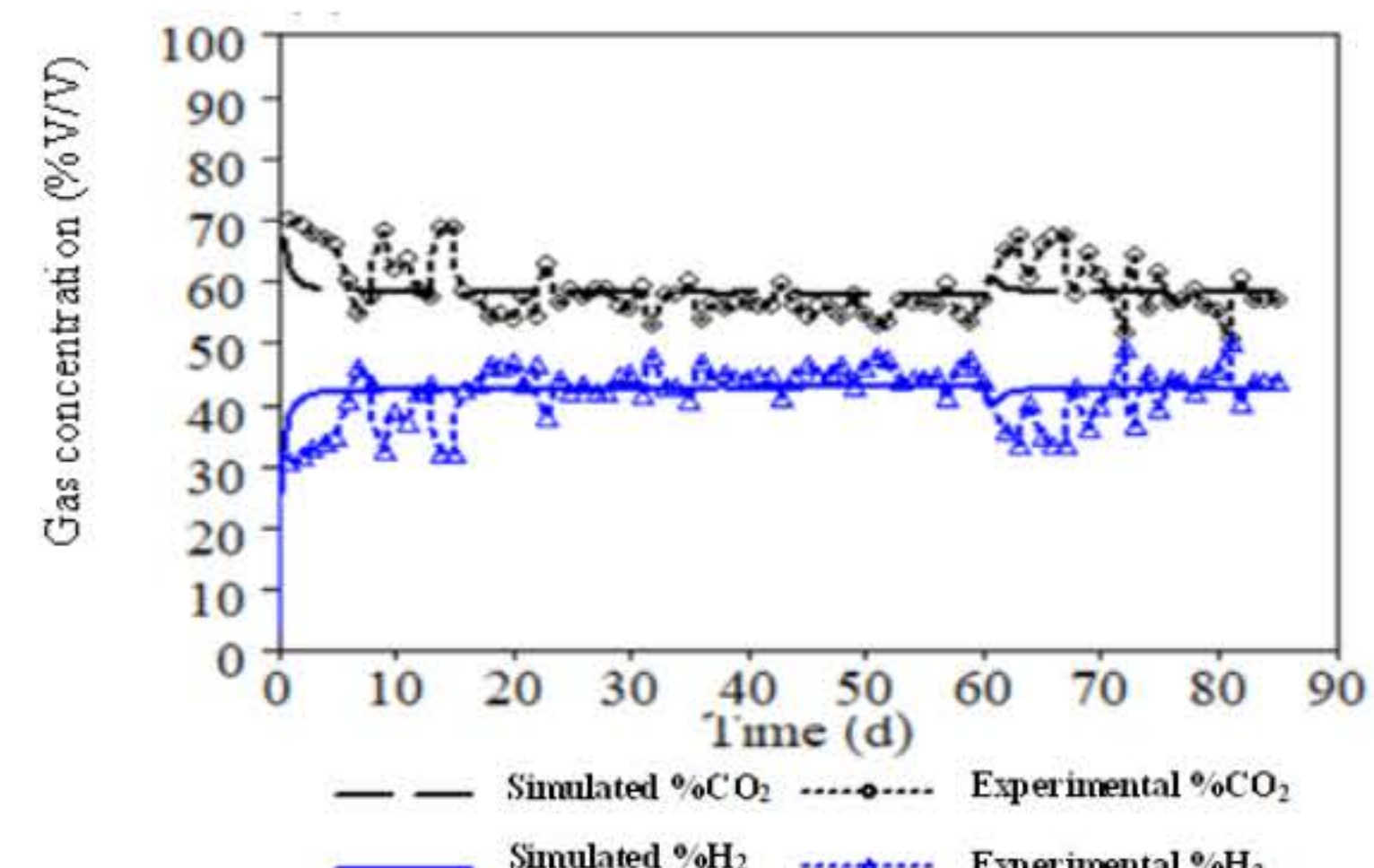


Fig. 4 gas concentration of H<sub>2</sub> production in the CSTR reactor

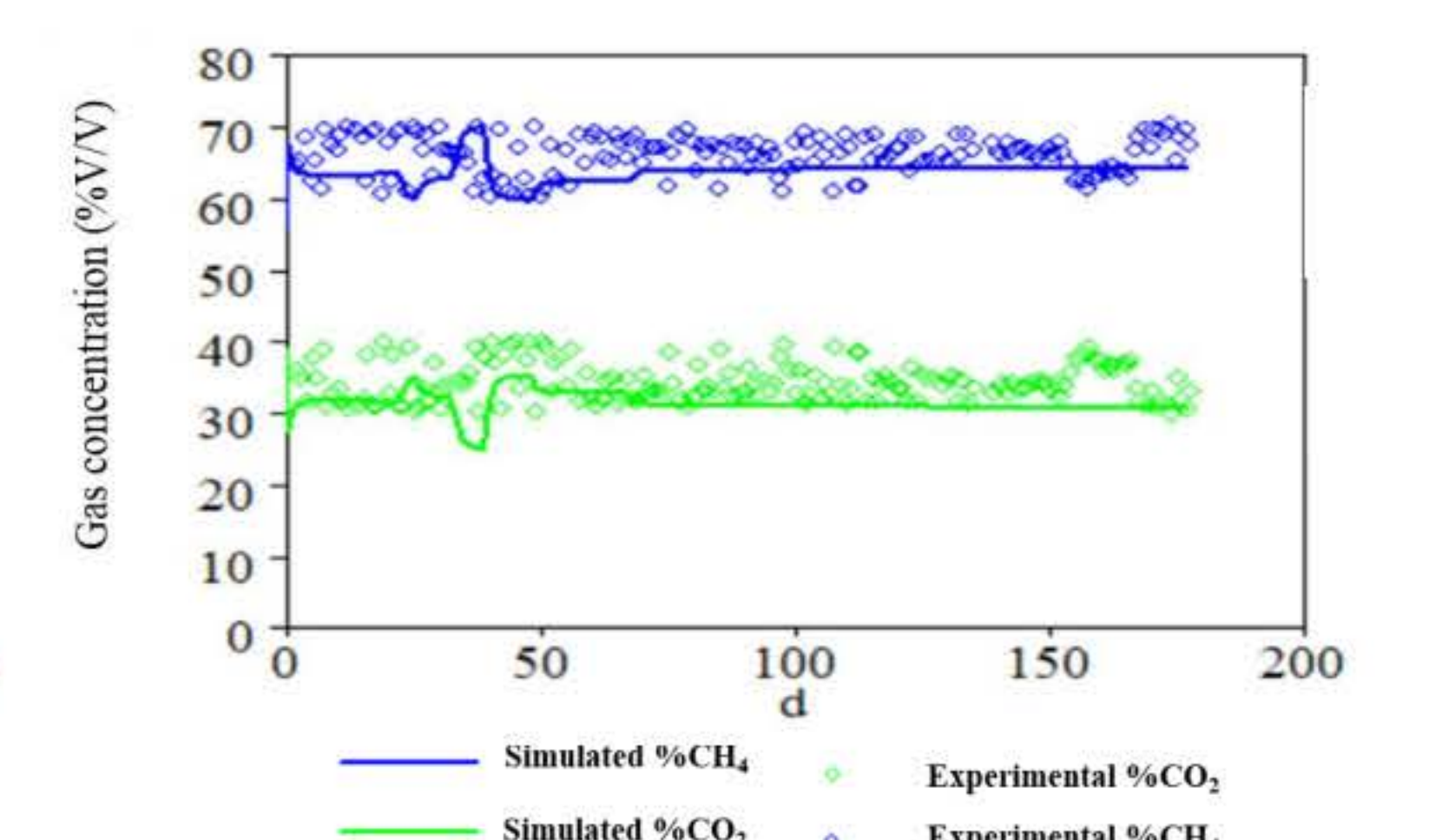


Fig. 5 gas concentration of CH<sub>4</sub> production in the UASB reactor

## Conclusion

- This study illustrates the possibility of co-digestion between POME and CLW. It proves that POME could enhance the biogas production yield of CLW by using the AD process.
- The optimum mixing ratio of POME:CLW was 70:30, achieved from the batch AD process. This ratio gave the highest total energy yield during the AD process and revealed the highest synergisms of about 9.21%.
- The different HRTs of POME:CLW at 70:30 mixing ratio was investigated in first stage AD process by using CSTR reactor for producing H<sub>2</sub> and the highest H<sub>2</sub> yield (95.45 mL/g-VS) was obtained from HTR 7 days and OLR 3.14 g-VS/L·d. Conversely, the 15 days of HRT with 1.20 g-VS/L·d of OLR was examined in second stage AD process by using UASB reactor for producing CH<sub>4</sub> with the yield 204.52 mL/g-VS.
- The model ADM-1 model framework was established, 9.10 % and 2.43 % of error fitting of H<sub>2</sub> and CH<sub>4</sub> gas between model simulation data and experimental data were found.
- The research work demonstrated a novel and feasible approach for co-digesting POME with CLW to efficiently generate valuable gaseous biofuel, mixed H<sub>2</sub> and CH<sub>4</sub> gas, at imminent optimal conditions.

## Acknowledgements

This research has received funding support from the NSRF via the Program Management Unit for Human Resources & Institutional Development, Research and Innovation [grant number B13F660062]. The authors would like to thank the ST Latex Co. Ltd., Sadao, Songkhla province, Chalong Concentrated Latex Industry Co. Ltd., Chana, Songkhla province, and Palm Pattana Southern Border Co., Ltd., Nong Chik, Pattani province for providing materials to our research.



References



Full text of the article



## Bio-hydrogen Production from Oil Palm Empty Fruit Bunches (OPEFB) by Process Series of Dark Fermentation (DF) and Microbial Electrolysis Cells (MEC)

Nikannapas Usmanbaha <sup>a</sup>, Rattana Jariyaboon <sup>a</sup>, Chonticha Mamimin <sup>b</sup>, Wanna Choorit <sup>c</sup>, Prawit Kongjan <sup>a,\*</sup>

<sup>a</sup> Bio-Mass Conversion to Energy and Chemicals (Bio-MEC) Research Unit, Faculty of Science and Technology, Prince of Songkla University, Pattani 94000, Thailand

<sup>b</sup> Department of Biotechnology, Faculty of Technology, Khon Kaen University, Khon Kaen 40002, Thailand; chonticha51@gmail.com

<sup>c</sup> Biomass and Oil Palm Research Center of Excellence, Walailak University, Tasala, Nakhon Si Thammarat 80161, Thailand

\* Corresponding author. E-mail address: prawit.k@psu.ac.th (P. Kongjan).

### Introduction

The crude palm oil extraction industry produces empty palm fruit bunches (EFB) approximately 230 kilograms/ton - Oil palm fresh fruit bunches (Chavalparit *et al.*, 2006). Some EFB is used as material for growing straw mushrooms and producing compost or mulch, which still has many EFB left, although some parts have been used. EFB contains 44.2% (w/w) cellulose, 33.5% (w/w) hemicellulose, and 20.4% (w/w) lignin (Suksong *et al.*, 2016), and has the potential for biofuel production. However, a hydrothermal method using water with temperatures in the range (150-220 °C) as a medium for cracking the structure of lignocellulose is used to condition the feedstock. To produce hydrogen gas by connecting dark fermentation in Continuous Stirred Tank Reactors (CSTR) and microbial electrolysis cells by mixed bacterial groups (Mixed cultures).

### Methods



Crush  
0.1-1 cm



Empty palm fruit bunches (EFB)



Hydrothermal pretreatment

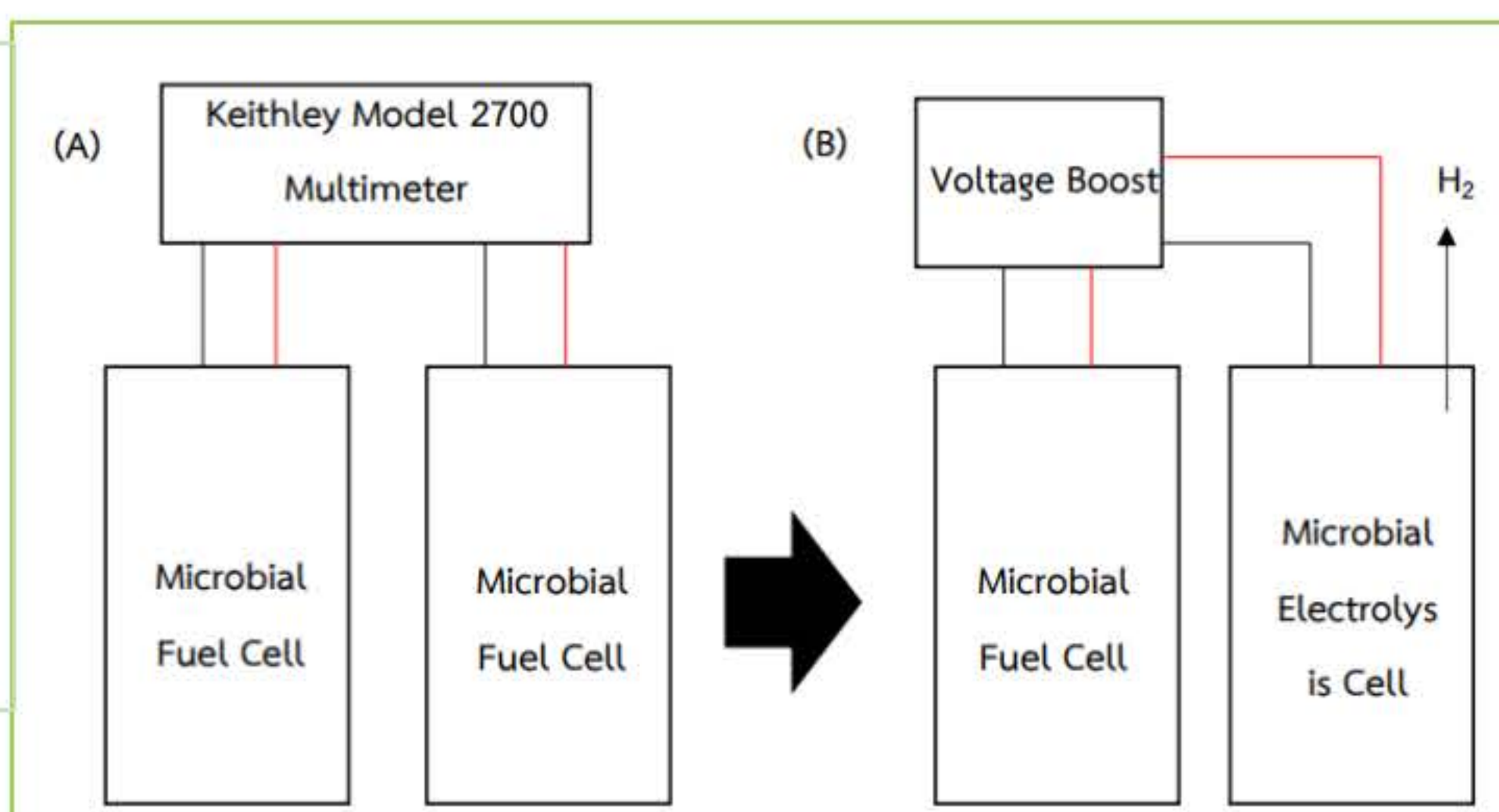


Hydrolysate of EFB from  
hydrothermal pretreatment

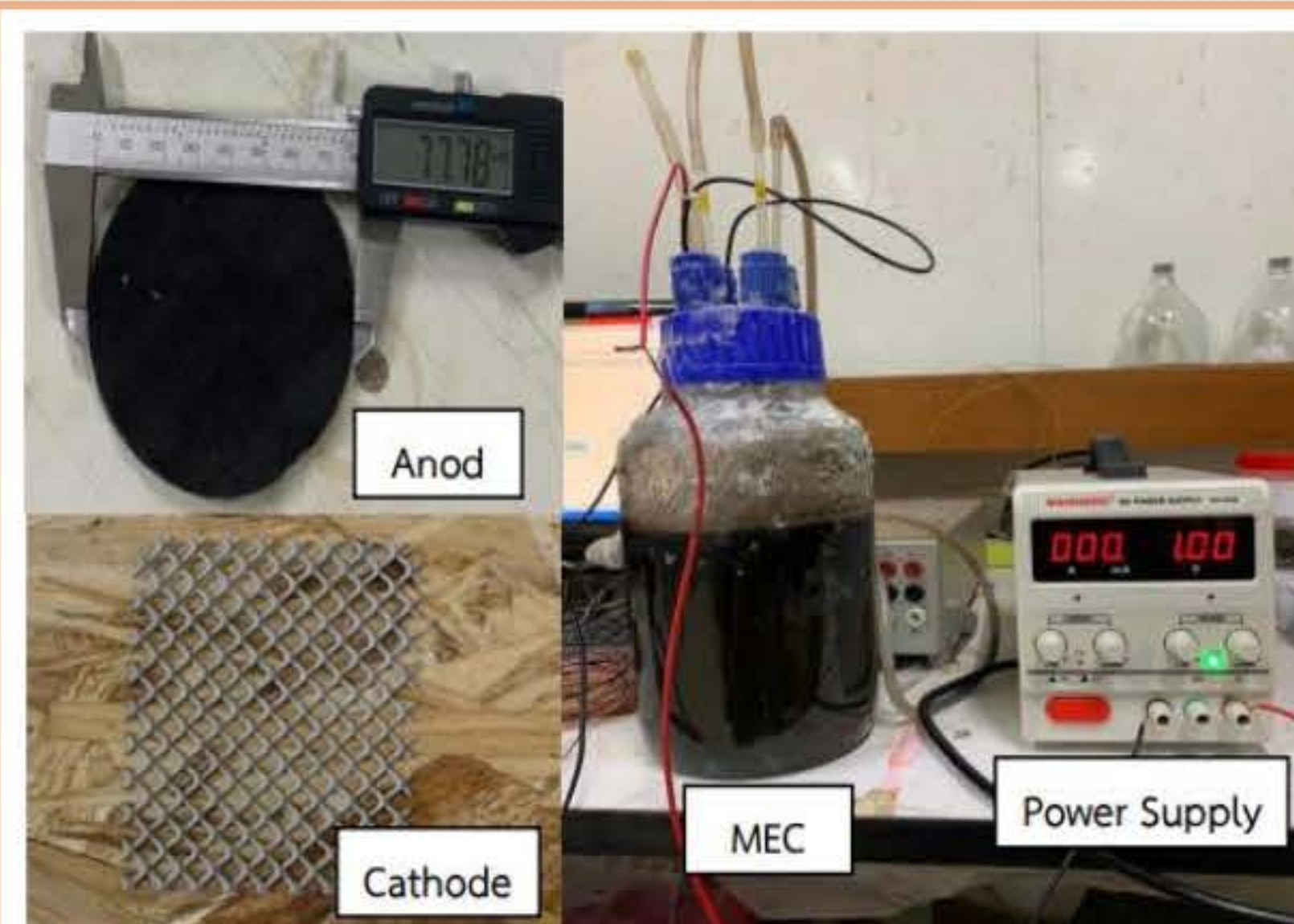


Acidogenic anaerobic dark fermentation 6 L  
working volume in CSTR

Initialization of hydrogen production in a microbial electrolysis cell  
(A) first step, startup of the system to 2 MFC cells,  
(B) second step modify one MFC cell to MEC for hydrogen production.



Design and initialize the MEC cell system



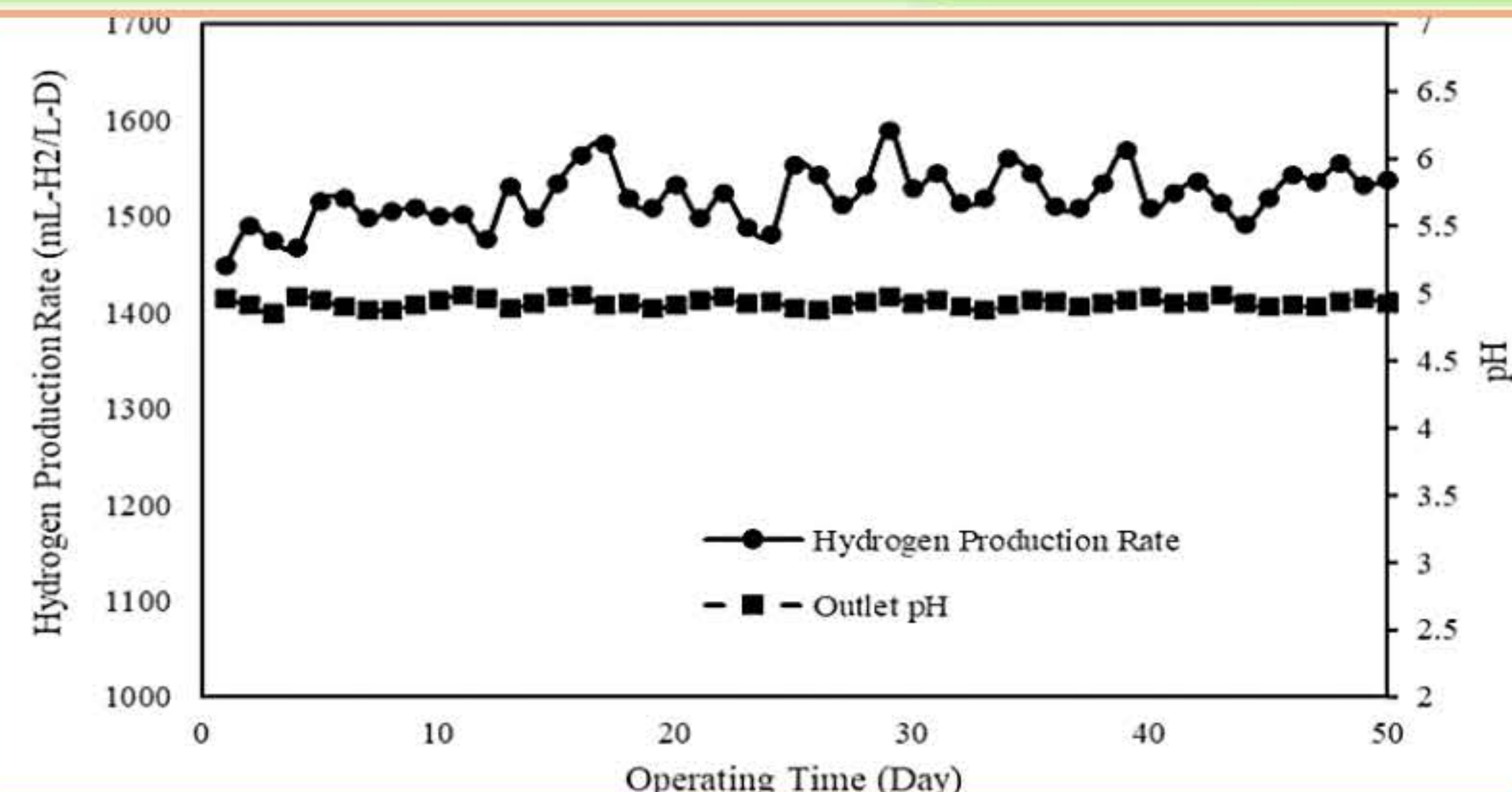
The performance of the dark fermentation  
process series and MEC cells.

Hydrogen production in a 2 L microbial electrolysis cell, working volume 1.8 liters. The effluent solution was then transferred to reactor with anode and insert the Platinum Coated-Titanium Mesh cathode into the reactor tank. Apply a potential difference of 0.8 volts from external power supply. The gases generated from the microbial electrolysis cell were measured using the water displacement method. The Gas components and concentration of volatile fatty acids were investigated with a machine GC-TCD and GC-FID, respectively.

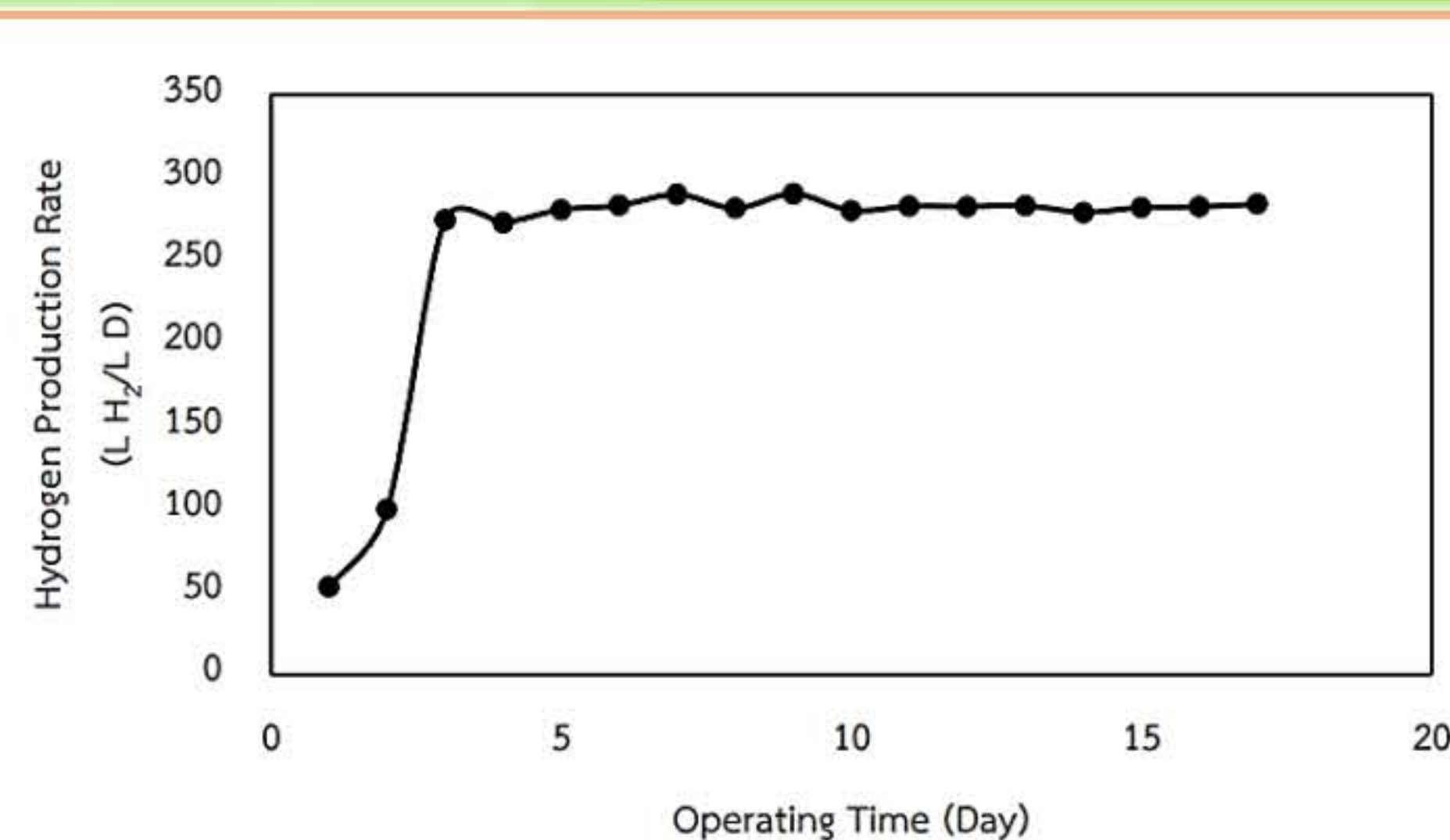
### Results & Discussion

#### Characterizations of the EFB hydrolysate

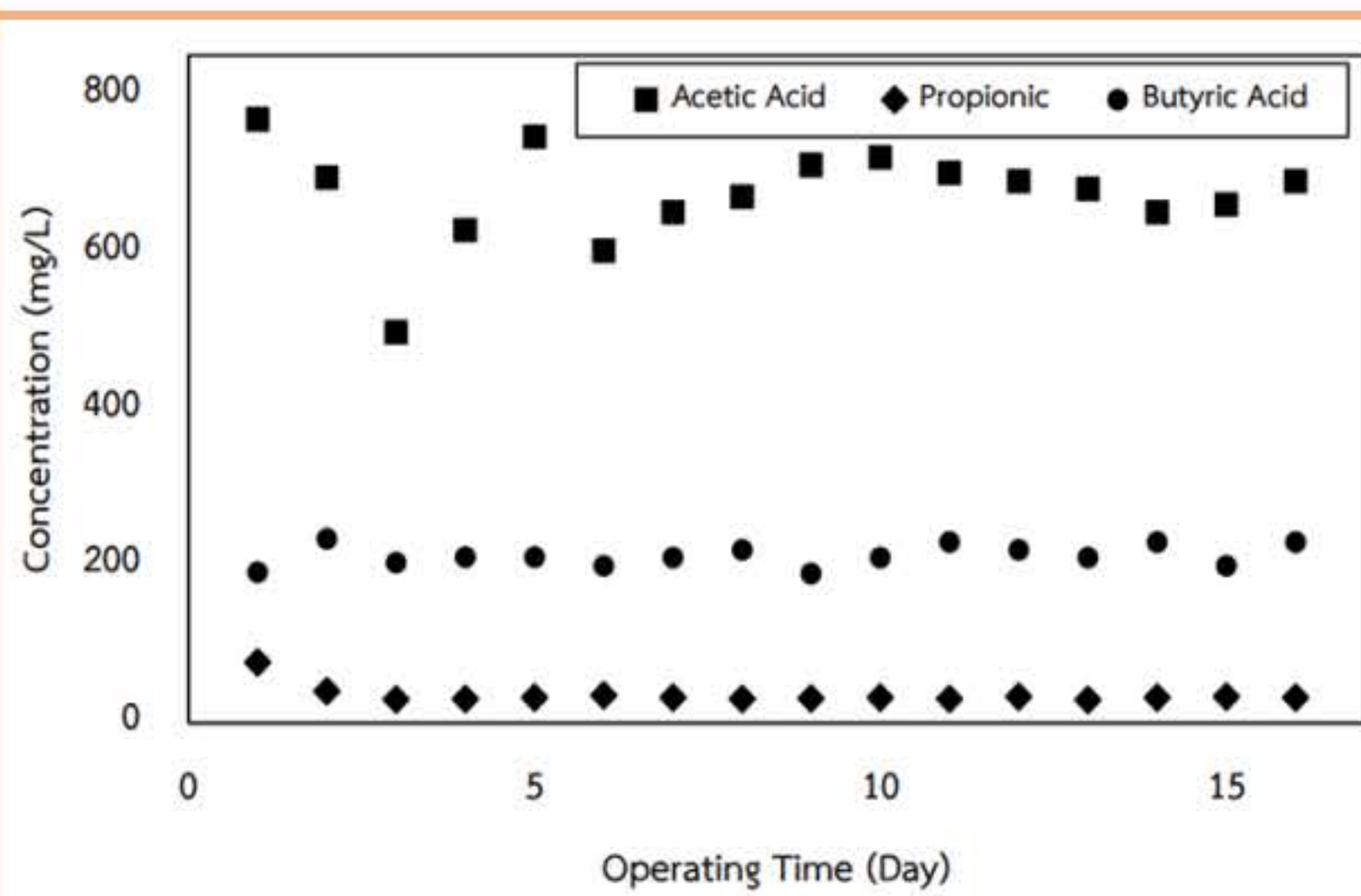
Character of hydrolysate	
Total Solid	2.77 ± 0.06 % (w/w)
Volatile Solid	2.10 ± 0.05 % (w/w)
Ash	0.67 ± 0.11 % (w/w)
Xylose	7.24 ± 0.06 g/L
COD	23,200 ± 3,064 mg/L
pH	4.5 – 5.6



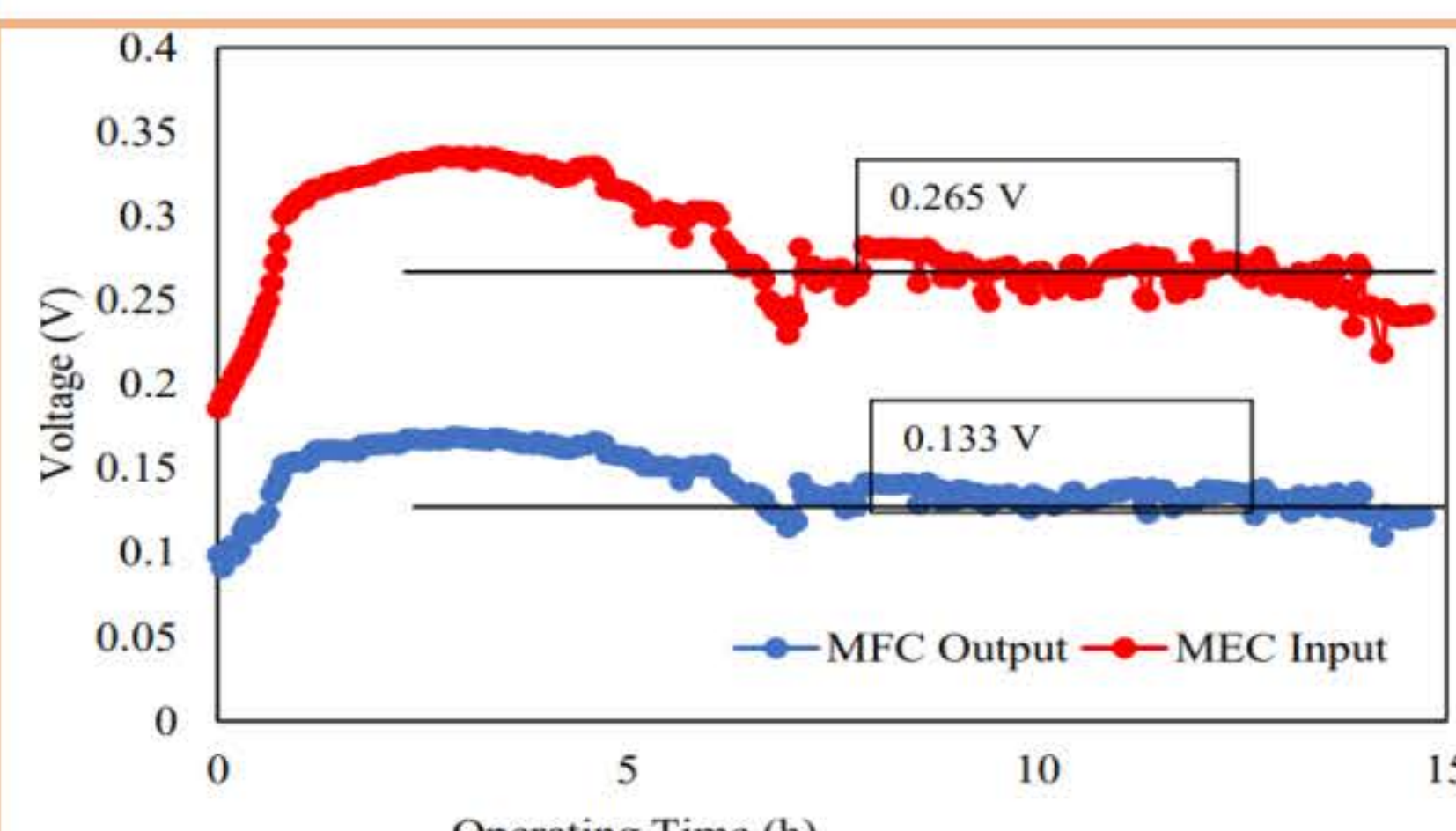
Hydrogen production rate and pH from xylose fermentation in CSTR



Hydrogen production rate from hydrolysate in CSTR



VFAs from the effluent of hydrolysate fermentation  
in CSTR



The potential difference from the biofuel cell and the  
potential difference fed to the microbial electrolysis cell

#### The efficiency of hydrogen gas production in microbial electrolysis cells

Substrate	MEC Volume (mL)	Input Voltage (V)	QMEC (mL H <sub>2</sub> /L·D)	YMEC (mmol-H <sub>2</sub> /g COD)	Reference
Dark Fermentation effluent	180	0.23	1061	32.44	This study
Dark Fermentation effluent	1,800	0.80	1,324	33.05	This study
Acetate	450	0.36	14	30.93	(Sun et al., 2008)
Dark Fermentation effluent	72	0.44	480	33.20	(Wang et al., 2011)

### Conclusion

- Anaerobic dark fermentation was carried out with 20 g/L xylose solution and BA Medium in a 6 L working volume CSTR reactor, with continuous feeding for a retention time of 72 h. Hydrogen gas production rate was 1,520.47±28.44 mL-H<sub>2</sub>/L-reactor·D. and the hydrogen yield was 1.40 ± 0.64 mol-H<sub>2</sub>/mol-Xylose, which was 42% compared to the theoretical yield. The concentrations of volatile fatty acids consisting of acetic acid at 677±24 mg/L, propionic acid 887±14 mg/L, and butyric acid 394±27 mg/L were investigated.
- Anaerobic dark fermentation from hydrolysate with BA Medium was operated continuously feed at a 6 day-HRT, revealing an increase in hydrogen production rate until the average constant was 206.91±10.96 mL-H<sub>2</sub>/L-reactor·D and had an average hydrogen yield of 1.51±0.08 mol-H<sub>2</sub>/mol-Xylose, which is 45% compared to the theoretical number of moles produced. The concentrations of volatile fatty acids consisting of 672.2±62.8 mg/L acetic acid, 34.9±11.4 mg/L propionic acid, and 212.6±13.8 mg/L butyric acid.
- In the section of hydrogen production in microbial electrolysis cells carrying out hydrogen production in a microbial electrolysis cell with effluent from the anaerobic fermentation process. Applying a potential difference of 0.233 V from the biofuel cell to a 180 mL microbial electrolysis cell, a hydrogen production rate of 1,061.72 mL-H<sub>2</sub>/L-reactor·D was found. While the hydrogen yield was 32.44 mmol-H<sub>2</sub>/g-COD, which is 51.9% compared to the hydrogen mol at theoretical production per gram COD. When applying a potential difference of 0.8 V to a 1.8 L microbial electrolysis cell, the maximum hydrogen production rate was 1,324 mL-H<sub>2</sub>/L·D and the hydrogen yield was 33.05 mmol-H<sub>2</sub>/g-COD, with hydrogen concentration of 61-62%.

### Acknowledgments

- This research has received funding support from the NSRF via the Program Management Unit for Human Resources & Institutional Development, Research and Innovation [grant number B13F660062].
- Thankful to Bio 4 gas (THAILAND) Company Limited for the support.
- Bio-Mass Conversion to Energy and Chemicals (Bio-MEC) Research Unit, Faculty of Science and Technology, Prince of Songkla University is great acknowledged to assist the experiment and provide materials.



## Impact of nickel, iron, and molybdenum addition on two-stage anaerobic digestion for enhanced hydrogen and methane production from palm oil mill effluent

Jiravut Seengenyong<sup>a</sup>, Sompong O-Thong<sup>a,b</sup>, Wanna Choorit<sup>c</sup>, Chonticha Mamimin<sup>d, e</sup>, and Sukonlarat Chanthong<sup>f</sup>

<sup>a</sup> International College, Thaksin University, Songkhla 90000, Thailand; <sup>b</sup> Biofuel and Biocatalysis Innovation Research Unit, Mahidol University, Nakhon Sawan 60130, Thailand; <sup>c</sup> Biomass and Oil Palm Research Center of Excellence, Walailak University, Tasala, Nakhon Si Thammarat 80161, Thailand; <sup>d</sup> Department of Biotechnology, Faculty of Technology, Khon Kaen University, Khon Kaen, 40002, Thailand; <sup>e</sup> Bio4gas (Thailand) Company Limited, Songkhla 90100, Thailand; <sup>f</sup> Energy Technology Program, Faculty of Engineering, Prince of Songkla University, Songkhla, 90110, Thailand

### ABSTRACT

The effect of trace element (Mo, Fe, Ni, and Co) addition on two-stage hydrogen and methane production from POME and change of microbial community under thermophilic conditions was investigated. The optimum condition for maximizing the two-stage hydrogen and methane was 10 mg·L<sup>-1</sup> of Mo, 6 mg·L<sup>-1</sup> of Co and 10 mg·L<sup>-1</sup> of Fe and 6 mg·L<sup>-1</sup> of Ni with hydrogen yield of 55 mL·H<sub>2</sub>·gVS<sup>-1</sup> and methane yield of 320 mL·CH<sub>4</sub>·gVS<sup>-1</sup>. Addition of Mo combine with Ni, Co and Fe can enhance hydrogen and methane yield via two-stage anaerobic digestion process. A quantitative real-time PCR of 16S rRNA genes was used for monitoring effect of trace element on responsible bacteria and archaea. The abundant bacterial population in hydrogen stage was related to *Thermoanaerobacterium thermosaccharolyticum* which is responsible for Fe and Ni addition. *Methanoculleus* sp. was dominant methanogen in methane reactor and responsible to Ni addition. Bacterial populations in methane reactor were responded to the addition of a combination of Fe and Mo, while archaeal populations were responded to the addition of Ni and Mo. A mixture of Fe, Ni, and Mo addition could enhance hydrogen and methane production, hydrogen-producing bacteria population, and methanogen population in two-stage anaerobic digestion process.

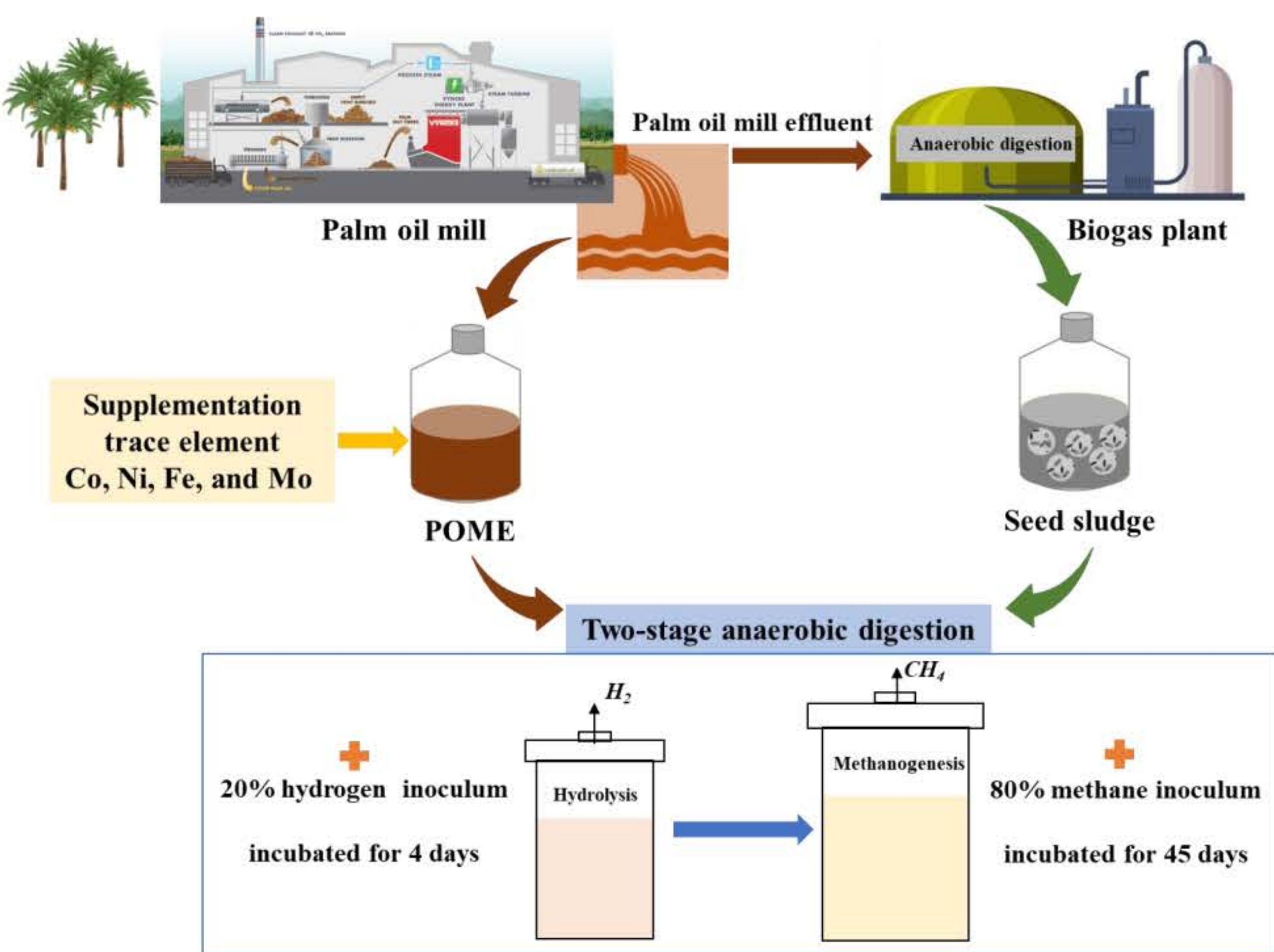
### INTRODUCTION / OBJECTIVES

The two-stage hydrogen and methane production has attracted growing attention worldwide due to its high potential to use as a vehicle fuel and probably an alternative to the fossil-based hythane (Liu et al., 2013). The two-stage hydrogen and methane production is also an environmentally friendly process and a promising way for both waste treatment and energy production from wastewater (Zahedi et al., 2016). Successfully two-stage hydrogen and methane production from palm oil mill effluent (POME) has a hydrogen yield of 210 L·H<sub>2</sub>·kgCOD<sup>-1</sup> and methane yield of 315 L·CH<sub>4</sub>·kgCOD<sup>-1</sup> with generating energy of 15.34 MJ·kgCOD<sup>-1</sup> (Mamimin et al., 2015).

Trace elements known to be crucial for the activity of enzymes in methanogenic systems are cobalt (Co), nickel (Ni), iron (Fe), and molybdenum (Mo) (Romero-Guiza et al., 2016). The addition of trace metals in the fermentation of waste can enhance biogas production to 14-50% (Zhang et al., 2011). Biogas production from the anaerobic digestion process with a high level of trace element, leading to inhibited anaerobic microbes results in low methane production (Romero-Guiza et al., 2016).

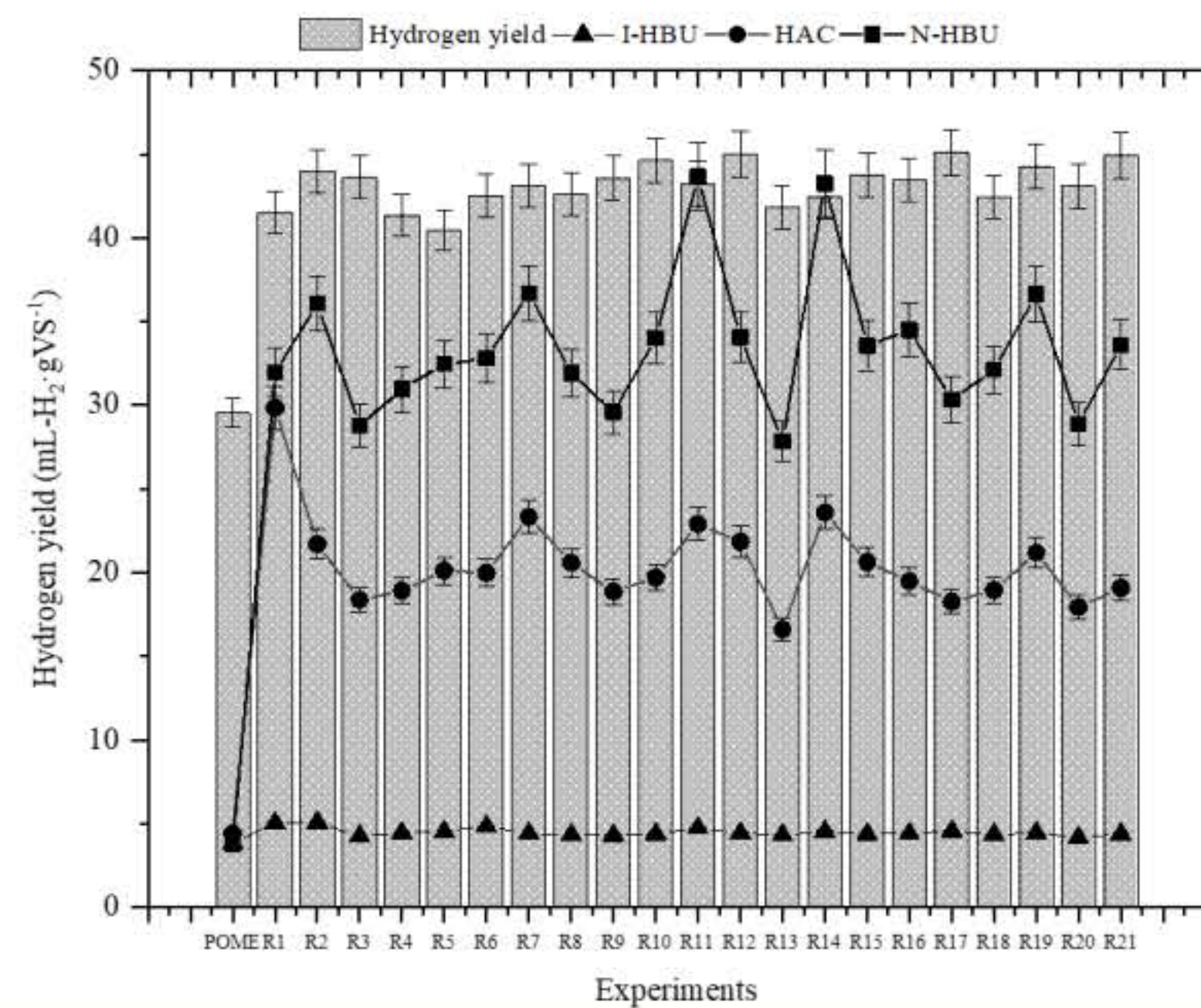
Until now, the optimal concentration of trace element and combination of trace element for anaerobic digestion process and two-stage hydrogen and methane process has been less extensively studied and also no report has linked the effect of trace element on process parameter to microbial community composition. This work aimed to investigate the effect of trace elements (cobalt, nickel, molybdenum, and iron) on two-stage hydrogen and methane production from POME under thermophilic conditions and change of microbial community.

### RESEARCH METHODOLOGY

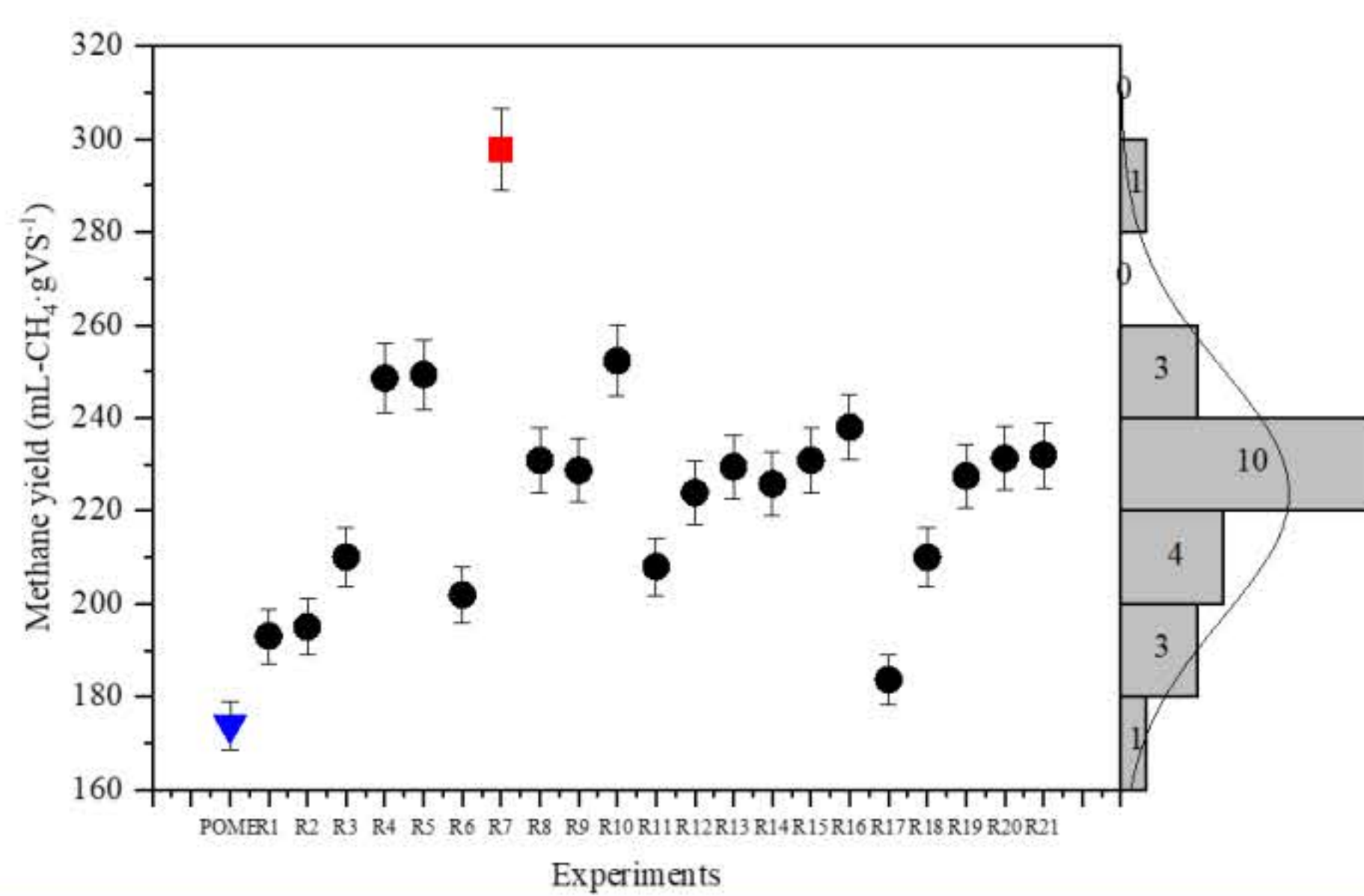


### RESULTS AND DISCUSSION

#### Effect of trace elements on hydrogen and methane production

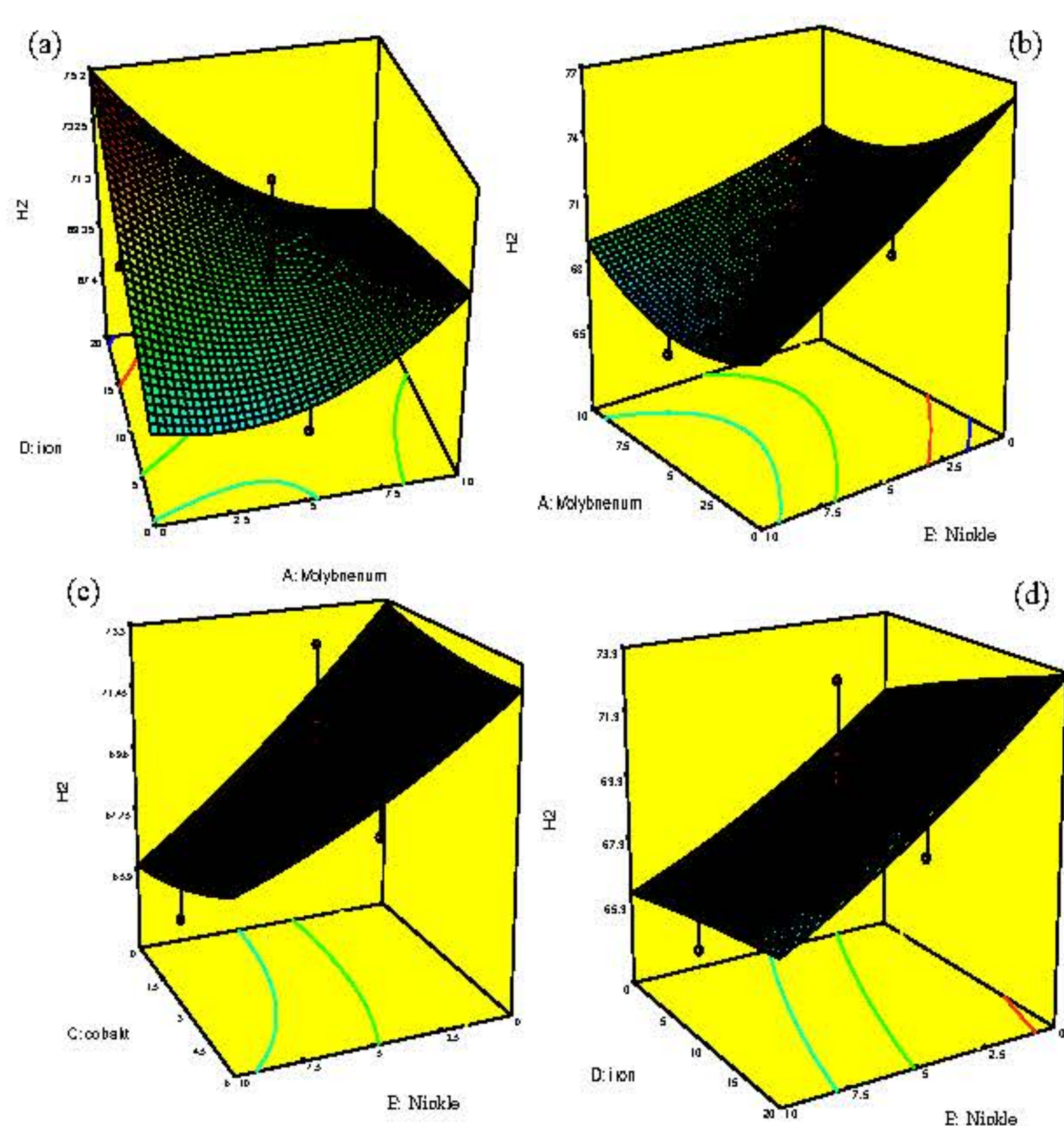


Effect of trace metal on hydrogen production in second stage found that 90% of hydrogen gas was produced during 4 day of incubation. Maximum hydrogen production was achieved at Fe, Ni and Co of 20, 10 and 6 mg·L<sup>-1</sup> (run 17) with hydrogen yield of 45.1 mL·H<sub>2</sub>·gVS<sup>-1</sup>. At concentration of 10 mg·L<sup>-1</sup> of iron (Fe), 5 mg·L<sup>-1</sup> of nickel (Ni) and 3 mg·L<sup>-1</sup> of cobalt (Co) and 5 mg·L<sup>-1</sup> of molybdenum (Mo) addition was also increases hydrogen production (run 21) with hydrogen yield of 44.9 mL·H<sub>2</sub>·gVS<sup>-1</sup>.



Methane production in second stage found that 90% of methane production was produced during 15 days of incubation with cumulative methane production ranged of 300-486 mL·CH<sub>4</sub>·gVS<sup>-1</sup>. The methane yields from POME hydrogenic effluent were ranged between 183-297 mL·CH<sub>4</sub>·gVS<sup>-1</sup>. The highest methane yield (297 mL·CH<sub>4</sub>·gVS<sup>-1</sup>) obtained from run7 with 20 mg·L<sup>-1</sup> of iron, 6 mg·L<sup>-1</sup> of cobalt and 10 mg·L<sup>-1</sup> of molybdenum. Lowest methane yield (183 mL·CH<sub>4</sub>·gVS<sup>-1</sup>) was achieved from run 17 which gave the maximum hydrogen yield.

#### Optimization of trace element concentration on two-stage hydrogen and methane production

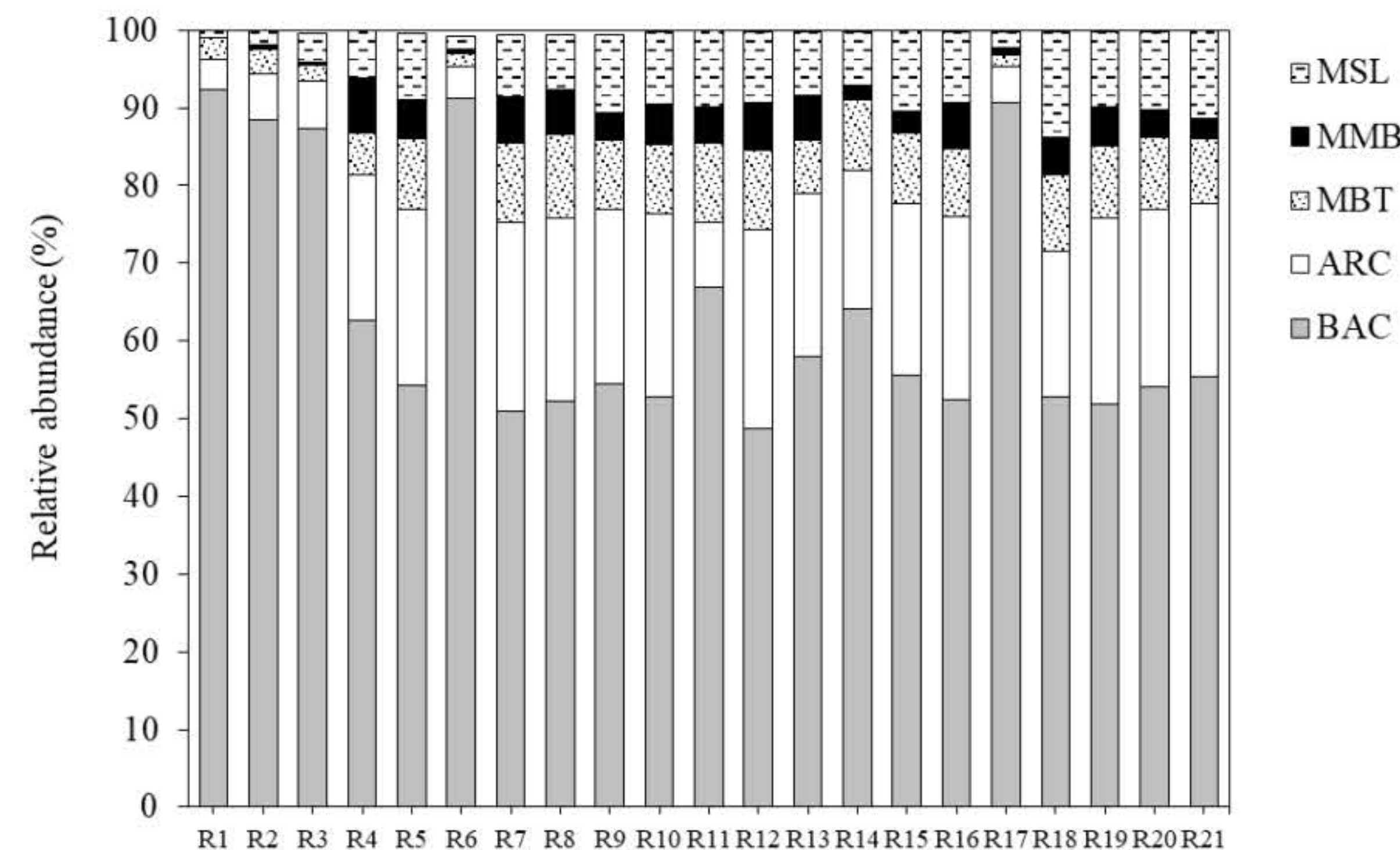


The 3D response surface of trace metal concentration on cumulative hydrogen, the optimum condition for maximizing the two-stage hydrogen and methane was 10 mg·L<sup>-1</sup> of Mo, 6 mg·L<sup>-1</sup> of Co and 10 mg·L<sup>-1</sup> of Fe and 6 mg·L<sup>-1</sup> of Ni with hydrogen yield of 55 mL·H<sub>2</sub>·gVS<sup>-1</sup> and methane yield of 320 mL·CH<sub>4</sub>·gVS<sup>-1</sup>. The highest concentration of iron (20 mg·L<sup>-1</sup>) resulted in increases of hydrogen production. Combination of Mo with Ni, Co, Fe can increase the rate of methane generation

After anaerobic digestion with trace element (Ni, Fe, Co and Mo) addition, the trace element (Co, Ni and Mo) present in effluent less than 5 mg·L<sup>-1</sup> from initial concentration of 3-10 mg·L<sup>-1</sup> except in run 7. However, iron was still remaining in effluent after anaerobic digestion process of 3-7 mg·L<sup>-1</sup>.

Run	Iron (mg·L <sup>-1</sup> )		Cobalt (mg·L <sup>-1</sup> )		Nickel (mg·L <sup>-1</sup> )		Molybdenum (mg·L <sup>-1</sup> )	
	Initial	final	Initial	final	Initial	final	Initial	final
POME	67	-	<0.5	-	<0.5	-	<0.5	-
R4	67	5	3	<0.5	5	<0.5	5	<0.5
R5	77	7.1	3	<0.5	10	<0.5	5	<0.5
R7	87	4.4	6	<0.5	<0.5	<0.5	10	1
R10	67	4.2	<0.5	<0.5	<0.5	<0.5	<0.5	<0.5
R17	87	5	6	<0.5	10	<0.5	<0.5	<0.5
R21	77	3.8	3	<0.5	5	<0.5	5	<0.5

#### Effect of trace element on microbial community



Thermophilic bacterium such as *Thermoanaerobacterium* sp., *Thermodesulfobacterium* sp. and *Rhodothermus* sp. were dominant and played an important role in hydrogen stage. The real time PCR show that, high methane production treatment composed of 50-60% bacteria and 17-25% archaea. High methane production treatment has relative archaea species abundance of in *Methanothermobacter* 10%, *Methanosarcina* 13% and *Methanomicrobial* 6%. Low methane production treatment composed of 88-90% bacteria and 3-6% archaea. Low methane production treatment has relative archaea species abundance of in *Methanothermobacter* 2%, *Methanosarcina* 3 and *Methanomicrobial* 1%

### Conclusion

- ✓ The optimum condition for maximizing the two-stage hydrogen and methane was 10 mg·L<sup>-1</sup> of Mo, 6 mg·L<sup>-1</sup> of Co and 10 mg·L<sup>-1</sup> of Fe and 6 mg·L<sup>-1</sup> of Ni with hydrogen yield of 55 mL·H<sub>2</sub>·gVS<sup>-1</sup> and methane yield of 320 mL·CH<sub>4</sub>·gVS<sup>-1</sup>.
- ✓ Addition of Mo combine with Ni, Co and Fe can enhance hydrogen and methane yield via two-stage anaerobic digestion process.
- ✓ The abundant bacterial population in hydrogen stage was related to *Thermoanaerobacterium thermosaccharolyticum* which responsible to Fe and Ni addition.
- ✓ *Methanoculleus* sp. was the dominant methanogen in methane reactor and responsible to Ni addition.
- ✓ Mixture of Fe, Ni and Mo addition could enhance hydrogen and methane production, hydrogen producing bacteria population and methanogen population in two-stage anaerobic digestion process.

### ACKNOWLEDGMENT

This research has received funding support from the NSRF via the Program Management Unit for Human Resources & Institutional Development, Research and Innovation [grant number B13F660062]

### References

- Liu Z, Zhang C, Lu Y, Wu X, Wang L, Wang L et al (2013) States and challenges for high-value biohythane production from waste biomass by dark fermentation technology. *Bioresour Technol* 135:292–303.
- Romero-Guiza, M.S., Vila, J., Mata-Alvarez, J., Chimenos, J.M., Astals, S., 2016. The role of additives on anaerobic digestion: A review. *Renewable Sustainable Energy Rev.* 58, 1486–1499.
- Zahedi, S., Solera, R., Miccolucci, F., Cavinato, C., Bolzonella, D., 2016. Changes in microbial community during hydrogen and methane production in two-stage thermophilic anaerobic co-digestion process from biowaste. *Waste Manage.* 49, 40–46.
- Zhang, L., Lee, Y.W., Jahng, D., 2011. Anaerobic digestion of food waste and piggy wastewater: Focusing on the role of trace elements. *Bioresour. Technol.* 102, 5048–5059.



## Preparation of oil palm wood for producing engineered wood products

Jaipet Tomad<sup>1</sup>, Suthon Srivaro<sup>1</sup>, Wanna Choorit<sup>2</sup>

<sup>1</sup>Center of Excellence in Wood and Biomaterials, Walailak University, Nakhon Si Thammarat, Thailand

<sup>2</sup>School of Agricultural Technology and Food Industry, Walailak University, Nakhon Si Thammarat, Thailand

### Introduction

Oil palm tree is one of the important economic crops widely planted in the South of Thailand. After 25 years of age, oil palm tree is generally cut down for replanting. Many attempts have been made to utilize oil palm trunk biomass for wood based products. The objective of this research project is to develop lumber based products from oil palm trunk for structural purpose. Since the quality of oil palm wood lumber is essential for the development of wood based product, here, we explored the characteristics of oil palm wood lumber dried with hot air oven at various drying temperatures. The reduction of moisture content and lumber quality of oil palm wood were examined.



### Methods

The oil palm trees used in this work were felled from a plantation area of Thasala district, Nakhon Si Thammarat province, Thailand. The trunk was converted into lumber with the dimensions of 100 mm x 70 mm (cross-section) x 150 mm (longitudinal) using circular saw. Before drying, oil palm specimens were impregnated with water in a pressure vessel at 12 bar for 60 min to attain the saturated moisture content with full cell process. These oil palm wood specimens were then dried with hot air oven at the temperatures of 50 °C, 75°C and 100°C. The moisture content and image of wood specimen were measured and taken, respectively every 6 hours until the final moisture content of 18% was attained.



### Results & Discussion

Figure 1 shows the reduction of moisture content of oil palm wood plotted against the drying time. It was found that the reduction of moisture content of oil palm wood was strongly dependent on drying temperature. At high drying temperature, drying rate was higher.

Figure 2 shows the appearance of oil palm wood lumber at the drying times of 12 h, 26 h and 148 h. It was found that oil palm wood dried at 50 °C had uniform thickness while those dried at high temperatures of 75 °C and 100 °C showed a distorted shape.

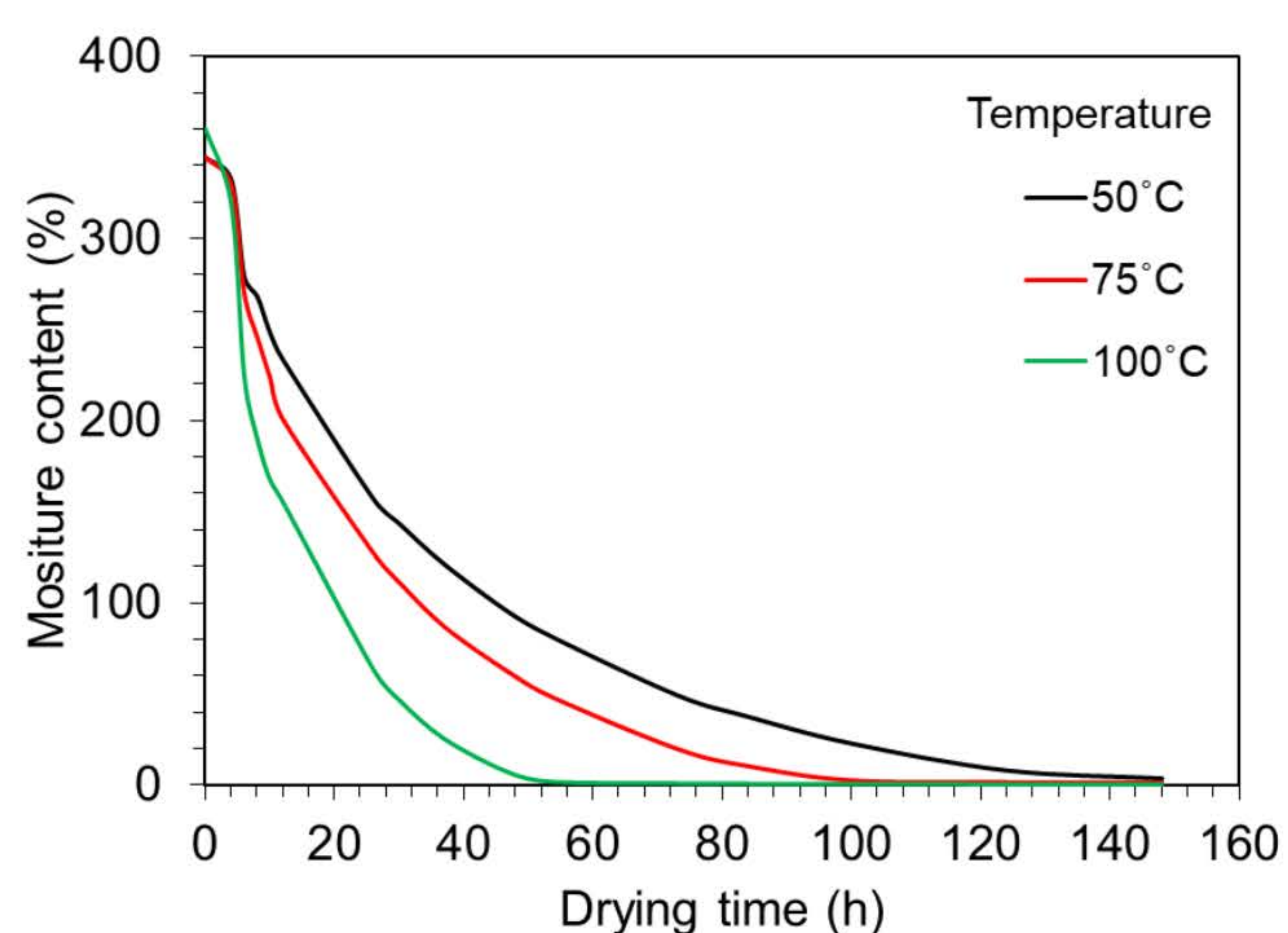


Figure 1. Effect of drying temperature on the drying rate.

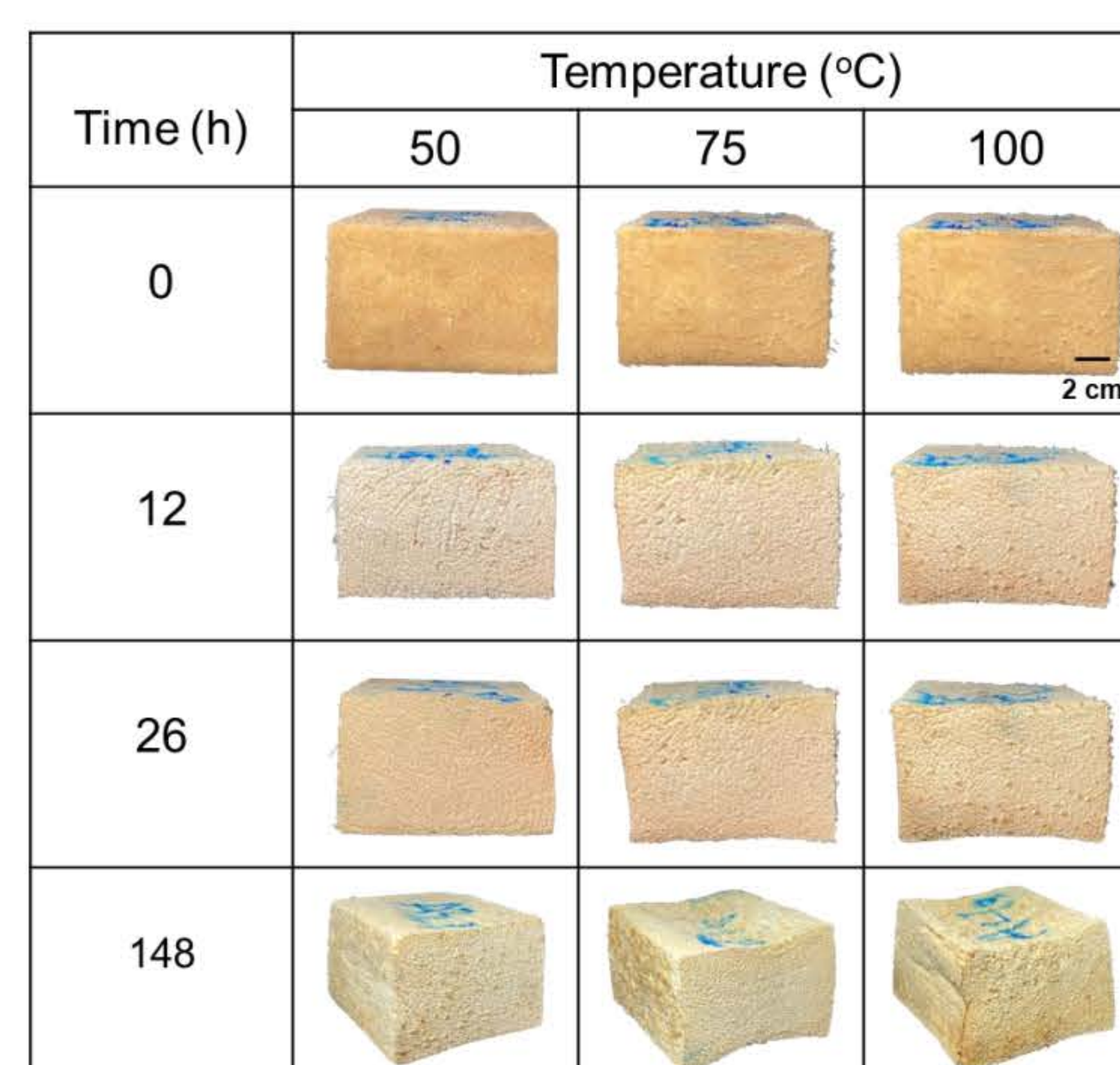


Figure 2. Image of oil palm wood at various drying times.

### Conclusion

Oil palm wood could be dried with hot air oven, and the drying temperature of 50 °C was recommended.

### Acknowledgements

This research has received funding support from the NSRF via the Program Management Unit for Human Resources & Institutional Development, Research and Innovation [grant number B13F660062]



## Promoting Climate-Neutral Rice Production: Methanotroph-Augmented Approach to Reduce GHG Emissions in Paddy

Chonticha Leamdarn<sup>1</sup>, Sompong O-Thong<sup>1,2\*</sup>, Wanna Choorit<sup>3</sup>, Jarupa Chuanklin<sup>4</sup>, Phawida Duangkhan<sup>4</sup>, Chaisit Niyasom<sup>5</sup>, Nils Kare Birkeland<sup>6</sup>

<sup>1</sup> International College, Thaksin University, Songkhla 90000, Thailand, <sup>2</sup> Water and Soil Environmental Research Unit, Nakhonsawan Campus, Mahidol University, Nakhonsawan 60130, Thailand,

<sup>3</sup> Biomass and Oil Palm Research Center of Excellence, Walailak University, Tasala, Nakhon Si Thammarat 80161, Thailand, <sup>4</sup> Paphayom Phitthayakhom School, Thaksin University, Phatthalung 93210, Thailand, <sup>5</sup> Department of Biology, Faculty of Science, Thaksin University, Phatthalung 93210, Thailand, <sup>6</sup> Department of Biological Sciences, University of Bergen, N- 5020, Norway

### ABSTRACT

The food sector plays a significant role in driving climate change, with rice cultivation alone accounting for 0.62% of CH<sub>4</sub> emissions and field burning contributing an additional 0.62% of CH<sub>4</sub> emissions to Thailand's agriculture sector's total greenhouse gas (GHG) emissions. In pursuit of climate neutrality in farms and farming systems, this study employs methanotrophs, specifically methane-oxidizing bacteria, to mitigate GHG emissions in flooded rice paddy systems by directly converting methane to methanol. Methanotrophic bacteria were enriched from various sources of soil in Phatthalung Province, Thailand, through cultivation on a medium with methane in the headspace of serum bottles. The enriched cultures were evaluated for methane consumption efficiency, considering different inoculation sizes (10%, 20%, 30%, and 40%), and subsequently applied to rice cultivation. The methane reduction efficacy of enriched bacteria derived from various sources, including cattle farm effluent, swamp field sediments, rice paddy soil, digested sludge, peat forest, and cattle farm soil, was determined to be 97.9%, 95.5%, 92.0%, 79.5%, 75.6%, and 95.2%, respectively. Notably, the enriched culture from cattle farm effluent exhibited the highest methane reduction efficiency. Furthermore, the optimal inoculum size of 20% effectively mitigated CH<sub>4</sub> emissions in rice cultivation. *Acinetobacter* sp., *Pseudomonas* sp., *Methylosarcina* sp., and *Methylomagnus* sp. dominated the enriched consortium. By leveraging methanotrophs and implementing a 20% inoculum size, this innovative approach holds promise for significantly reducing methane emissions from rice cultivation. This research fosters climate-neutral farming practices and enhances sustainability within the agricultural sector.

### INTRODUCTION / OBJECTIVES

Rice is a staple food and a key commodity in Thailand, rice cultivation accounts for 57.7% of the total GHG emission generated from agricultural activity in Thailand (CCAC, 2020). The food sector plays a significant role in driving climate change, with rice cultivation alone accounting for 0.62% of CH<sub>4</sub> emissions and field burning contributing an additional 0.62% of CH<sub>4</sub> emissions to Thailand's agriculture sector's total greenhouse gas (GHG) emissions.

Methanotrophs bacteria have the unique ability to grow on methane as their sole source of carbon and energy. They play a major role in the consumption of the atmospheric greenhouse gas methane and capturing biologically formed methane before it is released into the atmosphere (Kalyuzhnaya et al., 2019). Methanotrophs are used to reduce the global warming potential in a flooded paddy system, which is a progressive investigation in recent (Davamani et al., 2020). In pursuit of climate neutrality in farms and farming systems, this study employs methanotrophs, specifically methane-oxidizing bacteria, to mitigate GHG emissions in flooded rice paddy systems by directly converting methane to methanol.

### RESEARCH METHODOLOGY

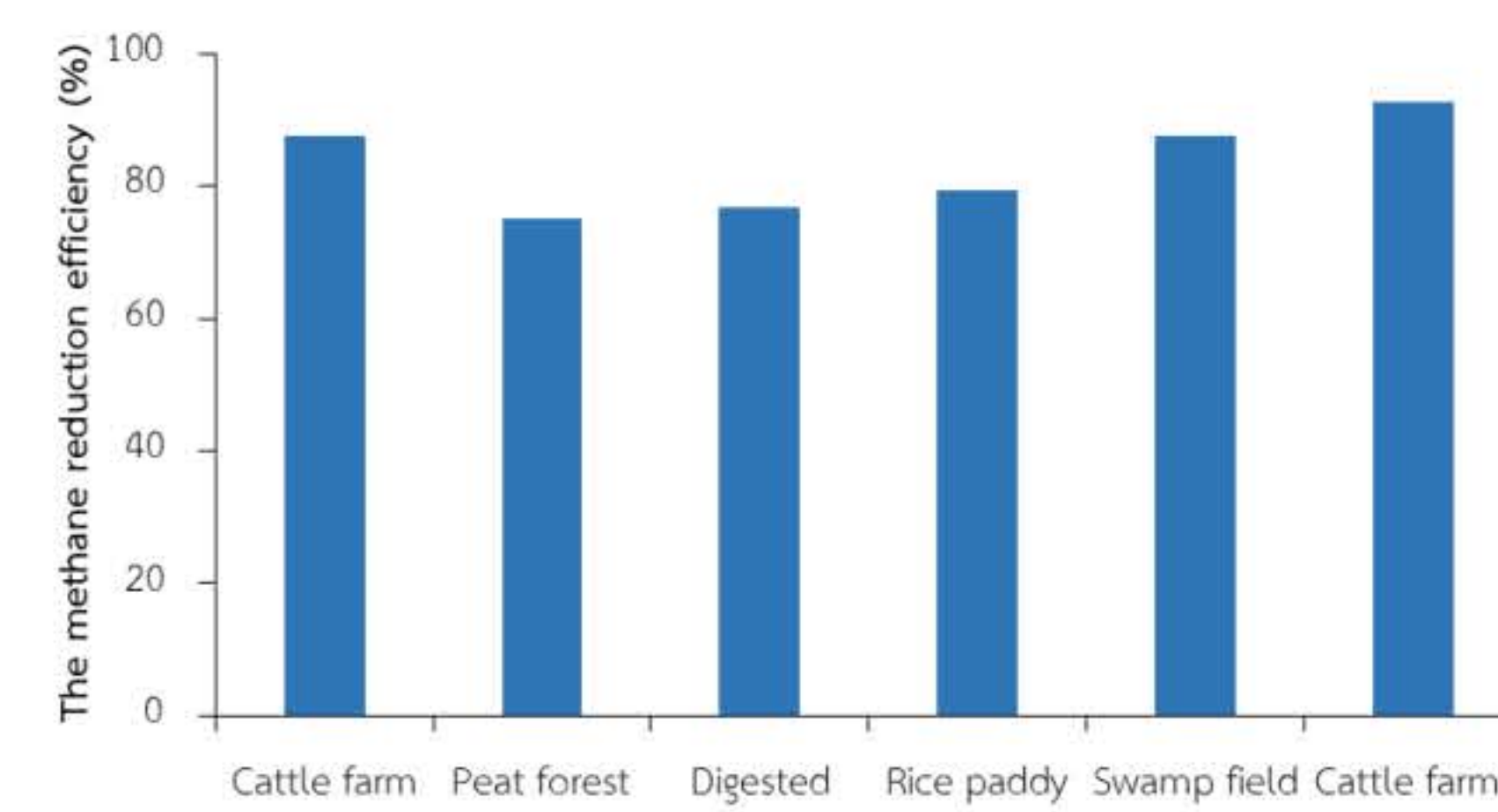
#### 1 Samples collection



### RESULTS AND DISCUSSION

The samples were collected from various sources of soil in Phatthalung Province, Thailand. The pH value of the samples is an acidic pH, except swamp field sediments is a natural pH, and the temperature of collected samples is in the range of 26-36 °C.

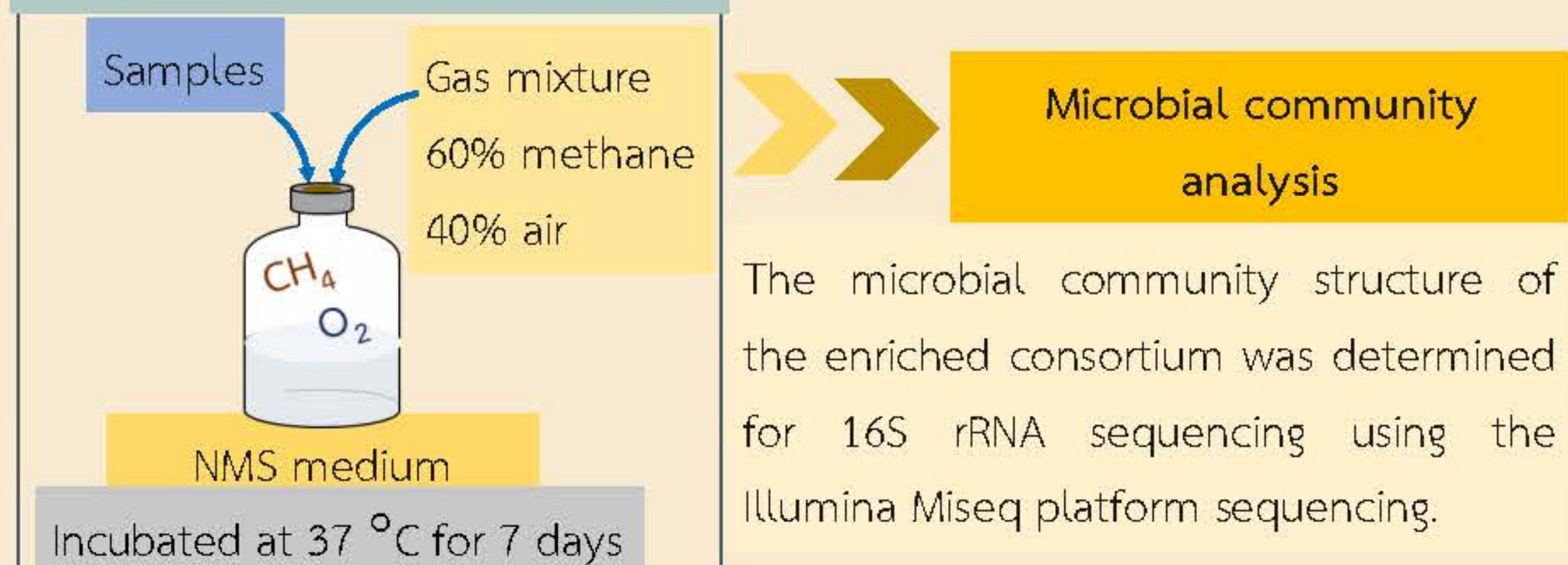
Samples	pH	Temperature (°C)
Cattle farm soil	2	32
Cattle farm effluent	2	32
Rice paddy soil	3	31
Peat forest soil	6	26
Digested sludge	6	36
Swamp field sediments	7	29



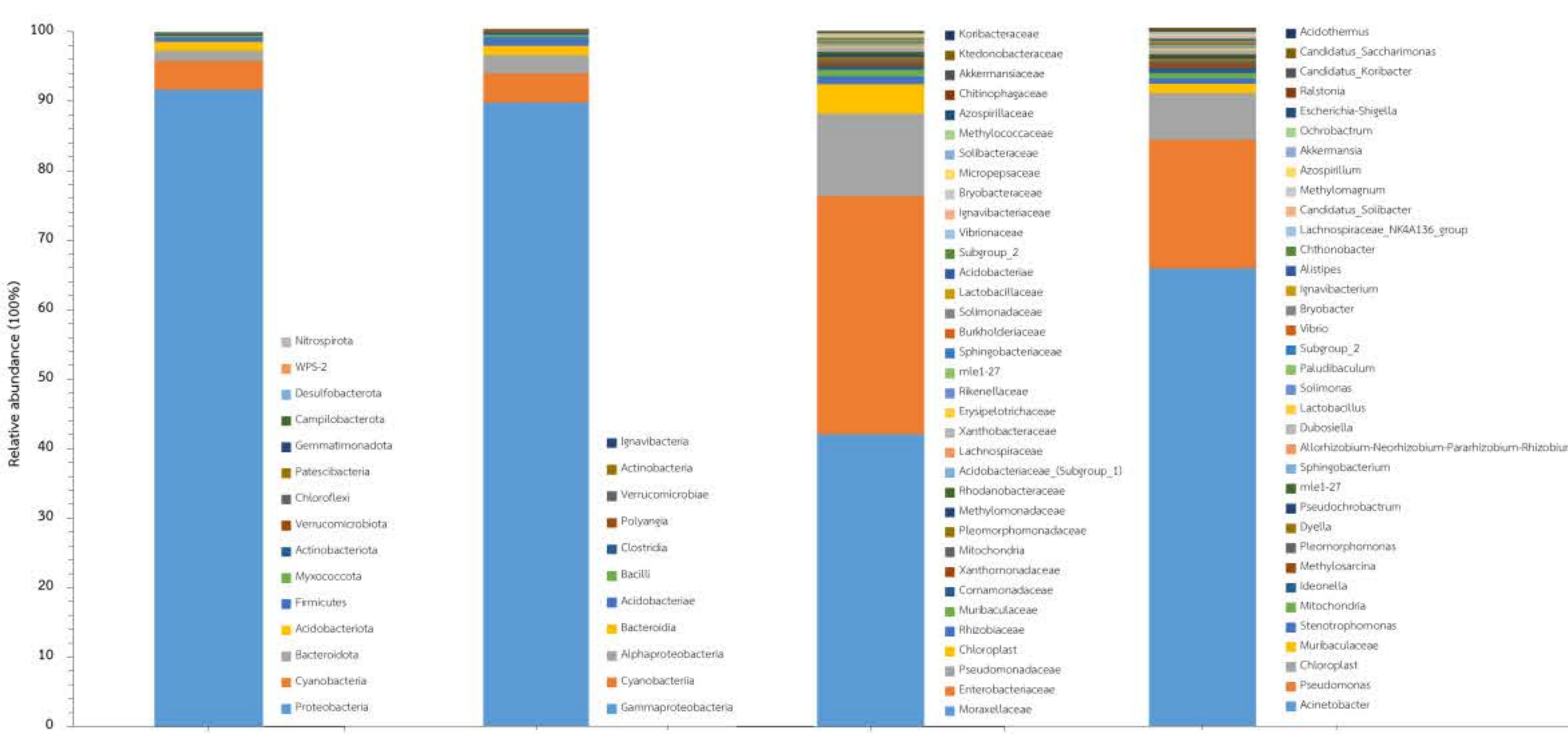
The collected samples were enriched with methane as the only carbon source. The enriched culture from cattle farm effluent exhibited the highest methane reduction efficiency (97.98%).

#### 2 Enrichment culture of methanotrophs bacteria

##### Three times enrichment cultures



The microbial community structure of the enriched consortium was determined for 16S rRNA sequencing using the Illumina Miseq platform sequencing.



The dominating bacteria belong to the phylum Proteobacteria (91%), and Gammaproteobacteria at the major class level (89%), which are responsible for enriched culture from cattle farm effluent. The dominant Family level was distributed across Moraxellaceae (41%), Enterobacteriaceae (34%), and Pseudomonadaceae (11%), which belong to the class Gammaproteobacteria, including dominated the genus level of *Acinetobacter* (65%) and *Pseudomonas* (18%).

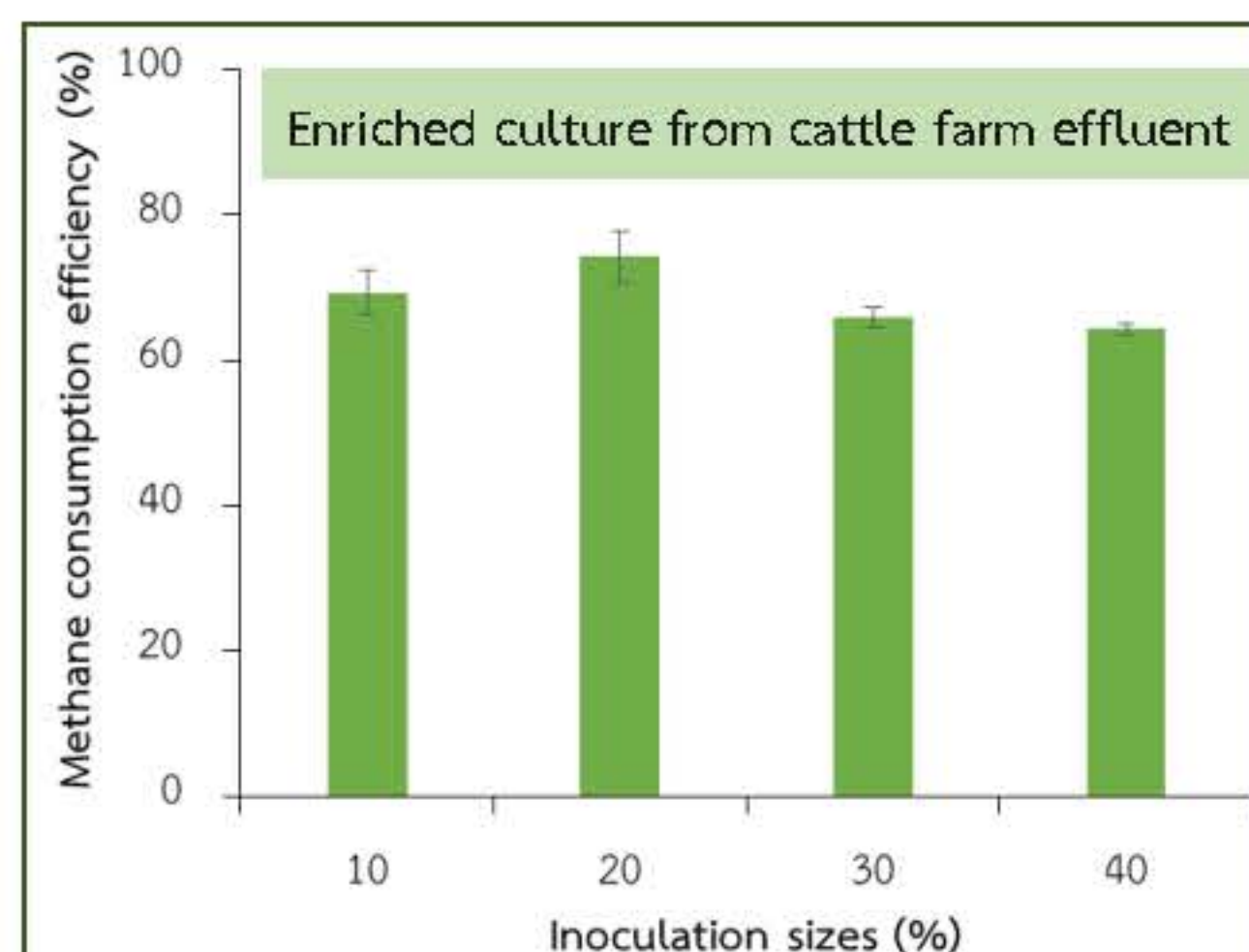
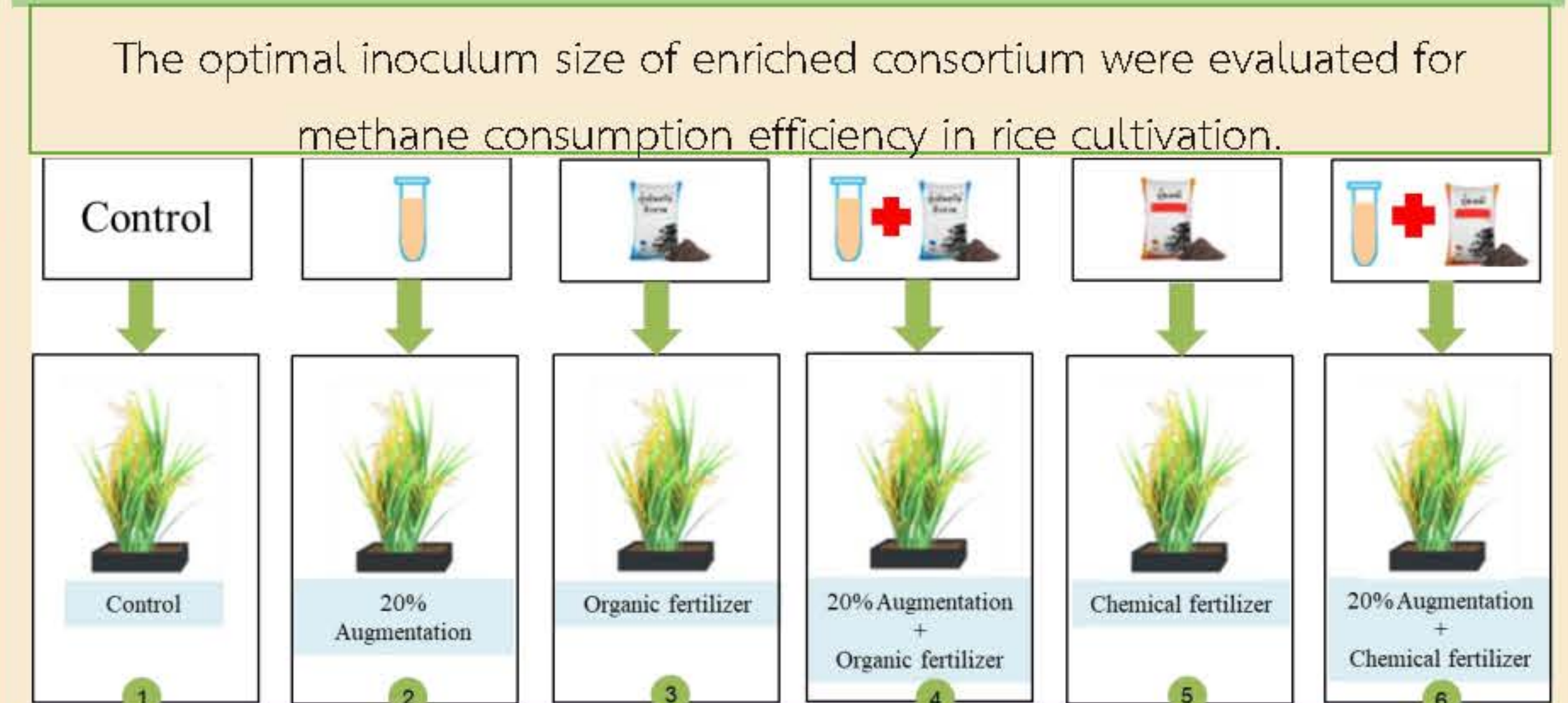
The relative abundance of phylogenetic groups in the enriched culture from cattle farm effluent at the Phylum, Class, Family and Genus level.

#### 3 Application

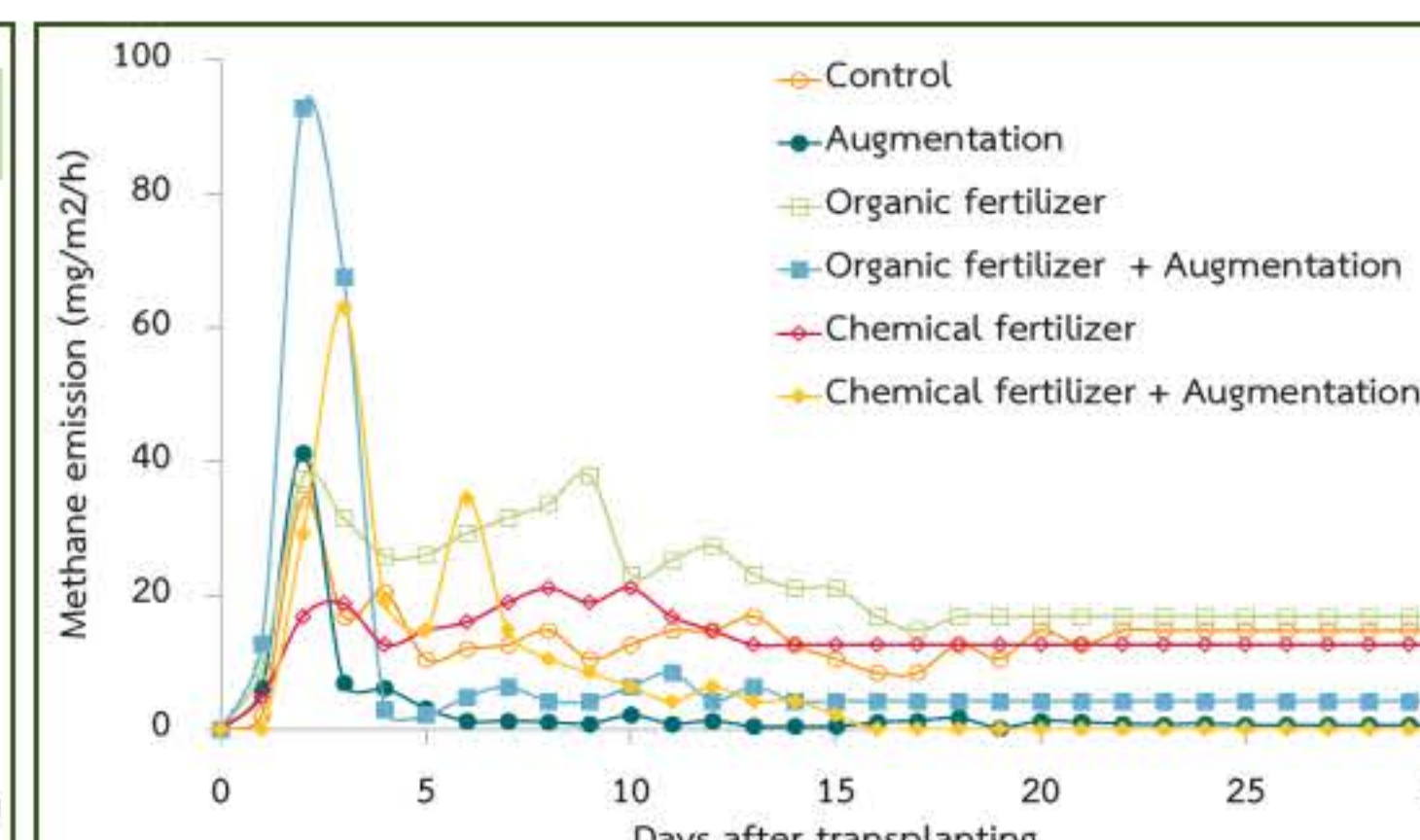
##### Evaluation of inoculation sizes for methane consumption efficiency

The enriched cultures were evaluated for methane consumption efficiency, considering different inoculation sizes (10%, 20%, 30%, and 40%).

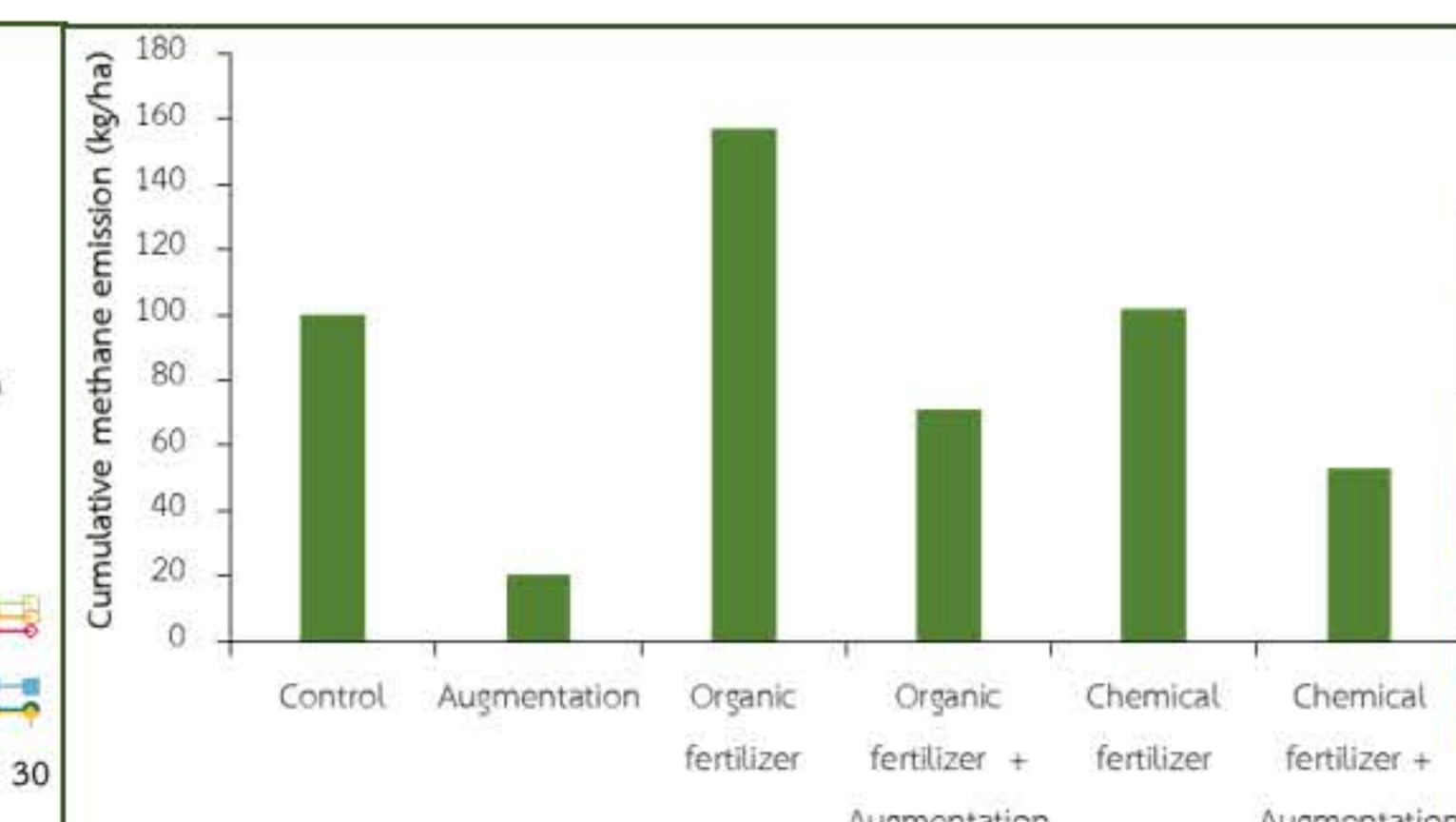
##### Methane reduction efficiency in rice cultivation



The optimal inoculum size at 20% effectively reduced CH<sub>4</sub> emissions, subsequently applied to rice cultivation.



Adding a 20% inoculum size of augmentation effectively mitigated CH<sub>4</sub> emissions in rice cultivation by 79% compared with the control. Rice cultivation with organic fertilizer and chemical fertilizer increased methane emission as a result, fertilizer had high nutrient content, which supports the methanogens growth in soil and enrichment culture.



### CONCLUSION

- Enriched cultures of methanotrophic bacteria from various soil sources exhibited high methane reduction efficiencies, with the culture from cattle farm effluent showing the highest efficacy.
- Implementing a 20% inoculum size effectively reduced CH<sub>4</sub> emissions in rice cultivation. *Acinetobacter* sp., *Pseudomonas* sp., *Methylosarcina* sp., and *Methylomagnus* sp. were dominant within the enriched consortium.
- Leveraging methanotrophs and adopting this innovative approach holds promise for significant methane emission reductions, promoting climate-neutral farming practices and enhancing agricultural sustainability.

### ACKNOWLEDGMENT

This research has received funding support from the NSRF via the Program Management Unit for Human Resources & Institutional Development, Research and Innovation [grant number B13F660062]

### References

- CCAC. 2020. Promoting low emissions rice production in Thailand | Climate & Clean Air Coalition (<https://www.ccacoalition.org/en/projects/promoting-low-emissions-rice-production-thailand>)
- Davamani, V., Parameswari, E., Arulmani, S. 2020. Mitigation of methane gas emissions in flooded paddy soil through the utilization of methanotrophs. Science of the Total Environment, 726: 138570.
- Kalyuzhnaya, M.G., Gomez, O.A., Murrell, J. C. 2019. The Methane-Oxidizing Bacteria (Methanotrophs). Taxonomy, Genomics and Ecophysiology of Hydrocarbon-Degrading Microbes, Handbook of Hydrocarbon and Lipid Microbiology, [https://doi.org/10.1007/978-3-319-60053-6\\_10-1](https://doi.org/10.1007/978-3-319-60053-6_10-1).
- Wassmann, R., Lantin, R.S., Neue, H.U., Buendia, L.V., Corton, T.M., Lu, Y. 2000. Characterization of Methane Emissions from Rice Fields in Asia. III. Mitigation Options and Future Research Needs. Nutrient Cycling in Agroecosystems, 58, 23-36.



# Application of Gamma Irradiation in Agriculture: Preparation and Testing of Coconut Peat as a Growing Media for Plant Tissue Acclimatization

Chatsuda Kongpeng<sup>1</sup>, Lamai Maikaeo<sup>1,\*</sup>, Tanagorn Sangtawesin<sup>1</sup>, Vichai Puripanyavanich<sup>1</sup>

<sup>1</sup> Nuclear Technology Research and Development Center, Thailand Institute of Nuclear Technology, Nakhon Nayok 26120 Thailand

\* Corresponding author, e-mail: lamai@tint.or.th

## Introduction



- 85% of coconut waste are discarded as waste, without any value.
- waste disposal cause pollution



The application of gamma irradiation in agriculture includes using gamma rays for modifying, microbial decontamination, mutation induction, as well as pathogen and pest control. Nowadays, plant tissue culture is experiencing economic growth. However, farmers often encounter issues during acclimatization, as the tissue-cultured plants may be weak in adapting to the environment, resulting in slow growth and even death. The selection of a suitable medium for acclimatization becomes crucial as it plays a significant role in reducing the risk of diseases during the germination and early growth stages of the plant.

Normally, the preferred medium for plant acclimatization is peat moss, which is imported from overseas to Thailand and is relatively expensive. However, in this study, there is a need to reduce the cost of acclimatization by utilizing materials available in Thailand. Coconut peat, derived from coconut, is an agricultural waste that is both inexpensive and possesses favorable properties for facilitating plant acclimatization.

A study by Sumet (2014) reported that coconut peat contains a high level of tannins. When these tannins dissolve in water, they transform into tannic acid, leading to calcium deficiency in plants and resulting in their death. Hence, it is necessary to process coconut peat to remove tannins before using them.

Therefore, this study is to evaluate the efficiency of gamma irradiation in removing tannins and providing for growing coconut peat as medium promoting the growth development of plant tissue for acclimatization of *Homalomena rubescens* mint var. and *Philodendron billetiae*.

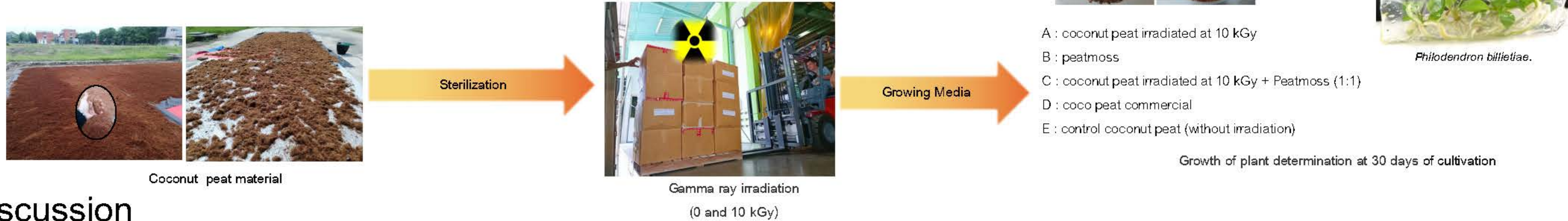


## Methods

### 1. Effect of gamma irradiation the electrical conductivity (EC) value in the leaching water of coconut peat samples



### 2. Effect of sterilization of coconut peat using gamma irradiation and its combinations on the growth of plantlets



## Results & Discussion

The electrical conductivity (EC) value in water was correlated with the concentration of tannic acid in leaching water (Table 1). The effects of gamma irradiation at doses of 0, 10, 20, and 30 kGy on EC in the leaching water of coconut peat samples showed no significant differences between treatments and controls. At 0.3-hour soak of coconut peat with tap water is optimal for leaching tannin. The third rinsing can reduce tannin and maintain the EC value lower than 500 µS/cm which is optimum for plant growth (Fig. 1).

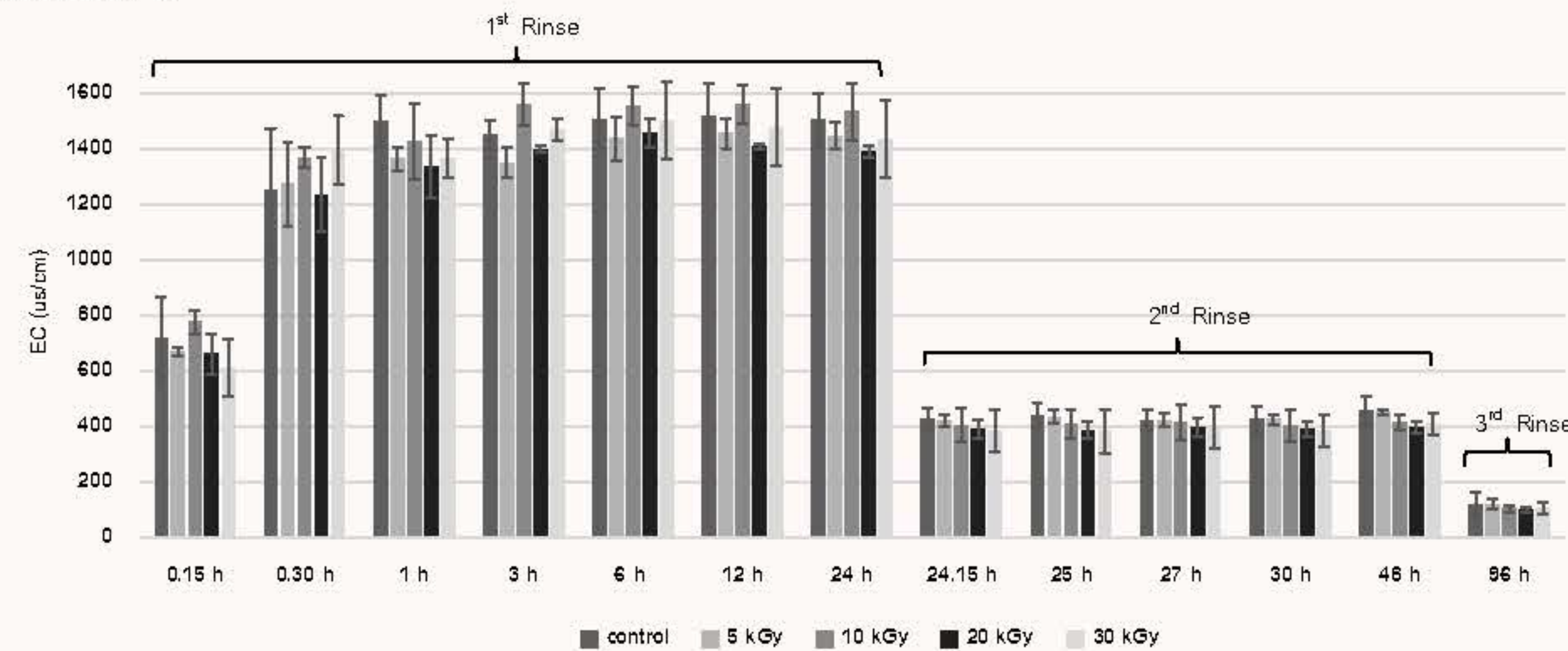


Figure 1: EC Values (µS/cm) after rinse water coconut peat irradiated at 5, 10, 20, 30 kGy, and Non-irradiated (control) at various time

Effect of sterilization of coconut peat using gamma irradiation and its combinations on the growth of plantlets. The experiment involved cultivating two types of plants in six different soil formulations, conducted in a temperature-controlled room at approximately 25±2 °C. The plants were exposed to continuous light for 24 hours within a closed cultivation system, with no additional watering for a period of one month.

In the experiment cultivating *H. rubescens* mint var. in various soil formulations, it was found that formulas B resulted in the highest number of leaves, following closely was formula C, showing no statistically significant difference at a 95% confidence level (Table 2). The formula with the fewest leaves was formula A, which did not differ statistically from formula E (coco peat commercial) and formula F (control).

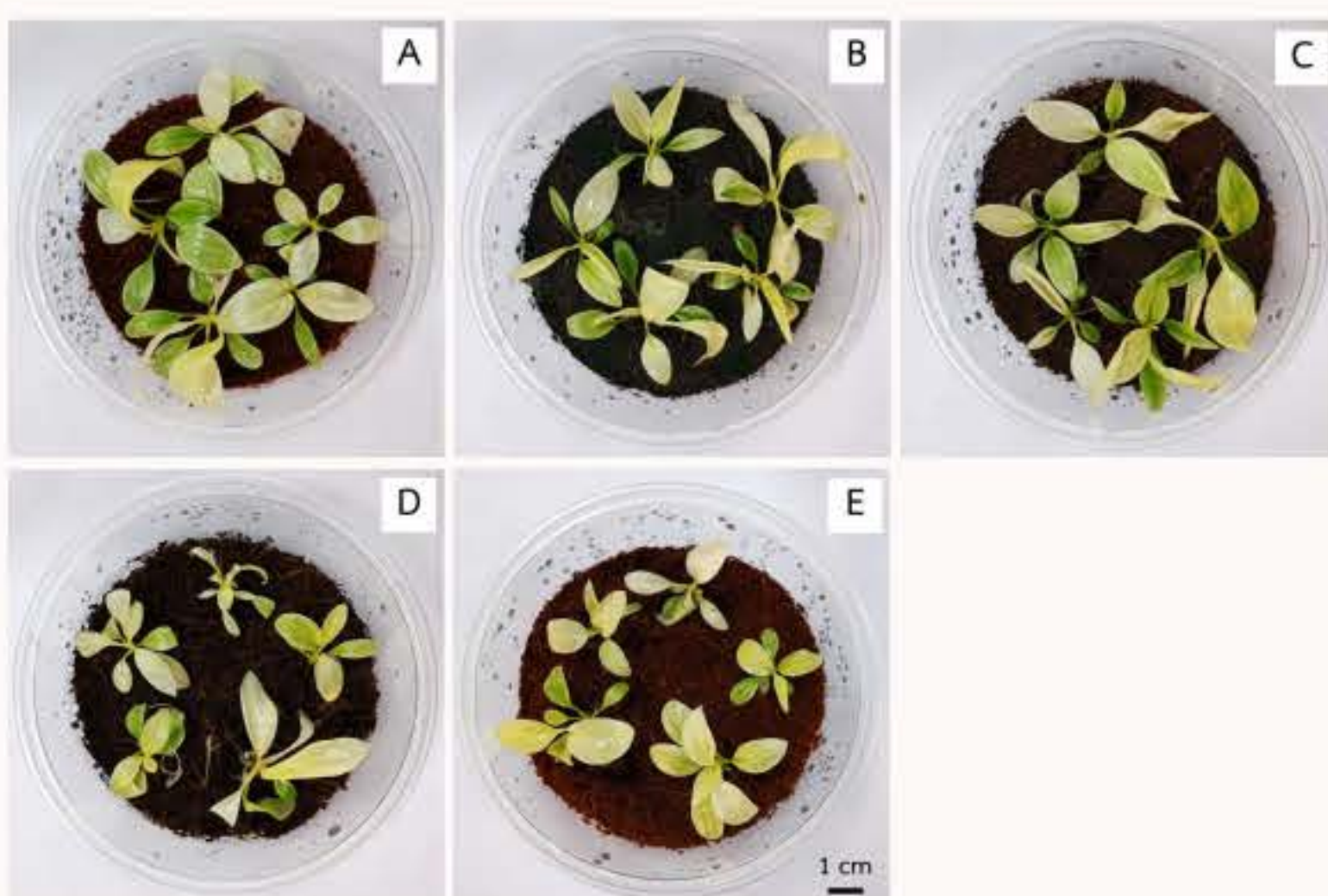


Table 2: Effects of different growing media on the number and size (length) of leaves of *Homalomena rubescens* mint var. after 30 days of cultivation.

Formula	No. of leaf ± SD	Leaf length (cm) ± SD
A	6.40 ± 1.36 <sup>b</sup>	2.39 ± 0.56 <sup>a</sup>
B	7.16 ± 1.26 <sup>a</sup>	2.27 ± 0.63 <sup>ab</sup>
C	7.08 ± 1.08 <sup>a</sup>	2.36 ± 0.79 <sup>ab</sup>
D	6.56 ± 1.30 <sup>b</sup>	2.00 ± 0.66 <sup>c</sup>
E	6.44 ± 0.79 <sup>b</sup>	2.11 ± 0.57 <sup>bc</sup>
F-test	*	*
LSD	0.51	0.25

Note \*: Means followed by different letters are statistically different at the 95% confidence level based on the LSD test.

Regarding leaf length, the soil formulation that resulted in the longest leaves for *H. rubescens* mint was formula A, showing no significant difference from formulas B to C. Formula D produced the smallest leaf size (Table 2). From the figure, it can be observed that in formula A, the plant exhibits a well-formed and aesthetically pleasing structure with beautifully spreading leaves.

In the experiment cultivating *P. billetiae* in various soil formulations, it was found that formula C resulted in the highest number of leaves and leaf length, formula C produced the largest leaves for *P. billetiae*, significantly different from the other formulas. Formula D resulted in the smallest leaf size (Table 3). From the figure, it can be observed that formula C promotes the vigorous growth and the leaves exhibit a healthy green color.

The results of the bacteriological analysis testing revealed that coconut peat + peat moss (1:1), irradiated at a dose of 10 kGy, showed reduced quantities of total plate count (81 CFU/mL), yeast and mold (<1 CFU/mL), and coliform (<0.3 MPN/mL) compared to the non-irradiated sample, which had values of 9.2x10<sup>6</sup> CFU/mL, 3.7x10<sup>4</sup> CFU/mL, and >110 MPN/mL, respectively.

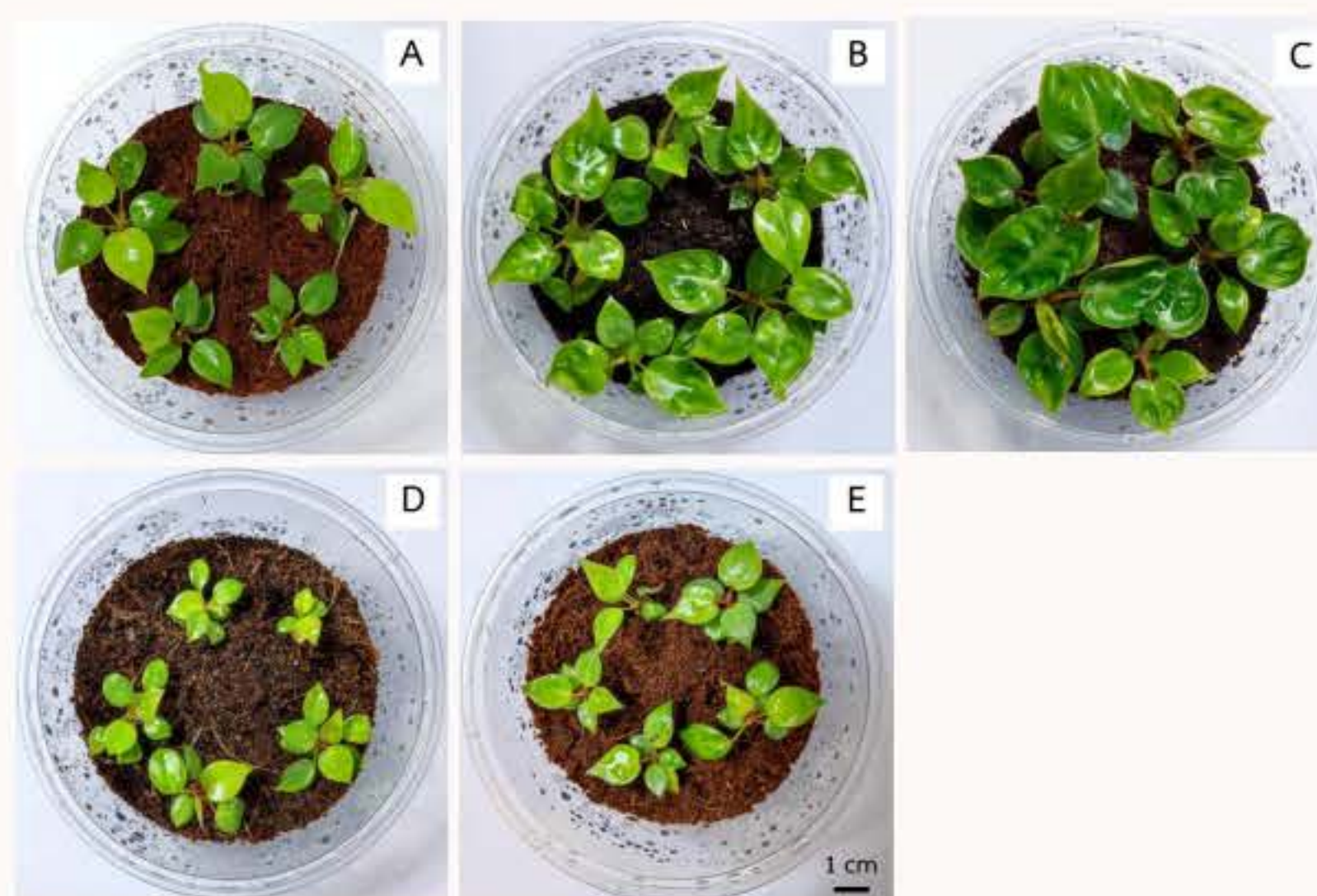


Table 3: Effects of different growing media on the number and size (length) of leaves of *Philodendron billetiae* after 30 days of cultivation.

Formula	No. of leaf ± SD	Leaf length (cm) ± SD
A	7.56 ± 0.64 <sup>cd</sup>	2.19 ± 0.40 <sup>c</sup>
B	8.92 ± 0.60 <sup>b</sup>	2.80 ± 0.47 <sup>b</sup>
C	9.04 ± 0.60 <sup>ab</sup>	3.25 ± 0.51 <sup>a</sup>
D	7.70 ± 0.65 <sup>c</sup>	1.59 ± 0.32 <sup>d</sup>
E	7.38 ± 0.67 <sup>d</sup>	2.23 ± 0.35 <sup>c</sup>
F-test	*	*
LSD	0.25	0.19

Note \*: Means followed by different letters are statistically different at the 95% confidence level based on the LSD test.

## Conclusion

Coconut peat is a valuable agricultural waste. The process of tannin reduction, achieved by soaking it three times in tap water for 30 minutes, minimizes tannin content to an optimum level for plantlet growth. Additionally, the sterilization process using gamma irradiation at 10 kGy reduces disease pathogens. Both the tannin reduction and sterilization processes of coconut peat promote the growth of plantlets, especially for economically valuable plants like *H. rubescens* mint and *P. billetiae*. Overall, this coconut peat demonstrates superior plant growth and can serve as a cost-effective alternative or mixture with peat moss, which is a more expensive material.

## Acknowledgements

This research has received funding support from the NSRF via the Program Management Unit for Human Resources & Institutional Development, Research and Innovation [grant number B13F660064]









**BRAINPOWER**  
CONGRESS 2023

ร่วมกับสร้างและขับเคลื่อนงานวิจัยขั้นแนวหน้า  
สู่อุตสาหกรรมแห่งอนาคต



by  
**SUK AI**  
สร้างคน  
ข้ามพรมแดน

**NANOTEC**  
a member of NSTDA

# Feasibility Study on Utilization of Hemp Hurd as Solid Biofuel

Jatuporn Parnthong, Sanchai Kuboon and Pongtanawat Khemthong

National Nanotechnology Center (NANOTEC),  
National Science and Technology Development Agency (NSTDA),  
Pathum Thani 12120, Thailand

## INTRODUCTION

In 2018, Thailand legalized hemp for industrial and medical purposes. Industrial hemp cultivation was promoted for a variety of uses, including textiles, construction materials, and food products. The government supported research and development efforts in this sector, and there were expectations of growth in hemp-related industries [1]. Hemp hurds are abundant biomass waste from hemp industry. It is lignocellulosic biomass waste which can be used as a solid fuel to generate heat or electricity. However, the utilization of conventional biomass as solid fuel is still inefficient due to its high moisture content, low heating value, and biodegradation during storage, etc. [2]. Torrefaction is a mild thermal conversion process of biomass typically operating at temperature between 200-300°C for 10-60 min under the absence of oxygen condition [3]. This process transforms raw biomass into a more energy-dense, stable, and improved solid fuel with enhanced combustion properties. The torrefied biomass called biocoal is more brittle and less hygroscopic than raw biomass, making it easier to grind, handle, and transport [4]. Therefore, this work aims to study biocoal production from hemp hurd via torrefaction process.



Hemp



Hemp hurd



Biocoal



Bio-green powerplant

## METHODS

### ❖ Biocoal production from hemp hurd via dry torrefaction process

#### Lab scale



#### Pilot scale



### ❖ Solid yield and energy yield were calculated as the following equation:

$$\text{Solid yield (\%)} = \frac{\text{Mass of torrefied sample (g)}}{\text{Mass of feedstock (g)}} \times 100 \quad (1)$$

$$\text{Energy yield (\%)} = \frac{\text{HHV of torrefied sample (MJ/kg)}}{\text{HHV of feedstock (MJ/kg)}} \times \text{Solid yield (\%)} \quad (2)$$

#### Analytical method

Bomb calorimeter (AC500 Isotherm Calorimeter, LECO, USA) was used to determine the calorific values of the biomass and biocoal samples. The proximate analysis of all samples was analyzed via thermogravimetry analysis (no. TA.129) to determine moisture content, volatile matter, ash content and fixed carbon. The weight percents of carbon (C), hydrogen (H), oxygen (O), nitrogen (N) and sulfur (S) were measured by CHNS elemental analyzer (LECO CHN628, LECO, USA).

## RESULTS & DISCUSSION

Table 1. HHV, solid yield and energy yield of biocoal from hemp hurd

Property	Value
HHV (MJ/kg)	> 20
Solid yield (%)	38.51 – 67.78
Energy yield (%)	44.49 – 82.02

Table 2. Ultimate composition of biocoal from hemp hurd

Ultimate composition	Value
C (%)	52.18 – 71.04
H (%)	3.89 – 5.53
N (%)	0.93 – 1.20
S (%)	< 0.05

Table 3. Proximate composition of biocoal from hemp hurd

Proximate composition	Value
Moisture (%)	< 5
Volatile matter (%)	28.37– 62.27
Fixed carbon (%)	33.53 – 68.84
Ash (%)	5.30 – 10.17

Table 4. Production cost estimation of biocoal from hemp hurd

Production	Cost (Baht/kg)
Lab scale	~ 1,000
Pilot scale	~ 100

The HHV of biocoal was higher than biomass feedstock and closed to the HHV of lignite and sub-bituminous coal. The solid yield was decreased with increasing temperature and retention time. On the other hand, the HHV of biocoal was increased with increasing temperature and retention time. For ultimate composition, the biocoal consisted of higher carbon content, lower hydrogen content than the biomass feedstock. For proximate composition, the biocoal consisted of higher fixed carbon and lower volatile matter than the feedstock. In addition, ash content in biocoal was higher than that in the feedstocks. These were due to dehydration, devolatilization, and decomposition of hemicellulose, cellulose and lignin during the process [5].

The production cost of biocoal for pilot scale was lower than that for lab scale, indicating that it has possibility for up-scaling biocoal production into industrial scale.

## METHODS

Hemp hurd could be utilized as feedstock for biocoal production. The HHV of biocoal from hemp hurd was more than 20 MJ/kg, which was comparable to sub-bituminous coal. However, hemp hurd has very high cost when compared to other biomass to use as a starting material for biochar production.

## REFERENCES

- [1] PACIFIC PRIME THAILAND. "Everything You Need to Know About Cannabis Usage in Thailand", <https://www.pacificprime.co.th/blog/cannabis-guide-thailand/>, accessed on 9 November 2023.
- [2] M.J. Prins, K.J. Ptasinski, and F.J.J.G. Janssen, "More efficient biomass gasification via torrefaction," *Energy*, Vol. 31, pp. 3458–3470, 2006, doi:10.1016/j.energy.2006.03.008.
- [3] T. R. Sarker, S. Nanda, A. K. Dalai, and V. Meda, "A Review of Torrefaction Technology for Upgrading Lignocellulosic Biomass to Solid Biofuels," *BioEnergy Research*, vol. 14, no. 2, pp. 645–669, 2021, doi: 10.1007/s12155-020-10236-2.
- [4] B. Batidzirai, A. P. R. Mignot, W. B. Schakel, H. M. Junginger, and A. P. C. Faaij, "Biomass torrefaction technology: Techno-economic status and future prospects," *Energy*, vol. 62, pp. 196–214, 2013, doi: 10.1016/j.energy.2013.09.035.
- [5] C. Lokmit, K. Nakason, S. Kuboon, A. Jiratanachotikul, and B. Panyapinyopol, "A comparison of char fuel properties derived from dry and wet torrefaction of oil palm leaf and its techno-economic feasibility", *Mater. Sci. Energy Technol.* Vol. 6, pp. 192–204, 2023, doi:10.1016/j.mset.2022.12.010.

## REFERENCES

This research has received funding support from the NSRF via the Program Management Unit for Human Resources & Institutional Development, Research and Innovation [grant number B13F660064] and funding support from Sukjai Co.,Ltd.



# Kilogram-Scale Production of Metal-Organic Framework Beads for Dehumidification Applications

Siriporn Kosawatthanakun<sup>1</sup>, Supaporn Nualyai<sup>1</sup>, Sanphat Chaonarin<sup>1</sup>, Nonthiya Theesakhu<sup>2</sup>,  
Pongtanawat Khemthong<sup>1</sup>, Kajornsak Faungnawakij<sup>1</sup>, Bunyarat Rungtaweeveranit<sup>1\*</sup>

<sup>1</sup>National Nanotechnology Center (NANOTEC), National Science and Technology Development Agency (NSTDA), Pathum Thani 12120, Thailand

<sup>2</sup>KRUGER ASIA INDUSTRIES (THAILAND) CO.,LTD., Khok Kham, Mueng, Samuthsakorn 74000, Thailand

\*E-mail: bunyarat.run@nanotec.or.th

## Introduction

### ■ Metal-organic frameworks for dehumidification

- Humidity control is crucial to maintaining a building's air quality and to prevent moisture-sensitive product.
- Solid or liquid desiccants are used in traditional systems but they lower moisture uptake capacity than mesoporous materials.
- Metal-organic frameworks (MOFs) are attractive due to large surface area, hydrothermal stability, albeit in different relative pressure, and excellent water adsorption for dehumidification.<sup>[1]</sup>

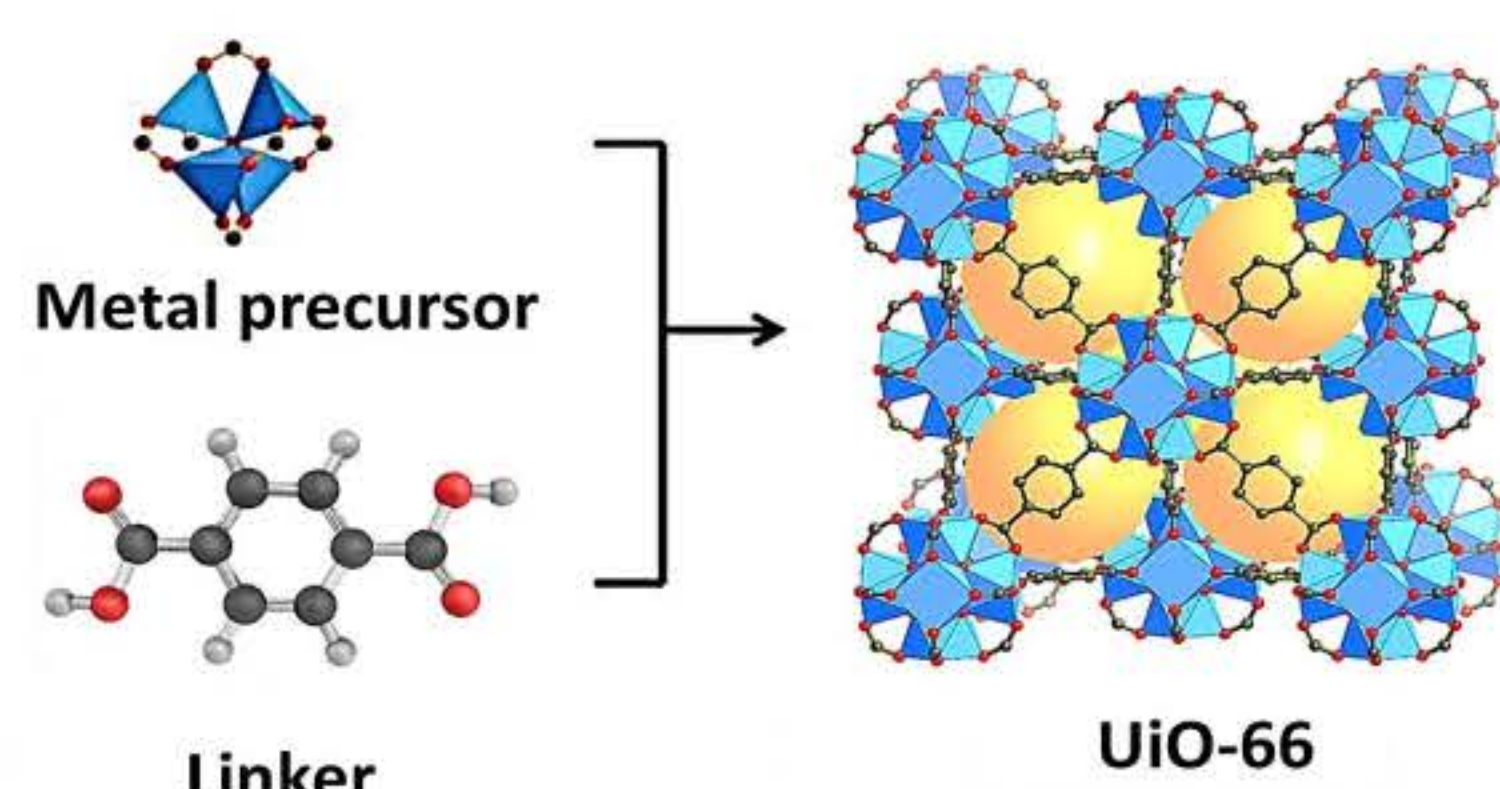
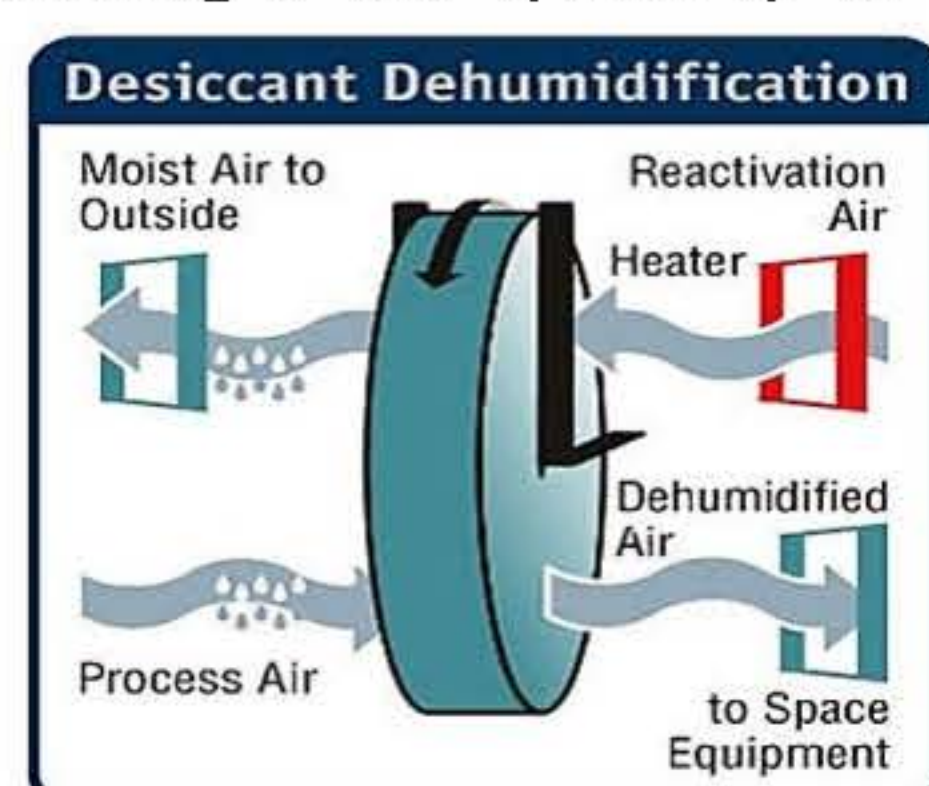


Fig. 1 Synthesis of MOF and Crystal structure of MOFs.<sup>[2]</sup>

### ■ MOF upscaling for industrial application

- Shaping of MOFs (see Fig.2), Beads are commonly formed due to robustness, ease of production, and high hardness tonality.<sup>[3-4]</sup>

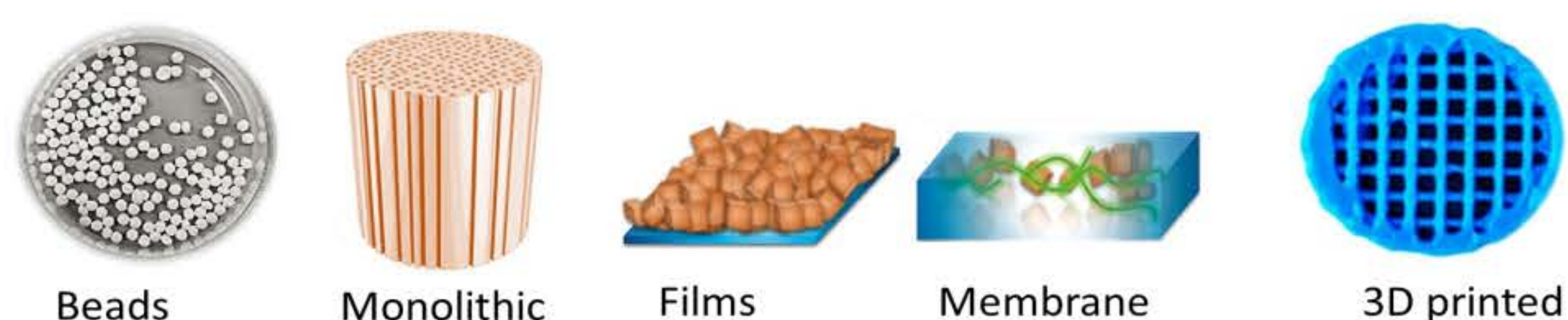


Fig. 2 Examples of MOFs with different shapes.

- In this work aims to investigate the effects of polymer binders on the physicochemical properties of the resulting beads. The production of beads with desired properties were then scaled to produce beads at kilogram scale.

## Results and Discussion

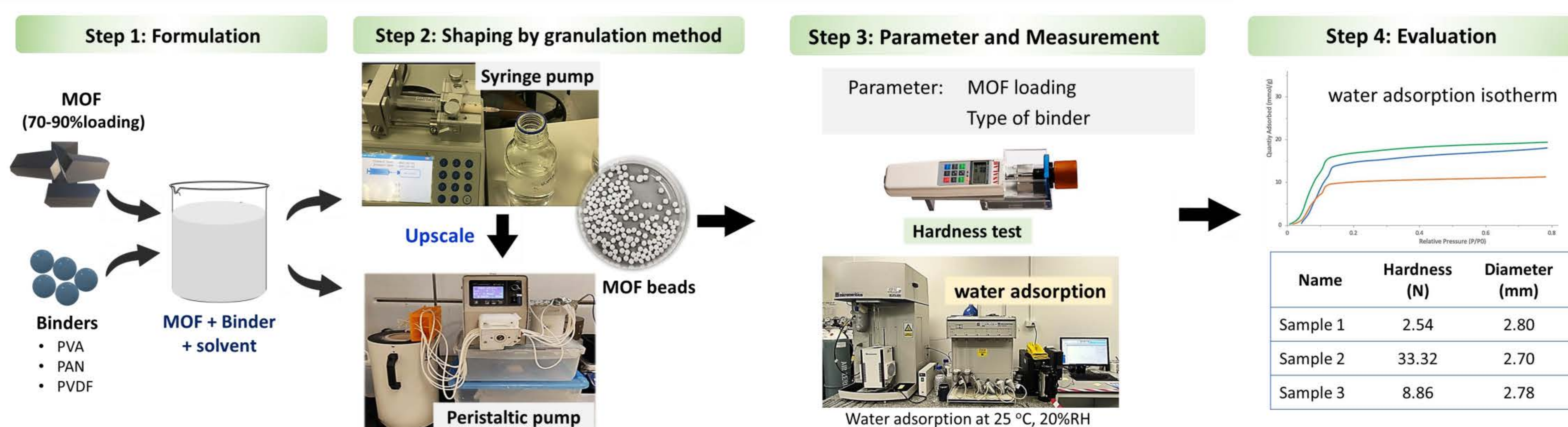
### ■ Effects of binders and MOF loading on water uptake and bead hardness

Conditions					
MOF loading (wt.%)	90	80	90	80	70
Polymer	PAN	PAN	PVDF	PVDF	PVDF
Coagulation solvent	DI water : Ethanol				
Hardness (N)	7.3	9.2	2.1	2.2	3.5
Water uptake at 25 °C, 20%RH ( $\frac{g_{H_2O}}{g_{MOF}}$ )	0.25	0.23	0.24	0.17	0.20

### ■ Continuous flow production of MOF beads on kilogram scale

Conditions			
MOF loading (wt.%)	80		
Polymer	PAN	PVA	PVDF
Coagulation	DI water : Ethanol		
Flow rate (mL/min)	0.50		
Hardness (N)	2.5	33.3	8.9
Water uptake at 25 °C, 20%RH ( $\frac{g_{H_2O}}{g_{MOF}}$ )	0.36	0.31	0.23

## Optimization and kilogram-scale production of MOF-beads



## Conclusions

- The effects of polymeric binders on the water adsorption properties and hardness were investigated.
- PVA was identified as a promising polymer for dehumidification applications.
- MOF beads were then made using a continuous process to produce MOF on a kilogram-scale.

## Acknowledgements

- This research has received funding support from the NSRF via the Program Management Unit for Human Resources & Institutional Development, Research and Innovation [grant number B13F660064]
- KRUGER ASIA INDUSTRIES (THAILAND) CO.,LTD and Nanocatalysis and Molecular simulation Research Group (NCAS) and CAT research team

## References

- [1] Cousin-Saint-Remi et al., *ACS Appl. Mater. Interfaces*, **2019**, 11, 13694–13703.  
[2] Abdel-Mageed et al., *J. Am. Chem. Soc.*, **2019**, 141, 13, 5201–5210.

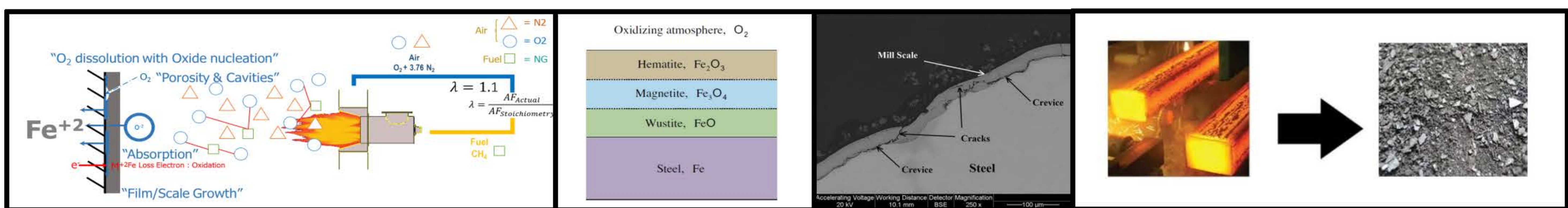
- [3] Dong et al., *Progress in chemistry*, **2021**, 33(12), 2173–2187.  
[4] Lim et al., *ACS Materials Lett*, **2019**, 1, 147–153



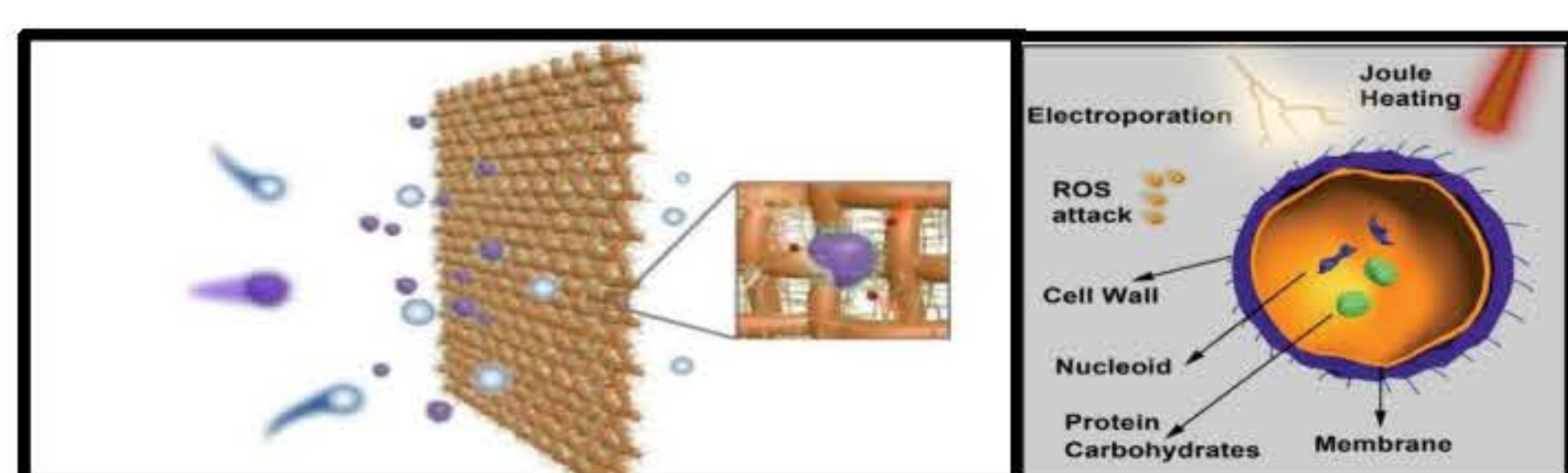
## Upcycling of industrial iron scale waste for reutilization as nanocomposite in environmental remediation: Air conditioner filter coating

**Researcher** Dr. Pitak Ngammuangtueng  
**Principle investigator** Dr. Nuttaporn Pimpha Ms. Thitirat Tancho  
**Co-researcher** Mr. Eknarin Thanayupong Dr. Peerakarn Banjerdki  
**Affiliation** National Nanotechnology Center (NANOTEC), National Science and Technology Development Agency

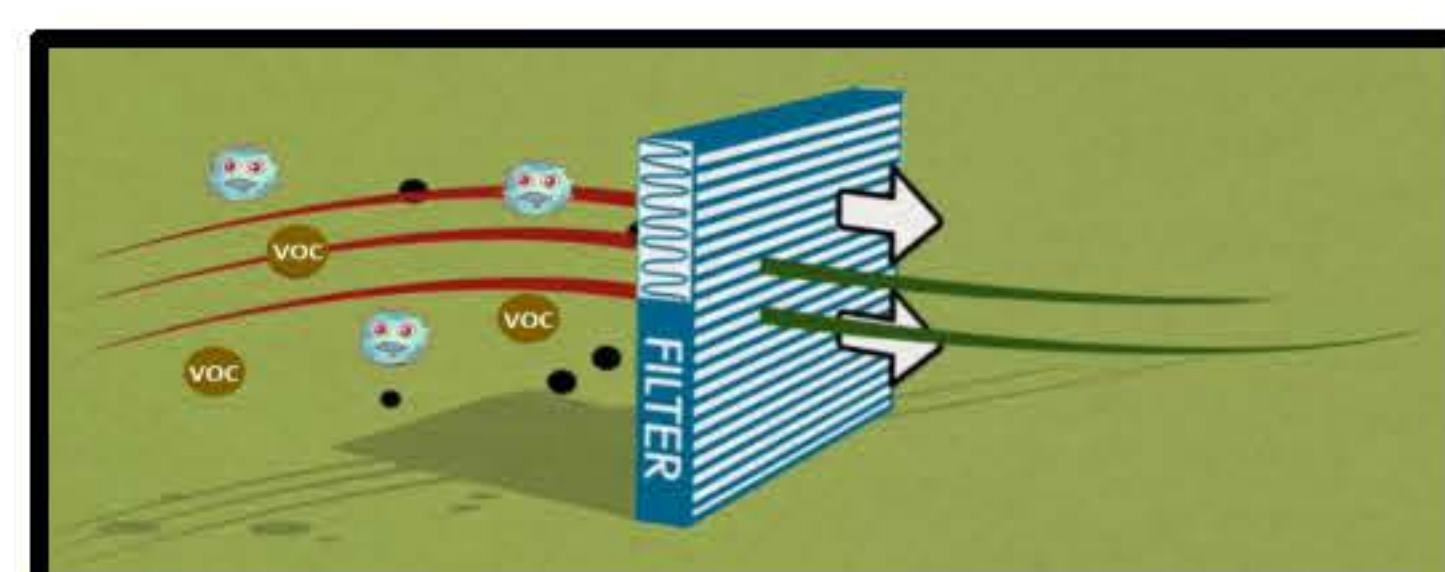
### Introduction and Rationale



- Iron mill scale is a flaky substance that forms on the outer surface of newly or previously heated steel or iron when it cools and oxidizes.
- Production of hot-rolled structural steel can reach **1,100,000 tons** per year. It is estimated that **13,360 tons** of iron mill scale was produced.
- This useful material was once considered a troublesome waste or by-product, but it is currently being repurposed to add value in many ways.

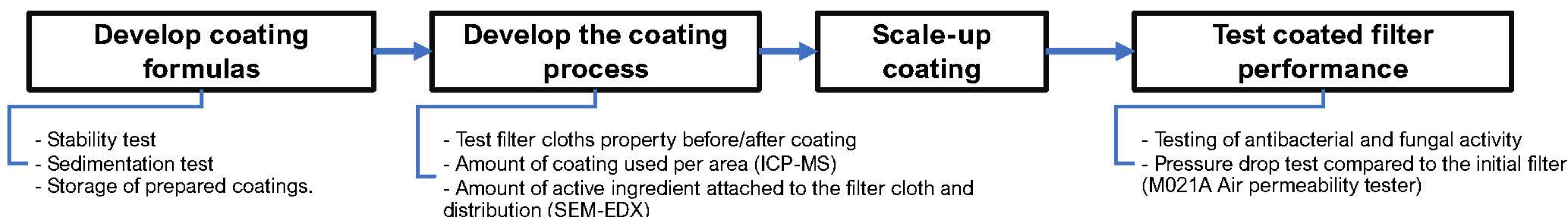


<sup>1</sup>Environ Sci Nano. 2018 May 1; 5: 1096–1106.



- Iron Oxide Nanowire-Based Filter for Inactivation of Airborne Bacteria<sup>1</sup>
- This study aims to add value to industrial waste steel scale for reuse as a nanocomposite material to increase air filter efficiency.

### Methods



### Results & Discussion

#### Filter property test

- The study result of 2 filter cloth groups (A and B) and 2 coating formulas (F1 and F2) indicated that both group A and B fibers have basically hydrophobic property implied from the contact angle test (Fig.1) and FTIR-ATR analysis (Fig.2).

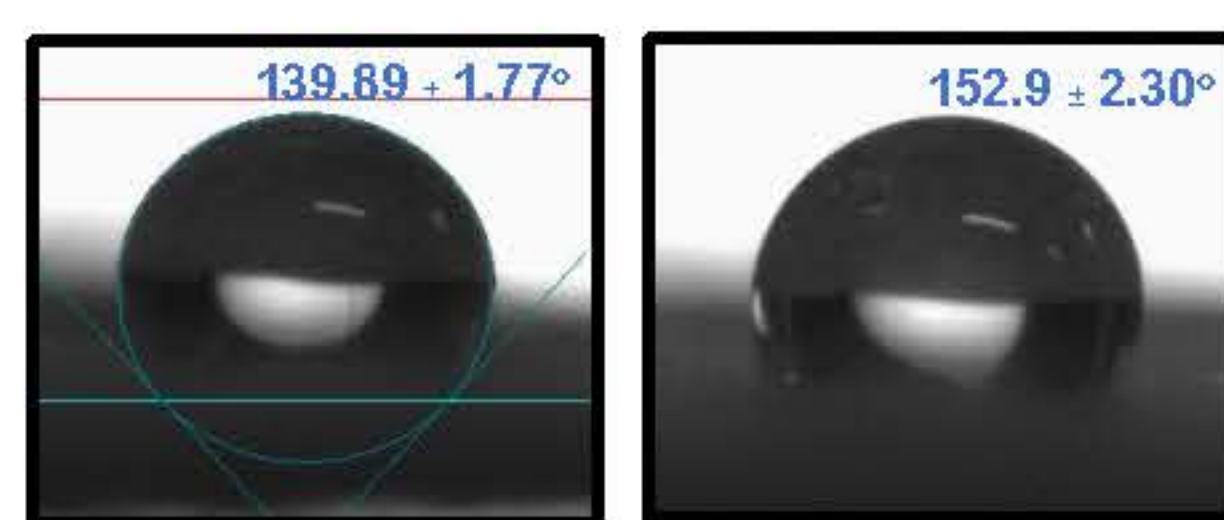


Fig.1 Contact angle of group A and B filter before coating

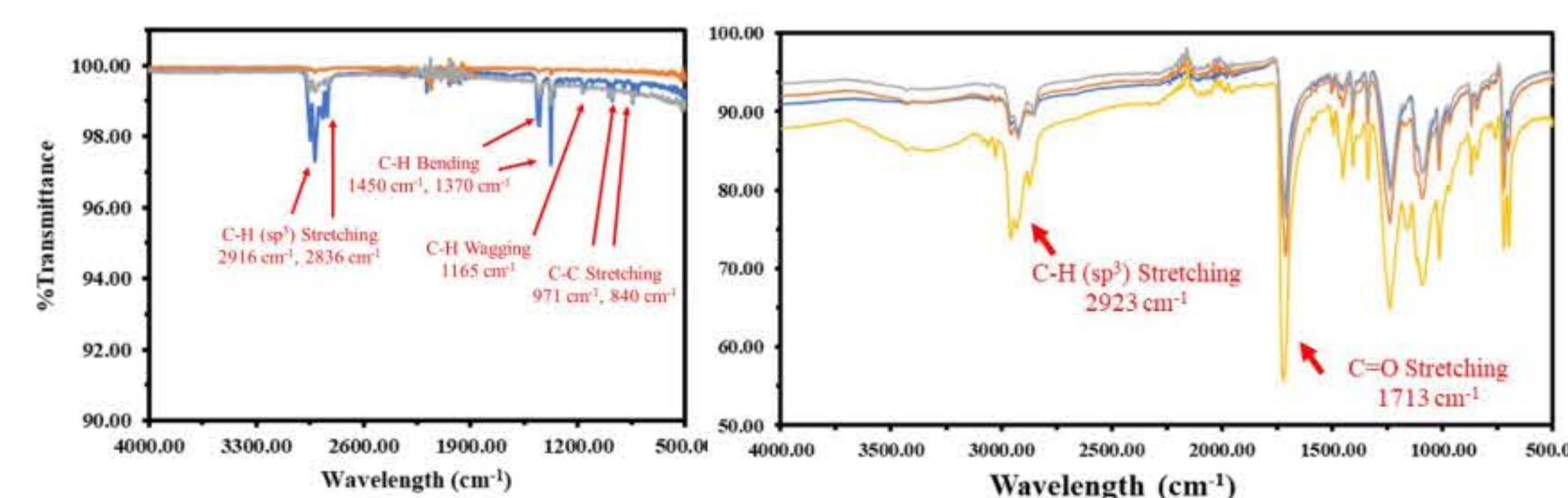


Fig.2 FTIR-ATR of group A and B filter before coating

- After coating process, the F1 coating makes both groups of fibers more hydrophilic properties. However, this property might affect the implement possibility due to the chance of humidity increasing in the filter.
- Coating F2 makes filter group A and B more hydrophilic (Fig.3) but still quite hydrophobic (Fig.4) while keep binding property of iron mill scale and other actives (Fig.5 SEM-EDX, ICP-MS). This makes F2 formula has better than F1 in case of making an air filter.

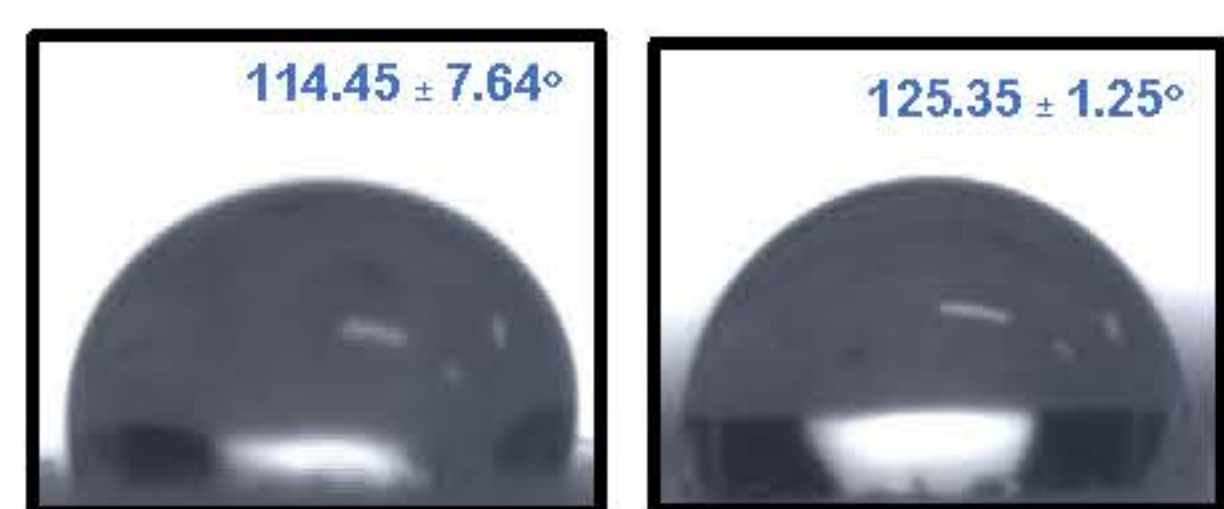


Fig.4 Contact angle of group A and B filter after F2 coating

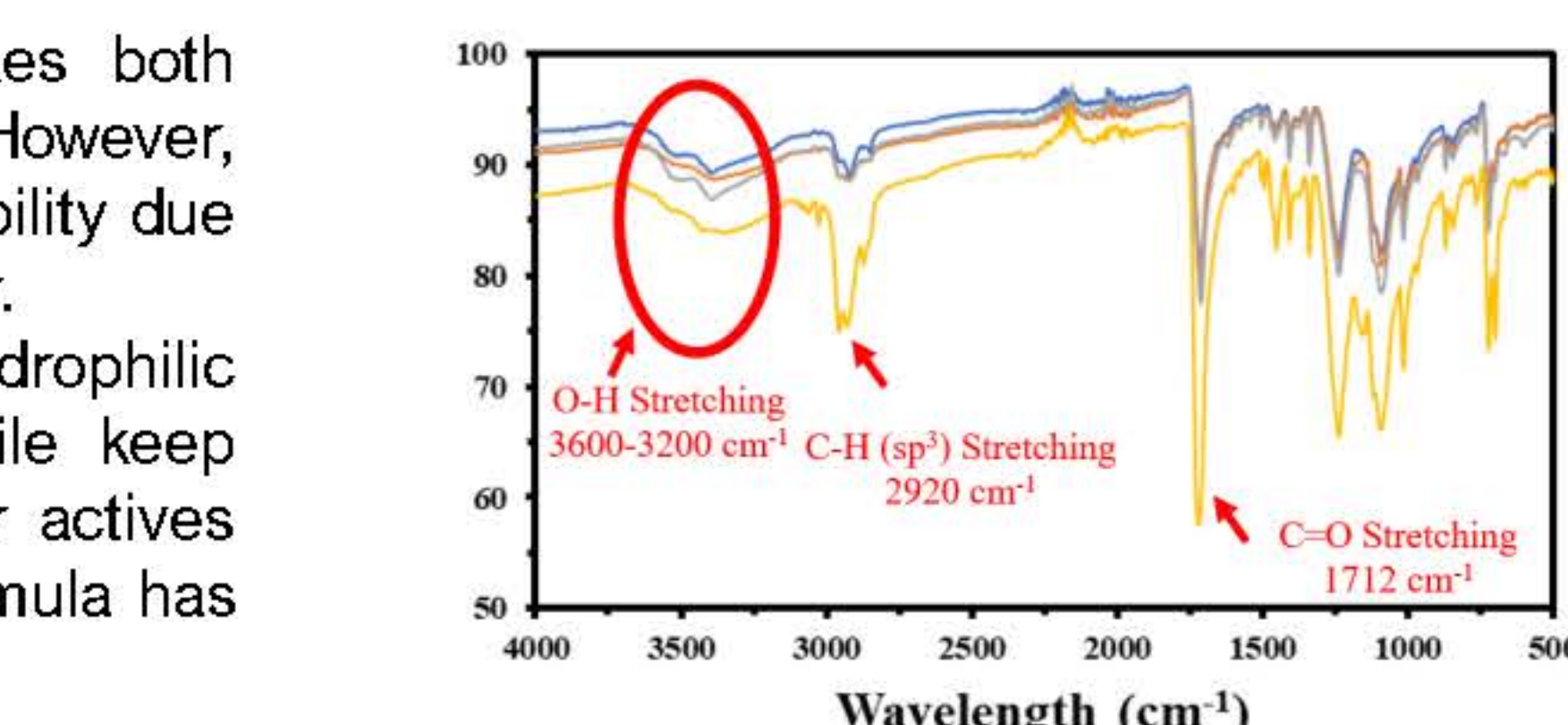


Fig.3 FTIR-ATR of B filter after coating

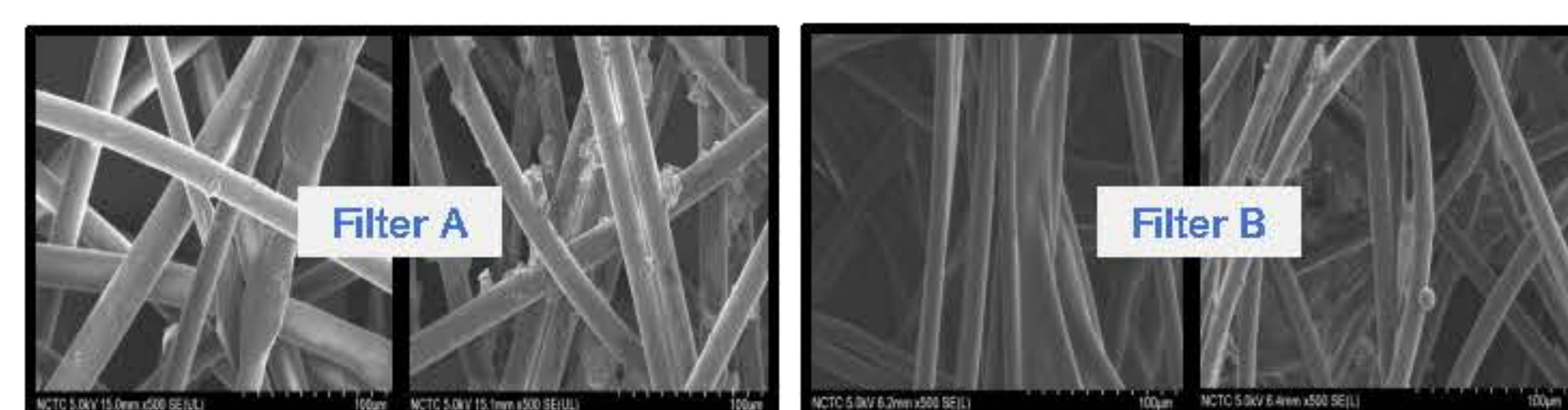


Fig.5 SEM-EDX of group A and B filters before and after F2 coating

#### Anti fungal and bacteria test

- After coating with F2 coated, only filter B can stop an *A. niger* growth (Fig. 6). In addition, filter B with F2 coated can stop the growth of *S. aureus* (7.6 cm clear zone), and *K. pneumoniae* (7.9 cm clear zone) (Fig. 7).

Fiber group	Formula 1		Formula 2	
	Fungal	Bacteria	Fungal	Bacteria
A	O	-	X	-
B	-	-	O	O

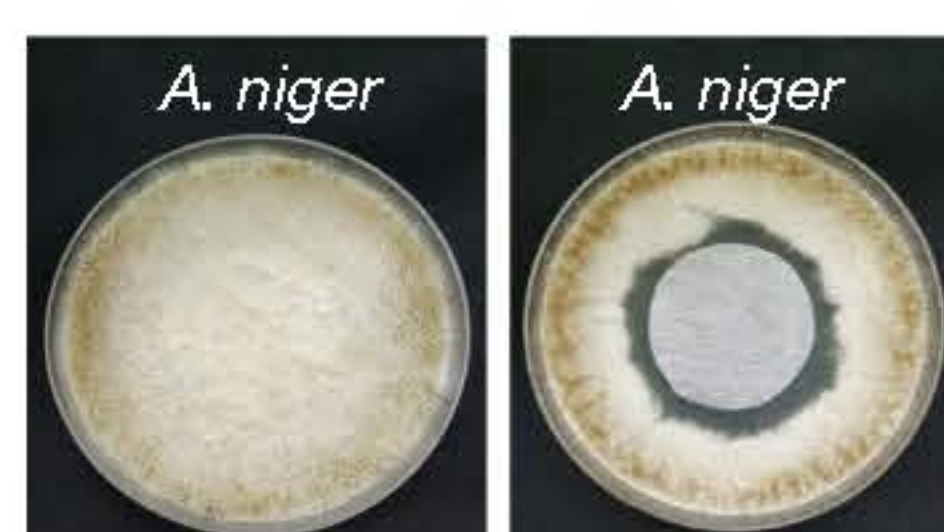


Fig. 6 Filter cloth B fungal test

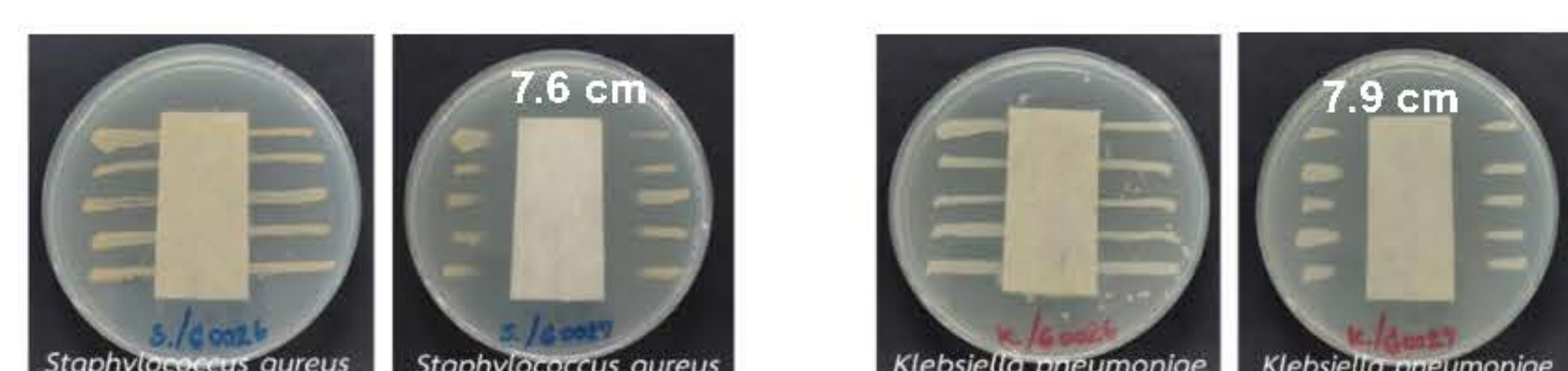


Fig. 7 Filter cloth B bacterial test

#### Air permeability test

- Filter B with F2 coated has reduced the air permeability 18.9% (Fig. 8).

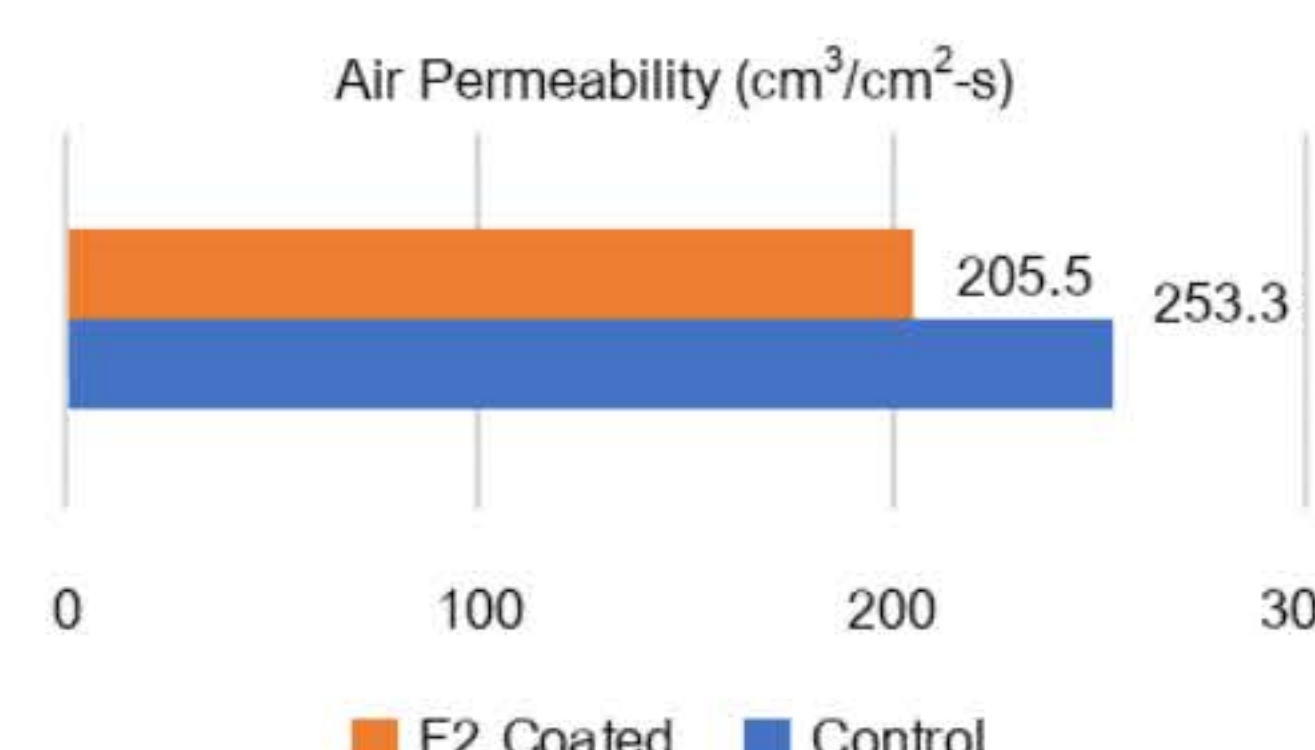


Fig. 8 Air permeability test of filter B

### Conclusion

Filter group B coated with the F2 coating formula has excellent physical properties and anti-fungal/bacterial capabilities, moreover, air permeability is reduced by just 18.9%. As a result, this form of coated filter is more suited for application in large-scale manufacturing.

### Acknowledgements

This research has received funding support from the NSRF via the Program Management Unit for Human Resources & Institutional Development, Research and Innovation [grant number B13F660064]



# Fabrication of Monolithic Metal-Organic Frameworks for Dehumidification Applications

Supaporn Nualyai<sup>1</sup>, Bunyarat Rungtaweeworanit<sup>1</sup>, Pongtanawat Khemthong<sup>1</sup>,  
Kajornsak Faungnawakij<sup>1</sup>, Sanpas Chaonarin<sup>1</sup>, Pawan Boonyoung<sup>1</sup>, Nonthiya Theesakhu<sup>2</sup>

<sup>1</sup>National Nanotechnology Center (NANOTEC)

<sup>2</sup>Kruger Asia Industries (Thailand) co. ltd

## Introduction

The imperative need for effective humidity control in diverse industrial sectors has fueled the exploration of innovative materials to enhance dehumidification technologies. Among these materials, metal-organic frameworks (MOFs) have garnered attention for their remarkable surface area, tunable structures, and moisture adsorption capabilities. However, to utilize MOFs, they must be shaped to prevent dusting. This work, thus, focuses on the scale up production of MOF powder to sub-kg scale and their shaping into monolithic form.

## Methodology

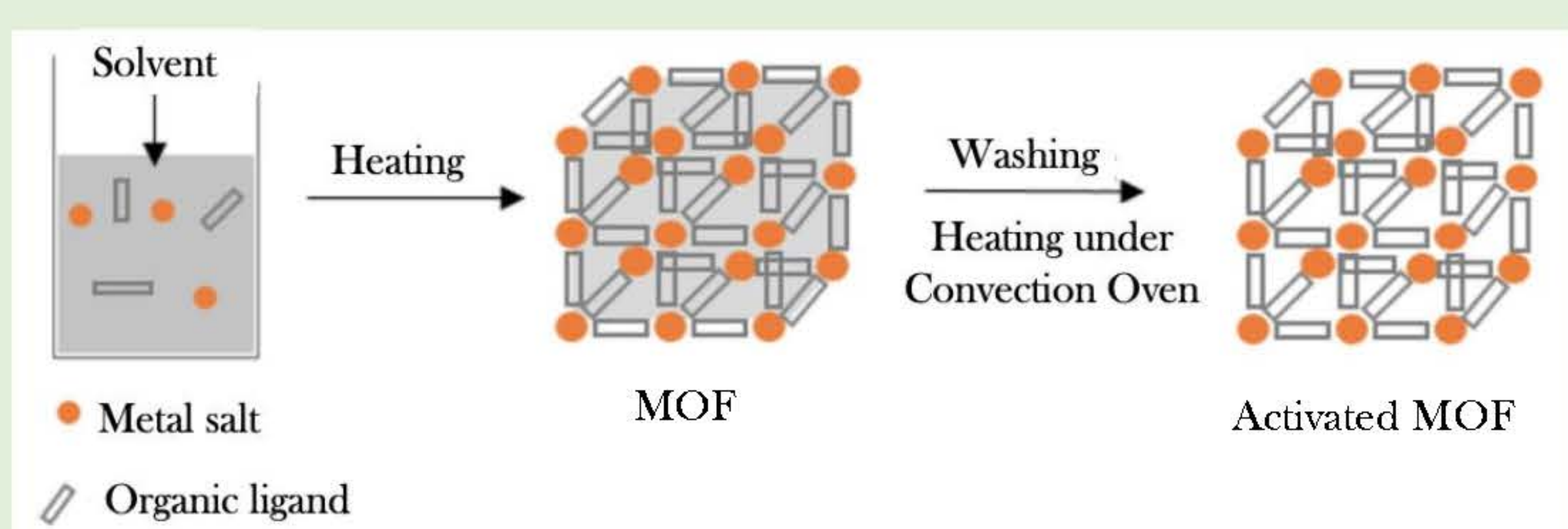


Figure 1. Synthesis of MOF powder.

## Results and discussion

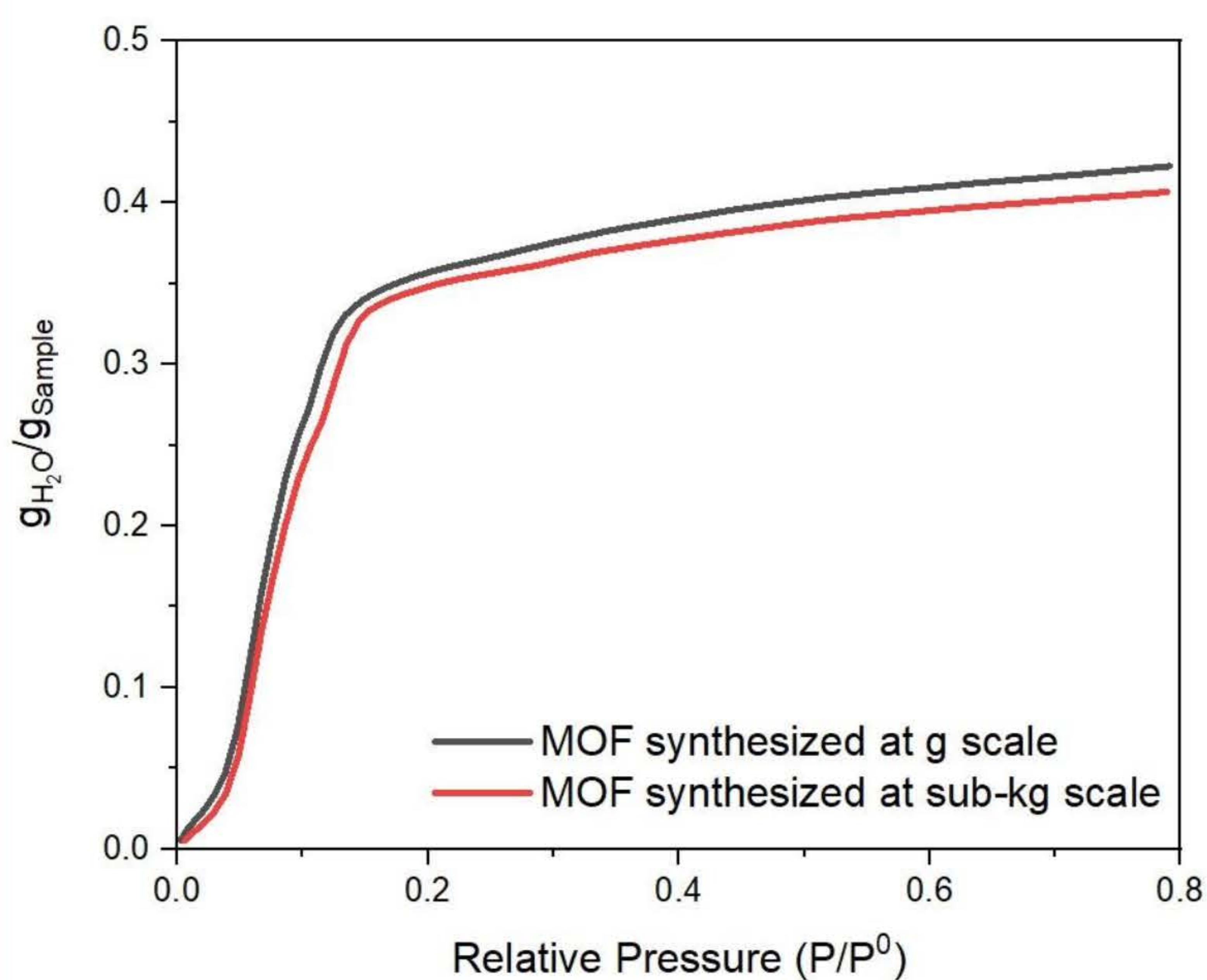


Figure 2. Water adsorption isotherms collected at 25 °C of MOF prepared at lab scale compared to MOF synthesized at sub-kg scale

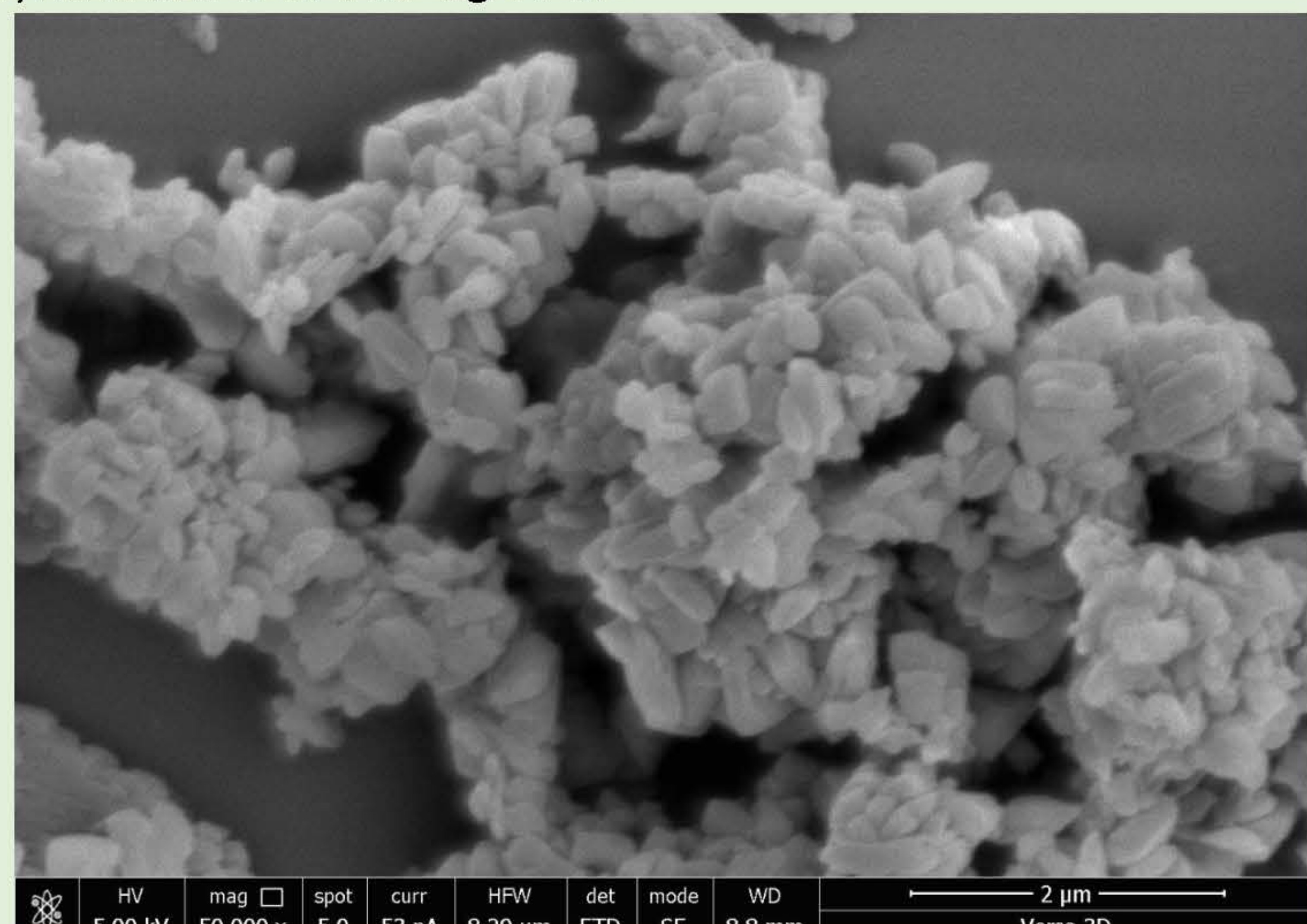


Figure 3. SEM image showing crystals of MOFs prepared at sub-kg scale

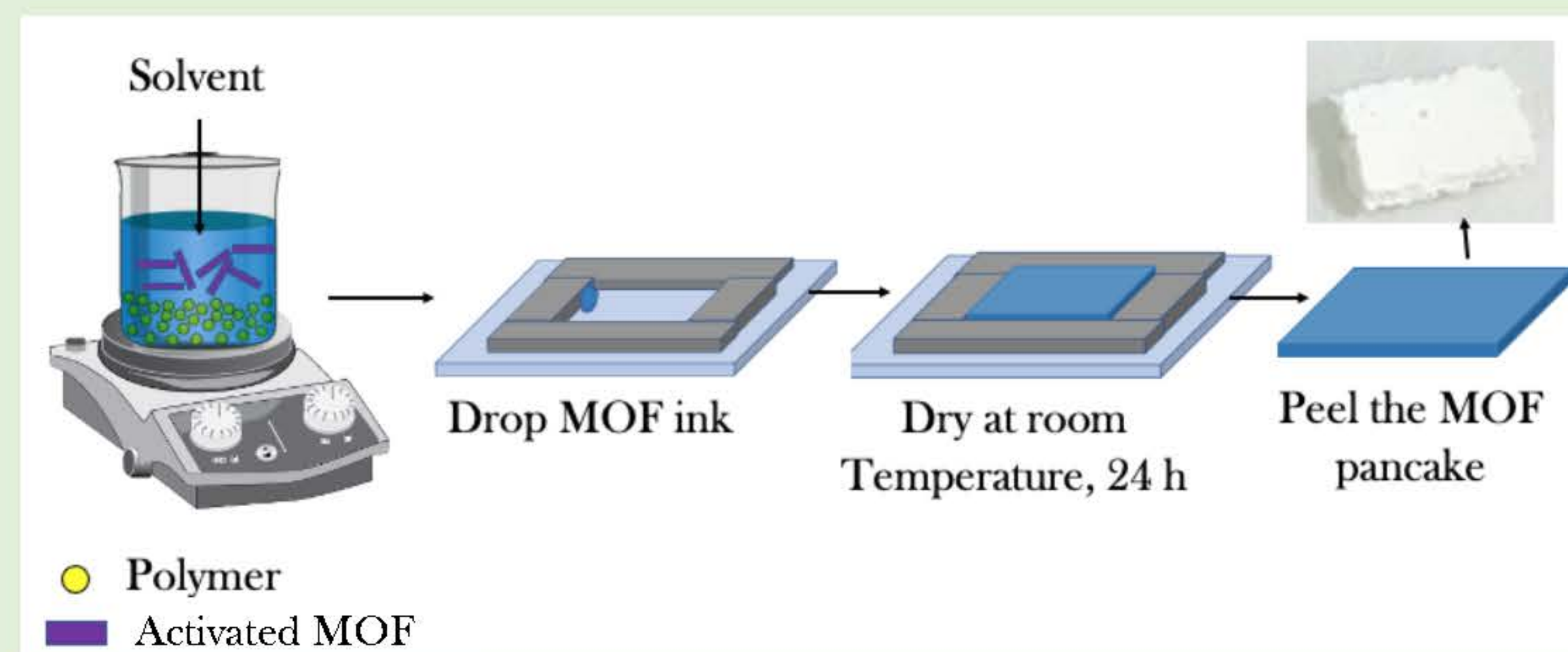


Figure 4. Fabrication of monolithic MOF.

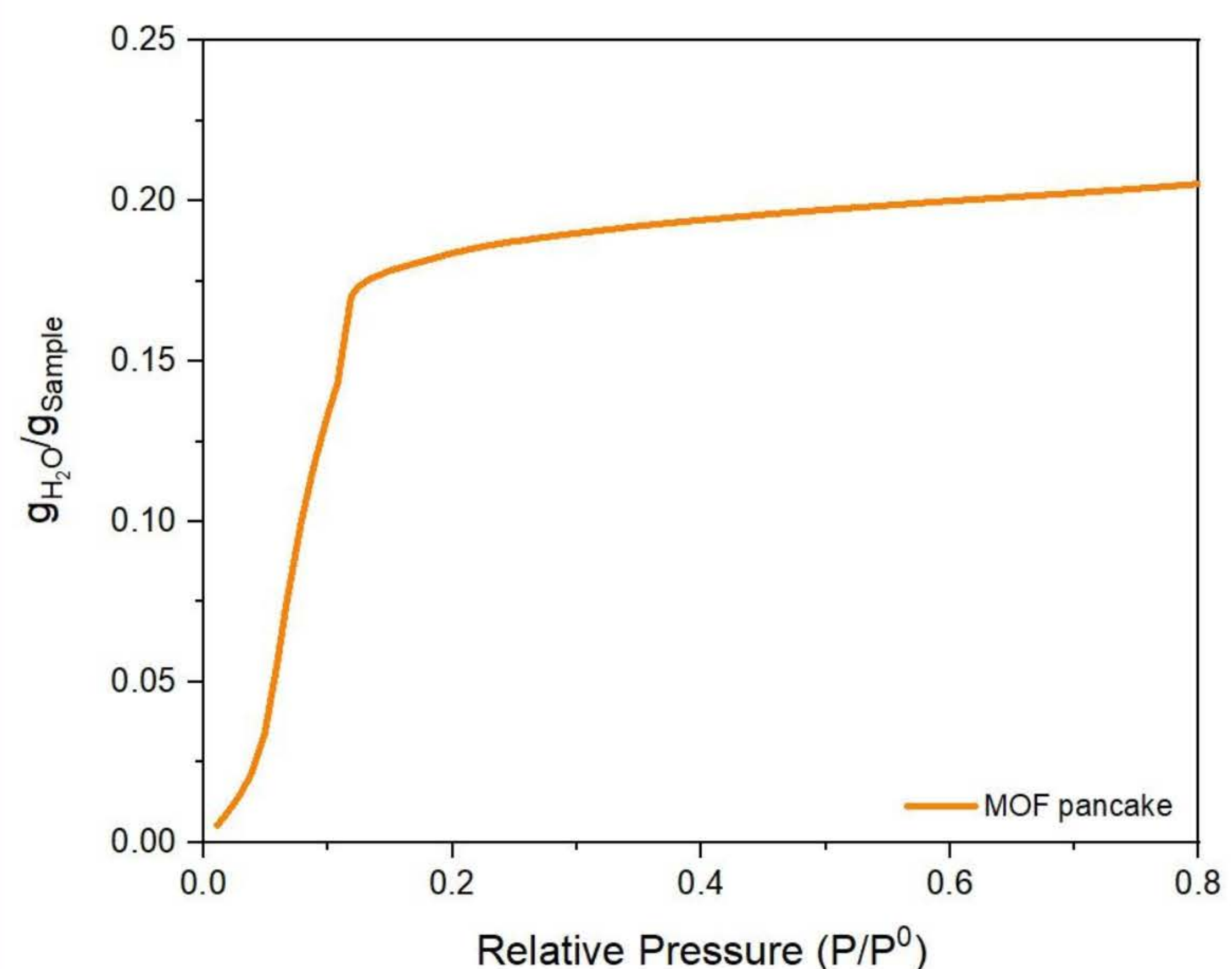


Figure 5. Water adsorption isotherm of monolithic MOF.

## Conclusion

Synthesis of MOF was scaled up from gram to sub-kg scale while the water uptake capacity remained similar. The MOF powder was then shaped into monolithic structure by mold casting technique which shows slightly decreased water uptake capacity due to the additional weight of the binder.

## Acknowledgements

This research has received funding support from the NSRF via the Program Management Unit for Human Resource & Institutional Development, Research and Innovation [grant number B13F660064]



# Feasibility study on utilization of hemp hurd as nanolignocellulosefiber

Pornnapa P Ipattanaporn, Wasawat Kraithong, Wanwitoo Wanmolee and Pongtanawat Khemthong

Nanocatalysis and Molecular Simulation Research Group, National Nanotechnology Center (NANOTEC),  
National Science and Technology Development Agency (NSTDA), Pathum Thani 12120, Thailand

## Abstract

Lignocellulosic biomass, is more than 40% in the plant dry matter, can be used to produce lignocellulose nanofibers (LCNFs) for a variety of applications such as in the biomedical, food, cosmetics, construction, automotive and aerospace industries. It mainly consists of cellulose, hemicellulose, and lignin of which properties pose challenges to specific applications. Therefore, it is necessary to study the composition and properties of the hemp hurd. This project has studied the physical properties and chemical properties of biomass from hemp hurd, and also studied the feasibility of hemp hurd as a precursor to produce LCNFs. The results of the study in this project found that hemp hurd can be used as a precursor for the production of the LCNFs with an average diameter of less than 100 nanometers.

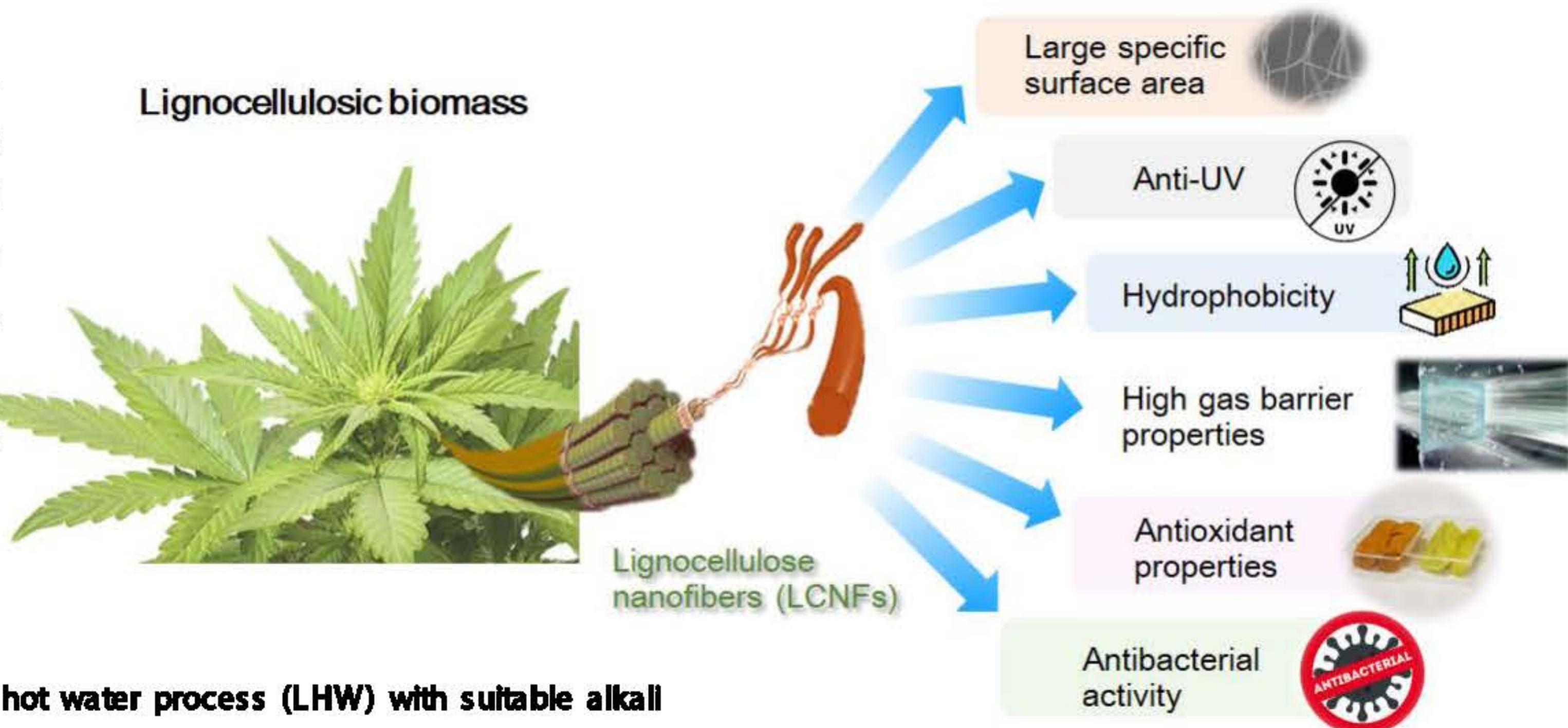


## Introduction

After the Ministry of Public Health announced that the parts of hemp are grown or produced in the country such as leaves (not attached to the inflorescence), branches, stalks, trunks, bark, roots and fibers, including seeds, oil and seed extract that the extracts contain Cannabidiol (CBD) as a component and the remaining residue from extraction must contain no more than 0.2% of Tetrahydrocannabinol (THC). These are not classified as a category 5 narcotic and can be used for medical purposes, research study for health products and others on December 15, 2020.<sup>[1]</sup> As a result, many areas are supporting the cultivation of hemp and it has become a new type of economic crop especially industrial pharmaceutical products, cosmetic products, food products, beverage products and dietary supplement products, paper products, etc. Therefore, hemp is being studied in more details both physical properties and chemical properties in the present due to it can be used in every part.

Production of bio-based materials (lignocellulose nanofibers; LCNFs) can improve mechanical properties. The heart of the process is to depolymerize lignocellulose to nano-level fibers. As a result, it is suitable for use as a reinforcing material and composite material to replace or compound with polymer materials, metals, and alloys including bio-based materials in the biomedical field.<sup>[2,3]</sup> For this work, the production of the LCNFs from hemp hurd requires chemical treatment to reduce the structural strength and resulting in high-purity of cellulose before being reduced into nano-scale fibers. Moreover, the processes required to condition and reduce biomass as well as the efficiency and ability to bring other elements that are not cellulose to be used as co-products were studied.

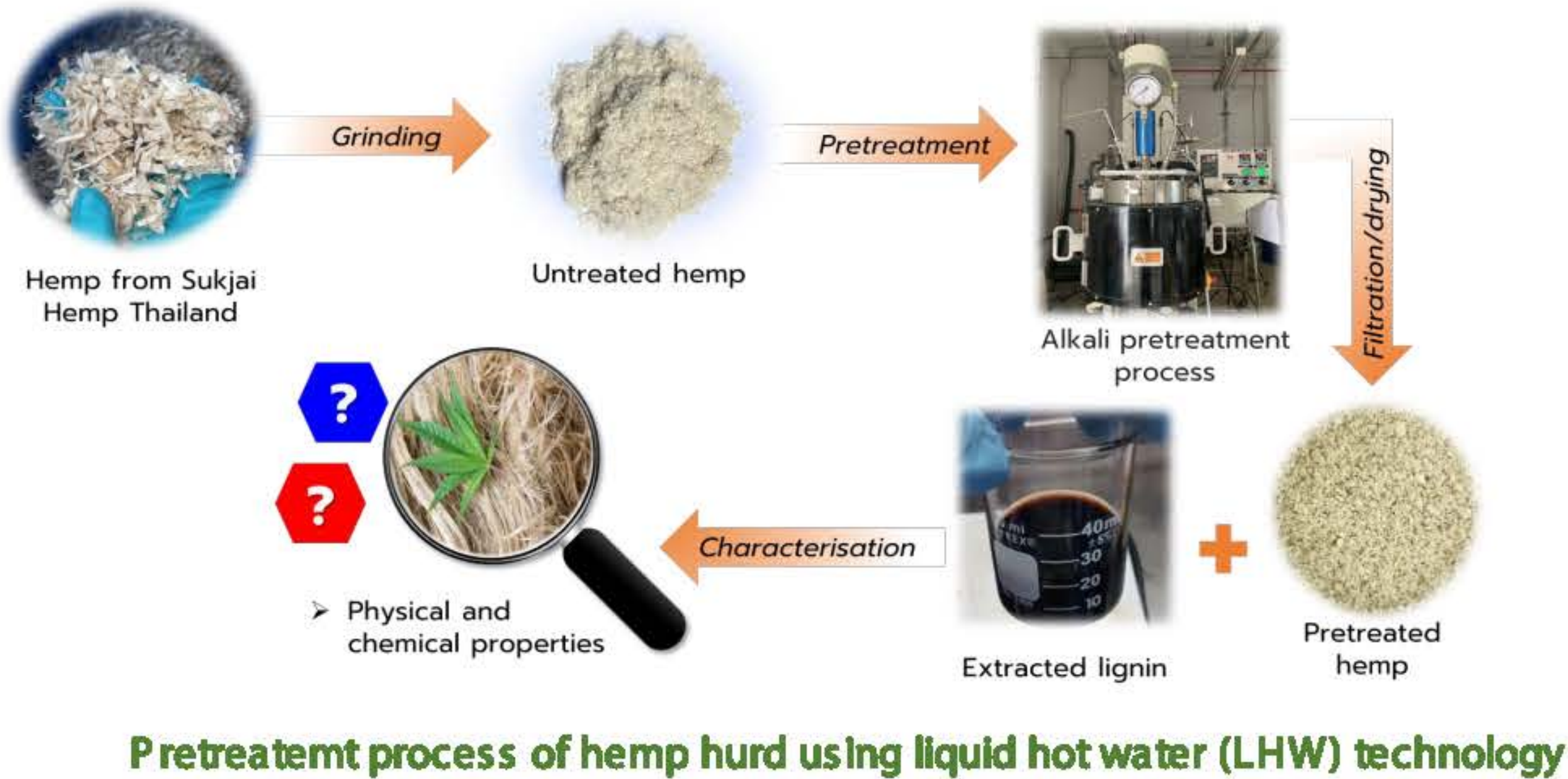
Lignocellulosic biomass



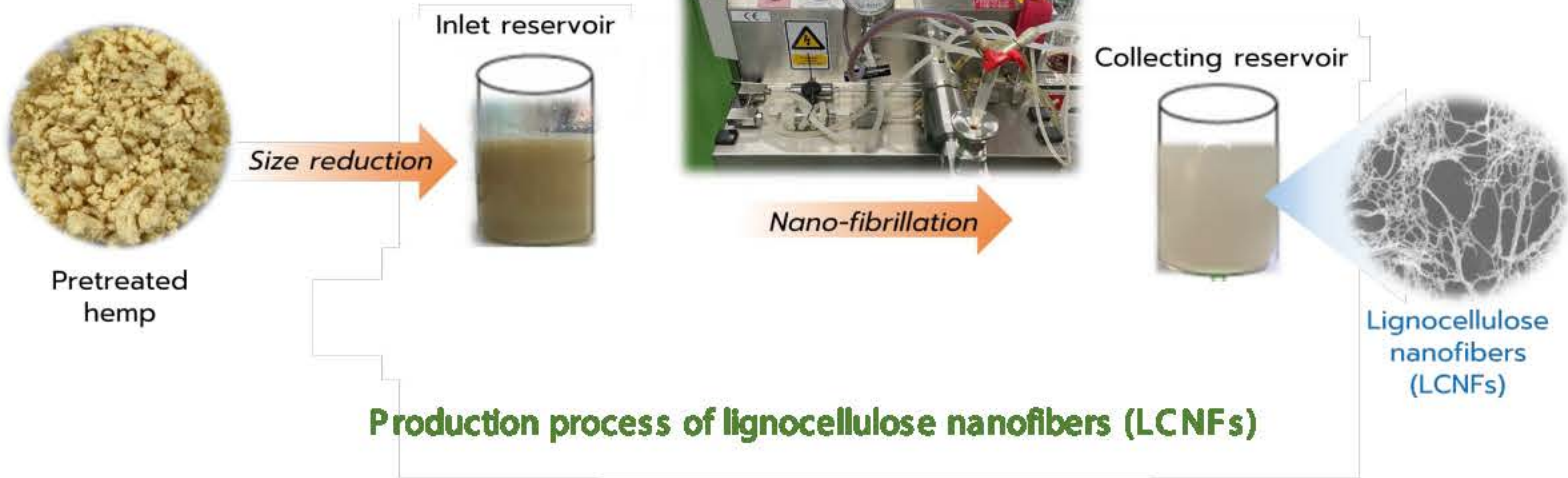
## Methods

**LCNFs production:** Dry hemp hurd was crushed into small sizes and adjusted the condition by the liquid hot water process (LHW) with suitable alkali concentration, temperature, time and water to biomass ratio. Upon completion of the reaction, rapid temperature reduction (quenching) was performed. The resulting products were filtrated to separate the pretreated hemp (solid) from the alkali solution containing hemicellulose and lignin. The pretreated hemp was washed with DI water to remove remaining any alkali until it was neutral.

The drying pretreated hemp was mixed with DI water at a concentration of 2% by weight. And then, the mixture was blended to reduce size by using a high-speed blender (Microfluidizer) until the LCNFs were obtained.



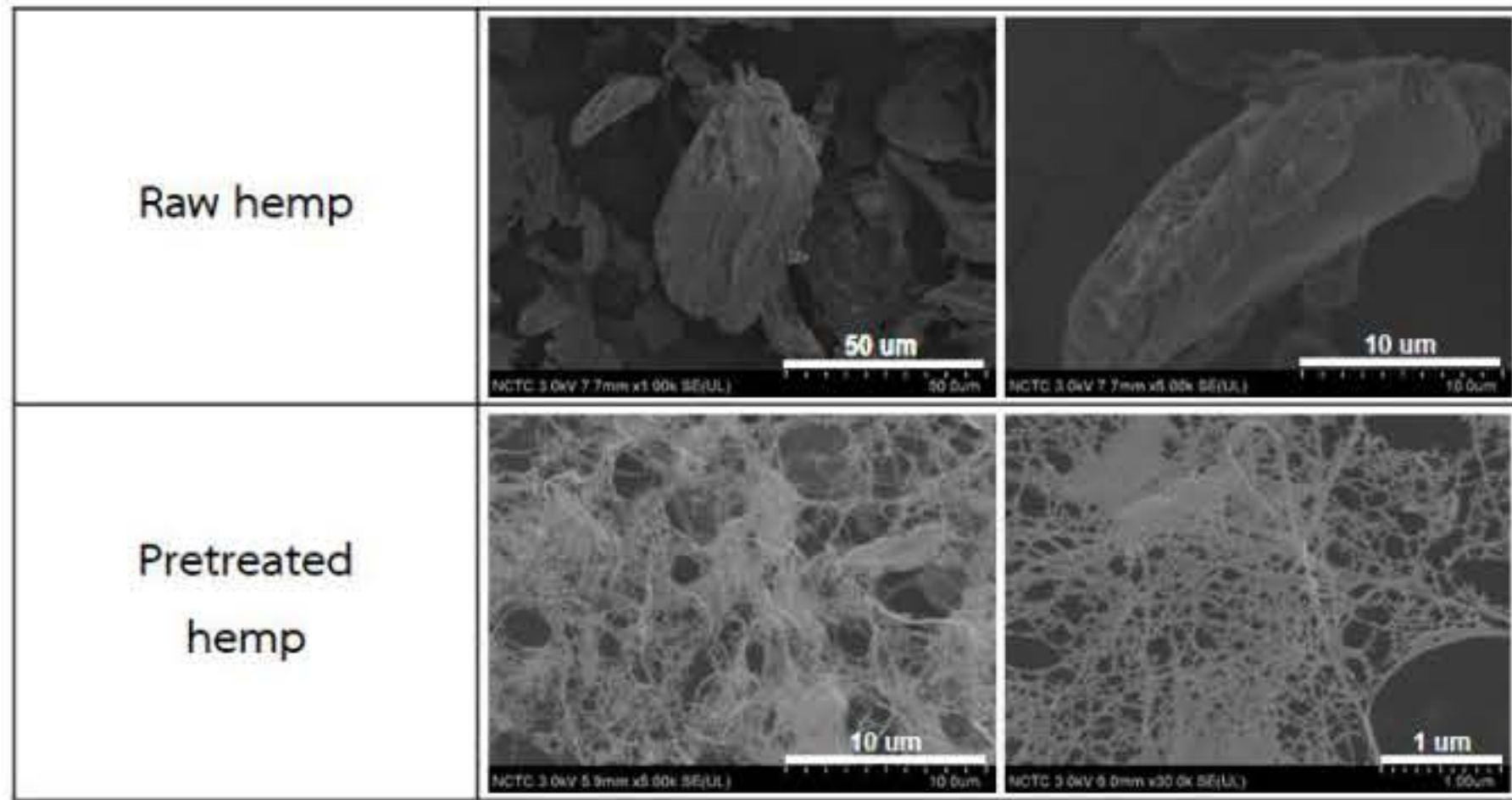
Production process of lignocellulose nanofibers (LCNFs)



## Results & Discussion

The results of component analysis before and after pretreatment of hemp stem with the LHW process and the suitable condition by using NREL technique are shown that hemicellulose and lignin contents of hemp were significantly reduce and obtained cellulose with the highest purity to 95% by weight. The morphology study of prepared lignocellulose nanofibers (LCNFs) by SEM was found that it has an average size of approximately 25 nanometers.

Materials	Solid yield (%)	Composition (%)			
		Cellulose	Hemicellulose	Lignin	Ash
Raw hemp	100	~40	~20	~26	~4
Pretreated hemp	30-40	75-85	8-10	5-20	1-2



The images of prepared lignocellulose nanofibers (LCNFs) by Scanning electron microscopy (SEM)

## Conclusion

Hemp stem can be produced the lignocellulose nanofibers (LCNFs) using the liquid hot water technology (LHW) combined with alkali pretreatment that able to remove ash, hemicellulose and lignin up to 90%, 80%, and 90% by weight, respectively. And the prepared LCNFs by Microfluidizer has an average size lower 100 nanometers.

## References

- [1] Hemp from Wikipedia The Free Encyclopedia. Retrieved 17 July 2022. Accessible from: <https://th.wikipedia.org/wiki/%E0%B8%81%E0%B8%B1%E0%B8%8D%E0%B8%8A%E0%B8%87>
- [2] R.J. Moon, A. Martini, J. Nairn, J. Simonsen, J. Youngblood, Cellulose nanomaterials review: Structure, properties and nanocomposites, 2011.
- [3] N. Lavoine, I. Desloges, A. Dufresne, J. Bras, Microfibrillated cellulose - Its barrier properties and applications in cellulosic materials: A review, Carbohydr. Polym. 90 (2012) 735 -764.

## Acknowledgements

This research has received funding support from the NSRF via the Program Management Unit for Human Resources & Institutional Development, Research and Innovation [grant number B13F660064] and Hemp by Sukjai co.,Ltd.



# Development of 316L stainless steel filament for metal 3D printing to produce lattice structure parts

Natthaphat Parsompech, Chanun Suwanpreecha, Bongkot Hararak, Charinee Winotapun, Siwat Linjee, Sukrit Songkuea, Anchalee Manonukul\*  
National Metal and Materials Technology Center (MTEC), National Sciences and Technology Development Agency (NSTDA), 111 Thailand Science Park, Klong Luang, Pathumthani 12120, Thailand

## Introduction

A lattice structure is an interconnected porous structure characterised by a large specific surface area, low material consumption, and weight control through volume fraction management. These structures are challenging to produce using conventional processes. Moreover, there is very limited study investigating the manufacture of lattice structures using the material extrusion additive manufacturing (MEX) technique. This project, therefore, aims to investigate the macro- and microstructure, defects, as well as the mechanical properties of 316L stainless steel lattice structures produced by MEX.

## Experimental procedures

The 316L filament was in-house developed and utilised for fabricating lattice specimens. The overall processing is shown in Fig. 1.

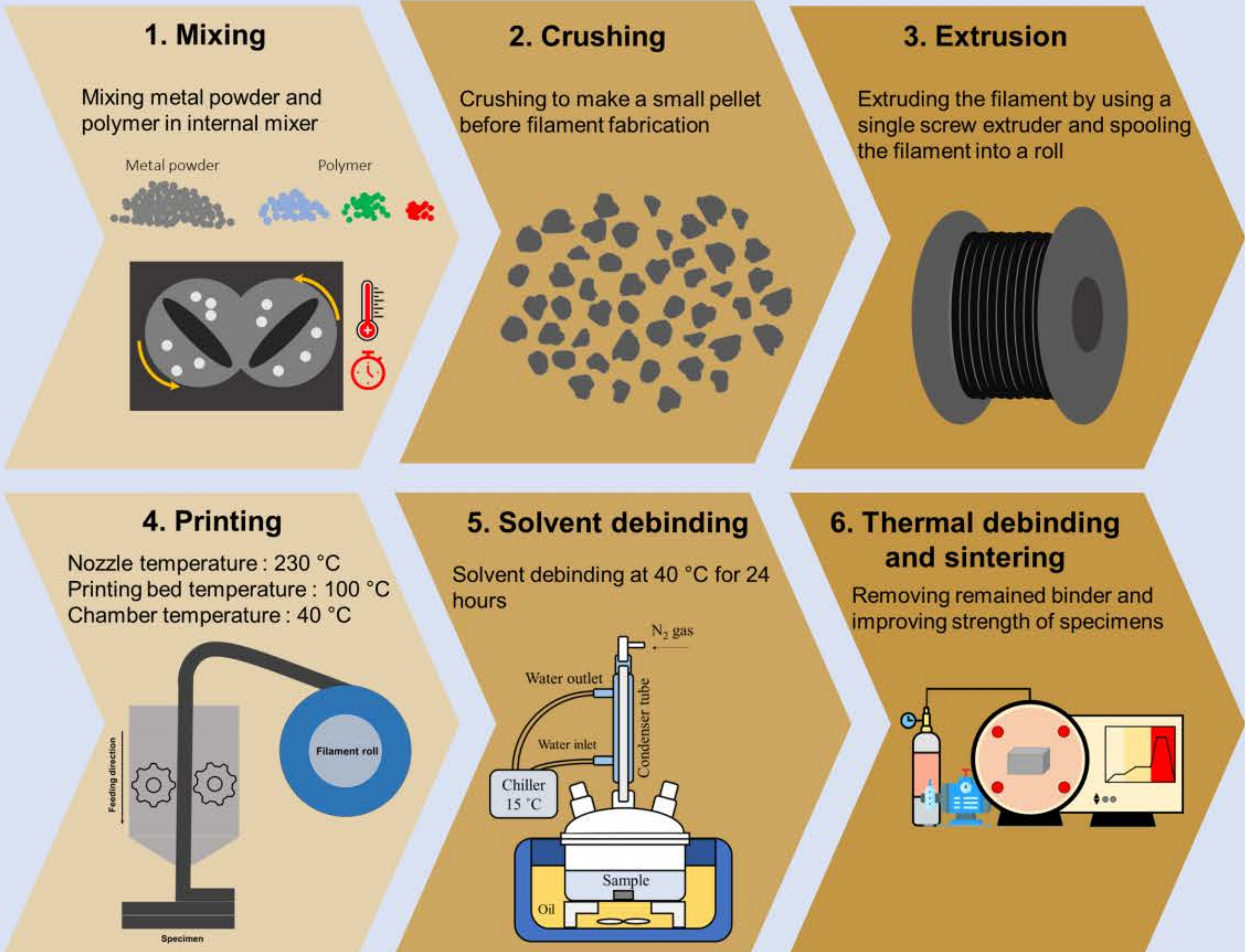
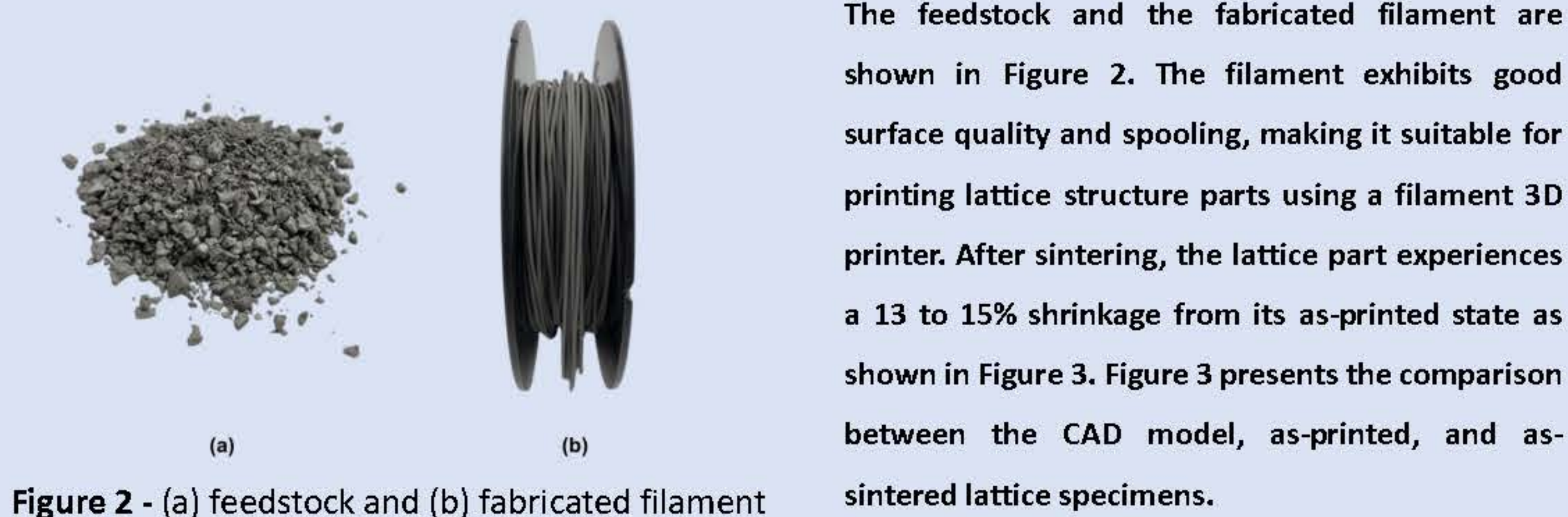


Figure 1 - Feedstock and specimen fabrication processes

## Results and discussion



The feedstock and the fabricated filament are shown in Figure 2. The filament exhibits good surface quality and spooling, making it suitable for printing lattice structure parts using a filament 3D printer. After sintering, the lattice part experiences a 13 to 15% shrinkage from its as-printed state as shown in Figure 3. Figure 3 presents the comparison between the CAD model, as-printed, and as-sintered lattice specimens.

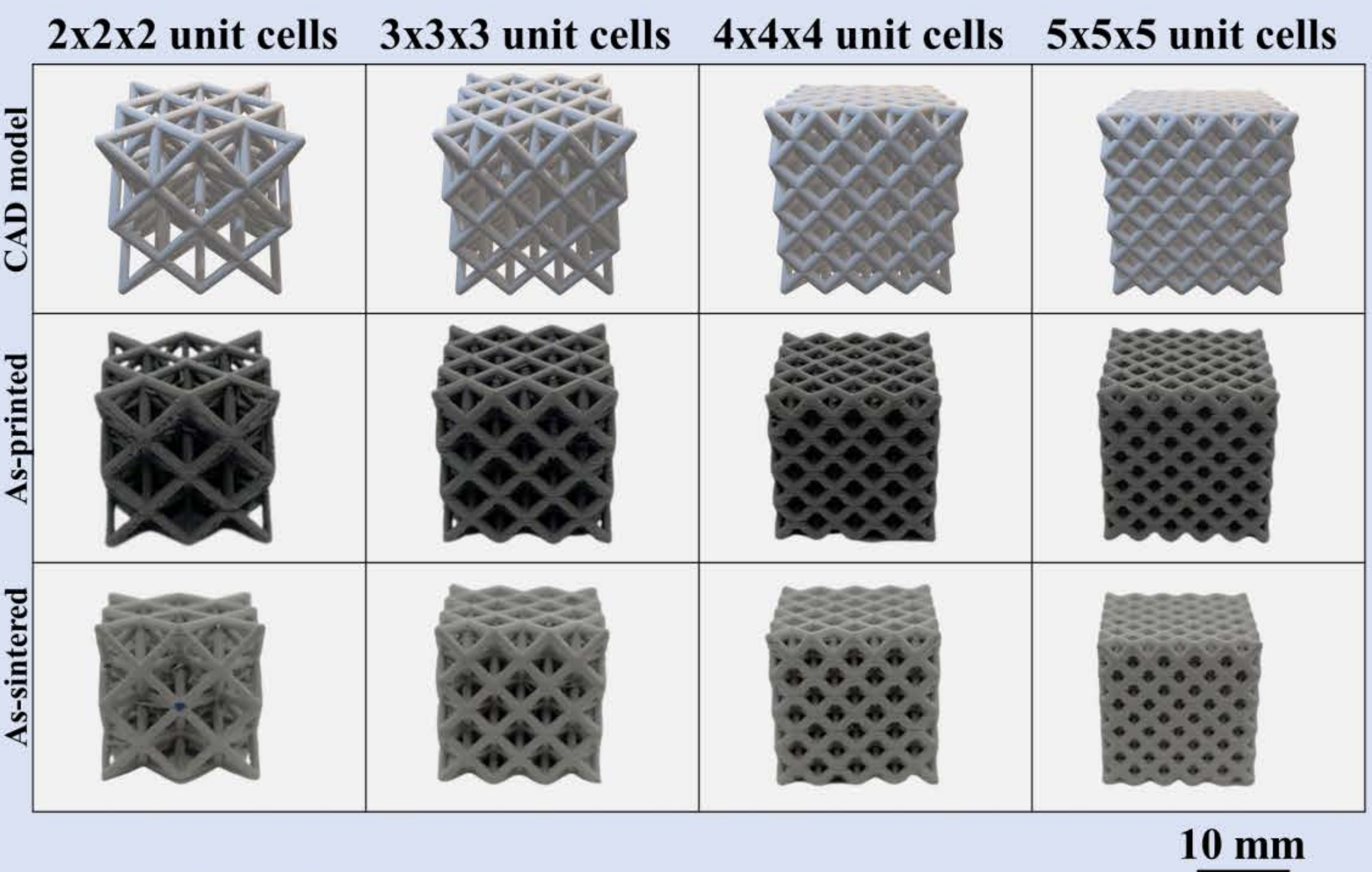


Figure 3. The comparison between CAD model, as-printed and as-sintered parts

The mechanical properties of the as-sintered specimens were determined through compressive testing. At the moment, only 3x3x3 unit cells were tested with different loading directions, i.e. (i) printing direction (PD) is parallel to compression direction (CD) and (ii) PD is perpendicular to CD, as shown in Figure 4(a). The compressive stress vs strain curves are expressed in Figure 4 (b). The results show high repeatability in both loading directions.

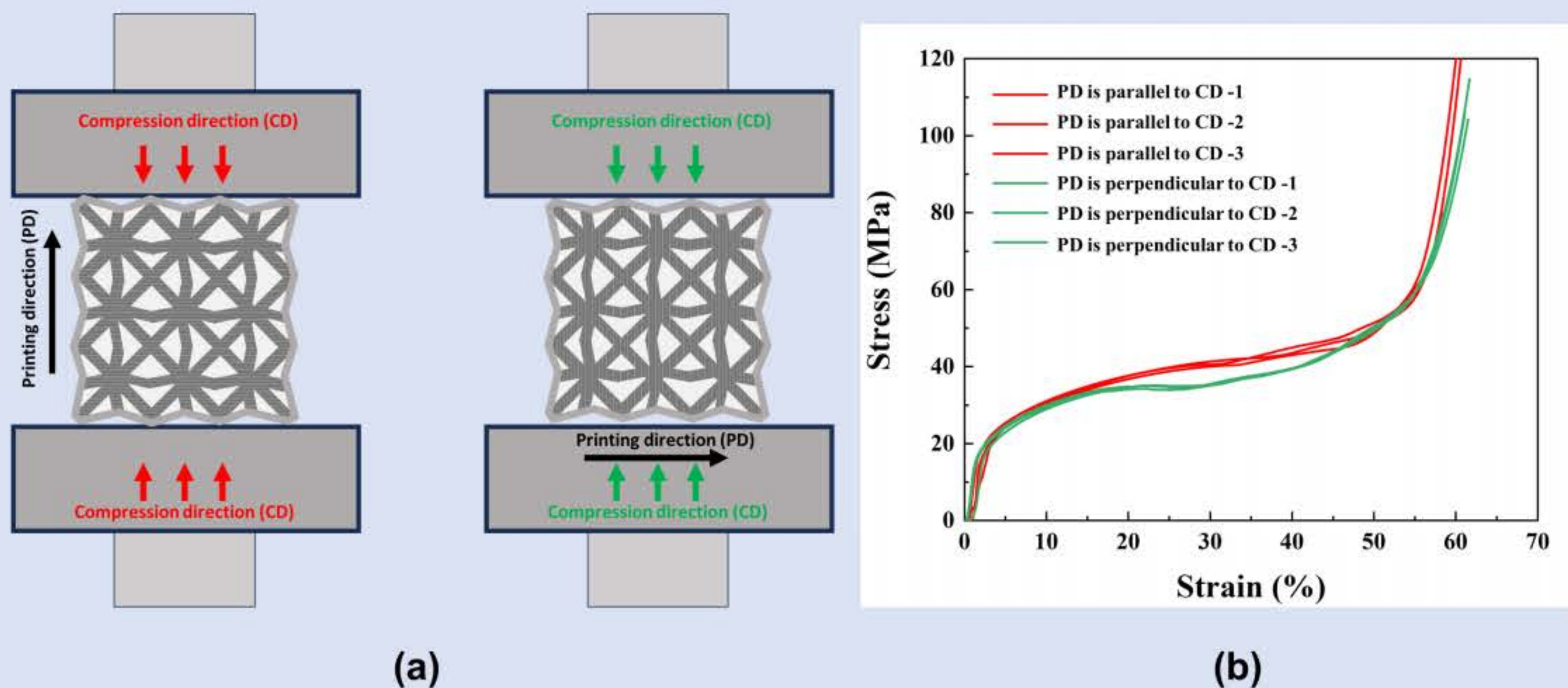


Figure 4. (a) Printing direction of lattice metal with respect to compression direction and (b) corresponding stress-strain curves

The CT scans of the lattice specimens show a small sagging (red arrows) and void (green arrows) under some struts and nodes. There are some voids that occur at struts. The cross section of the lattice structure in 2 directions is shown in Figure 5. The Z-direction cross sections with a parallel view to the printing direction show a smoother area than a perpendicular X-direction because of the interlayer areas.

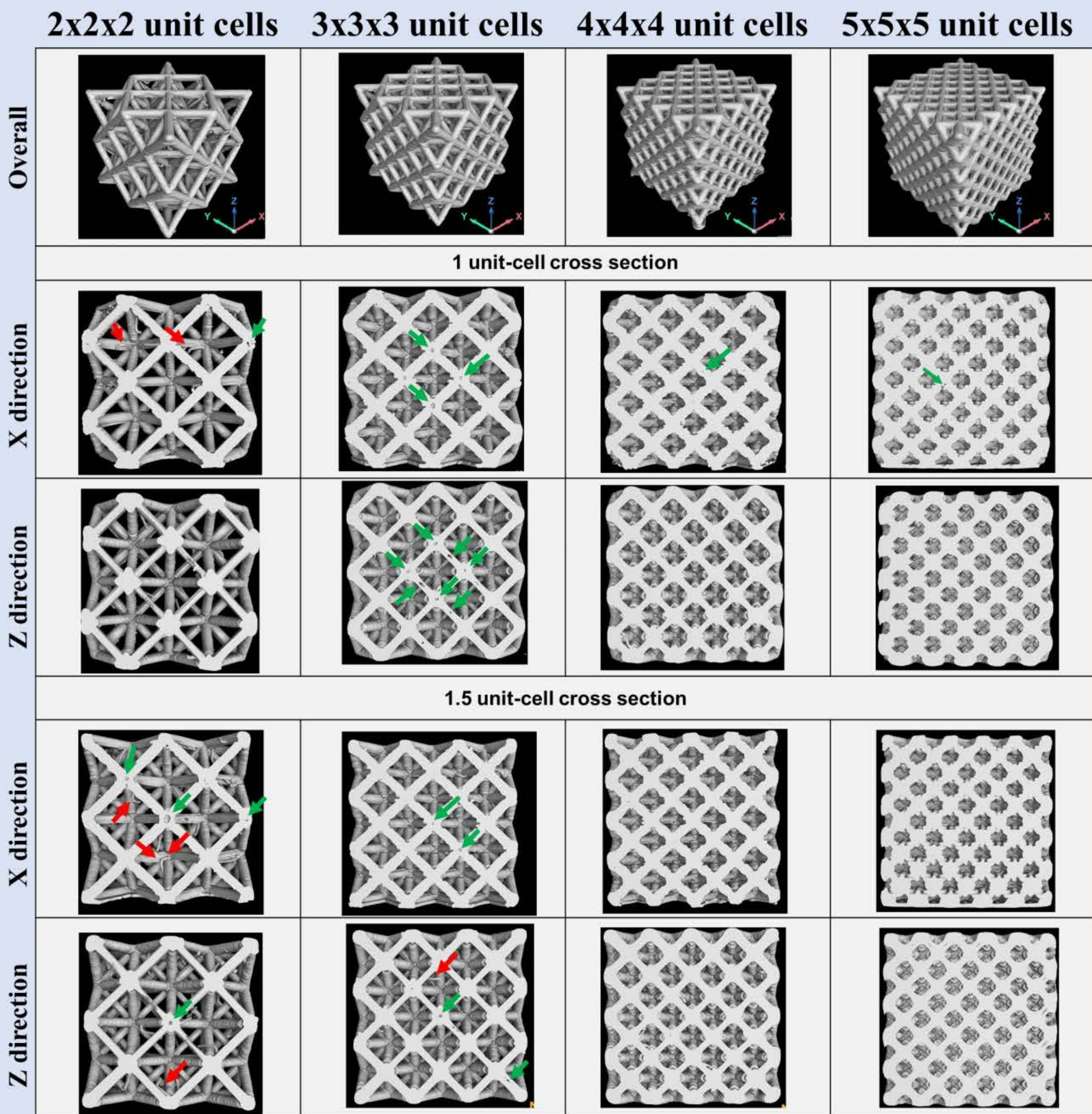


Figure 5. CT scans of the lattice specimens

The microstructure of as-sintered 316L austenitic stainless steel (at strut region) shows twins (yellow arrow) and rounded pores, which are typical for 316L stainless steel manufactured by pressureless sintering. Moreover, the Mn-Si-O-rich (pink arrow) and SiO<sub>2</sub> (light blue arrow) particles were also found, which is contaminated during the powder production and usually found in conventional powder metallurgy processes [1].

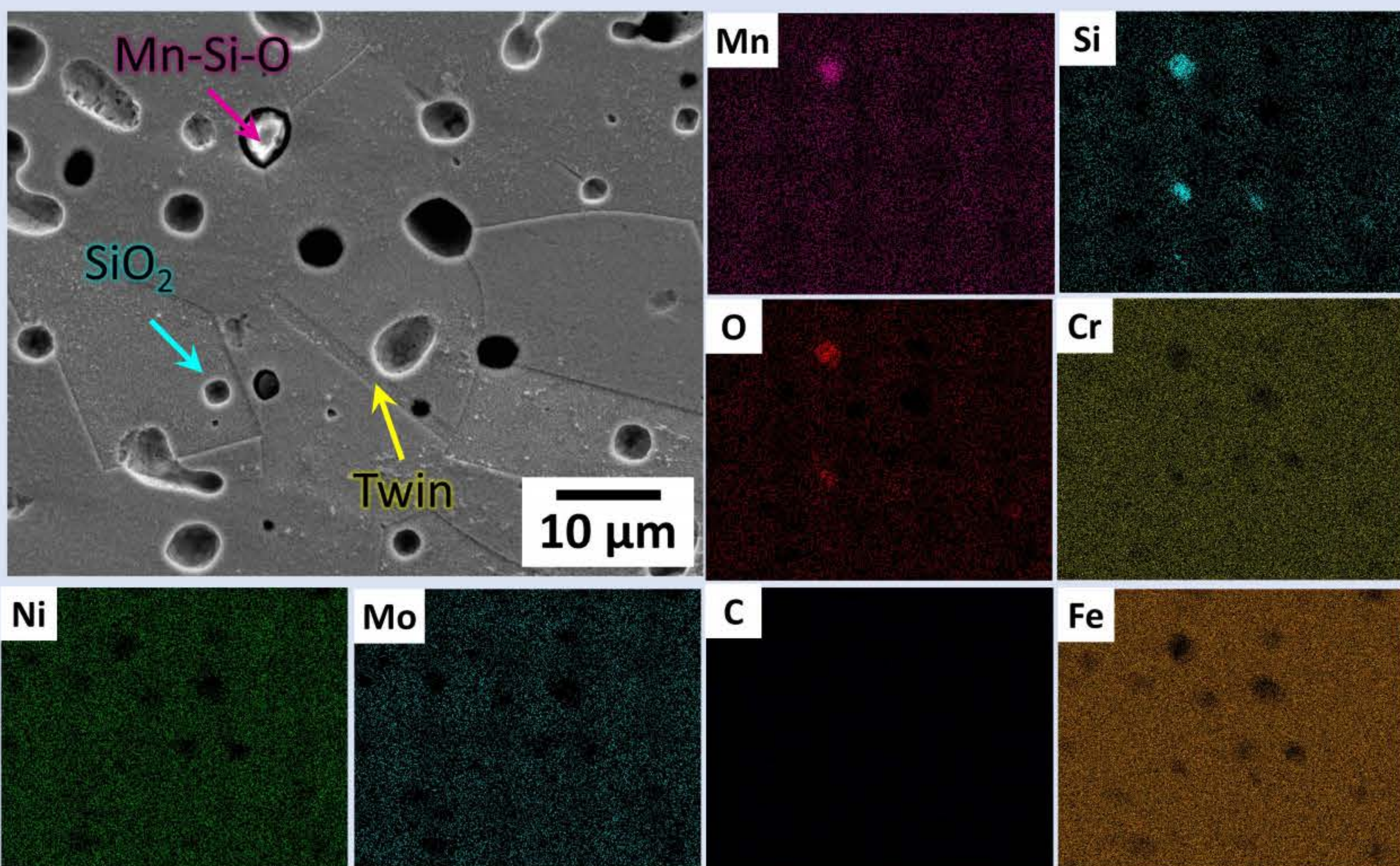


Figure 6. SEM micrograph in 3x3x3 unit cells

## Conclusions

- The fabricated filament shows good surface quality and consistency.
- The 316L lattice structure can be produced using MEX technique, even though there are some internal defects.
- The lattice structure shows high repeatability of compressive properties.
- Loading directions have no significant effect on the elastic properties of 316L lattice structure.
- The microstructure of 316L lattice shows typical austenitic stainless steel with the inclusions of SiO<sub>2</sub> and Cr-Si-O.

## References

- [1] Chanun Suwanpreecha, Sukrit Songkuea, Siwat Linjee, Suksan Muengto, Mongkol Bumrungron, Anchalee Manonukul, Tensile and axial fatigue properties of AISI 316 L stainless steel fabricated by materials extrusion additive manufacturing, Materials Today Communications, Volume 35, 2023, 105667, ISSN 2352-4928, <https://doi.org/10.1016/j.mtcomm.2023.105667>.

## Acknowledgements

This research has received equipment support from Septillion Co., Ltd. and funding support from the NSRF via the Program Management Unit for Human Resources & Institutional Development, Research and Innovation (PMU-B) [grant number B13F60064].





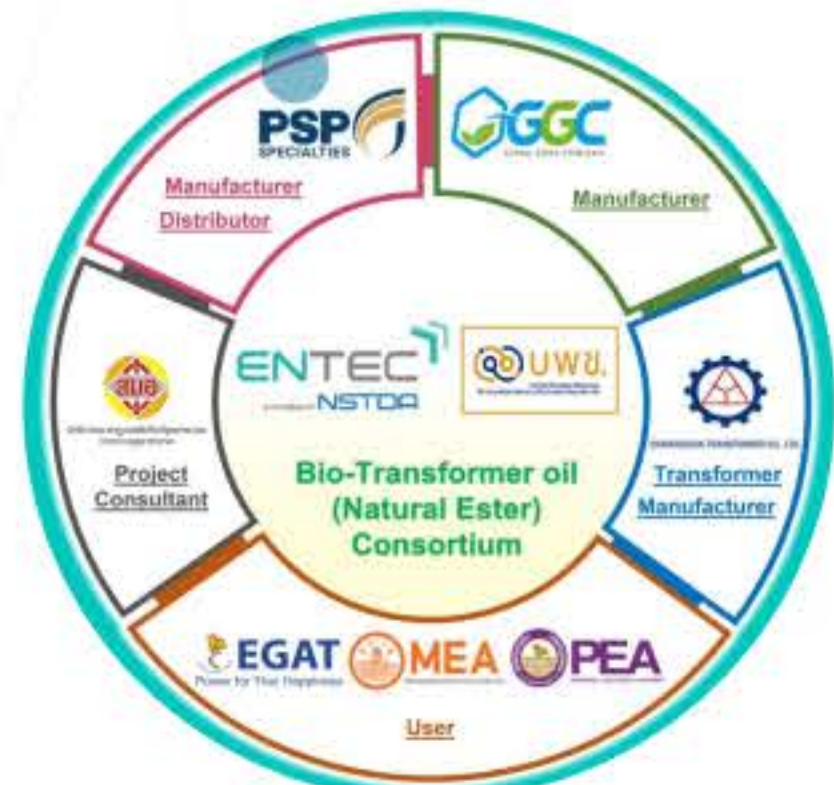
BRainPOWER  
CONGRESS 2023

ร่วมกันสร้างและขับเคลื่อนงานวิจัยขั้นแนวหน้า  
สู่อุตสาหกรรมแห่งอนาคต

# Development of **Less Flammable Bio Transformer Oil** from **Palm Oil** and Integrated Pilot Field Test to Promote Its Commercial and Sustainable Use

Sareena Mhadmhan\*, Boonyawan Yoosuk, Pornpong Siriratsakul, Bowornchai Chareonteraboon,  
Pathompong Janetaisong, Pawnprapa Pitakjakpipop, Suparoek Henpraserttae, Parncheewa Udomsap

Clean Fuel Technology and Advanced Chemistry Research Team, National Energy Technology Center,  
National Science and Technology Development Agency, Pathum Thani 12120, Thailand.  
Emails: sareena.mha@ncr.nstda.or.th / Boonyawan.yoo@entec.or.th



Mineral oil (MO) has been used as the insulating oil in most of the high voltage equipment. However, lack of petroleum oil, impact on environment, and disposal problem of used oil, the development of green and environment-friendly insulating oil has become a hot topic in insulating oil research. In order to alleviate the problem of palm oil oversupply in the market, this research propose the development of less flammable bio-transformer oil from palm oil, and it conduct field tests in the transformer. This will increase the value of palm oil in Thailand, reduce fire risks in power transformers and generate income for palm oil farmers.

## Bio Transformer Oil Production



**EnPAT**

Bio transformer oil



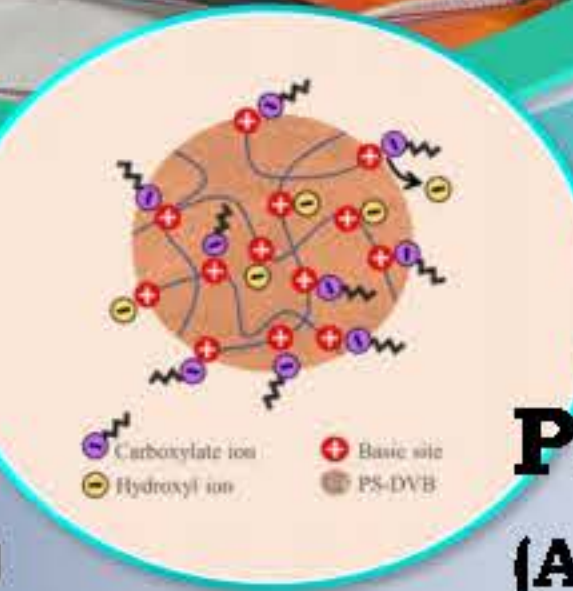
Properties analysis

(Physicochemical and electrical properties)

Properties modification

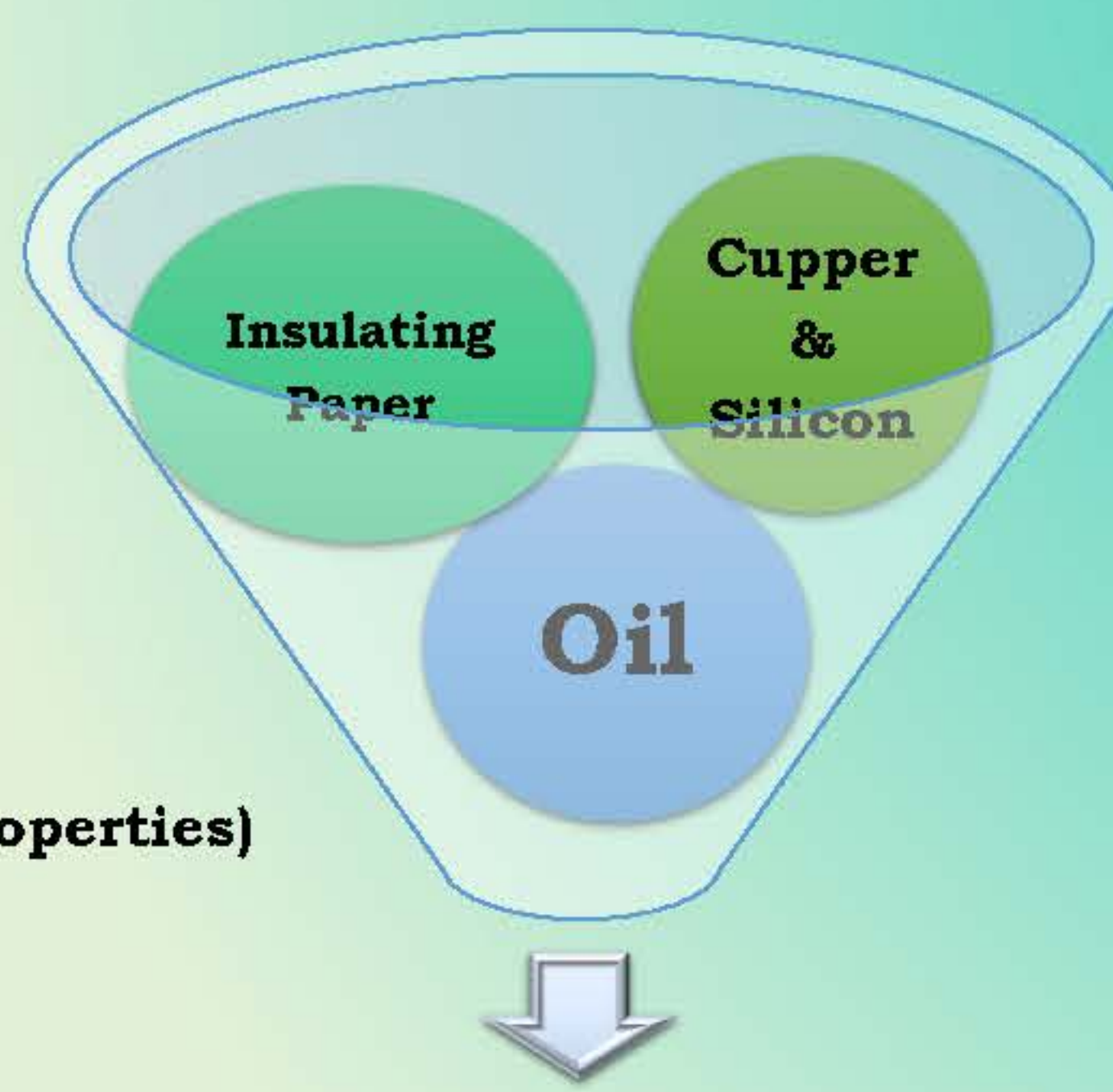


RPO  
(Refined palm oil)



Physical Pretreatment  
(Adsorption process)

## Thermal Accelerated Aging Test



Thermal aging

150 °C for 720-4,008 h



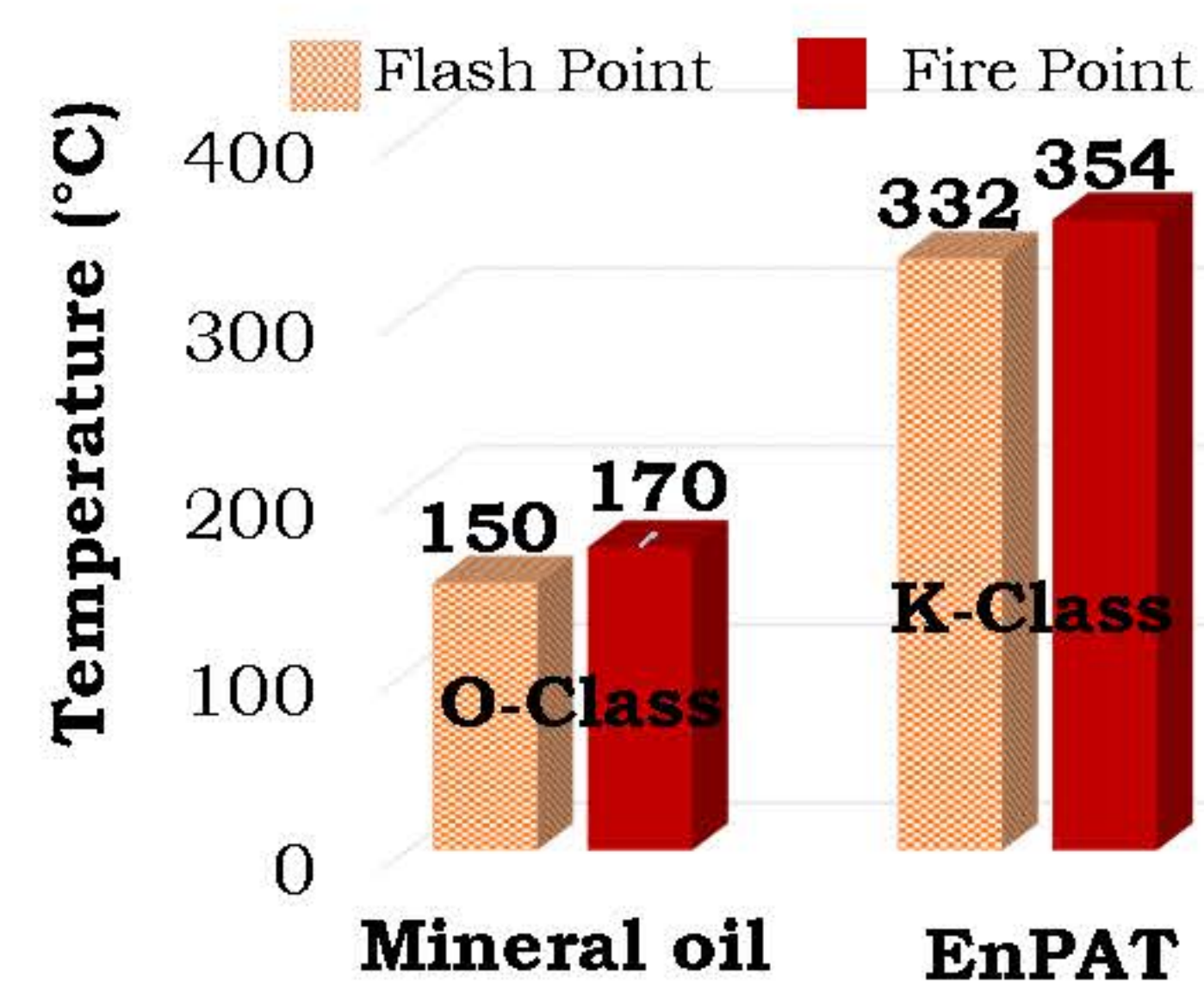
## IEC 62770

### Fluids for electrochemical applications

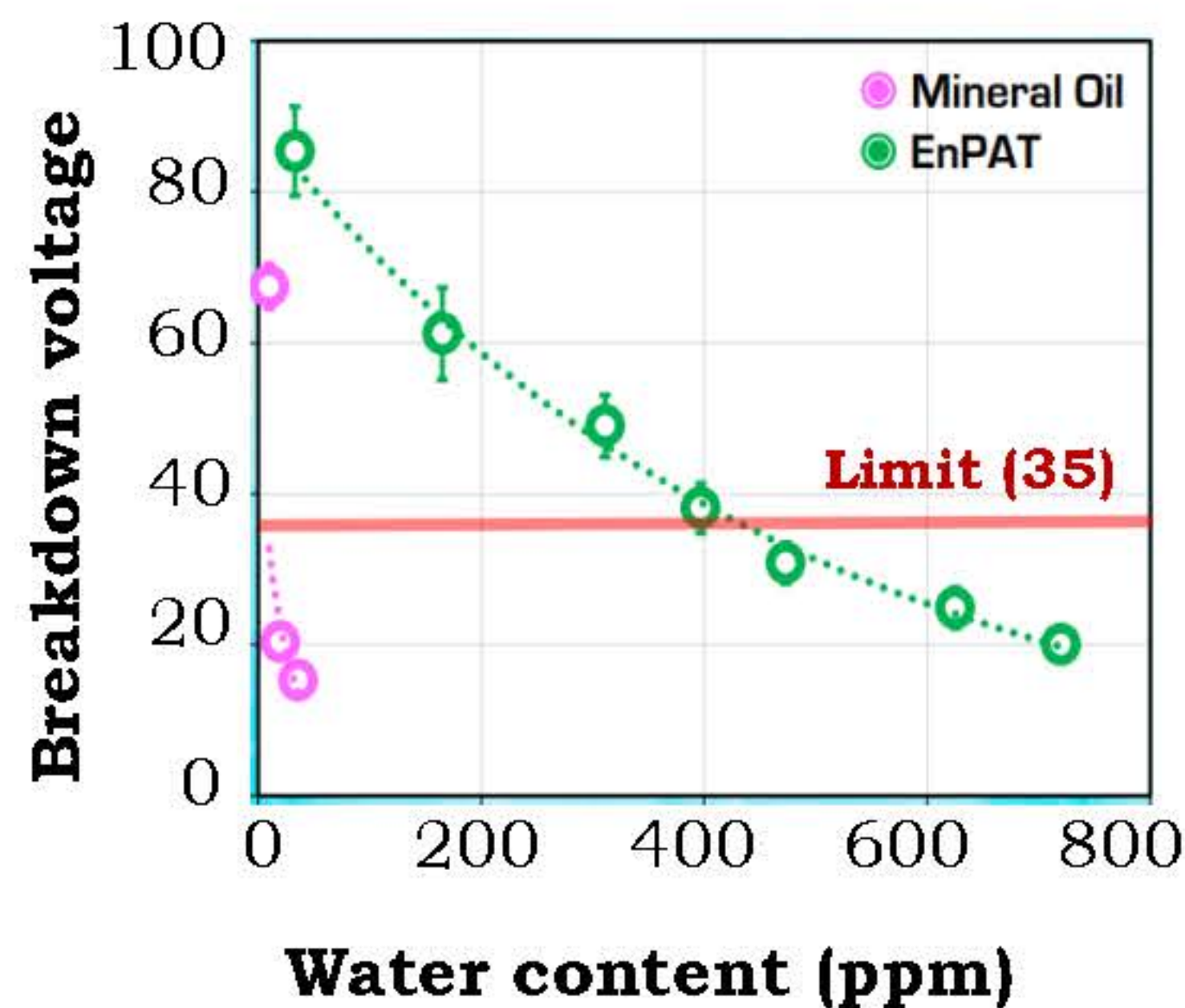
Properties	Methods	Limit	MO	EnPAT
<b>Physical properties</b>				
Viscosity at100 °C (mm <sup>2</sup> /s)	ASTM D445	≤ 15	-	<b>8.30</b>
Viscosity at40 °C (mm <sup>2</sup> /s)	ASTM D445	≤ 50	8.1	<b>39.72</b>
Pour point (°C)	ASTM D97	≤ -10	-51	<b>3</b>
<b>Chemical properties</b>				
Water content (ppm)	IEC 60814	≤ 200	10	<b>&lt;50</b>
Acid number (mg-KOH/g)	IEC 62021.3	≤ 0.06	0.01	<b>&lt;0.02</b>
Oxidation stability (h)	EN15751	-	-	<b>&gt;80</b>
<b>Electrical properties</b>				
Dissipation factor at 90 °C	IEC 60247	≤ 0.05	0.007	<b>0.02</b>
Dielectric breakdown (kV)	IEC 60156	≥ 35	67.9	<b>&gt;100</b>
Dielectric constant	IEC 60247	-	-	<b>2.86</b>
Resistivity (m, x10 <sup>10</sup> )	IEC 60247	-	-	<b>1.09</b>

**Flash point;** The lowest temperature forming ignitable vapor

**Fire point;** The most critical factor for transformer fire safety

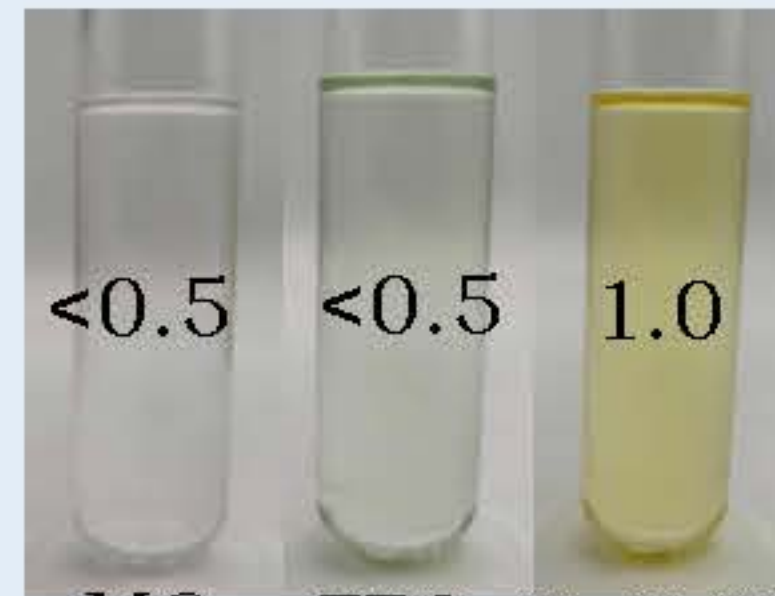


EnPAT has a very high moisture tolerance and can also trap more water which may slow down cellulose aging.

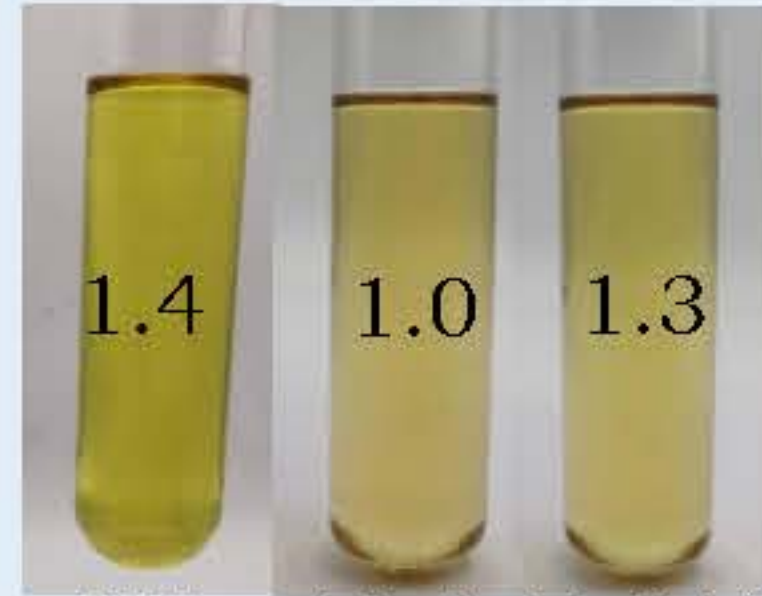


### Color change

#### Before aging



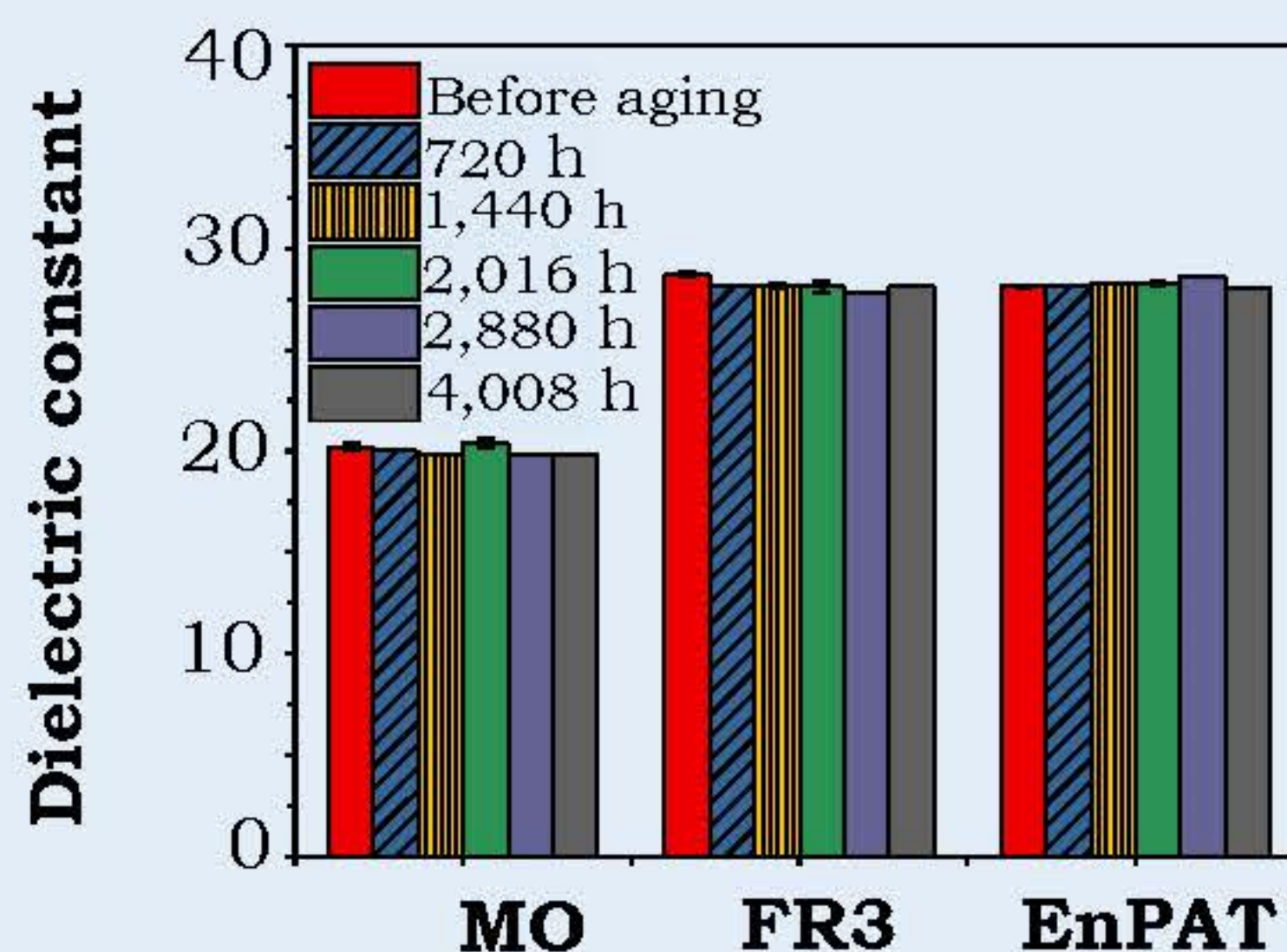
#### After aging (150 °C/ 4,008h)



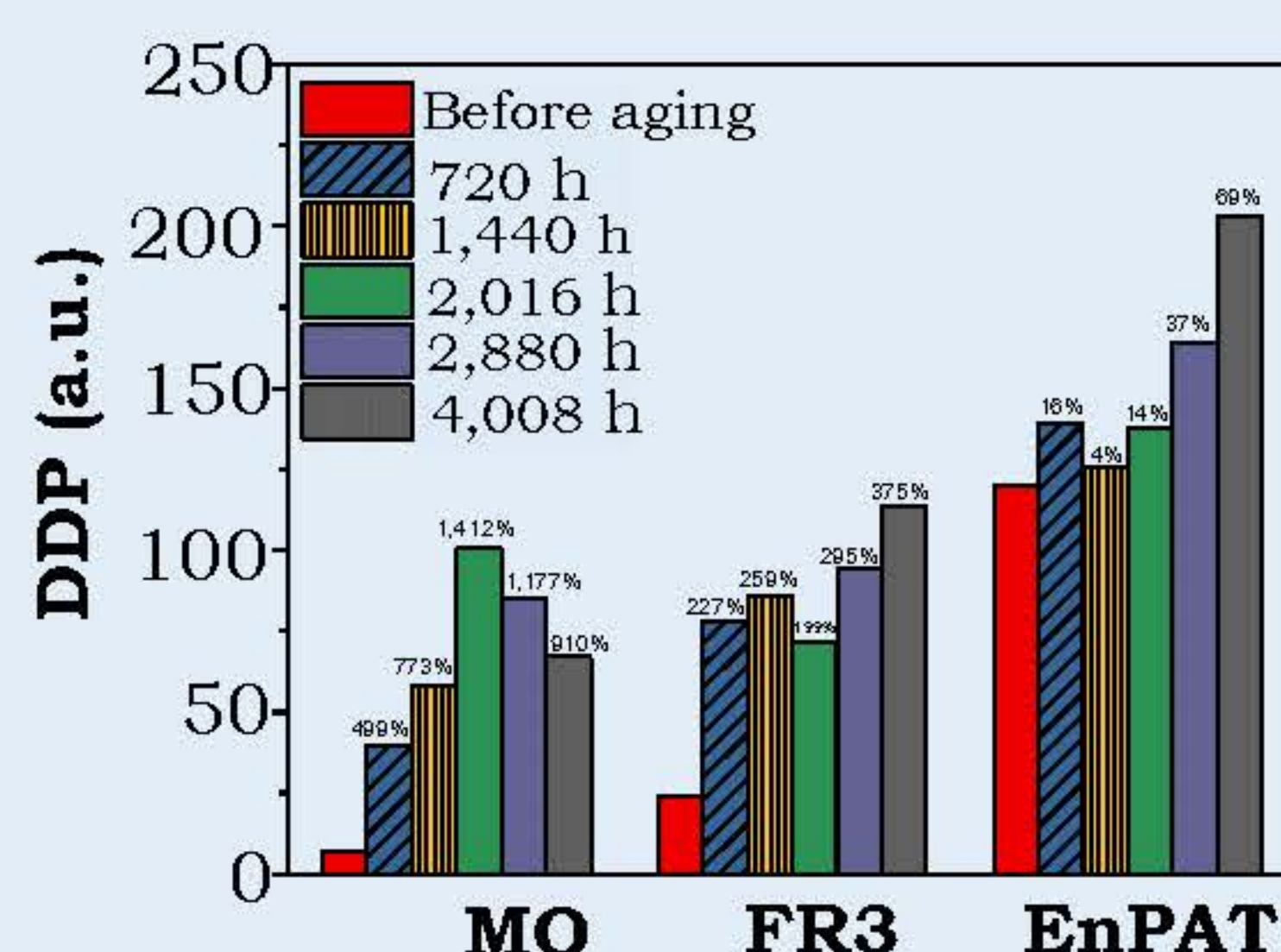
The color of **EnPAT** is slightly changed after aging test.

### Electrical property change

**EnPAT** demonstrates that the dielectric constant (permittivity) remains vary stable and constant with aging duration.



### Chemical property change



The percent increase of dissolved decay product (DDP) in **EnPAT** is lower as compared to MO.

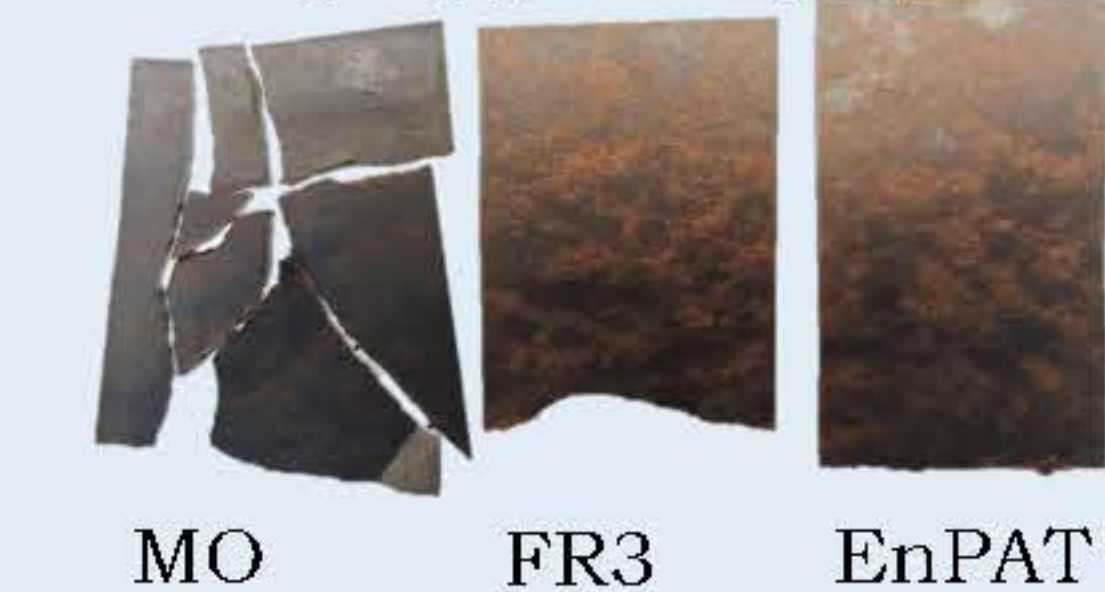
### Degradation of insulating paper

#### After aging (150 °C/ 2,880h)

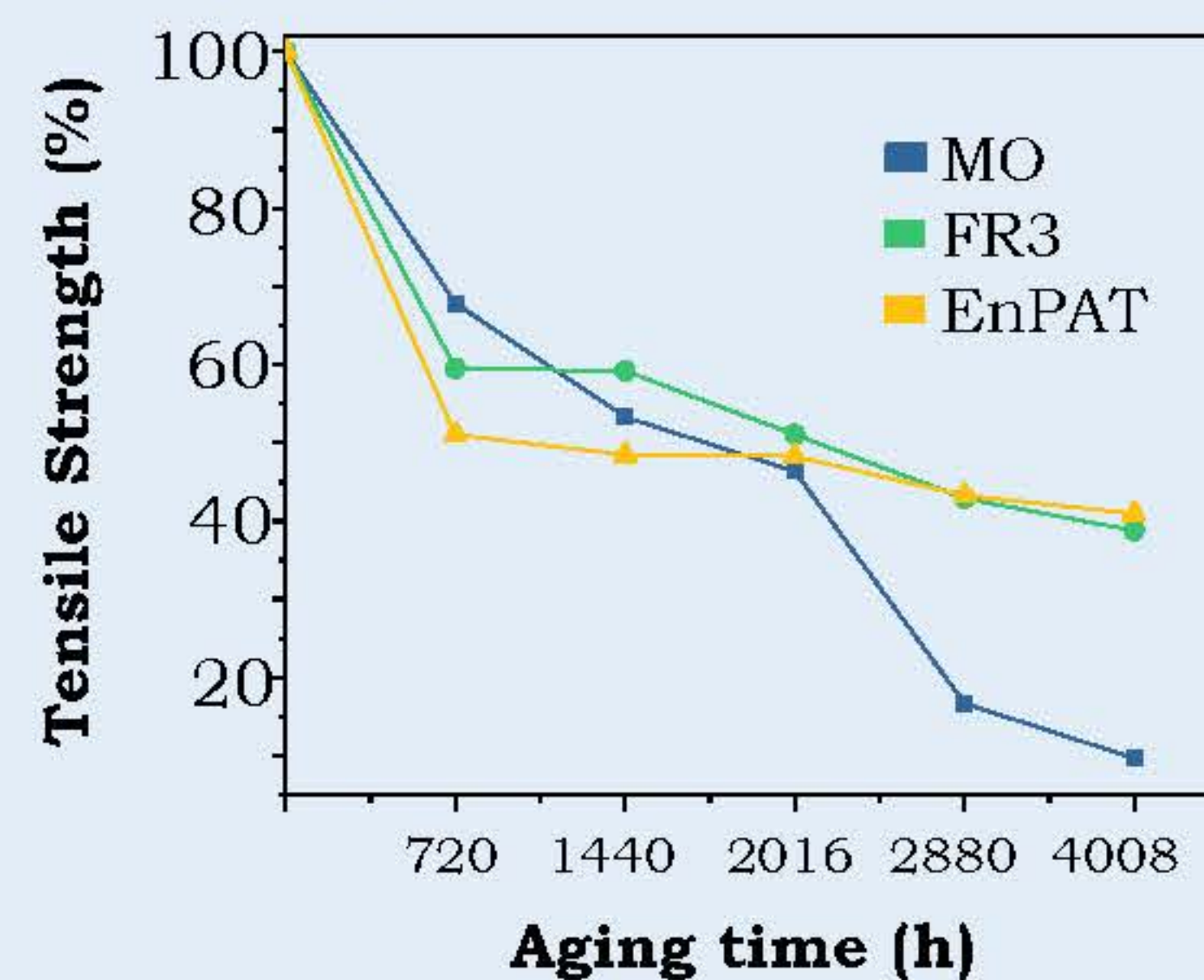


#### Before aging

#### After aging (150 °C/ 4,008h)



### Tensile strength of insulating paper aged in MO, FR3, and EnPAT at 150 °C



### Degree of polymerization (DP)

Aging time (h)	Samples	DP
Before aging	-	<b>1,086</b>
2,016	MO	286
	FR3	367
	EnPAT	<b>356</b>
2,088	MO	150
	FR3	367
	EnPAT	<b>356</b>

**EnPAT** helps to reduce the degradation rate of insulation paper as compared to the MO, extending the longevity of the insulation performance.

- Flash point and fire point are 2 times higher than MO
- Prevent the ignition from transformer explosion (Save life and properties)
- Greater reliability in transformer uses
- Properties comply with IEC 62770 and ASTM D6871

- Biodegradable (Not classified as hazardous to health)
- Recyclable (Raw material for biodiesel production)
- Sustainable (net-zero emission value)
- High value added (Premium product from palm oil)



### Reference

Mhadmhan, S.; Yoosuk, B.; Chareonteraboon, B.; Janetaisong, P.; Pitakjakpipop, P.; Henpraserttae, S.; Udomsap, P. *Separation and Purification Technology* **2023**, 310.

### Acknowledgements

This research has received the funding support from the NSRF via the Program Management Unit for Human Resources & Institutional Development, Research and Innovation (grant number B13F660064) and the National Energy Technology Center (ENTEC), National Science and Technology Development Agency.





**BRAINPOWER**  
CONGRESS 2023

ร่วมกันสร้างและขับเคลื่อนงานวิจัยชั้นนำ  
สู่อุตสาหกรรมแห่งอนาคต



## Superoxide Dismutase Produced from Recombinant Yeast and Its Function as Free Radical Scavengers

KANOK WONGRATPANYA<sup>1</sup>, NASSAPAT BOONVITTHYA<sup>2</sup>, PHITSANU PINMANEE<sup>1</sup>, PAWEENA THONGKRED<sup>1</sup>, JUTHAMAS SUWANPRATEEP<sup>1</sup>, THIDARAT NIMCHUA<sup>1\*</sup>

1. Enzyme Technology Research Team, Biorefinery and Bioproduct Technology Research Group, National Center for Genetic Engineering and Biotechnology, National Science and Technology Development Agency.

2. PTT Public Company Limited

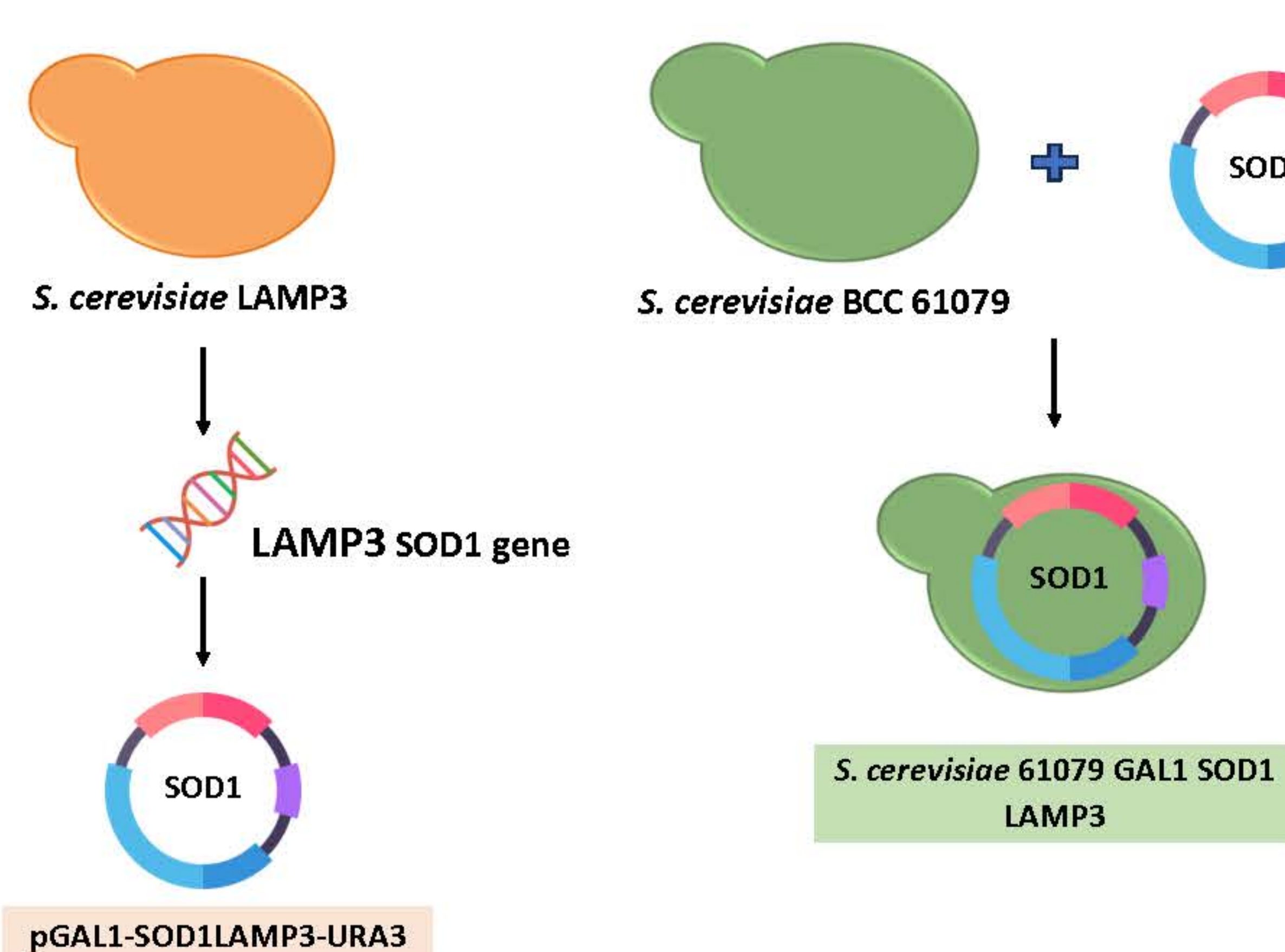
\* Correspondence: Thidarat.nim@biotec.or.th

### Introduction

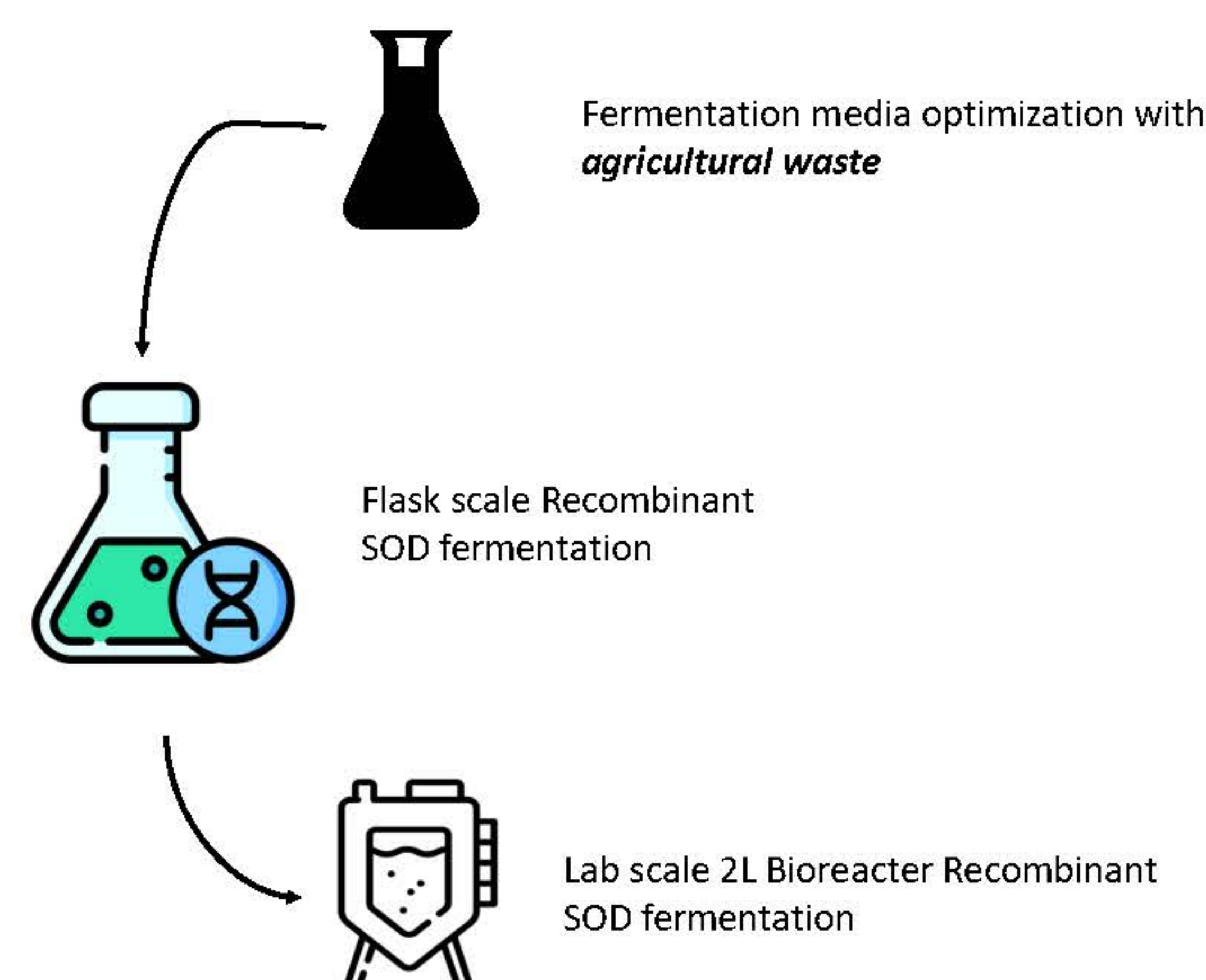
Superoxide dismutase (SOD) plays a role as free radical scavenging agent and shows inflammation reduction caused by oxidative stress inside the living cell. SOD has been applied to various kinds of industries such as food, food supplement, and pharmacy. Cosmeceuticals and personal care products industry are industrial sector that showed high demand of SOD. However, there are few candidate players in SOD market. In Thailand there was no domestic SOD producer, hence, the supply of SOD in Thailand are totally imported. Hence, this study aimed to develop recombinant SOD from yeast platform. The recombinant *Saccharomyces cerevisiae* harbored SOD1 gene was constructed. The fermentation process by using low-cost medium for recombinant SOD production was conducted for enzyme production cost reduction. We aim that this low-cost SOD production process could be implemented in industrial production scale and boost up the Thailand specialty enzyme production sector. The domestic enzyme production could reduce the trade deficit and leading to a sustainability economic expansion of bioeconomy in Thailand.

### Technology development

#### Recombinant strain construction

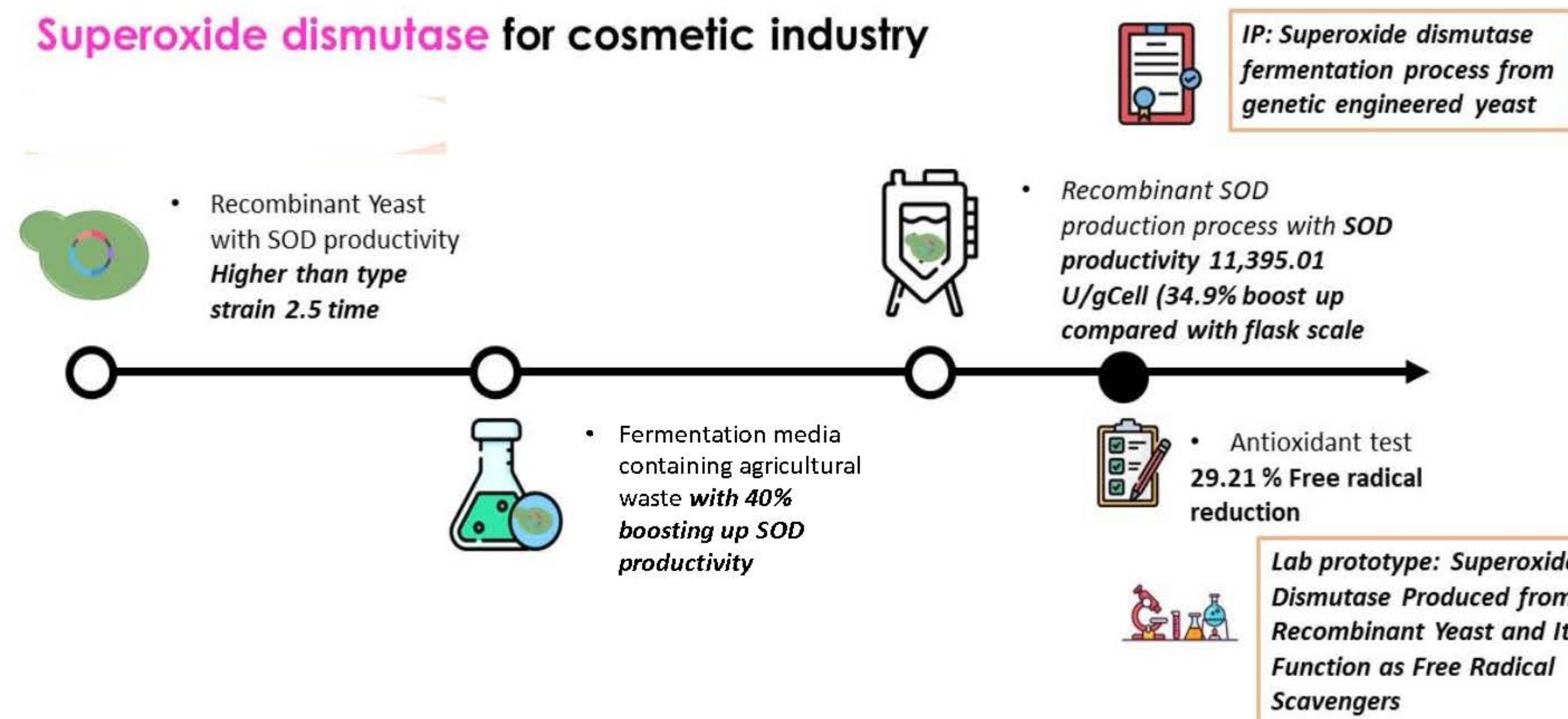


#### Recombinant SOD Fermentation



### Results and Discussion

#### Superoxide dismutase for cosmetic industry



In this study we constructed a recombinant *S. cerevisiae* strain harbored SOD1 gene which showed a SOD production efficiency 2.5 time higher than type strain. The media optimization for recombinant SOD production revealed that low-cost fermentation media which developed in this study could increased the SOD productivity up to 40% and the productivity of SOD was achieved 11,395.01 U/g cell in 2 L fermentation. The anti oxidant test of recombinant SOD showed that recombinant SOD exhibited 29.21% free radical Scavengers reduction

### Conclusion

*Saccharomyces cerevisiae* a GRAS strain which suitable for using as a host cell for bioactive compound production This study revealed that, development of recombinant SOD production by using agricultural waste could increased the productivity of SOD compared with type strain. A low-cost SOD production process showed economic feasibility for industrial production. Furthermore, recombinant SOD in this study could reduce free radical means that recombinant SOD from this study could apply to cosmeceuticals and personal care products industry.

### Acknowledgements

This research has received funding support from the NSRF via the Program Management Unit for Human Resources & Institutional Development, Research and Innovation [grant number B01F640033]



# Production of xylooligosaccharides (XOS) using an enzymatic process

Katesuda Aiewviriyasakul<sup>1</sup>, Katewadee Boonyapakron<sup>1</sup>, Srisakul Trakarnpaiboon<sup>1</sup>, Wipawee Sritusnee<sup>1</sup>, Hataikarn Lekakarn<sup>2</sup>, Morakot Sakulsombat<sup>3</sup>, and Benjarat Bunternngsook<sup>1,\*</sup>

\*Corresponding author,  
benjarat.bun@biotec.or.th

<sup>1</sup>Enzyme Technology Research Team, Biorefinery Technology and Bioproduct Research Group, National Center for Genetic Engineering and Biotechnology, 113 Thailand Science Park, Phahonyothin Road, Khlong Luang, Pathumthani 12120, Thailand, <sup>2</sup>Department of Biotechnology, Faculty of Science and Technology, Thammasat University, Rangsit Campus, Patumthani 12120, Thailand, <sup>3</sup>Mitr Phol Innovation & Research Center 399 Moo 1, Chumpae – Phu Khieo Road, Kok Sa-ard sub-district, Phu Khieo district, Chaiyaphum 36110

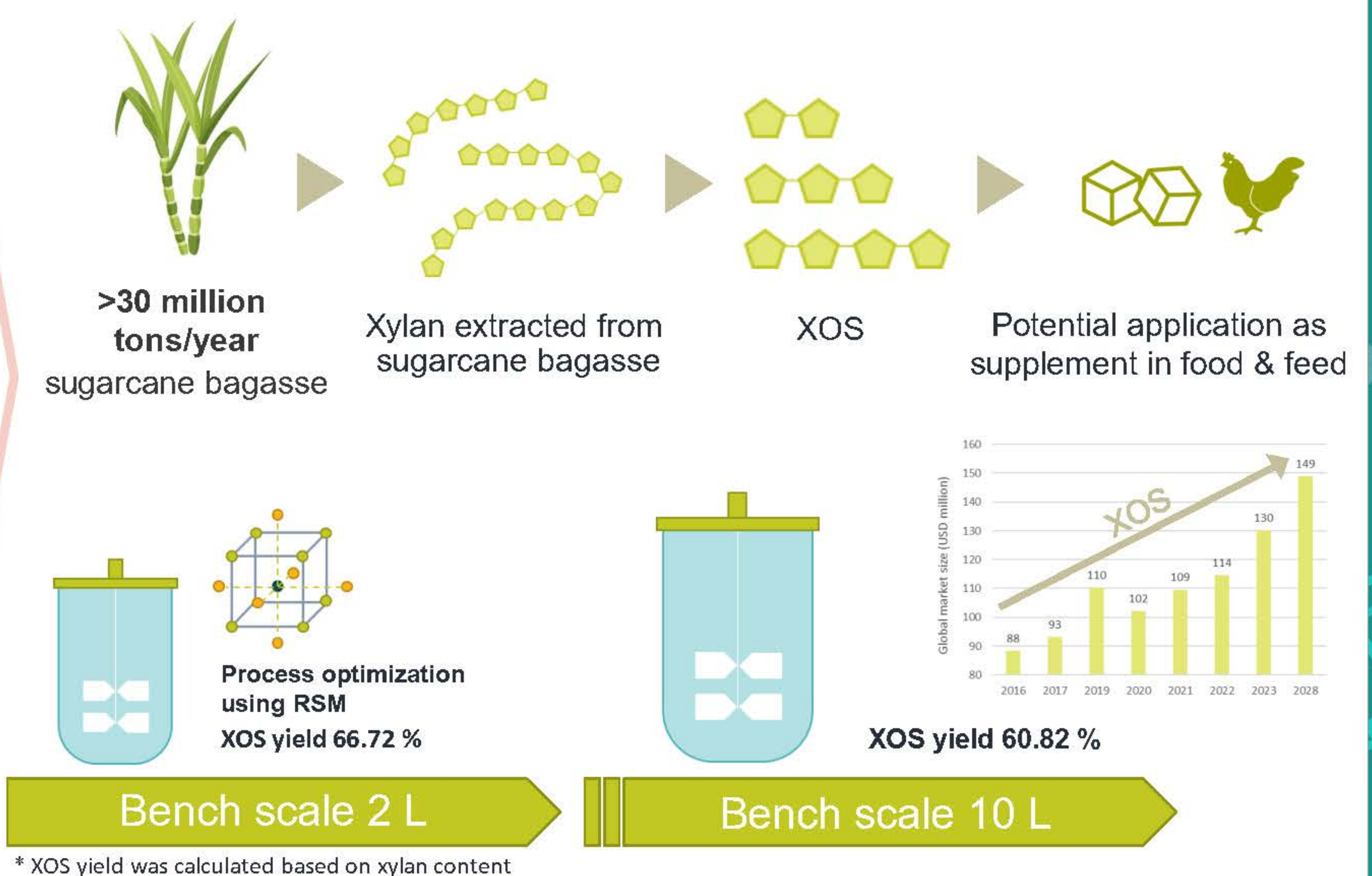
## Introduction

Xylooligosaccharide (XOS) has been indicated as an emerging biomass-derived biochemical with potential prebiotic and bioactive properties. XOS is applied as a functional ingredient in food and cosmeceutical industries. The global market value of XOS is predicted to be USD 148.75 million by 2028, with a 4.48% growth rate per year. Currently, XOS is produced from lignocellulosic biomass using chemical or enzymatic processes. The traditional chemical process uses acid to hydrolyze raw material; therefore, it produces a lot of acid waste, leading to environmental problems. Moreover, the acid hydrolysis process generates a high yield of xylose and a wide range of degree of polymerization. These low specific properties and high by-products lead to higher costs for the downstream process step.

Therefore, this project aims to develop a highly efficient enzymatic XOS production process using xylanase enzymes to hydrolyze xylan by cleaving beta-1,4-glycosidic bonds to produce XOS. This process has high specificity to the oligosaccharide products with a desirable range and is environmentally friendly.

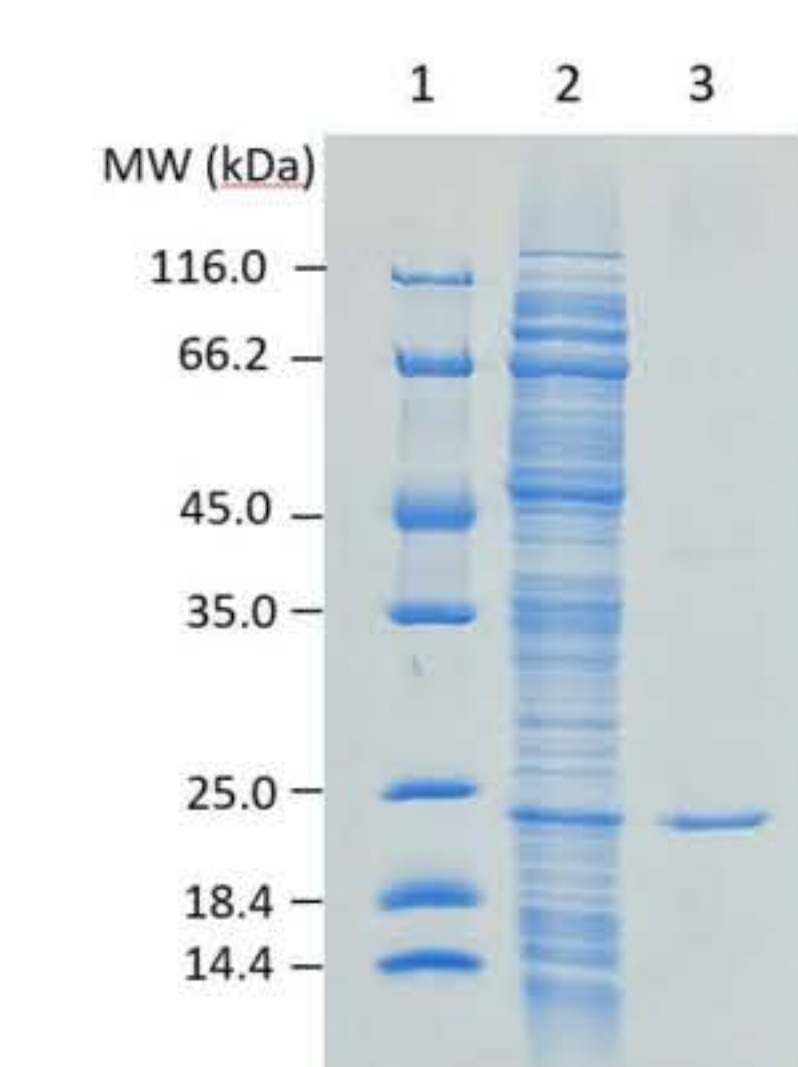
## Xylooligosaccharide production process

The enzymatic process for the production of controllable chain-length xylooligosaccharides



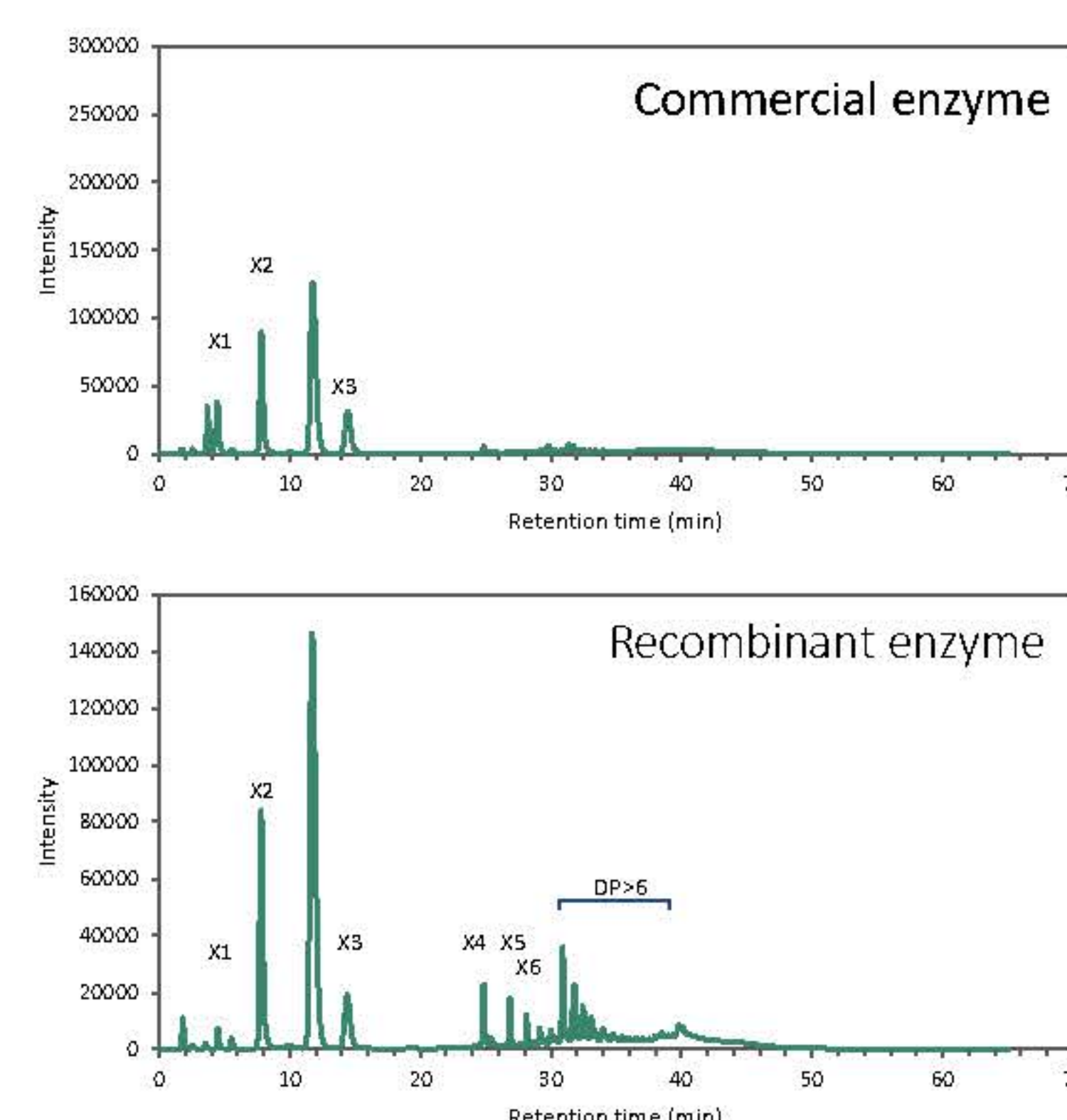
**Goal** To study optimal conditions for xylan hydrolysis to produce XOS using commercial enzyme and recombinant enzyme of BIOTEC

## Expression protein



Recombinant enzyme expressed in *E. coli* BL21(DE3)  
Lane 1: protein marker  
Lane 2: crude enzyme  
Lane 3: purified enzyme

## Product profile



## Conclusion

This project developed a digestion process for producing XOS from xylan extracted from bagasse, using commercial xylanase enzyme and recombinant xylanase enzyme developed by the enzyme technology research team, BIOTEC. Yields of the developed process were short-chain XOS at the degree of polymerization between DP2 and DP6. The two enzymes produced different proportions of specific products. The production at a 10-liter reactor obtained a 60% yield of XOS.

## Acknowledgement

This research has received funding support from the NSRF via the Program Management Unit for Human Resources & Institutional Development, Research and Innovation [grant number B13F660064]. The authors acknowledge the support provided by Enzyme Technology Research Team, National Center for Genetic Engineering and Biotechnology.



### Advantages

- High yield

### Disadvantages

- Require robust equipment
- High temperature and pressure
- Require noxious chemicals
- Preferred to produce XOS mixtures with a wide DP range (DP2 - DP20)
- Undesired by-products: furfural and HMF
- Require downstream step (high costs)

### Chemical Hydrolysis

## References

- Nabarlatz, D., Montané, D., Kardosová, A., Bekesová, S., Hřibálová, V., Ebringerová, A. 2007. Almond shell xylo-oligosaccharides exhibiting immunostimulatory activity. *Carbohydr Res*, 342(8), 1122-8.
- Amorim, C., Silvério, S.C., Prather, K.L.J., Rodrigues, L.R. 2019. From lignocellulosic residues to market: Production and commercial potential of xylooligosaccharides. *Biotechnology Advances*, 37(7), 107397.
- Poletto, P., Pereira, G.N., Monteiro, C.R.M., Pereira, M.A.F., Bordignon, S.E., de Oliveira, D. 2020. Xylooligosaccharides: Transforming the lignocellulosic biomasses into valuable 5-carbon sugar prebiotics. *Process Biochemistry*, 91, 352-363.

## Enzymatic Hydrolysis

### Advantages

- Environment-friendly
- High efficiency and specificity
- Reduce undesired by-products
- Prefer in food and pharmaceutical industries
- Low DP (DP2–DP4) (higher prebiotic potential)
- Reduce formation of degradation products

### Disadvantages

- Low yield
- High cost (depends on enzyme prices)
- Require pretreatment step to increase enzymatic accessibility



# Production of a high strength product using a thixoforging process

Monthakam Chanthiwong<sup>1</sup>, Sutean Mungkan<sup>2</sup>, Chulada Domrong<sup>1</sup>, Sompong Sriranasoawapak<sup>1\*</sup>

<sup>1</sup> Nation Metal and Materials Technology Center, Thailand Science Park, Pathumthani, Thailand

<sup>2</sup> UMC Diecasting Co., Ltd. 1/35 Village No.2 Samut Sakhon industrial estate5, Samut Sakhon 74000

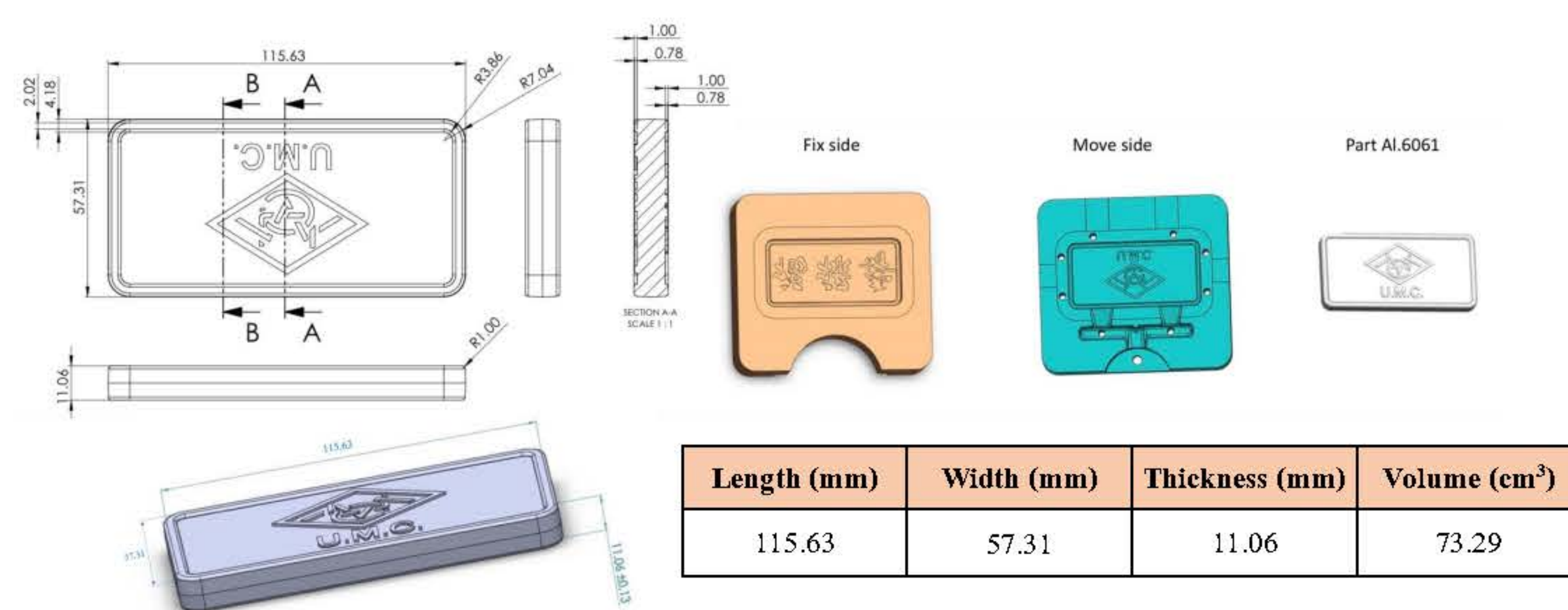
\* Corresponding Author

## Introduction

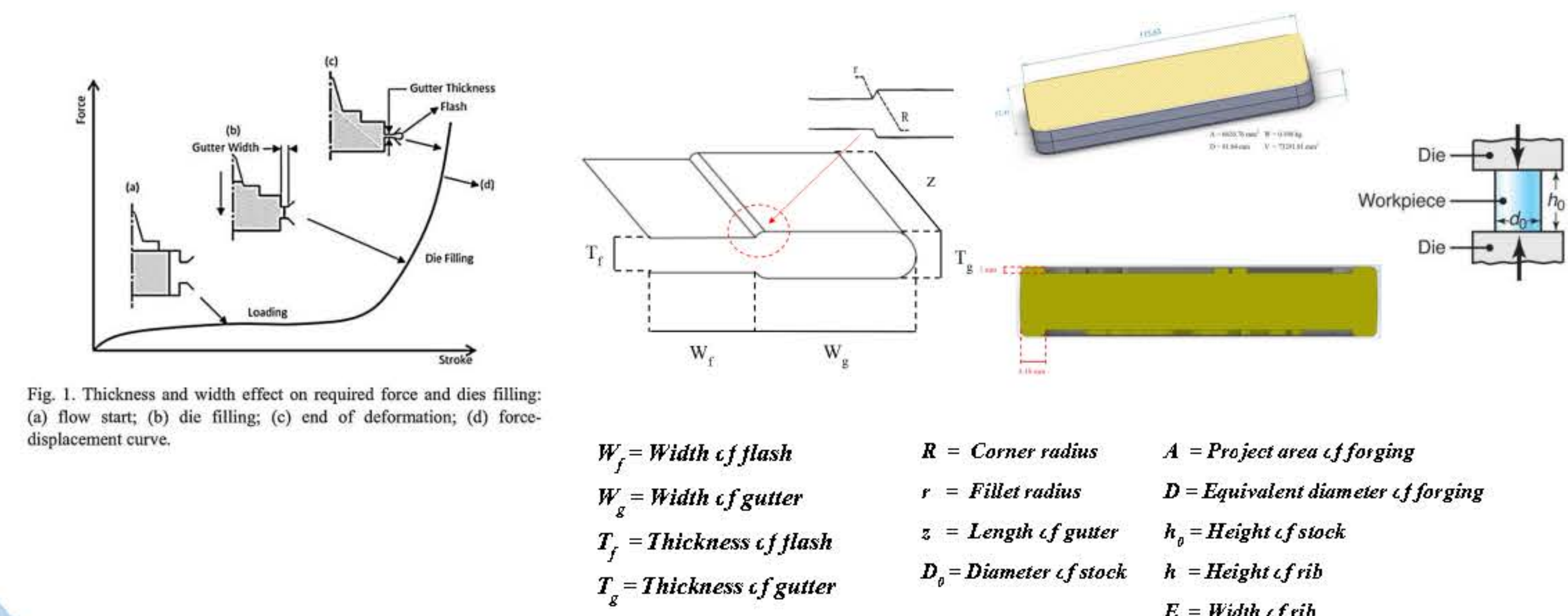
Forging is a manufacturing process involving the shaping of metal using compressive forces. It is classified according to the temperature at which it is performed: cold forging, warm forging, or hot forging. It is typically used for producing components with high strength requirements. However, the complexity of the component is limited due to the massive compressive forces required, resulting in significant capital expenditure for machinery and tooling. Thixoforging is an alternative forging capable of producing a component with fewer compressive forces but more complex shapes. The component is forged using metals at temperatures between the solid and liquid states, allowing for the manufacture of components to reduce the number of shaping steps and the raw material involved in the manufacturing process. However, knowledge in terms of die design and forming parameters is still far less existing compared with those of the conventional forging process. This research aims to provide a recipe for die design and forming parameters for thixoforging to guide industries to obtain high integrity and complexity shape components.

## Methods

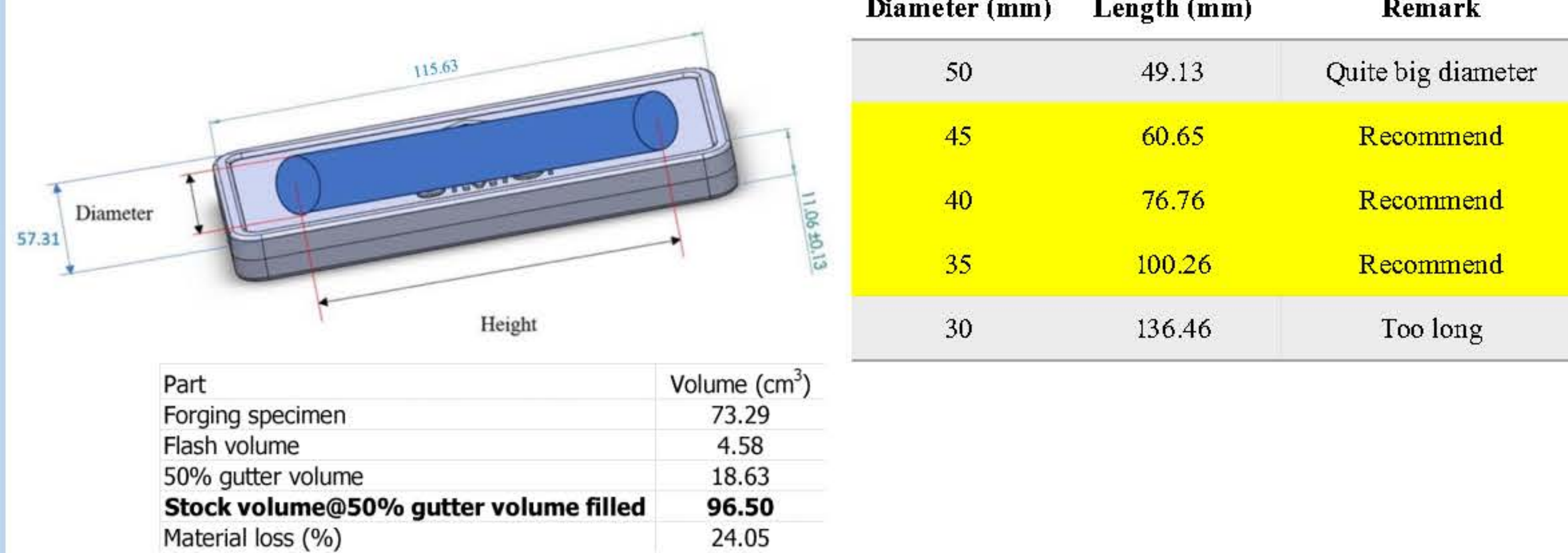
### Forging specimen



### Effect of thickness and width of flash on forging and die filling



### Stock dimension



### Flash and gutter design

No.	Reference	Method of calculation	$W_f$	$W_g$	$T_f$	$T_g$	$R$
1.	[1]	$T_f = 0.015 \sqrt{D}$					
2.	[1], [2], [3]	$W_f = 0.015 \sqrt{D}$					
3.	[1], [2], [3]	$W_g = 0.015 \sqrt{D}$					
4.	[1], [2], [3], [4]	$W_f = 0.015 \sqrt{D}$					
5.	[2]	$W_f = 0.015 \sqrt{D}$					
6.	[3]	$W_f = 0.015 \sqrt{D}$					
7.	[3]	$W_f = 0.015 \sqrt{D}$					
8.	[3]	$W_f = 0.015 \sqrt{D}$					
9.	[3]	$W_f = 0.015 \sqrt{D}$					
10.	[3]	$W_f = 0.015 \sqrt{D}$					

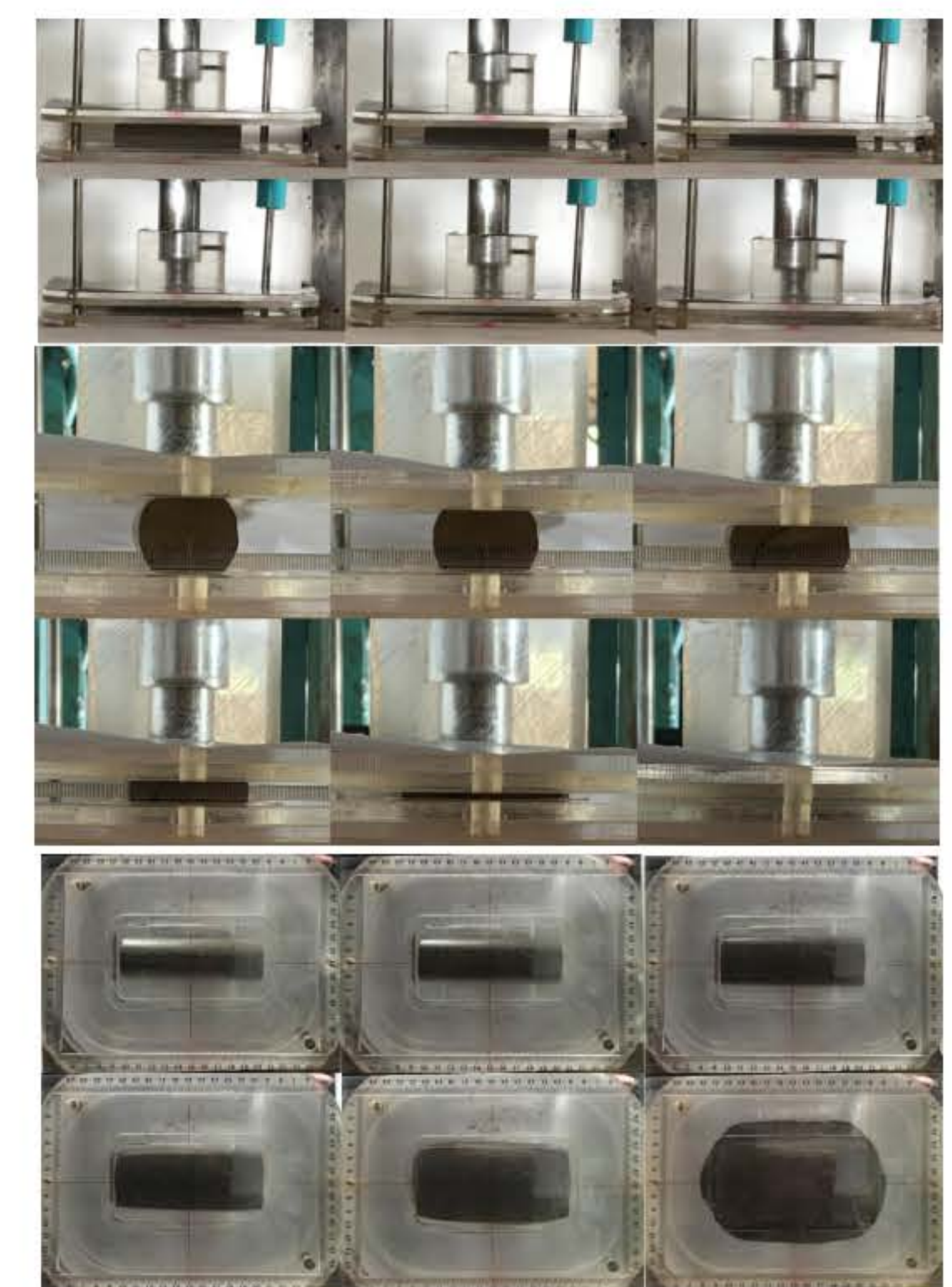
No.	Reference	Calculate value (mm)	$W_f$	$W_g$	$T_f$	$T_g$	$R$
1.	[1]	1.22	NEA	-	-	-	-
2.	[1], [2], [3]	1.66	6.29	18.45	-	-	-
3.	[1], [2], [3]	1.67	6.42	7.11	-	-	-
4.	[1], [2], [3], [4]	1.52	3.97	6.04	-	-	-
5.	[2]	1.38	-	-	-	-	-
6.	[3]	1.71	5.59	9.66	-	-	-
7.	[3]	1.71	5.59	9.66	-	-	-
8.	[3]	1.68	4.33	7.29	-	-	-
9.	[3]	1.22	4.57	8.83	4.88	24.08	-
10.	[3]	1.52	3.97	6.04	2.44	24.16	1.52
11.	[3]	1.47	N/A	-	-	-	-
12.	[3]	1.89	3.64	6.54	-	-	-

\*Average  $T_f = 1.61$  mm and  $W_g = 7.93$  mm, calculate [5]  $T_g = 2.57$  mm and  $W_f = 31.73$  mm

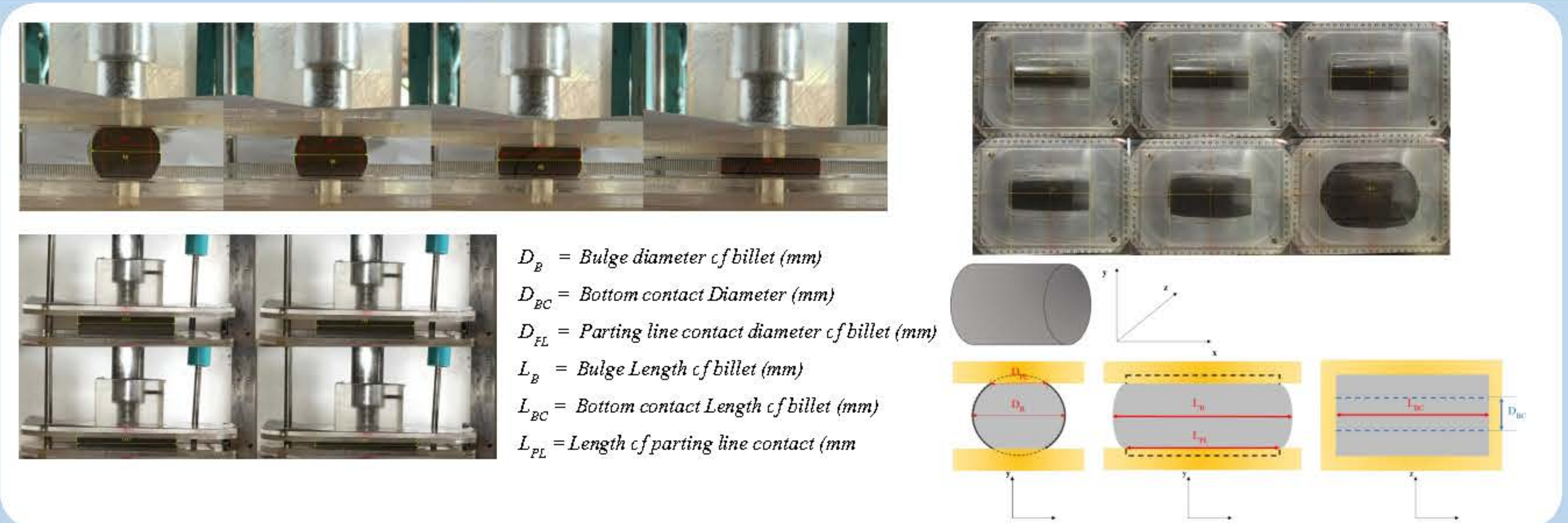
\*\*Unknown parameters:  $h_p$ ,  $h_r$  and  $z$

### Experiment

No.	Condition	Diameter (mm)	Length (mm)
1.	1A	33.61	110.15
2.	2A	40.57	77.31
3.	3A	42.95	65.33
4.	1B	33.85	111.84
5.	2B	39.88	77.73
6.	3B	42.83	65.66
7.	1C	33.41	111.27
8.	2C	40.40	77.70
9.	3C	42.72	65.39
10.	1D	34.6	110.76
11.	2D	41.04	76.52
12.	3D	42.7	67.63



## Results and Discussion



## Conclusions

Parameters for die design for the thixoforging process were primarily recommended based on the average values of the parameters suggested for the die design of the conventional forging process. Due to the different rheology properties of the stock materials between both forging processes, it is expected that the thixoforging die would require less space for flashing. Four different clays with different strengths and dimensions were used as stock materials to simulate the die filling in an acrylic die under compression. It was found that with the same stock volume, the one with the higher upsetting sectional area to available die cavity space ratio and less strength is more progressive in cavity filling. The remaining work is to investigate the effect of the flashing space of the die on the integrity of the forging product under the thixoforging of a real semi-solid metal.

## Acknowledgements

This research has received funding support from the NSRF via the Program Management Unit for Human Resources & Institutional Development, Research and Innovation [grant number B13F660064]

## References

- [1] S. Chandan. Study of parameters towards improving efficiency of closed die hot forging process (master's thesis). India: National Institute of Technology Rourkela, 2014.
- [2] B. Tomov et al. Influence of flash design upon process parameters of hot die forging. Journal of Materials Processing Technology 157-158 pp. 620-623, 2004.
- [3] M. Sedighi and M. Pourbashi. Variable gutter technique as a novel method to reduce waste material in closed die-forging process. Journal of Mechanical Science and Technology Vol. 28, Issue 12, pp. 5129-5134, 2014.
- [4] M. Velibor and J. Predrag. Application of regression method for determining the die land dimensions based on data from industry. FME Transactions 45, pp. 590-596, 2017.
- [5] E. Nauberger and L. Mockel. Richtwerte zur Ermittlung der Gratdicke unter Gratabverhältnissen beim Gesenkschmieden von Stahl. Werkstattstechnik Vol. 51, p. 725, 1961.
- [6] V. Kulkarni, S. Gawande, N. Gite, A. Avhad and Y. Sonawane. Forging die design for gear blank. International Research Journal of Engineering and Technology, Volume. 04 Issue. 03, 2018.
- [7] Peak Eiko. Metal flow simulation and design of dies for closed die forging (doctor's thesis). Scientific studies and research center. CAVASOLS - SYRIA 1992.
- [8] K. Mancj and S. Naveen. Forging die design & simulation of automotive component clutch release fork. JETIR Issue8, ISSN 2349-5162, 2018.



# STUDY AND DEVELOPMENT OF POROUS NANOFIBERS, GRAPHENE OXIDE QUANTUM DOT NANOFIBER COMPOSITE, AND METAL DOPED GRAPHENE OXIDE QUANTUM DOT NANOFIBER COMPOSITE FOR CARBON DIOXIDE REDUCTION AND CAPTURE



Sougata Ghosh<sup>1,2</sup> and Sirikanjana Thongmee<sup>1\*</sup>

<sup>1</sup>Department of Physics, Faculty of Science, Kasetsart University, Bangkok - 10900, Thailand; and  
<sup>2</sup>Department of Microbiology, School of Science, RK. University, Rajkot - 360020, Gujarat, India

## 1. Introduction

The unique physical, chemical, optical and electronic properties of semiconductor quantum dots (QDs) have resulted in broad-spectrum applications in therapeutics, diagnosis, bioimaging, sensors, and others (Ajibade and Oloyede, 2022). The fluorescent QDs are zero-dimensional materials with quantum confinement in all three dimensions. They are generally 1–10 nm in size. The tunable size and shape of the QDs are dependent on the method of synthesis and various reaction parameters such as precursor concentration, temperature, time, pressure, and pH (Jara et al. 2014). The exciton generation, tunable energy band gaps, and high absorption coefficients of QDs make them the most suitable candidates for their application in photovoltaic devices (Stolle et al. 2014). Among various nanomaterials developed to date, semiconductor quantum dots were some of the first nanostructures explored for biomedical applications that include cadmium and zinc selenide based core-shell nanoparticles (Deerinck et al. 2008). Carbon-based QDs are more advantageous due to their good water solubility, biocompatibility, and stable fluorescence. The fluorescent emission wavelength of graphene quantum dots (GQDs) can be in various regions, including deep ultraviolet light, blue light, green light, yellow light, and red light. The fluorescent property of the QDs is largely dependent on their sizes, surface-associated functional groups, and excitation wavelength (Chen et al. 2018).

Various synthesis processes for the fabrication of luminescent QDs include carbonization, electrochemical oxidation, hydrothermal, microwave-assisted, oxidative cleavage, solvothermal ultrasonic-assisted methods (Adersh et al. 2015; Kitture et al. 2015; Kitture et al. 2012). However, the extensive use of hazardous chemicals for reduction and stabilization in the aforementioned physical and chemical processes are major limitations for their biomedical applications due to compromised biocompatibility (Ghosh et al. 2011; Ghosh et al. 2012a,b). Hence, biological methods are most preferred for the synthesis of luminescent QDs using bacteria, fungi, algae, and plants (Salunke et al. 2014; Sant et al. 2013). The extracts prepared from the biomass are rich in metabolites such as enzymes, reducing sugars, flavonoids, phenolics, starch, saponin, citric and ascorbic acids which can play a significant role in the synthesis, shape evolution, and capping of the biofabricated nanoparticles (Ghosh et al. 2015a-f; Mallick et al. 2015).

Although the biological synthesis of QDs is in its infancy, the past decade has witnessed extensive efforts to improve the synthesis methods for QDs with control over the size and shape to yield monodispersed particles with desired morphological and functional properties (Ghosh et al. 2014; Ghosh et al. 2013). In view of the background, the following report gives an elaborate account of the synthesis of carbon quantum dots (CQDs) using *Syzygium samarangense* popularly known as Java apple. The CQDs were characterized and will be used further to incorporate within electrospun polymeric nanofibers for carbon dioxide reduction and capture.

## Methods

**Plant extract preparation:** Fresh Java apple were collected from the local market in Bangkok, Thailand which were washed thoroughly under running tap water for 5 minutes. The fruits were cut into small pieces and converted to juice using an electric juicer. The resulting juice was strained to remove any particles and stored at 4°C for further use.

**Synthesis of CQDs:** CQDs were synthesized by a facile hydrothermal treatment of Java apple juice. Filtered fresh juice was poured into a 100mL stainless-steel autoclave with a Teflon lining and thermolyzed for 36h at 180 °C. The oven was cooled to room temperature. The CQDs were collected by filtration with a 0.22 µm membrane filter as an orange-brown highly viscous liquid. Photocatalytic activity measurements.

**Characterization:** The CQDs were characterized using UV-visible spectroscopy, Fourier transform infrared spectroscopy, and transmission electron microscope (TEM) analysis.

## Results and Discussion



**Figure 1.** Preparation of plant extract. A) Weighing of fresh Java apples; B) sliced pieces inside electric juicer; C) fruit juice preparation; D) straining the fruit juice; E) filtration through Whatman filter paper No 1.; F) Filtered fruit juice stored for further use.



**Figure 2.** Hydrothermal synthesis of CQDs using a stainless-steel autoclave with a Teflon lining.

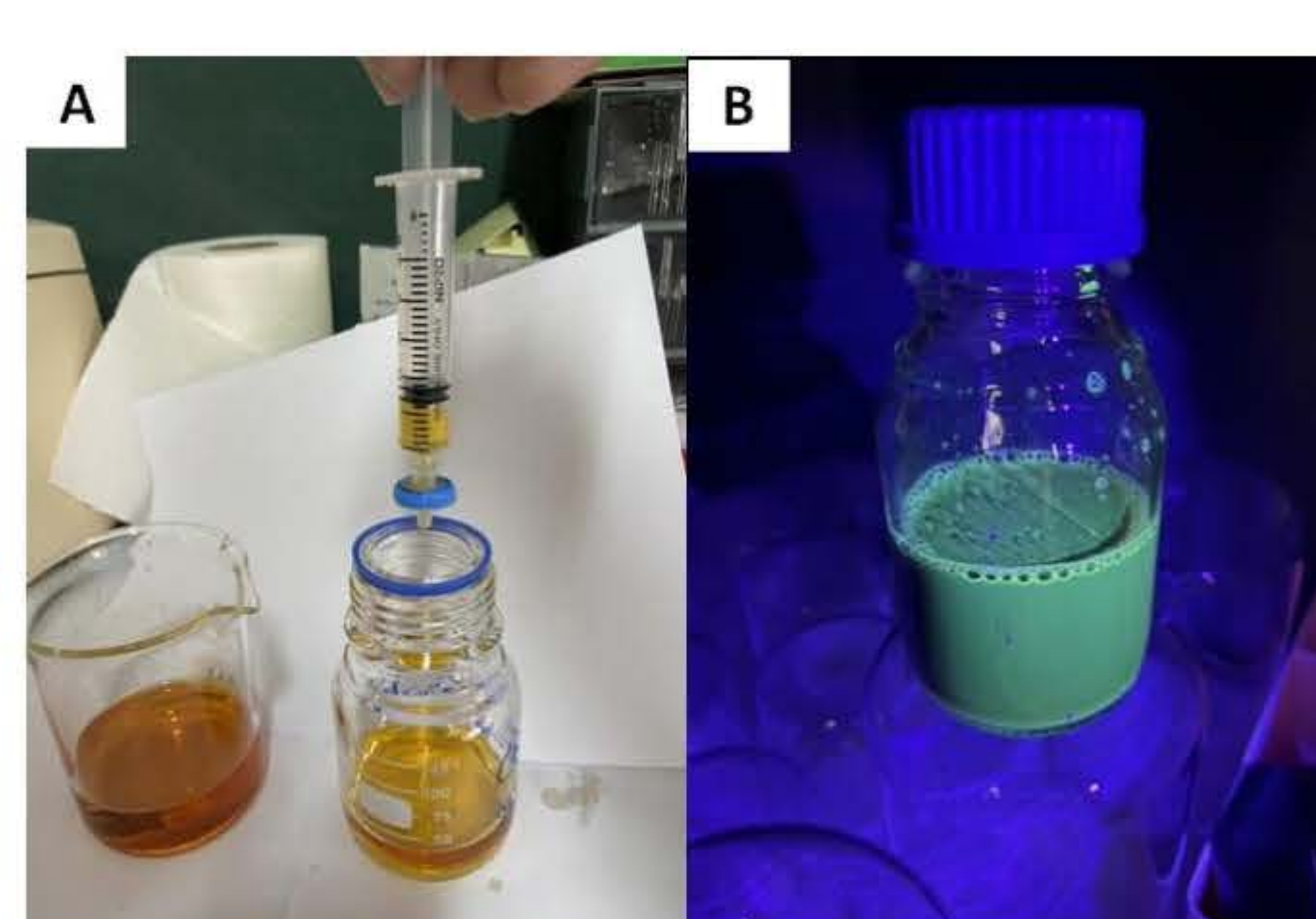


**Figure 3.** A) Recovery of the CQDs using syringe filtration and B) fluorescence of the CQDs under the UV light.

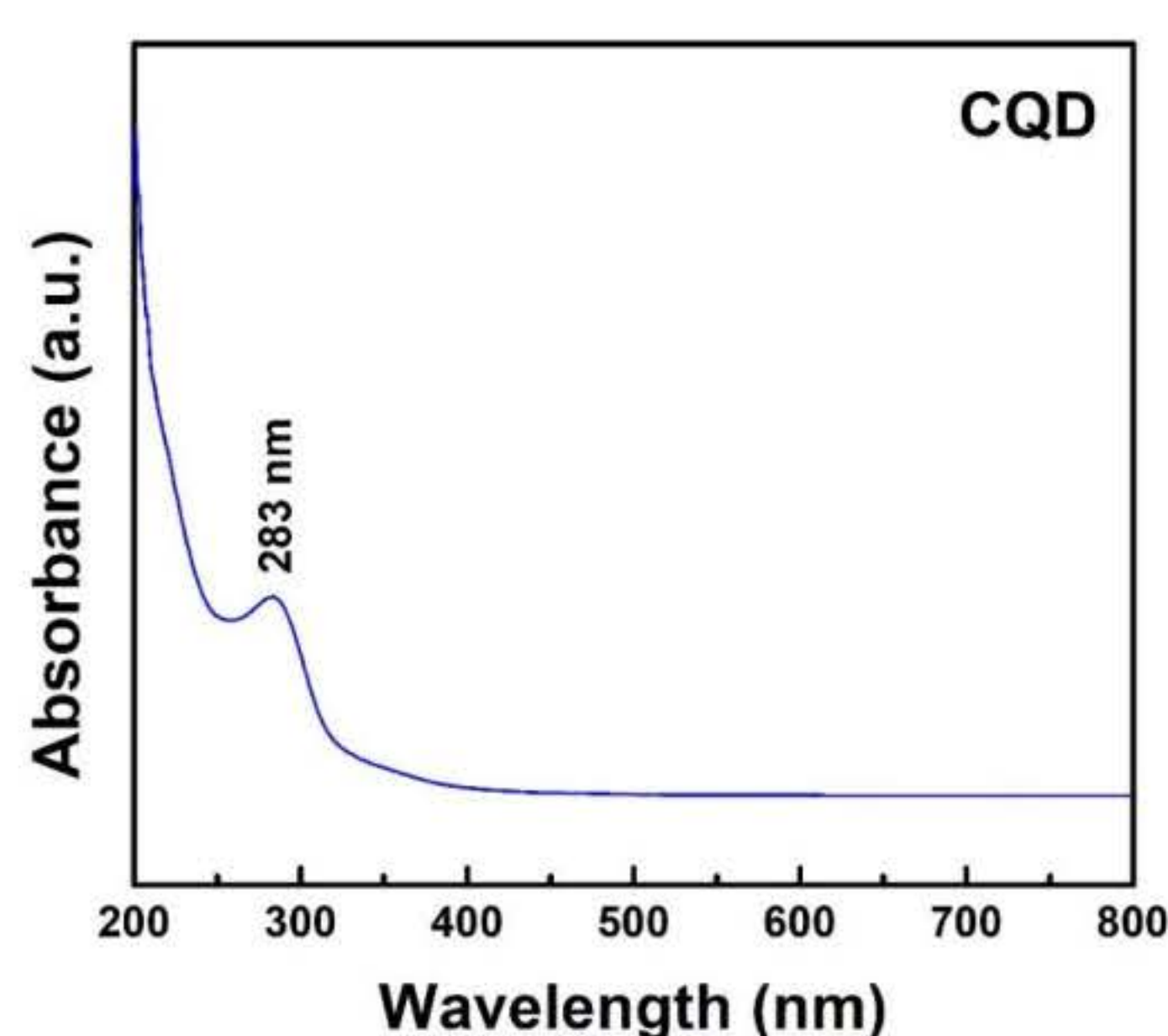


**Figure 4.** The UV-visible spectra of the CQDs

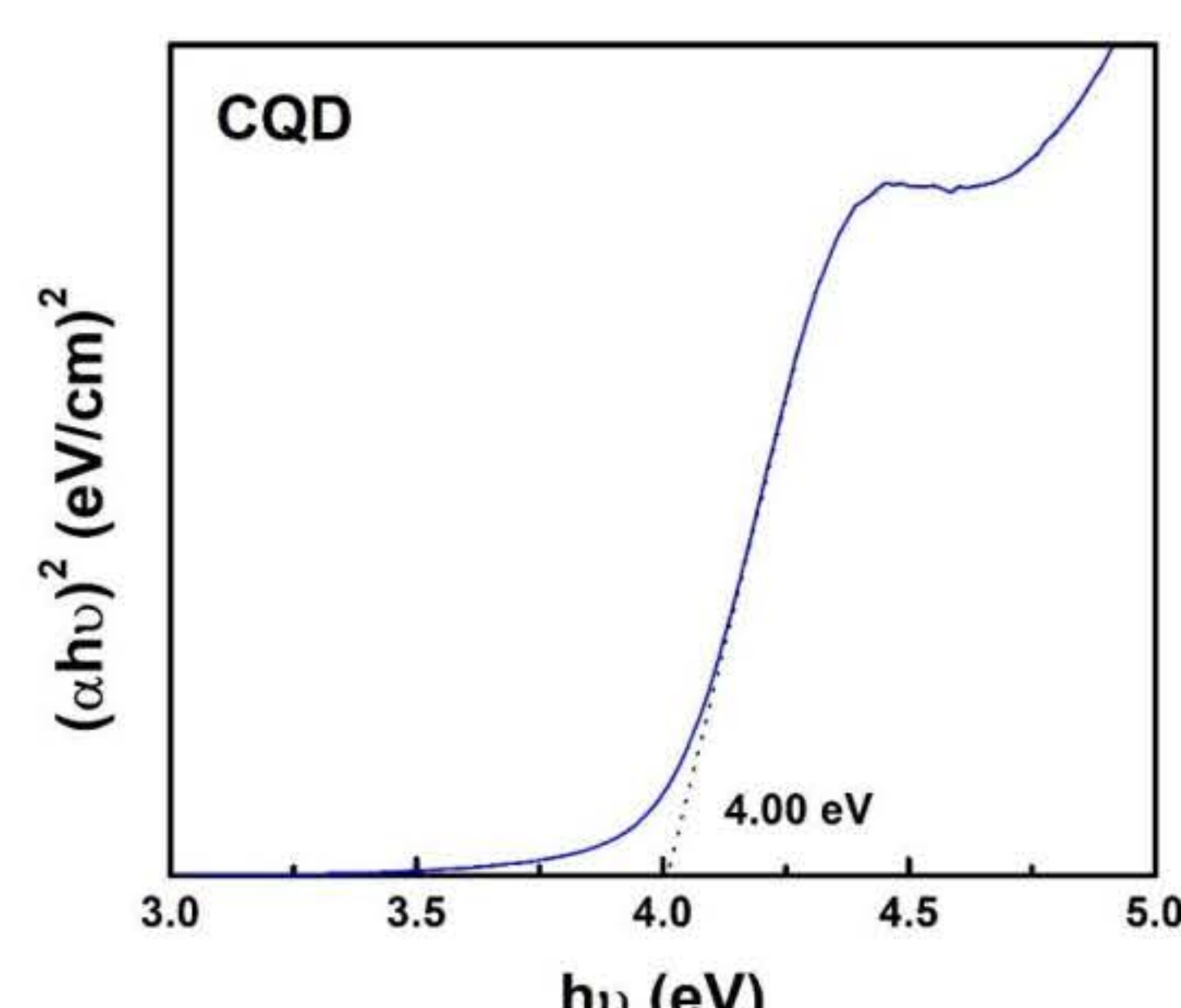


**Figure 5.** The UV-Vis absorption data fitted by Tauc's formula for direct band gap.

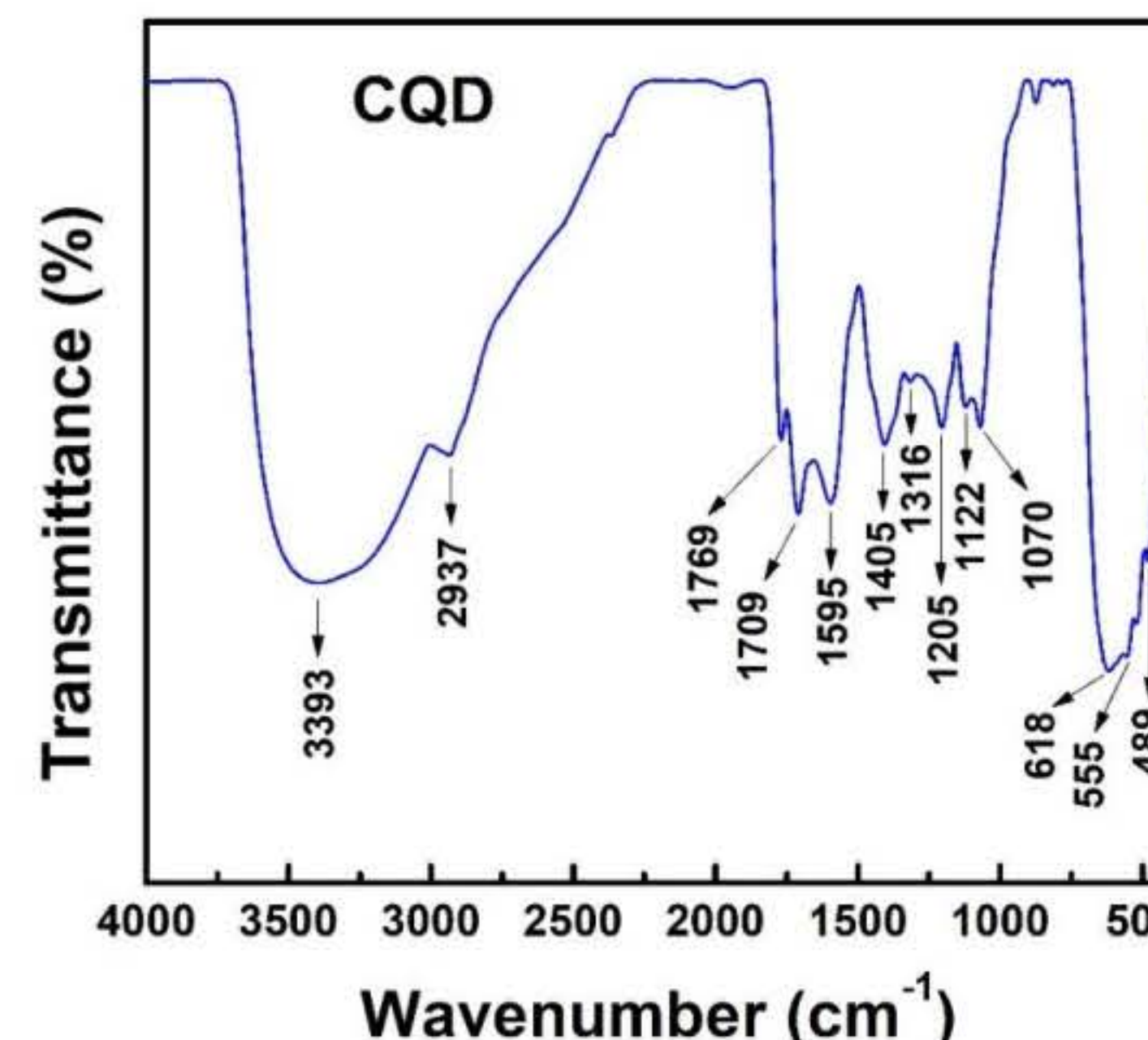


**Figure 6.** The FTIR spectrum of the CQDs

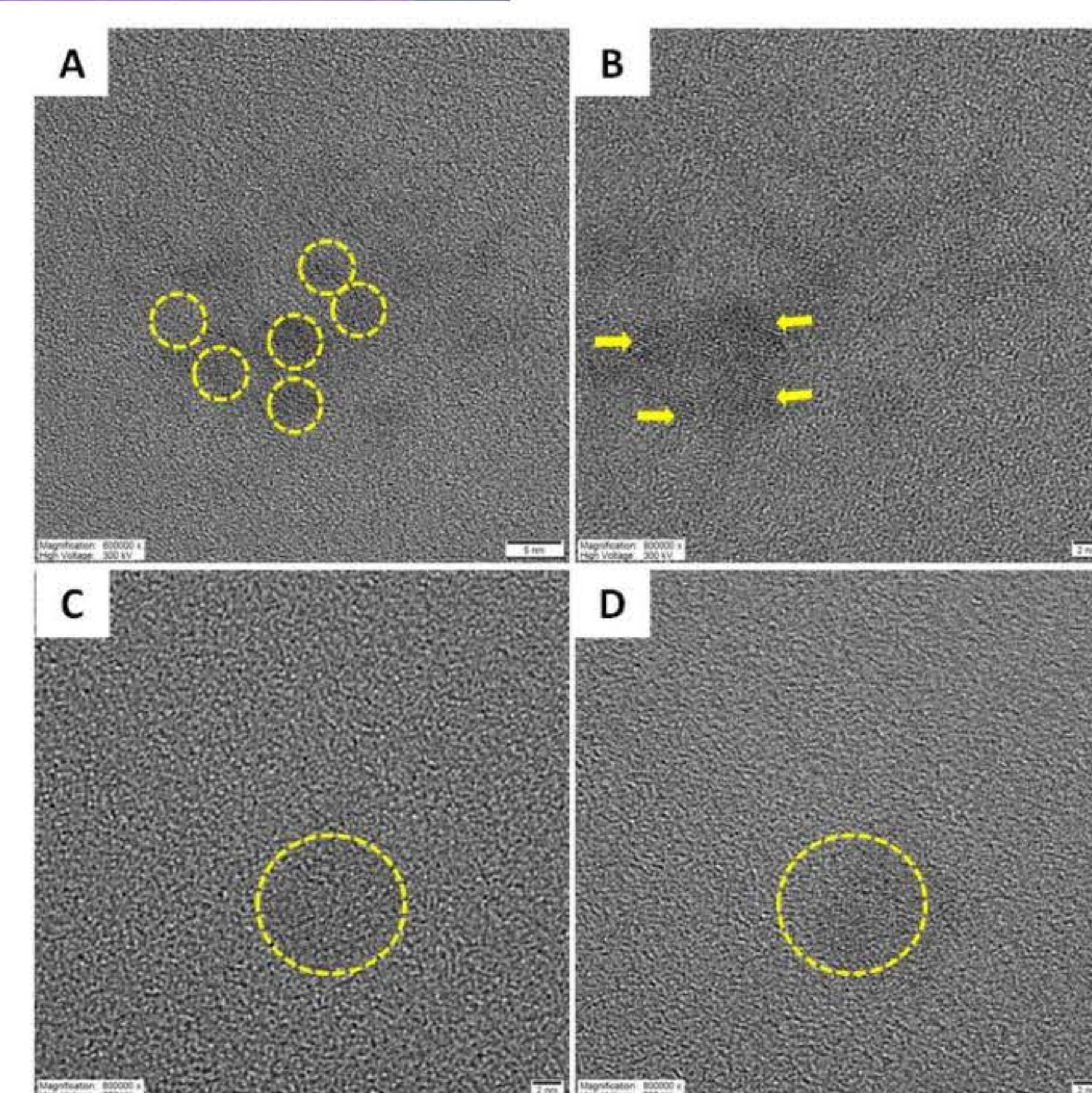


**Figure 7.** TEM images of picture of CQD. A) Inset showing scale bar of 5 nm; B) CQDs attached together with inset scale bar of 2 nm; C and D) Discrete CQDs with visible lattice fringes with inset scale bar of 2 nm.

**Synthesis of CQDs:** The fresh Java apples were used for the preparation of the plant extract. **Figure 1** shows the stepwise processing of the fruits eventually getting the pure fruit juice which was used for further CQDs preparation. The CQDs were synthesized by direct hydrothermal treatment of the fruit juice at 180 °C for 36 h as shown in **Figure 2**. Then the resulting CQDs were collected by filtration with a 0.22 µm membrane that showed brown colour in visible light while it exhibited bright fluorescence under UV light as shown in **Figure 3**. The use of Java apple juice as a natural precursor and low synthesis temperature allowed for the highly scalable and sustainable synthesis of CQDs.

## UV-visible spectroscopy:

An aqueous dispersion of the CQDs was highly stable without any sign of precipitation even after four months. On irradiation with 365 nm UV light, the aqueous solution of CQDs showed an intense greenish blue color indicating its potential in the optoelectronic and biomedical fields. The UV-visible spectroscopy revealed a sharp peak at 283 nm which indicated the successful synthesis of the CQDs from the plant extract as evident from **Figure 4**. Further, the UV-Vis absorption data was fitted by Tauc's formula for direct band gap evaluation that is presented in **Figure 5**.

## FTIR analysis:

The Fourier transform infrared (FTIR) spectrum in **Figure 6** shows the presence of significant surface functional groups. The merged peaks at ~1595 cm<sup>-1</sup> were assigned to C=O and C=C stretching in the conjugated structure. The C=O and C-O stretching vibrations at ~1595 cm<sup>-1</sup> and ~1405 cm<sup>-1</sup>, respectively, indicate the presence of oxygenated carboxyl and hydroxyl functional groups. Furthermore, the intense band at ~3393 cm<sup>-1</sup> can be assigned to typical -O-H stretching vibrations. The doublet at ~2937 represents C-H stretching. The broad band at ~618 cm<sup>-1</sup> was ascribed to =C-H stretching.

## TEM analysis:

The morphology and microstructure of the CQDs were investigated using transmission electron microscope (TEM) analysis. Typical TEM image in **Figure 7** show that the CQDs were nearly monodispersed and almost spherical. The CQDs exhibited a narrow size distribution in the range of 4–7 nm. The CQDs were highly crystalline with a d-spacing of 0.24 nm.

**Conclusion:** Biogenic CQDs with attractive morphological and optical properties hold great promise for biomedical, environmental, and industrial applications. The route for synthesis is rapid, efficient, and environmentally benign where the generated CQDs are highly fluorescent and biocompatible. The smaller size of the biogenic CQDs makes them attractive for easy uptake and elimination after activity from the cells. However, in order to ensure their clinical translatability, thorough toxicity studies along with pharmacokinetic and pharmacodynamic investigations are warranted. Moreover, the various synthesis parameters like fruit juice concentration, reaction time, temperature, and pH, should be carefully optimized to improve scalability that would ensure higher yield and decrease the production cost. Incorporating the biogenic CQDs into polymeric nanofibers can yield significant properties for ideal carbon dioxide reduction and capture. Thus, with a systematic approach coupled with global R&D and commercialization efforts, biogenic CQDs have a high probability to revolutionize the future of environmental nanotechnology.

**Acknowledgements:** This research has received funding support from the The Program Management Unit for Human Resources & Institutional Development and Innovation (PMU-B) under the Program of National Postdoctoral and Postgraduate System approved by PMU-B Board Committees (Contract No. B13F660065).



## Synthesis of Water Hyacinth-Derived Hard Carbon as an Anode for Sodium-Ion Batteries

Wikanda Wongsombat\*, and Assoc. Prof. Dr. Nikom Klomkliang\*,<sup>1</sup>

\* School of Chemical Engineering, Institute of Engineering, Suranaree University of Technology, Nakhon Ratchasima 30000, Thailand

<sup>1</sup> Corresponding author: nikom.klo@sut.ac.th

### INTRODUCTION

Currently, lithium-ion batteries are widely used as electrical energy storage devices. However, due to the limited quantity and high price of lithium compounds, an interesting alternative is being considered to address this issue: replacing them with sodium-ion batteries. Sodium-ion batteries are considered a cost-effective and environmentally friendly option, as sufficient sodium sources are readily available, and anode electrodes can be obtained by burning biomass. With inexpensive chemical components, a scaled-up industry should be capable of producing batteries that cost less than their lithium counterparts, with the added benefit of a significantly improved environmental profile.

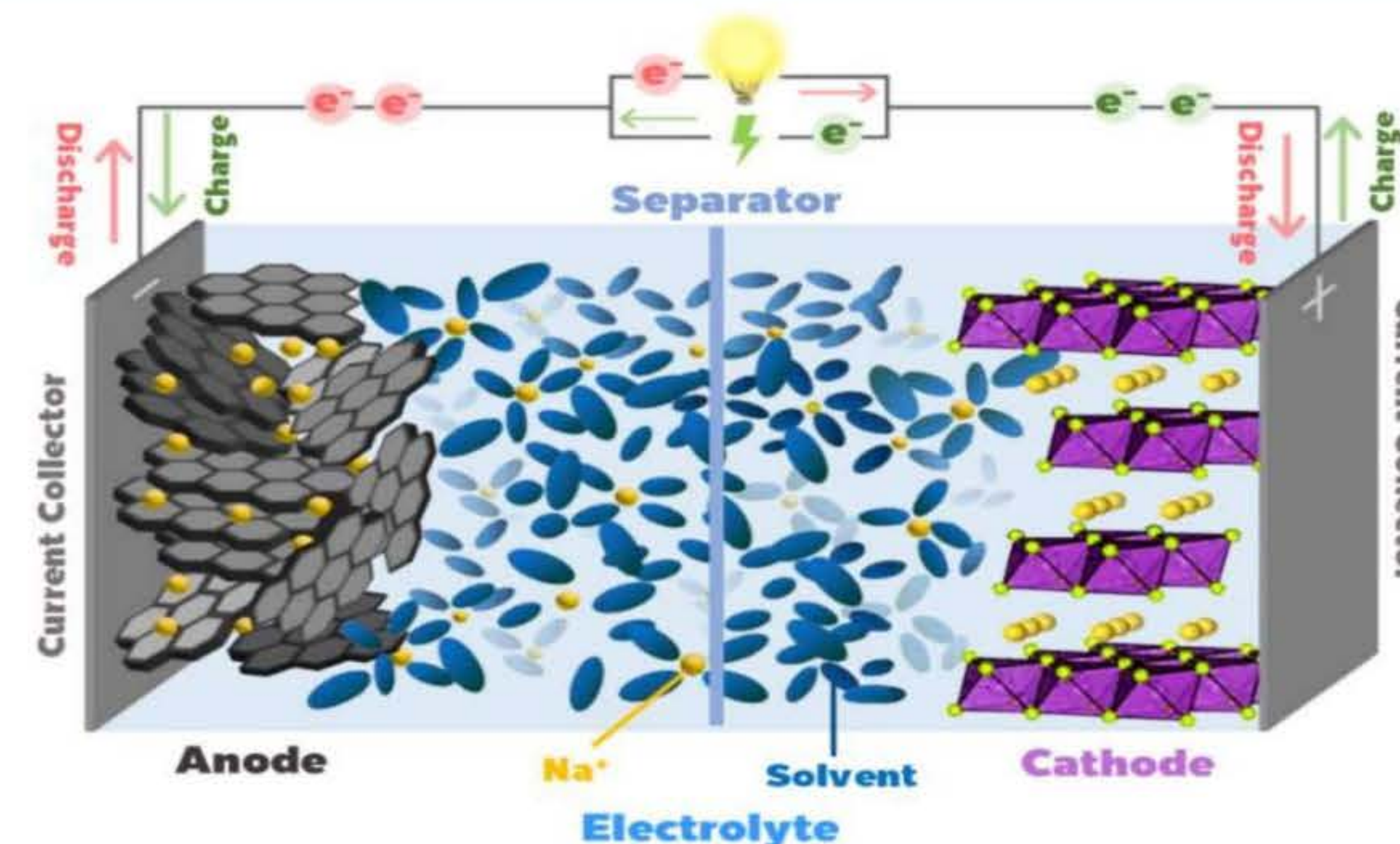


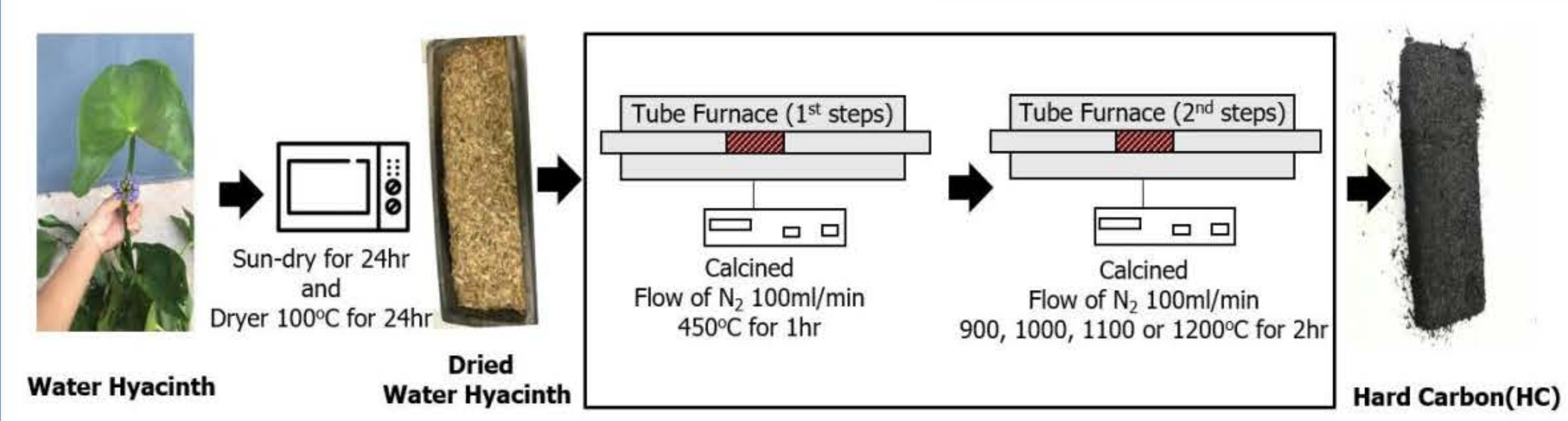
Fig. 1. Components and Working Principles of Sodium-Ion Batteries During Charging and Discharging (Palomares, Serras et al. 2012)

### OBJECTIVE

This research project, therefore, synthesizes hard carbon material from biomass by using water hyacinth as the anode for sodium-ion batteries. This is because the hard carbon material has a large amount of pores and a high surface area. It has a high charge and discharge capacity, it is cheap, and it increases the value of weeds.

### METHODS

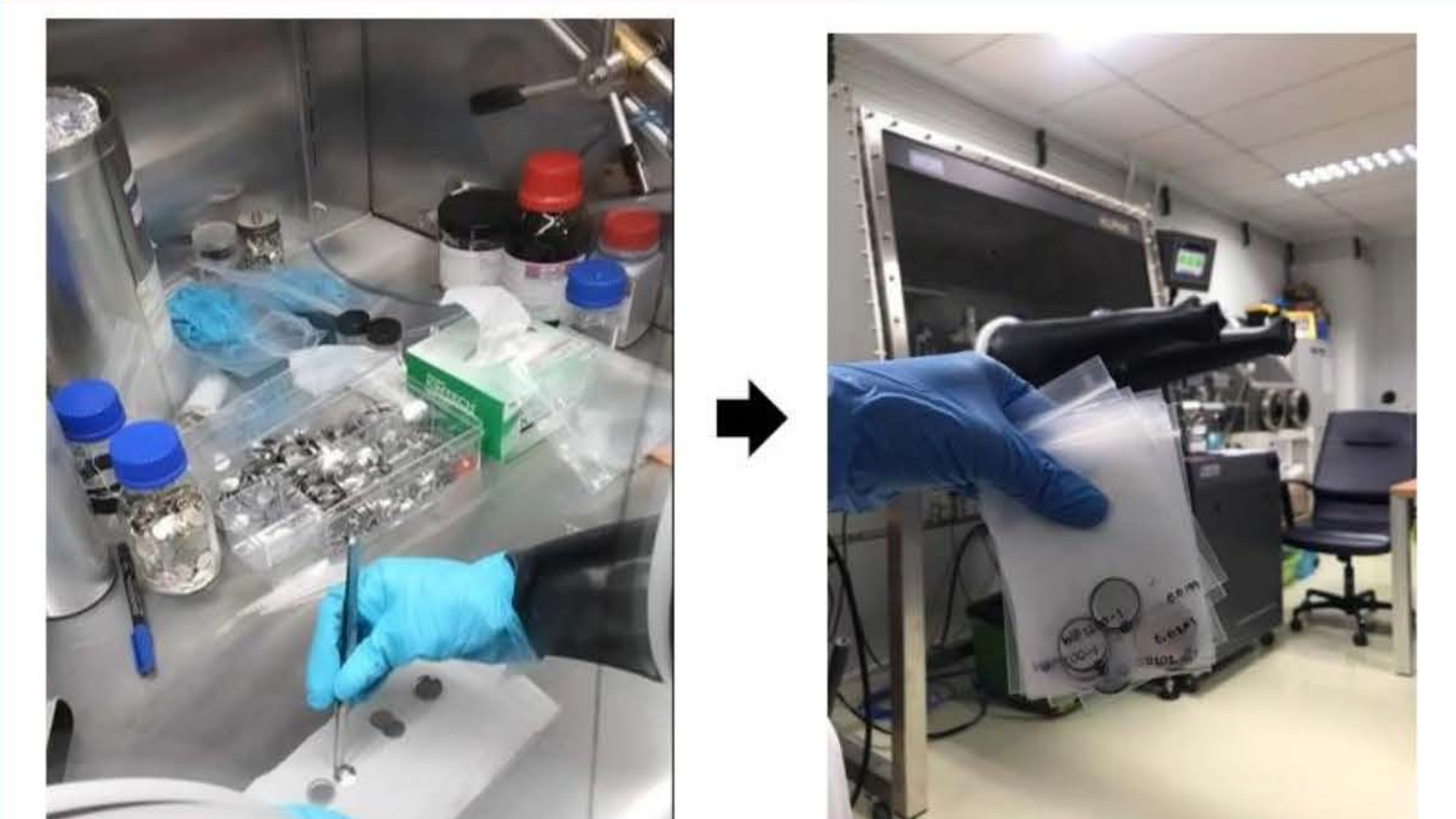
#### Synthesis of Hard Carbon from Water Hyacinth



#### Synthesis of Hard Carbon electrode



#### Forming coin cell battery inside an Argon glovebox



### RESULTS AND DISCUSSION

#### CHN analysis

Table 1. Average percentage of Carbon, Hydrogen and Nitrogen elements

Sample	Carbon	Hydrogen	Nitrogen
WH900-2	40.74	1.74	0.98
WH1000-2	46.13	1.39	0.69
WH1100-2	53.26	1.19	0.34
WH1200-2	55.87	0.50	1.35

Sample	Carbon	Hydrogen	Nitrogen
WH1100-1	50.14	0.77	0.31
WH1100-2	53.26	1.19	0.34
WH1100-3	49.30	0.91	0.31
WH1100-4	52.15	1.01	0.30

Sample	Carbon	Hydrogen	Nitrogen
WH1200-1	60.09	0.26	1.19
WH1200-2	55.87	0.50	1.35
WH1200-3	52.19	0.26	1.22
WH1200-4	52.36	0.20	1.06

#### X-ray diffraction (XRD)

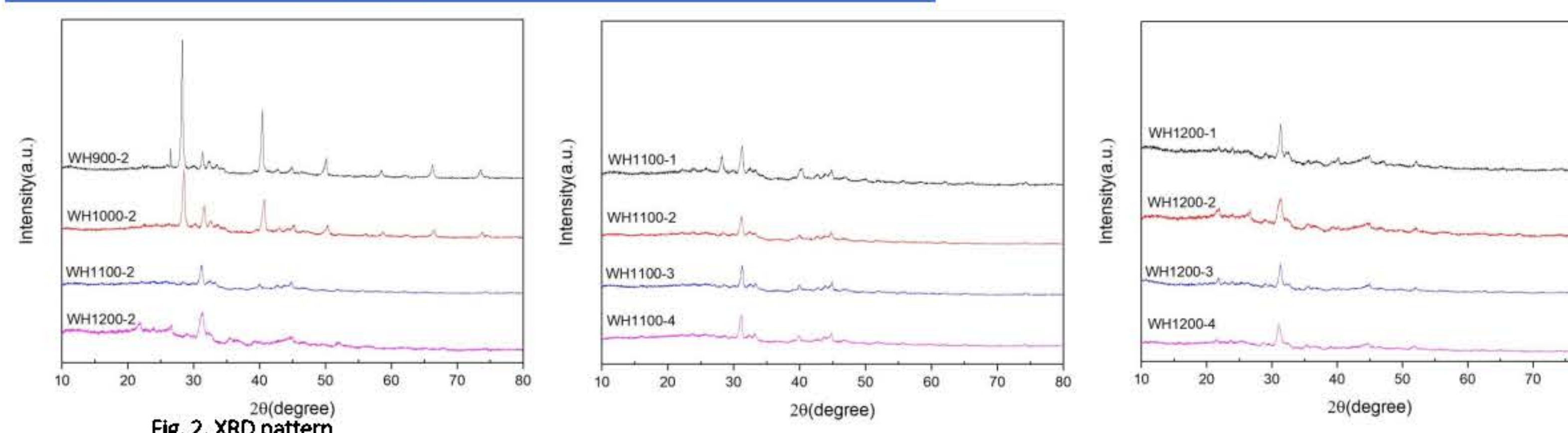


Fig. 2. XRD pattern

#### ASAP2020 Plus

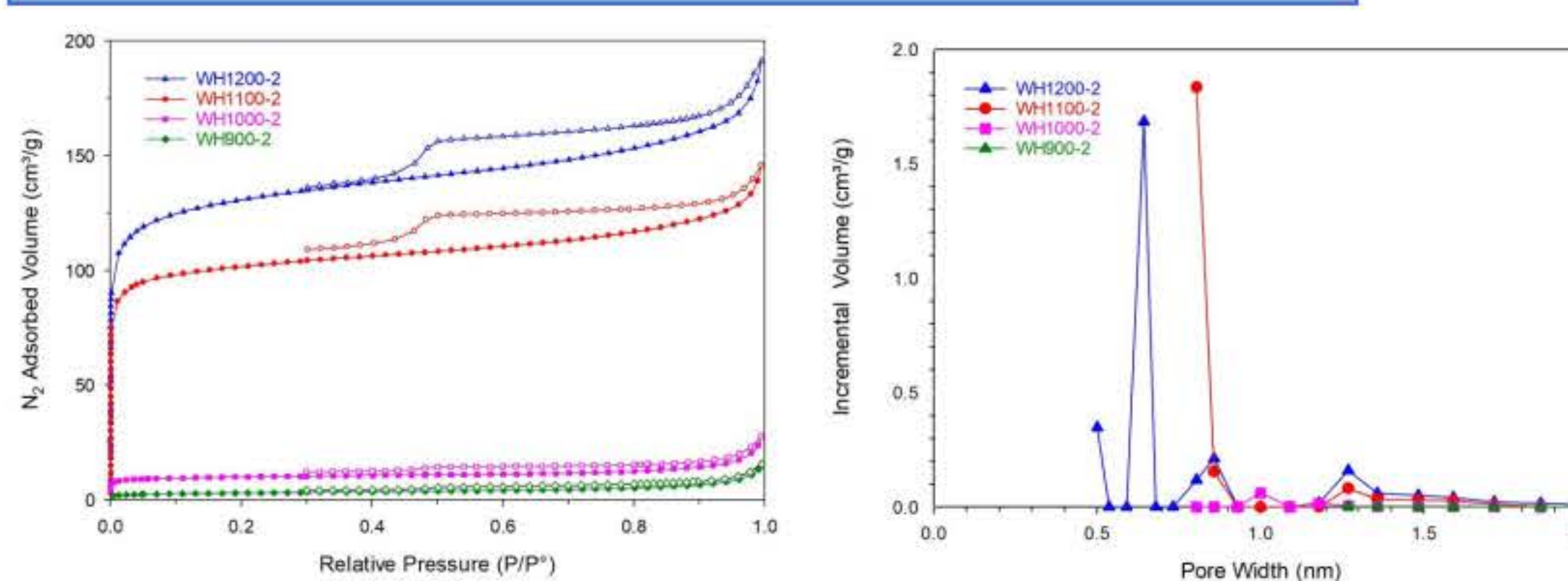


Fig. 3. N<sub>2</sub> adsorption-desorption isotherm and the distribution of pore sizes

Table 2. Physical parameters of HW products

Sample	S <sub>BET</sub> (m <sup>2</sup> g <sup>-1</sup> )	Pore volume (cm <sup>3</sup> g <sup>-1</sup> )
WH900-2	10.21	0.0239
WH1000-2	34.53	0.0427
WH1100-2	357.22	0.2256
WH1200-2	458.81	0.2960

### CONCLUSIONS

Synthesis of Hard Carbon from Water Hyacinth for Use as an Anode Electrode. The most suitable pyrolysis condition, determined at 1200°C for 2 hours, was identified as optimal for anode. Physical properties were investigated through XRD, CHN analysis, and N<sub>2</sub> adsorption-desorption techniques. The analysis revealed a high nitrogen content of 1.35 wt% in its structure and a surface area of 458.81 m<sup>2</sup> g<sup>-1</sup>. These properties positively influence the performance of the anode for Sodium-Ion Batteries.

#### ACKNOWLEDGEMENTS

This research has received funding support from (i) Suranaree University of Technology (SUT) and (ii) the NSRF via the Program Management Unit for Human Resources & Institutional Development, Research and Innovation (PMU-B) [grant number B13F60067]





BRAINPOWER  
CONGRESS 2023

ร่วมกับสร้างและขับเคลื่อนงานวิจัยชั้นแนวหน้า  
สู่อุตสาหกรรมแห่งอนาคต



# Production of bioactive peptides with *Bacillus subtilis* from agro-industrial wastes for plant health-promoting

Chanon Saengchan<sup>1</sup> and Kumrai Buensanteai<sup>1\*</sup>

<sup>1</sup>School of Crop Production Technology, Institute of Agriculture Technology, Suranaree University of Technology, Nakhon Ratchasima, 30000, Thailand

Corresponding author: kumrai@sut.ac.th

## Introduction

The chemical fertilizer industry is experiencing a growing trend, with an expected annual increase in demand of around 1-2%. This growth is primarily driven by the expansion of agricultural areas for key economic crops such as rice, corn for livestock feed, and cassava. These crops collectively account for approximately 60% of the total chemical fertilizer usage. However, the fertilizer industry faces various challenges, including unpredictable weather conditions, fluctuating prices of raw materials dependent on global fertilizer prices, and exposure to currency exchange rate risks.

Nevertheless, challenges to the chemical fertilizer industry arise from the increasing adoption of organic farming practices and the popularity of biofertilizers. Consumers are showing a preference for products that are environmentally friendly and promote health. Additionally, these products contribute significantly to the added value of Thai agricultural products, estimated at 18-188 times. The global and Thai markets for these products continue to grow, supported by strong government backing.

Therefore, the aim of this study is to develop factors of bioactive peptide products aimed at elevating production capabilities in the industry, and enhancing product features for practical use is crucial. The focus should be on promoting plant growth, inducing resistance, and improving overall plant health. These strategies contribute to the plant's ability to establish its own defense mechanisms against pathogenic agents, thereby increasing its resistance to diseases and adding value to the entire agricultural cycle.

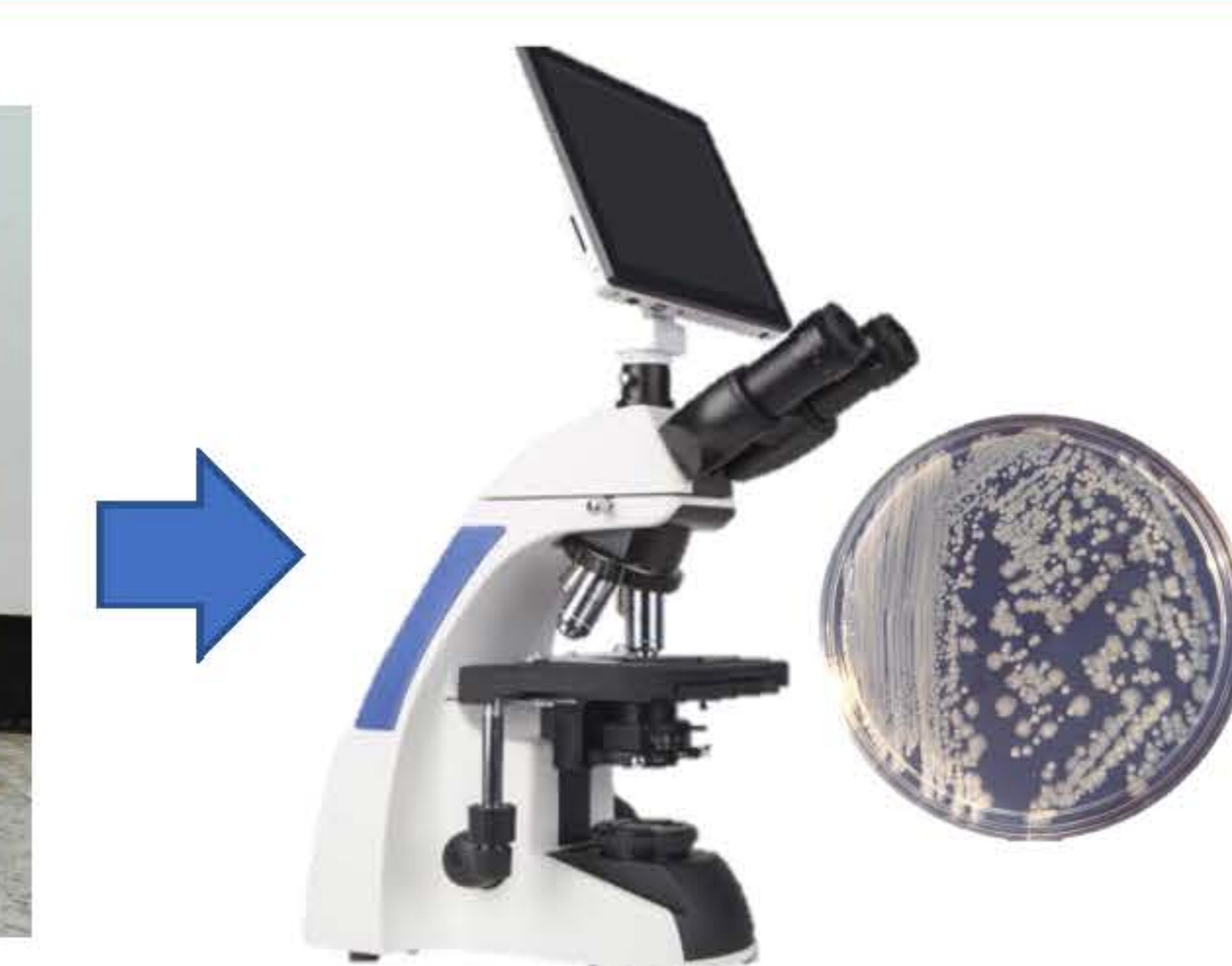
## Materials and methods



Preparing agro-industrial wastes materials in the cassava industry (soil peelings, cassava residue) for use as nutrient sources for *Bacillus subtilis*



Checking the increase in the quantity of *B. subtilis* cultivated in different nutrient media

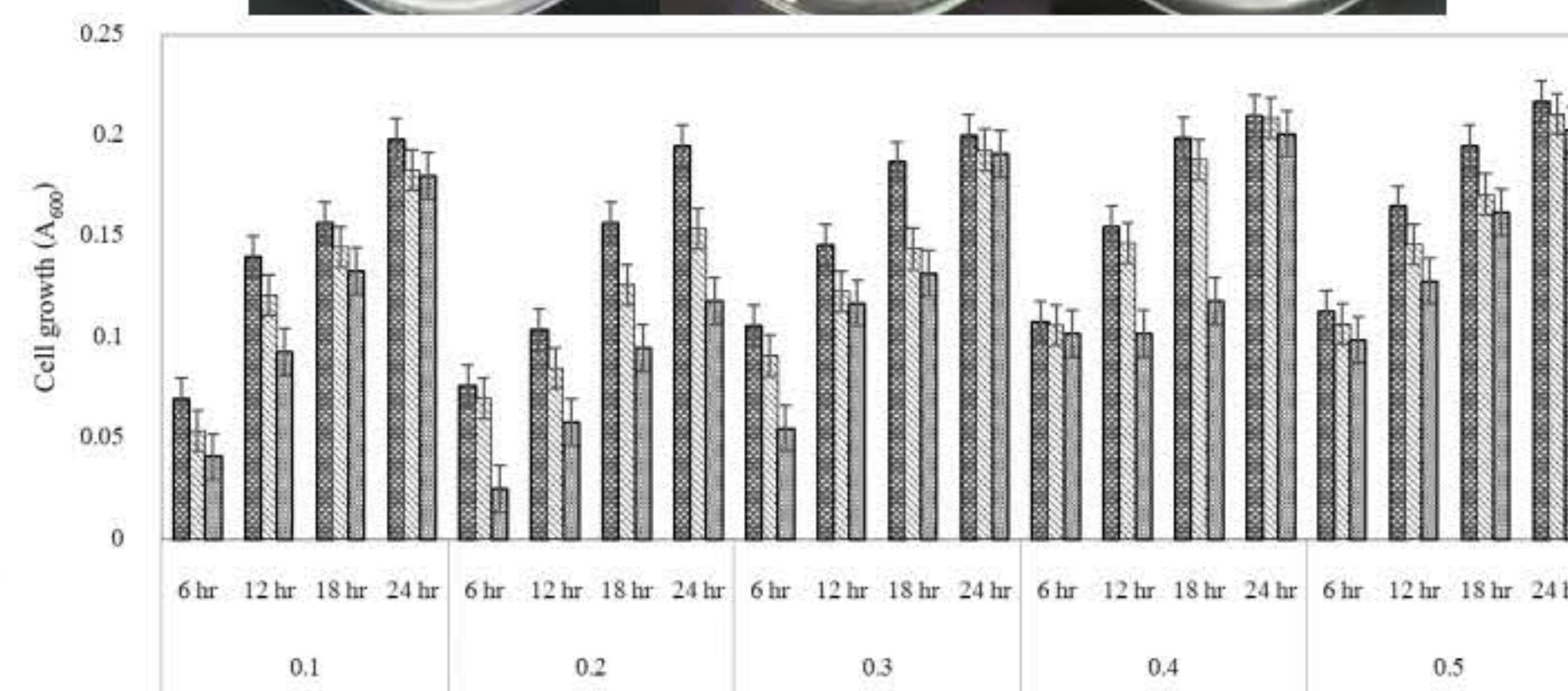


Percentage of microbial (other fungi and bacteria) contamination for 6 months

## Results & Discussion

Months	Percentage of microbial contamination (%)	
	Fungi	Bacteria
0	2.92	1.45
1	5.65	1.18
2	7.09	2.46
3	9.31	3.1
4	11.53	2.24
5	9.99	1.37
6	8.07	1.67

After 6 months of incubation, it was found that the contamination of other types of fungi was 2.92, 5.65, 7.09, 9.31, 11.53, 9.99, and 8.07 percent, while the contamination of other types of bacteria was 1.45, 1.18, 2.46, 3.1, 2.24, 1.37, and 1.67 percent.



Molasses diamonium phosphate and yeast extract (MDY) has the highest amount of bacteria added were  $2.57 \pm 0.27 \times 10^8$  cfu.ml<sup>-1</sup>.

## Conclusion

### Action plan for the next period

- ☐ Prototype of bioactive peptides with *Bacillus subtilis*.
- ☐ Analyzed for moisture content and percentage of survival.
- ☐ Percentage of microbial contamination.
- ☐ Analysis of changes in biochemical composition within plant cells using FT-IR spectroscopy.
- ☐ The draft manuscript for the accepted journal.
- ☐ Statistical analysis

## Acknowledgements

This research has received funding support from (i) Suranaree University of Technology (SUT) and (ii) the NSRF via the Program Management Unit for Human Resources & Institutional Development, Research and Innovation (PMU-B) [grant number B13F660067]



# Study of anti-microbial food packaging film from biodegradable plastics containing nano Ag-eggshell $\text{CaCO}_3$ particle

Mohammad Hossein Azarian<sup>1</sup>, TirapornJunyusen<sup>2</sup>, WimonlakSutapun<sup>1,3</sup>

<sup>1</sup> Research centre for Biocomposite Materials for Medical, Agricultural and Food Industry, Suranaree University of Technology, Nakhon Ratchasima, 30000, Thailand

<sup>2</sup> School of Agricultural Engineering, Institute of Engineering, SuranareeUniversity of Technology, Nakhon Ratchasima, 30000, Thailand

<sup>3</sup> School of Polymer Engineering, Suranaree University of Technology, Nakhon Ratchasima, 30000, Thailand

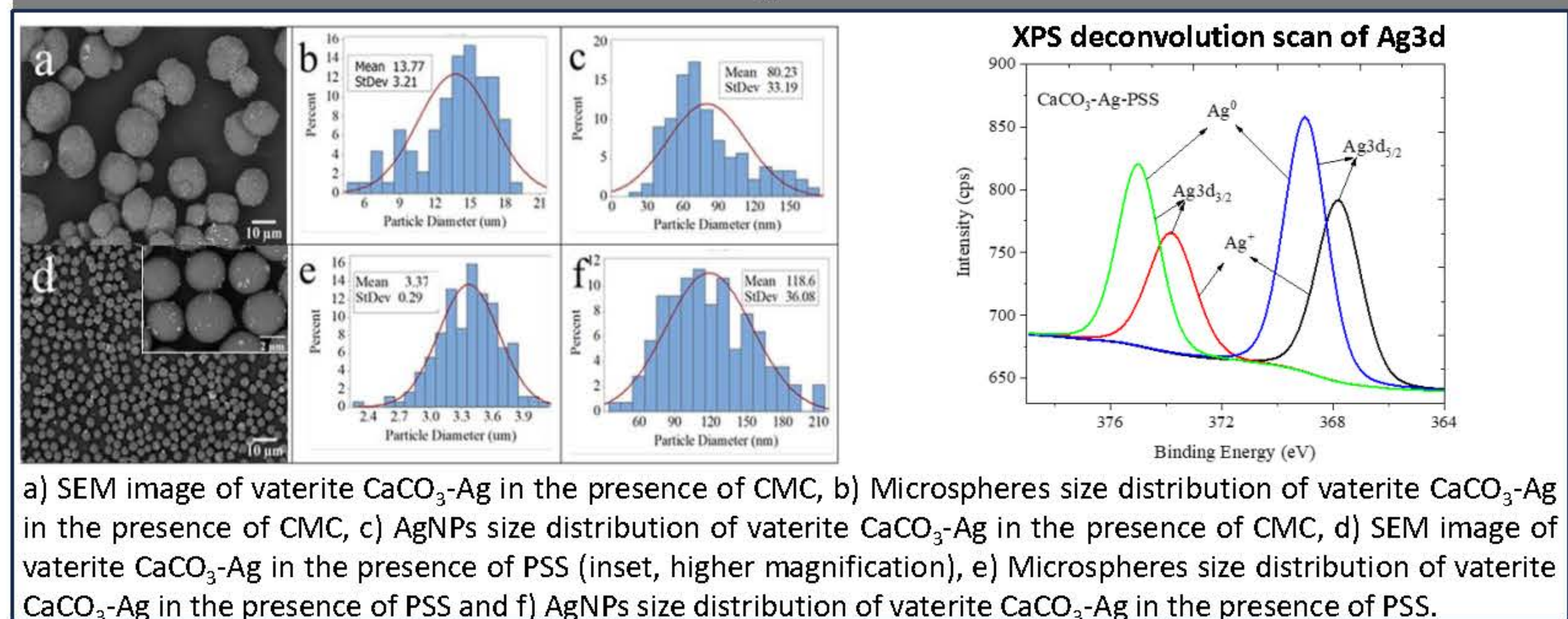
## Introduction

The development of biocompatible absorbent materials, combining inorganic and organic constituents, holds crucial significance across biomedical, food industry, and pharmaceutical realms, primarily for moisture management and bacterial growth prevention. Antimicrobial superabsorbent pads play a critical role in active food packaging by managing moisture and inhibiting pathogens, thereby extending food shelf life and substantially reducing food waste. Moreover, shifting from synthetic to biopolymer-based choices, particularly with the utilization of carboxy methyl cellulose (CMC), presents an eco-friendly and sustainable approach in packaging solutions. In wound dressing applications, the use of metal nanoparticles, especially silver, emerges as a promising alternative to antibiotics due to their broad-spectrum antimicrobial properties and their capability to prevent the development of resistance. Silver nanoparticles (AgNPs) demonstrate remarkable antimicrobial efficacy, especially when integrated into diverse polymer matrices like PVA, thereby exhibiting immense potential for enhancing healing processes and safeguarding against bacterial infections.

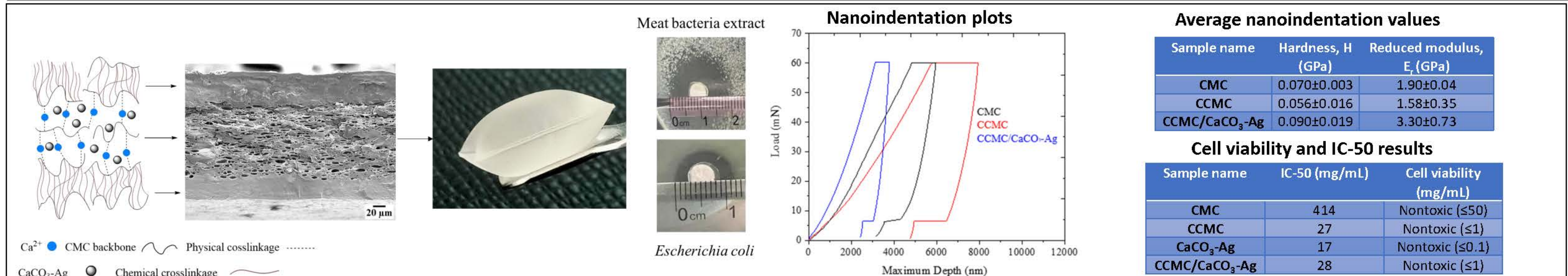
## Objective

Developing antimicrobial superabsorbent pads by integrating CMC and vaterite  $\text{CaCO}_3$ -Ag microspheres aims to enhance mechanical properties, increase water absorption, and improve antimicrobial efficacy against *Escherichia coli* and minced pork bacteria, specifically targeting potential applications in meat packaging. Investigate the influence of vaterite  $\text{CaCO}_3$ -Ag on structural changes and mechanical properties of PVA films and assess the release behaviour of AgNPs in diverse environments, simulating wound conditions, and examining biocompatibility with human dermal fibroblast cells.

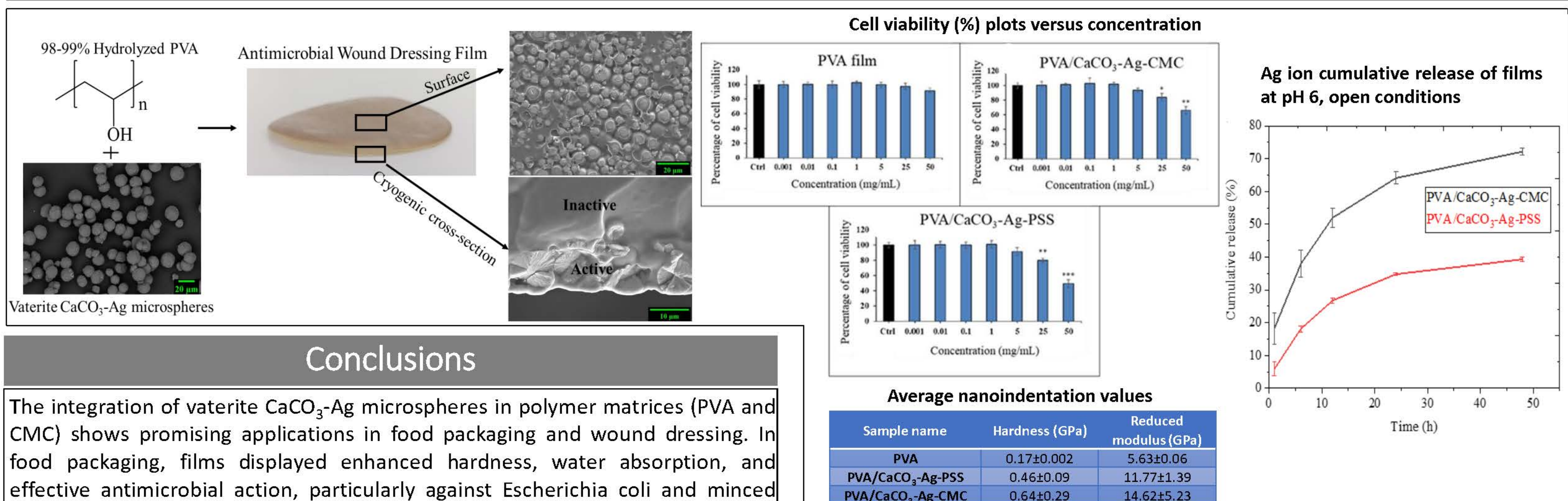
## biogenic vaterite $\text{CaCO}_3$ -Ag hybrid microspheres



## Tailoring microstructure of superabsorbent film for active food packaging using carboxy methyl cellulose and biogenic vaterite $\text{CaCO}_3$ -Ag hybrid microspheres



## Biogenic vaterite calcium carbonate-silver/poly(Vinyl Alcohol) film for wound dressing



## Conclusions

The integration of vaterite  $\text{CaCO}_3$ -Ag microspheres in polymer matrices (PVA and CMC) shows promising applications in food packaging and wound dressing. In food packaging, films displayed enhanced hardness, water absorption, and effective antimicrobial action, particularly against *Escherichia coli* and minced pork bacteria. In wound dressing, the films exhibited improved mechanical properties and potent antimicrobial activity against *Escherichia coli*, demonstrating potential controlled AgNPs release. Both studies reveal the versatility and potential multifunctionality of vaterite  $\text{CaCO}_3$ -Ag hybrid microspheres as carriers for AgNPs in distinct applications, emphasizing their significant role in these industries.

## Acknowledgment

This research has received funding support from (i) Suranaree University of Technology (SUT) and (ii) the NSRF via the Program Management Unit for Human Resources & Institutional Development, Research and Innovation (PMU-B) [grant number B13F660067].





BRAINPOWER  
CONGRESS 2023

ร่วมกับสร้างและขับเคลื่อนงานวิจัยขั้นแนวหน้า  
สู่อุตสาหกรรมแห่งอนาคต



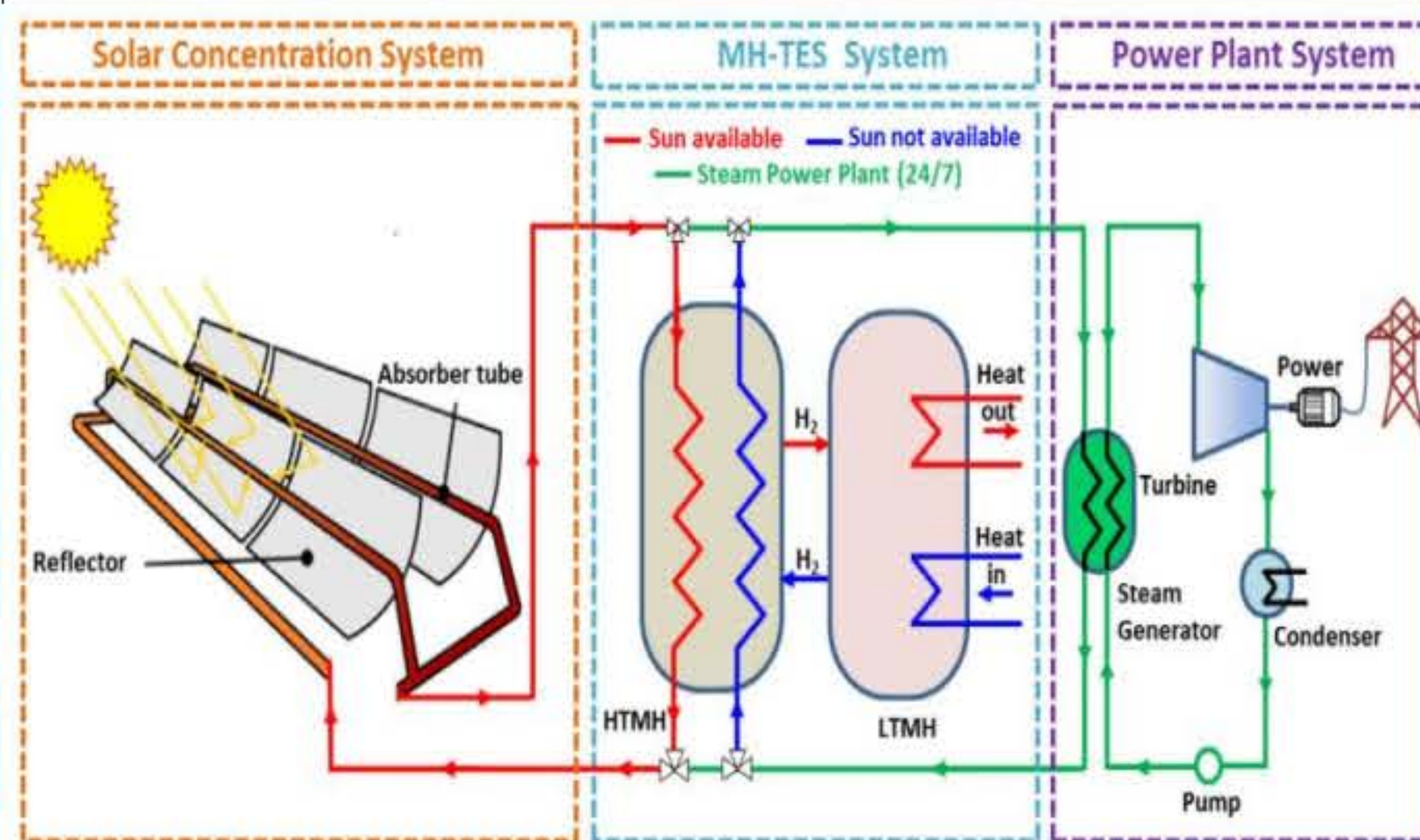
# Heat charging and discharging of coupled $\text{MgH}_2$ - $\text{LaNi}_5$ based thermal storage: Cycling stability and hydrogen exchange reactions

Sophida Thiangviriya, Phuttimet Thongtan, Natthaporn Thaweelap, Prapatsorn Plerdsranoy, Rapee Utke\*

School of Chemistry, Institute of Science, Suranaree University of Technology, Nakhon Ratchasima, 30000 Thailand

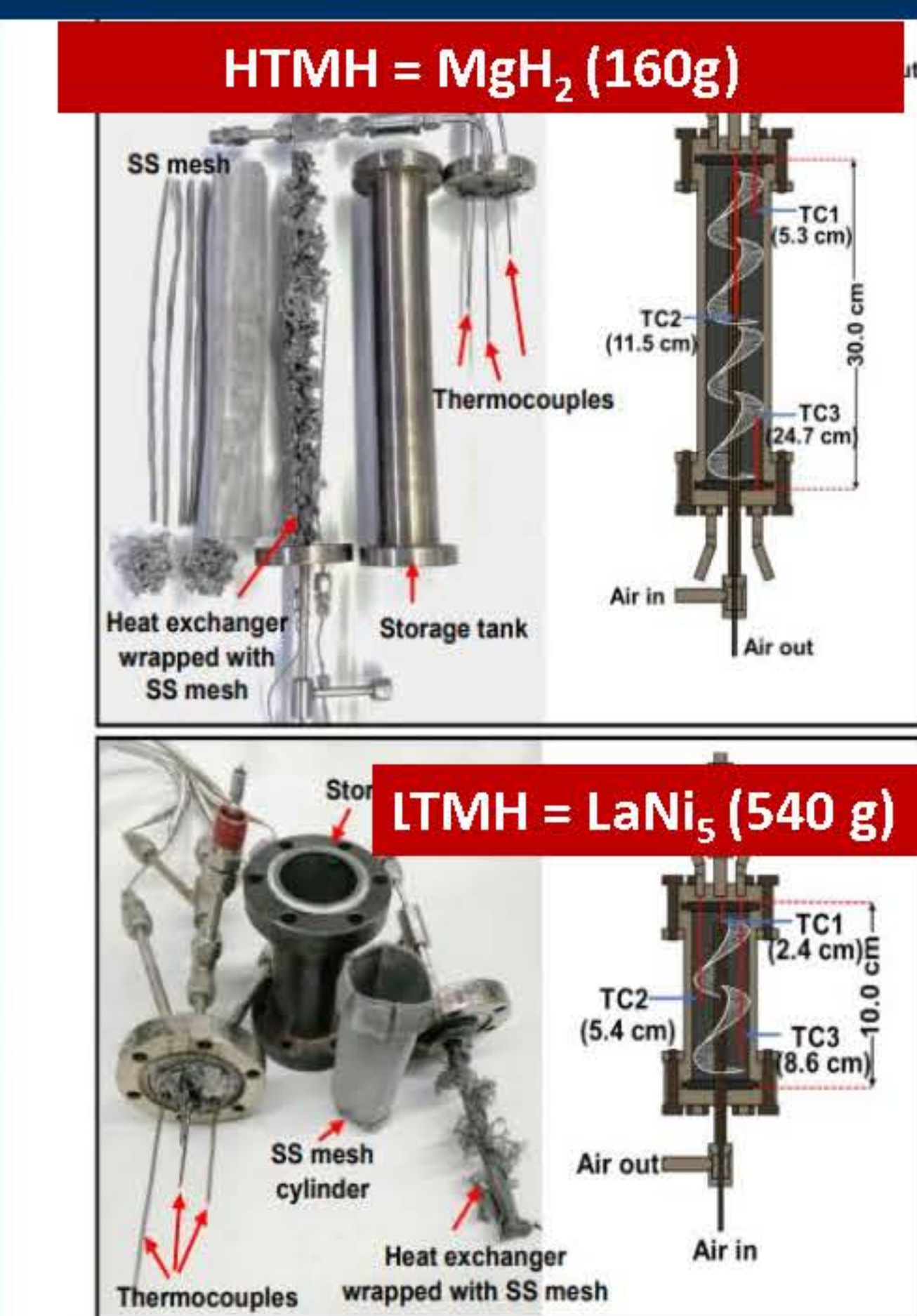
\*Corresponding author (Email: rapee.g@sut.ac.th)

## Introduction

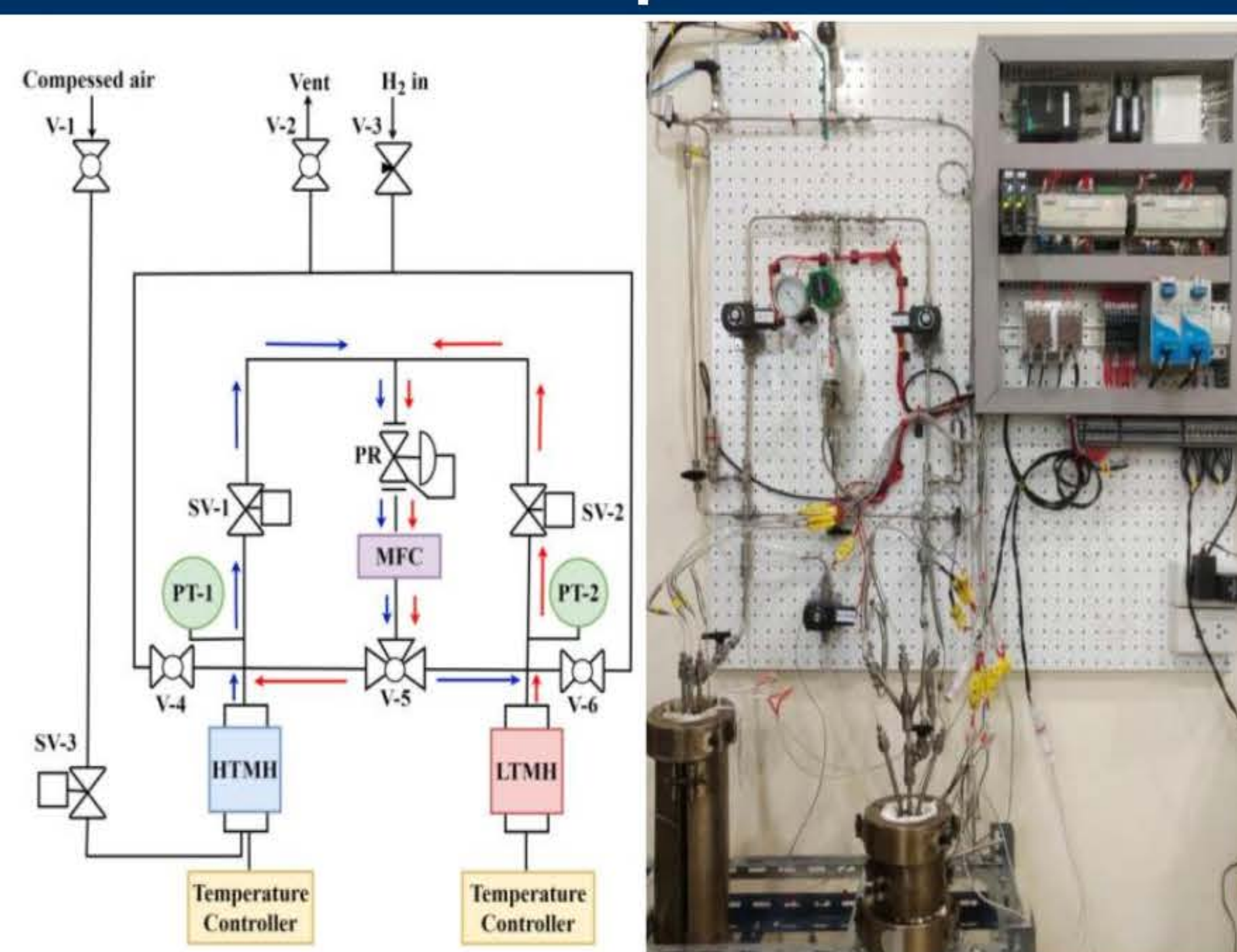


Solar energy can be converted into electricity without emitting greenhouse gases using photovoltaic cells or concentrated solar power (CSP). For CSP plants, integration with thermal energy storage (TES) is required to continuously produce electricity from thermal energy throughout day and night. Considering current TES technologies of sensible heat, latent heat, and thermochemical heat, the last category based on endothermic and exothermic reactions upon de/rehydrogenation of metal hydrides has drawn significant attention due to high energy densities (10 times more than molten salt, wide operating temperature range (300-850 °C), delivery at nearly constant temperature, and cycling stability. The idea of coupled high- and low-temperature hydrides (HTMH-LTMH) with suitable thermodynamics has been proposed for highly efficient TES systems. HTMH acts as thermal battery charging and discharging heat during hydrogen desorption (endothermic) and absorption (exothermic), respectively.

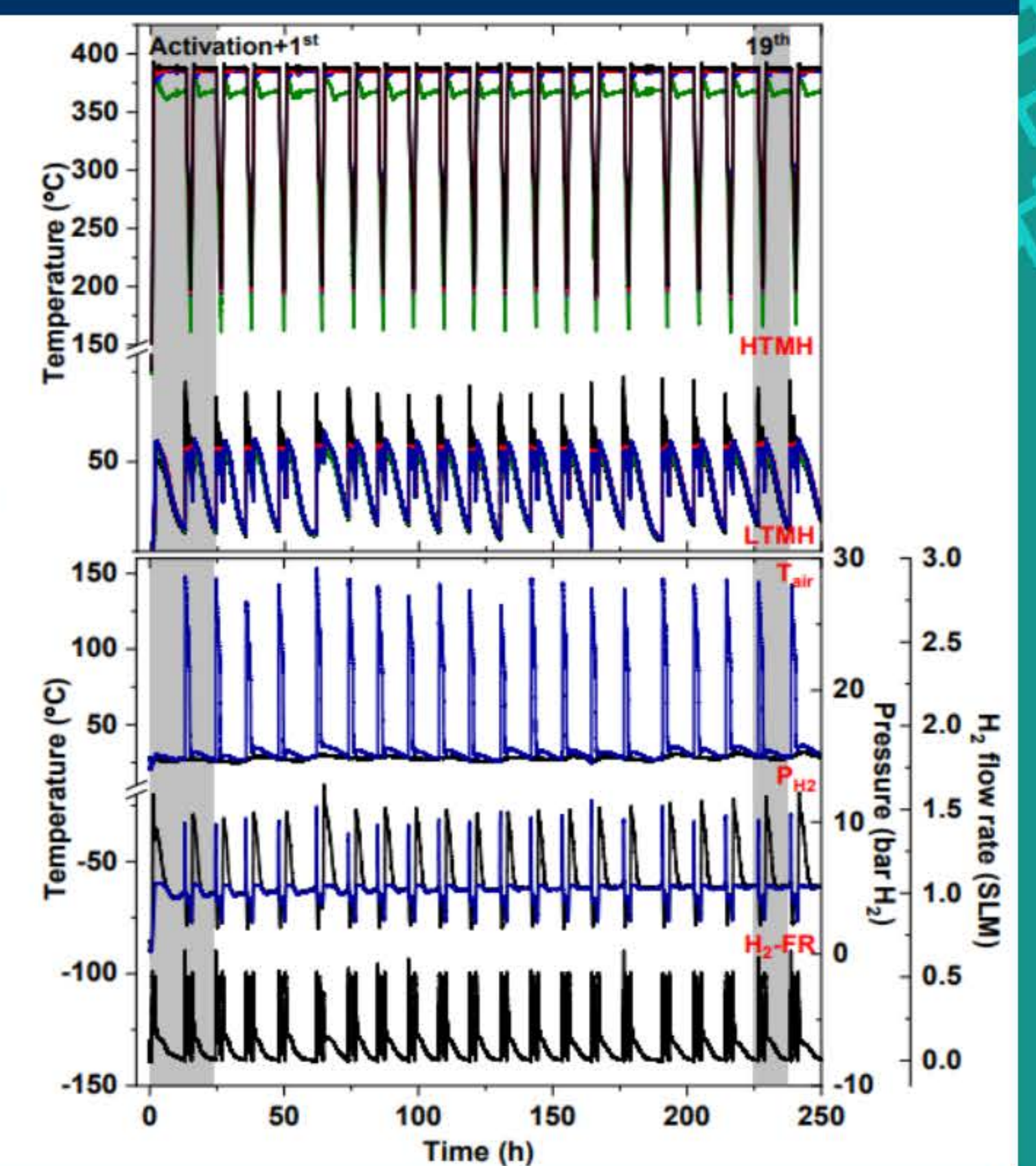
## Experiments



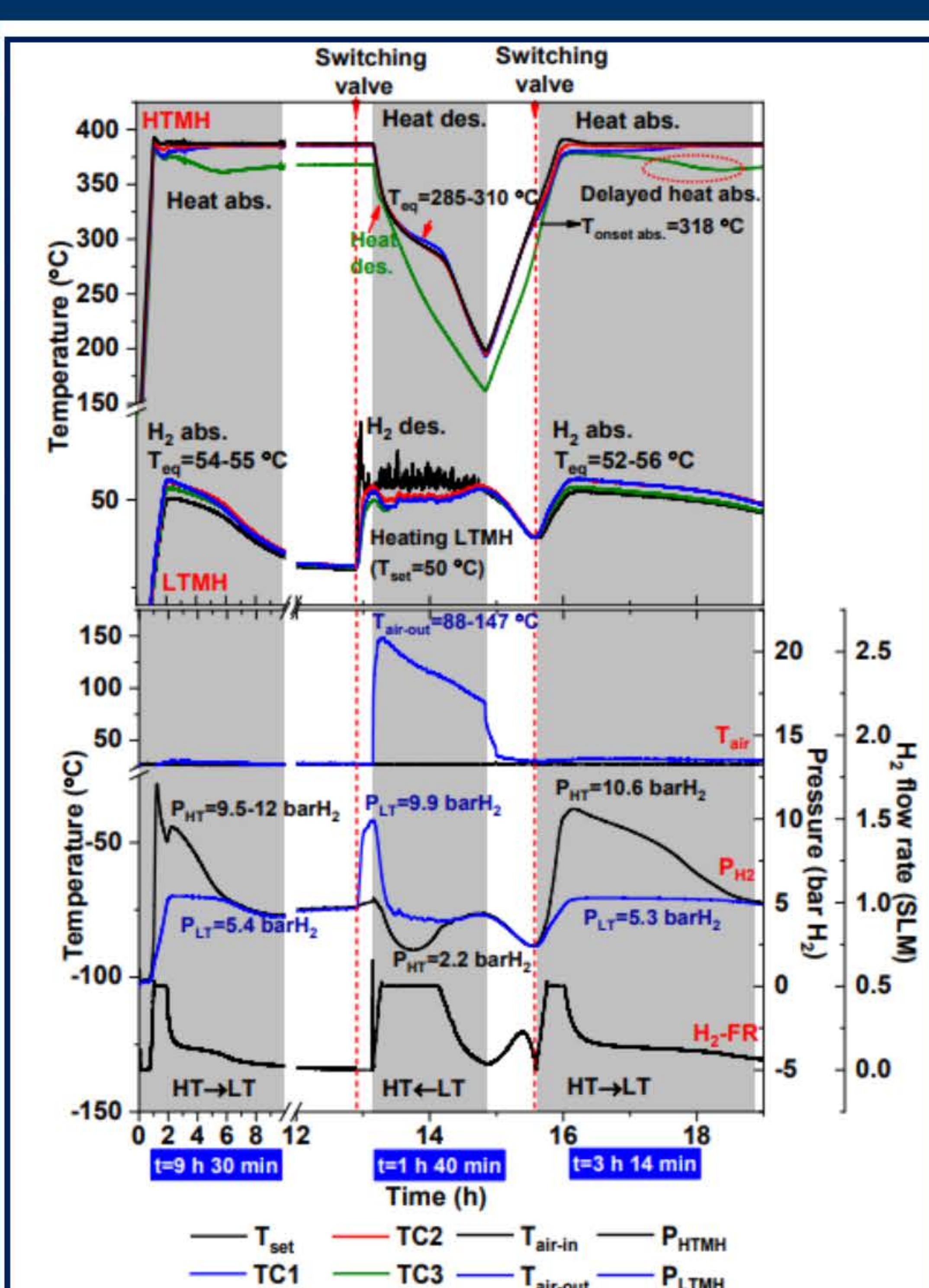
The component and schematic diagrams of HTMH and LTMH tanks.



Schematic diagram and photo of the test station for investigating heat charging and discharging performances

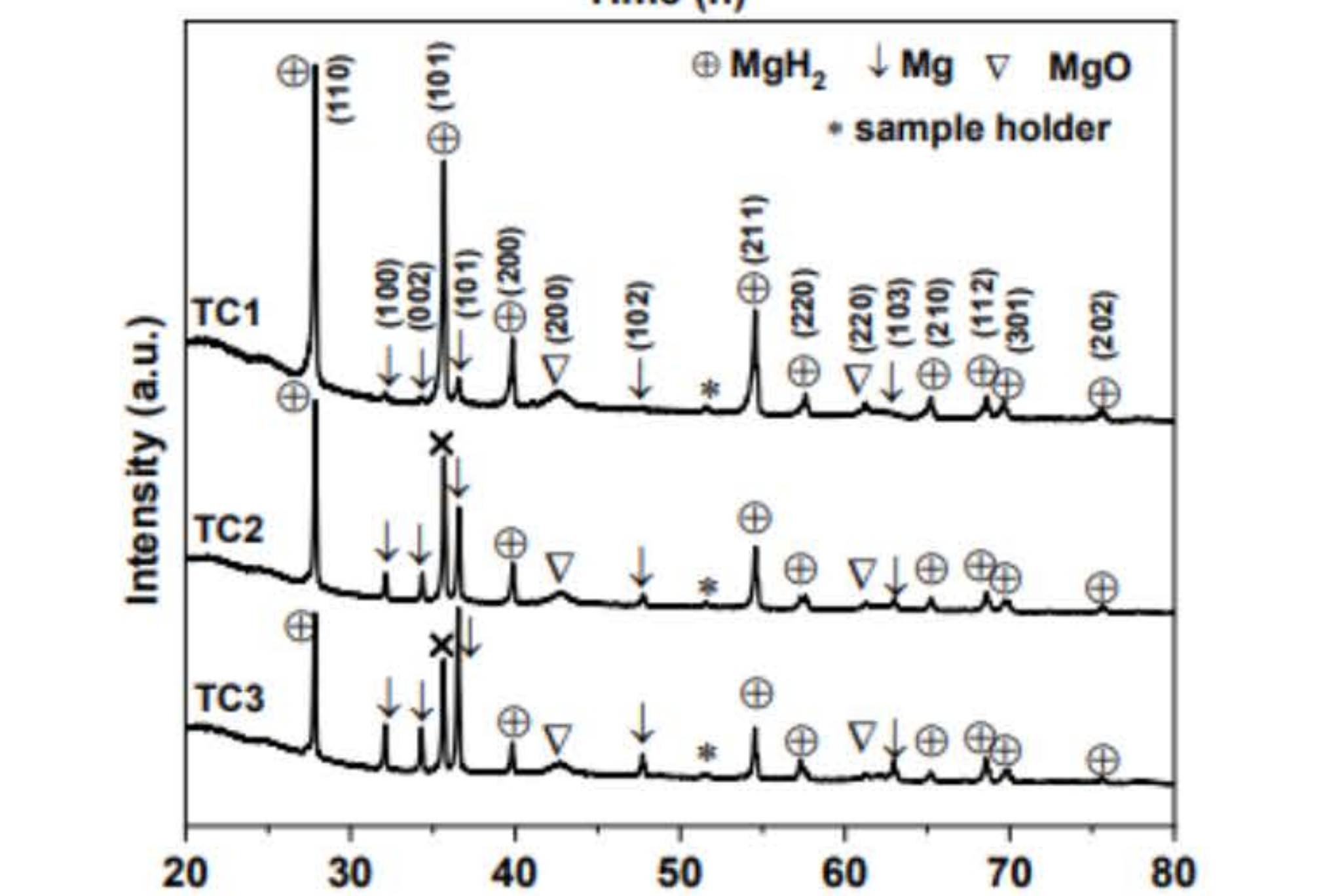
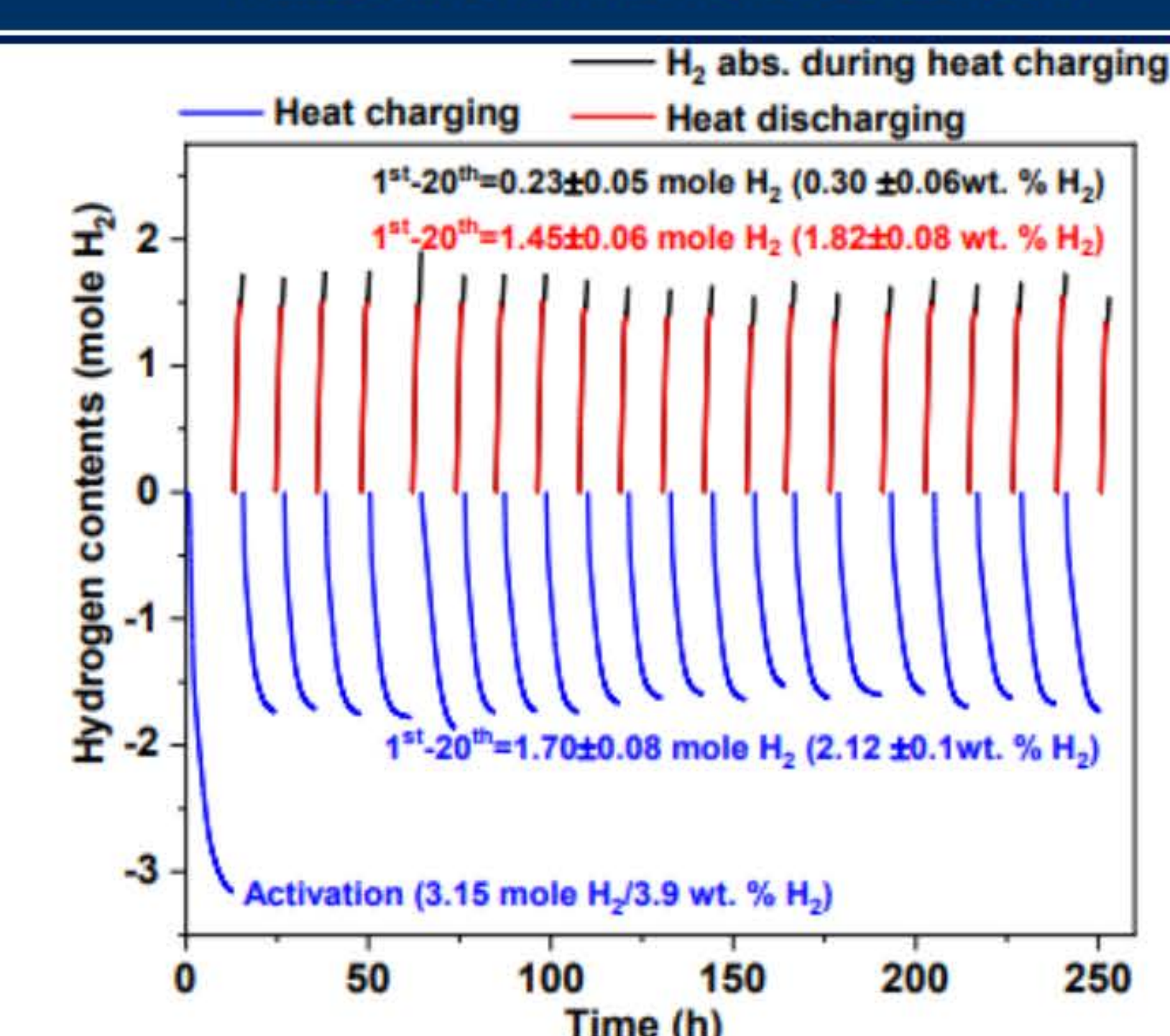


## RESULTS AND DISCUSSION



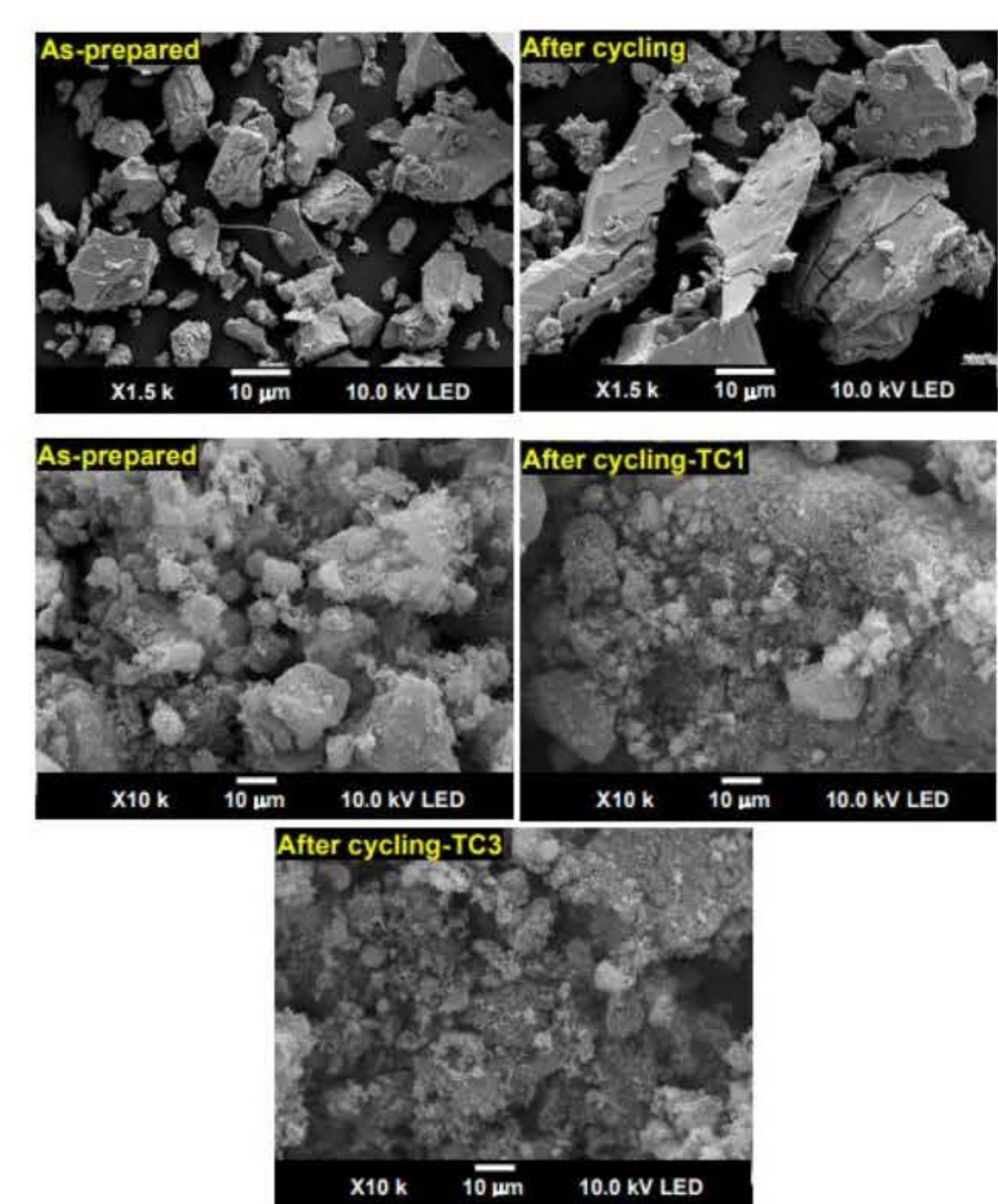
Temperatures of HTMH, LTMH, and HTF, pressures of HTMH and LTMH, and  $\text{H}_2$ -FR exchanging between HTMH and LTMH during activation and the 1<sup>st</sup> cycle of the coupled  $\text{MgH}_2$ - $\text{LaNi}_5$  thermal storage

- Temperatures and pressures of both HTMH and LTMH as well as  $\text{H}_2$ -FR during the 19<sup>th</sup> cycle are comparable to those of the 1<sup>st</sup> cycle.
- HTF temperature ( $T_{\text{air-out}}$ ) is 88–147 °C.
- HTMH store heat (release hydrogen) at 318 °C
- LTMH absorb  $\text{H}_2$  at all TCs to 52–56 °C



$\text{H}_2$  contents exchange between HTMH and LTMH upon 20 cycles and PXRD spectra of HTMH after the 20<sup>th</sup> heat discharging at different positions in the HTMH tank.

- 3.15 mol  $\text{H}_2$  transfer from HTMH to LTMH during activation (3.9 wt. %  $\text{H}_2$ ).
- Stability upon 20 cycles  $\text{H}_2$  contents exchanging between HTMH and LTMH up to  $1.70 \pm 0.08$  mol  $\text{H}_2$  ( $2.12 \pm 0.1$  wt. %  $\text{H}_2$ ).
- Superior cycling stability of the coupled  $\text{MgH}_2$ - $\text{LaNi}_5$  thermal storage



SEM images of LTMH and HTMH powder samples in the as-prepared state and after the 20<sup>th</sup> heat storage cycle.

- Particle agglomeration of both LTMH and HTMH powder samples upon 20 heat storage cycles

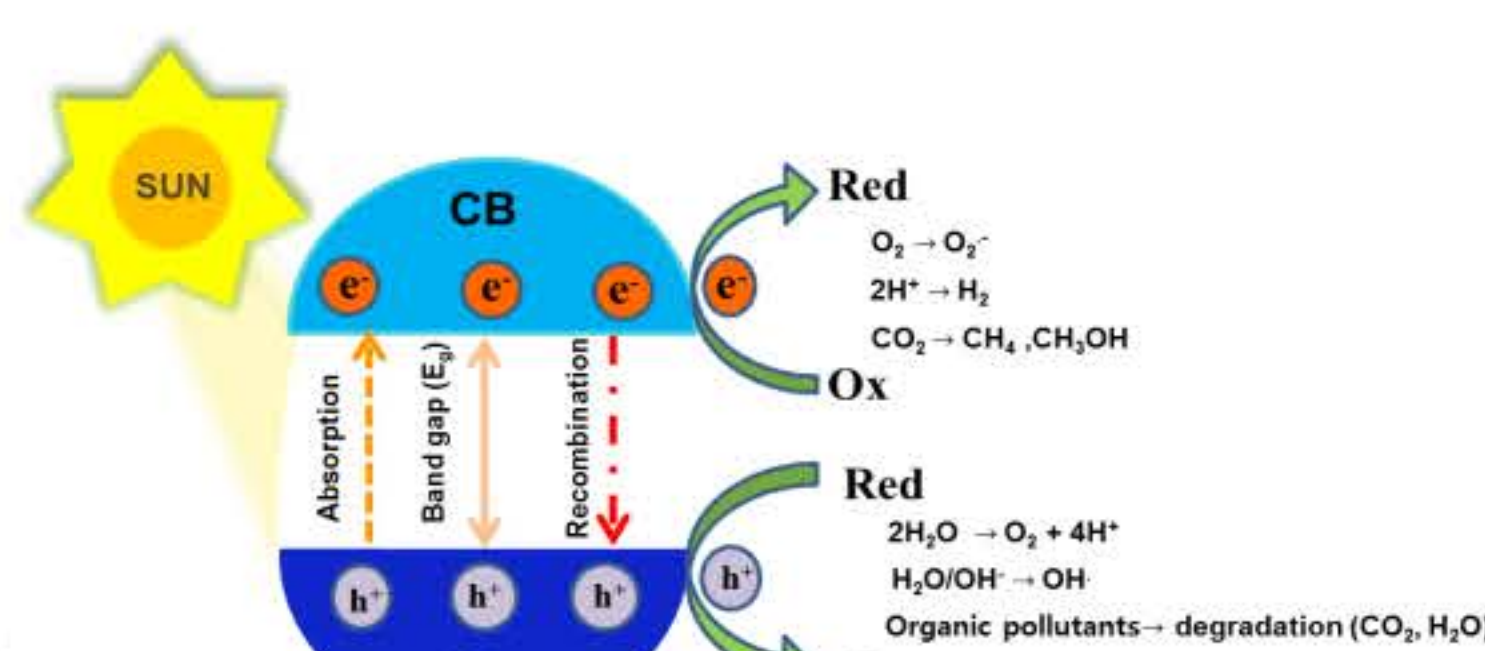
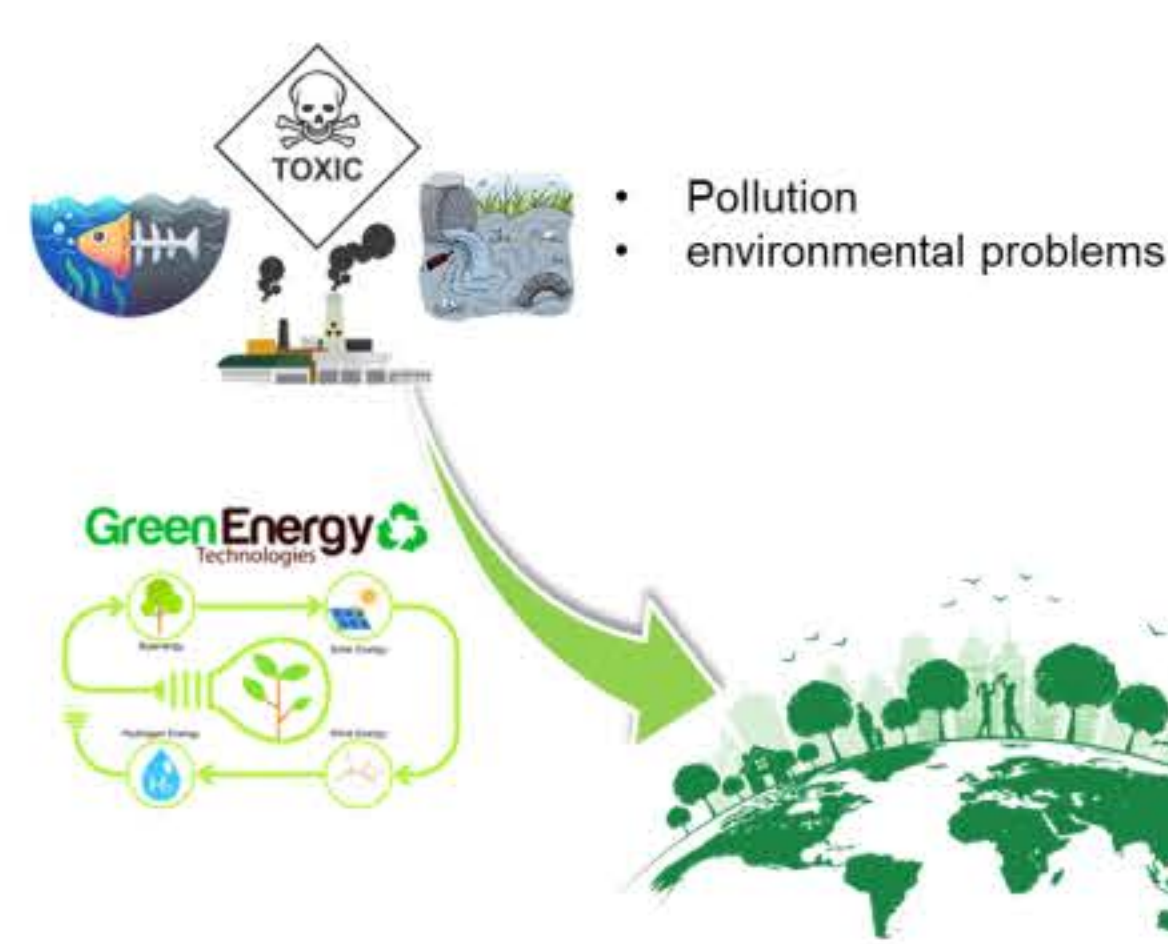
## Conclusions

- Heat charging and discharging of HTMH were at 380 and 285–310 °C.
- $\text{H}_2$  de/absorption of LTMH were at 25–50 °C.
- Heat storage densities during charging and discharging were  $797 \pm 37.5$  and  $680 \pm 28$  kJ/kg, respectively.
- Poor reaction was detected at the bottom of the tank due to deficient hydrogen diffusion and thermal conductivity in the hydride beds.

**Acknowledgements:** This research has received funding support from (i) Suranaree University of Technology (SUT) and (ii) the NSRF via the Program Management Unit for Human Resources & Institutional Development, Research and Innovation (PMU-B) [grant number B13F660067].



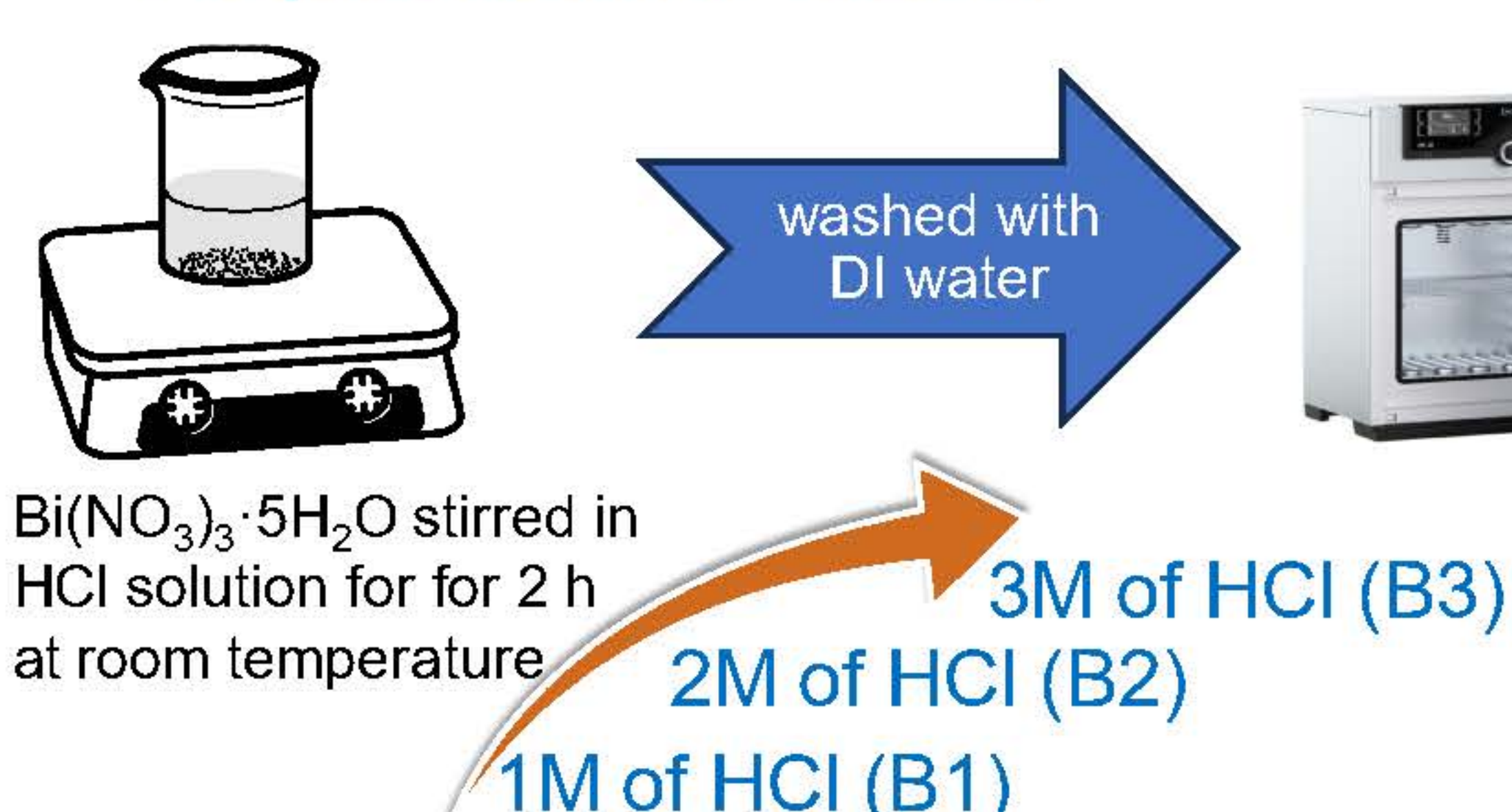
## Introduction



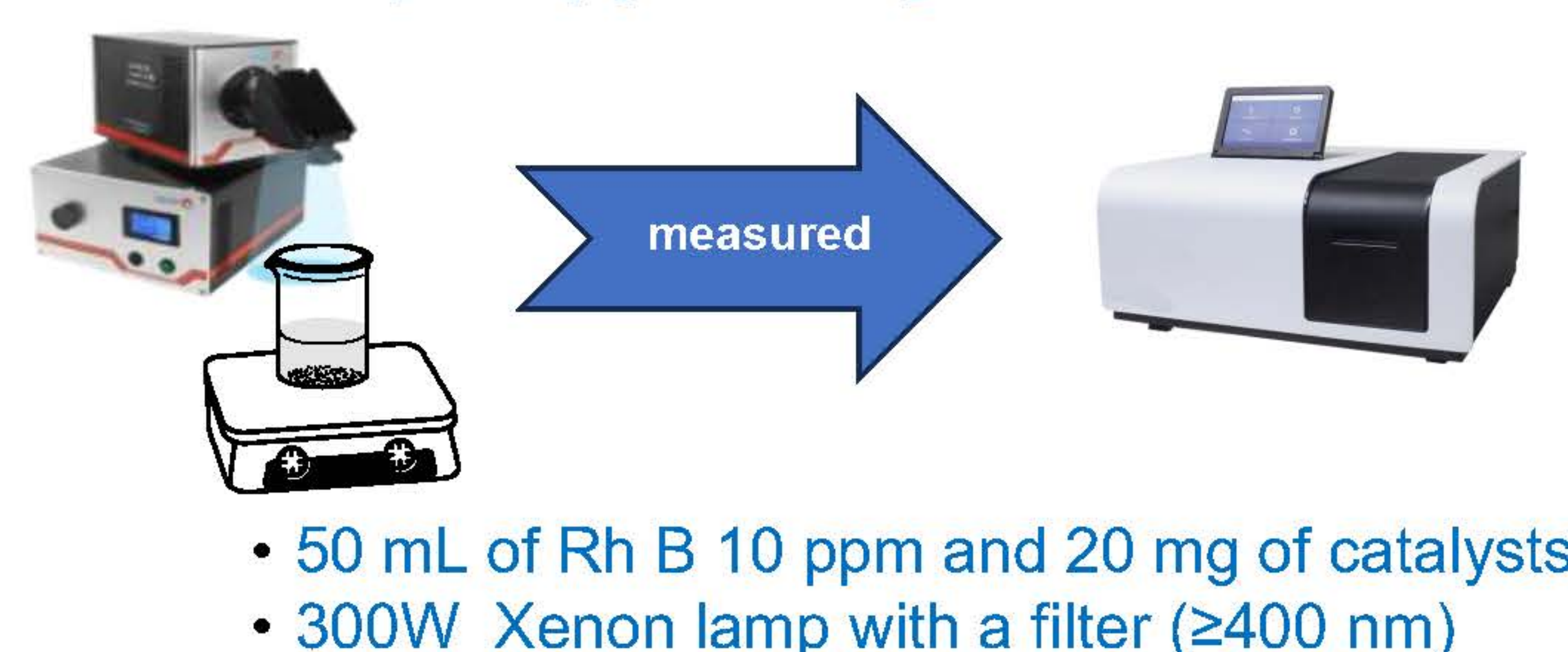
- We face an increasing need for renewable energy sources and clean environment.
- Photocatalysis is a promising approach to harvest solar energy and decompose organic pollutants.
- BiOCl is one of the promising photocatalysts since it has the appropriate  $E_g$  value (3.2 eV)
- We investigate the defect formation in BiOCl, resulting in photoresponse in the visible region.

## Methods

### Preparation of BiOCl

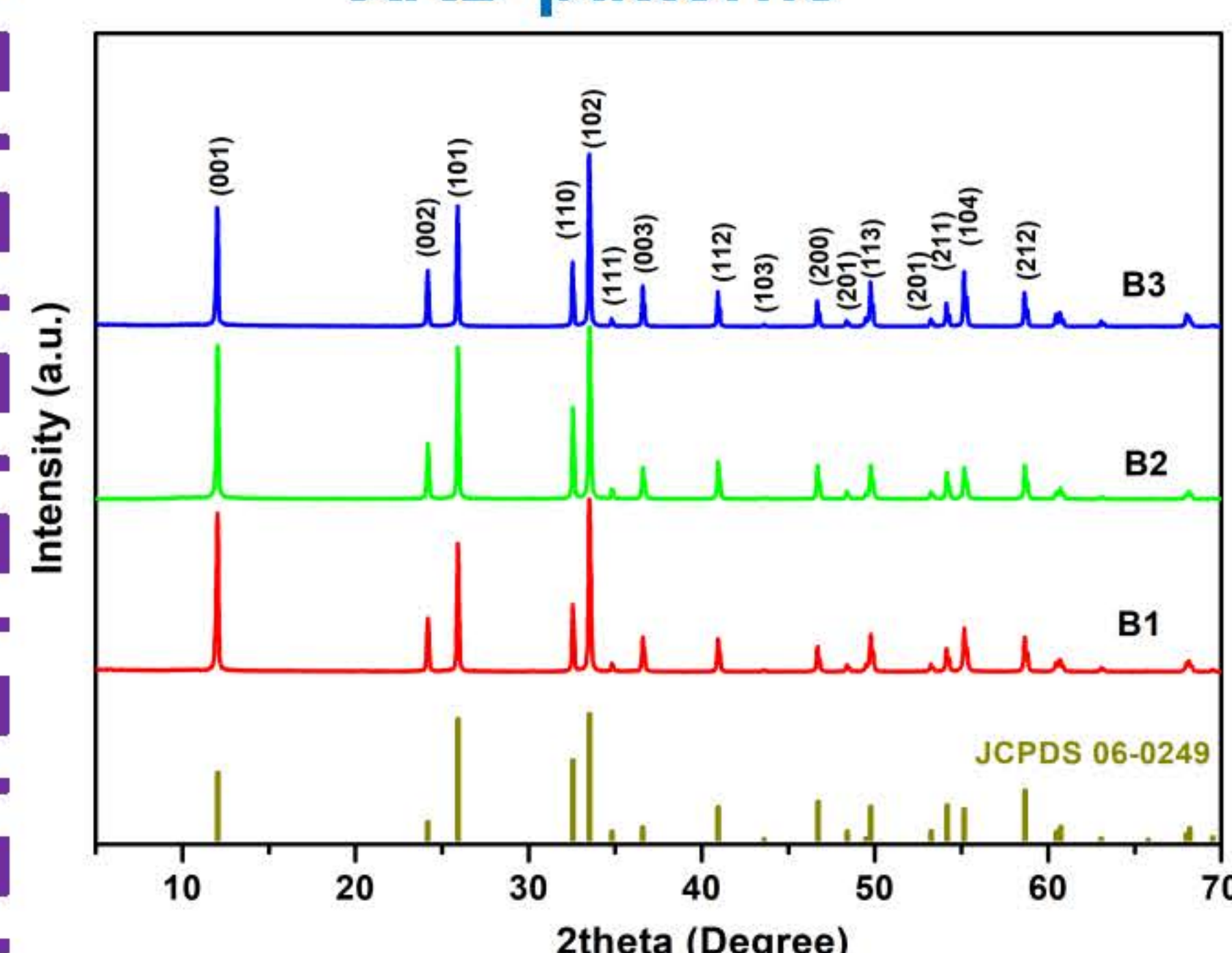


### Rhodamine B (Rh B) photodegradation

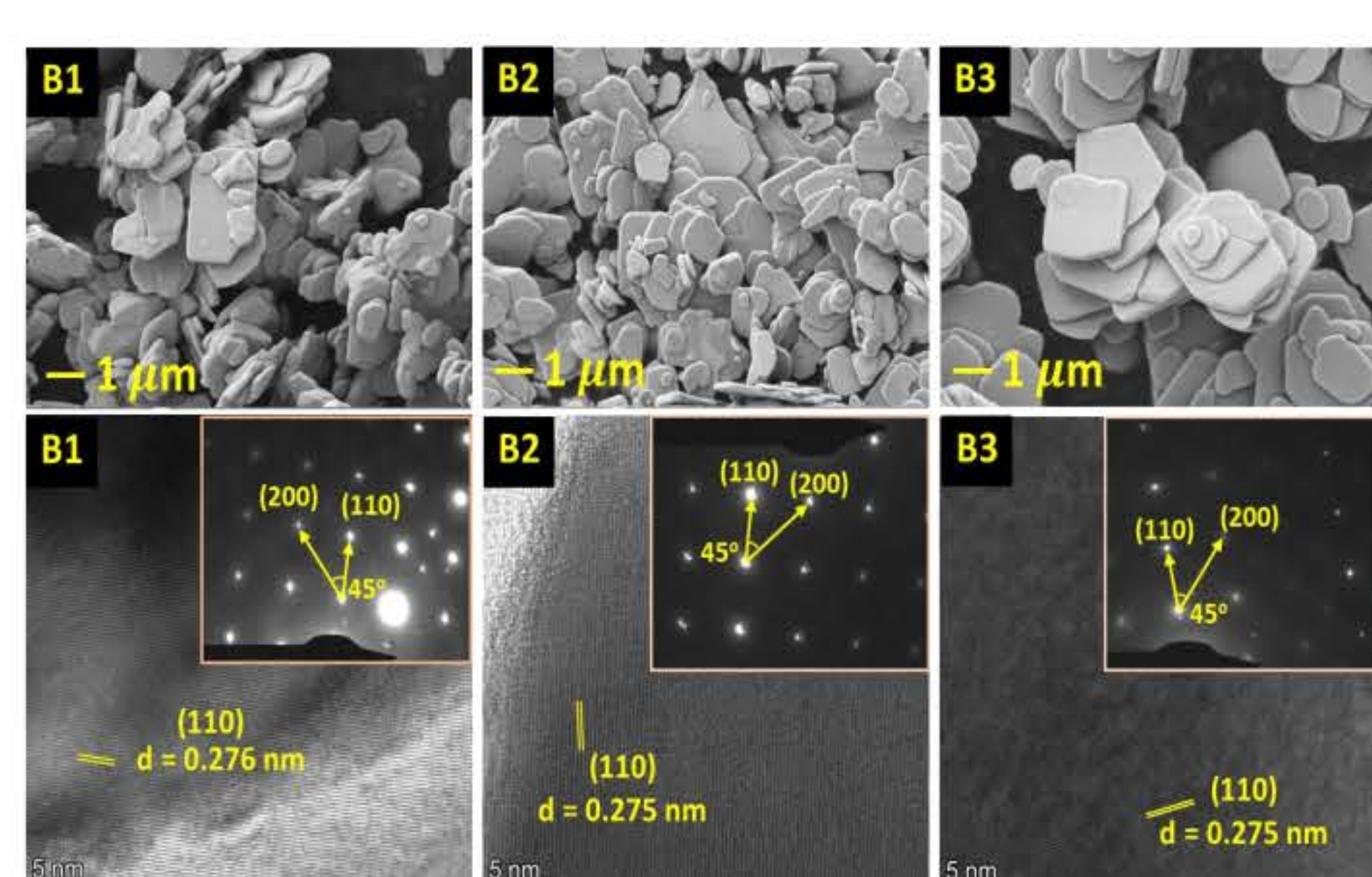


## Results & Discussion

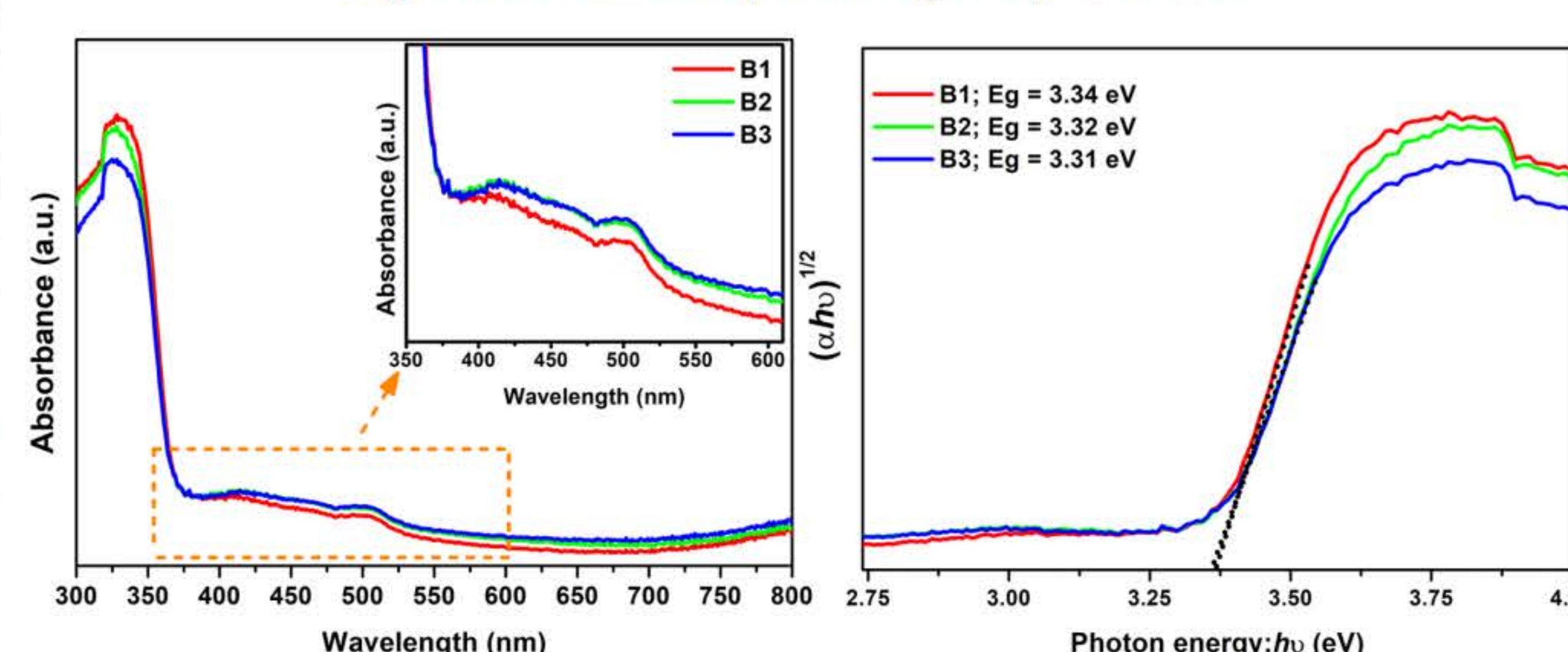
### XRD patterns



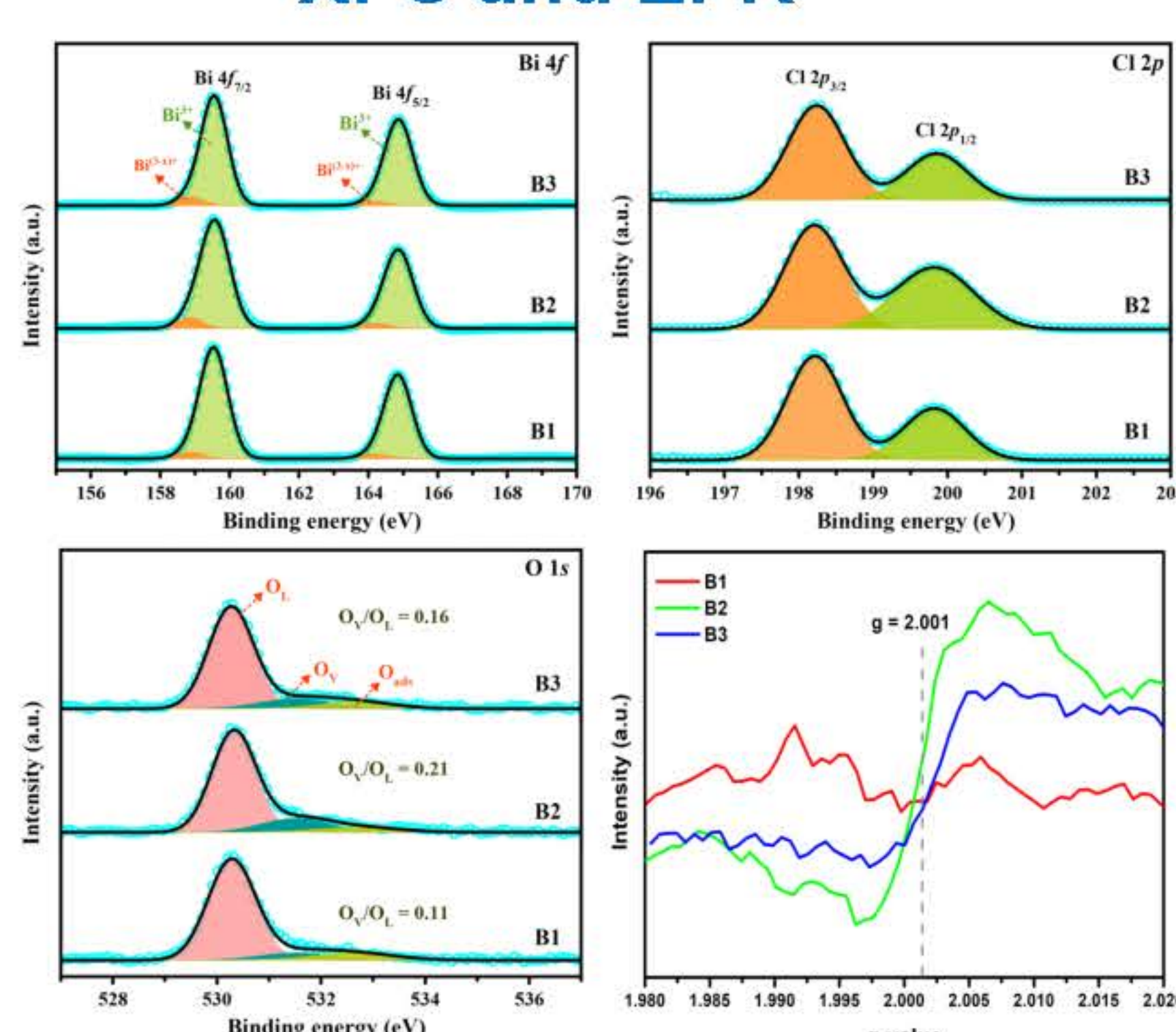
### SEM/TEM



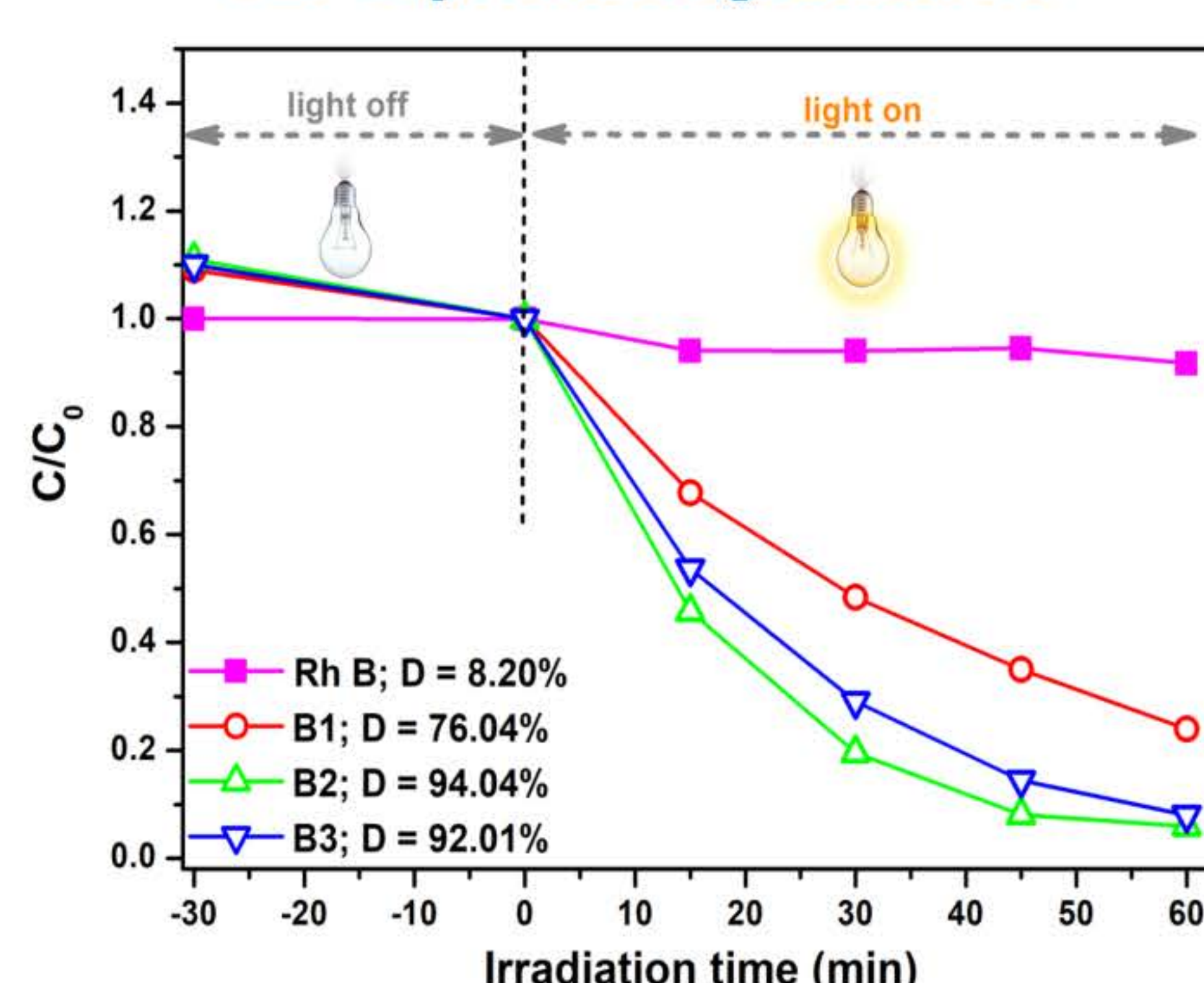
### Optical absorption properties



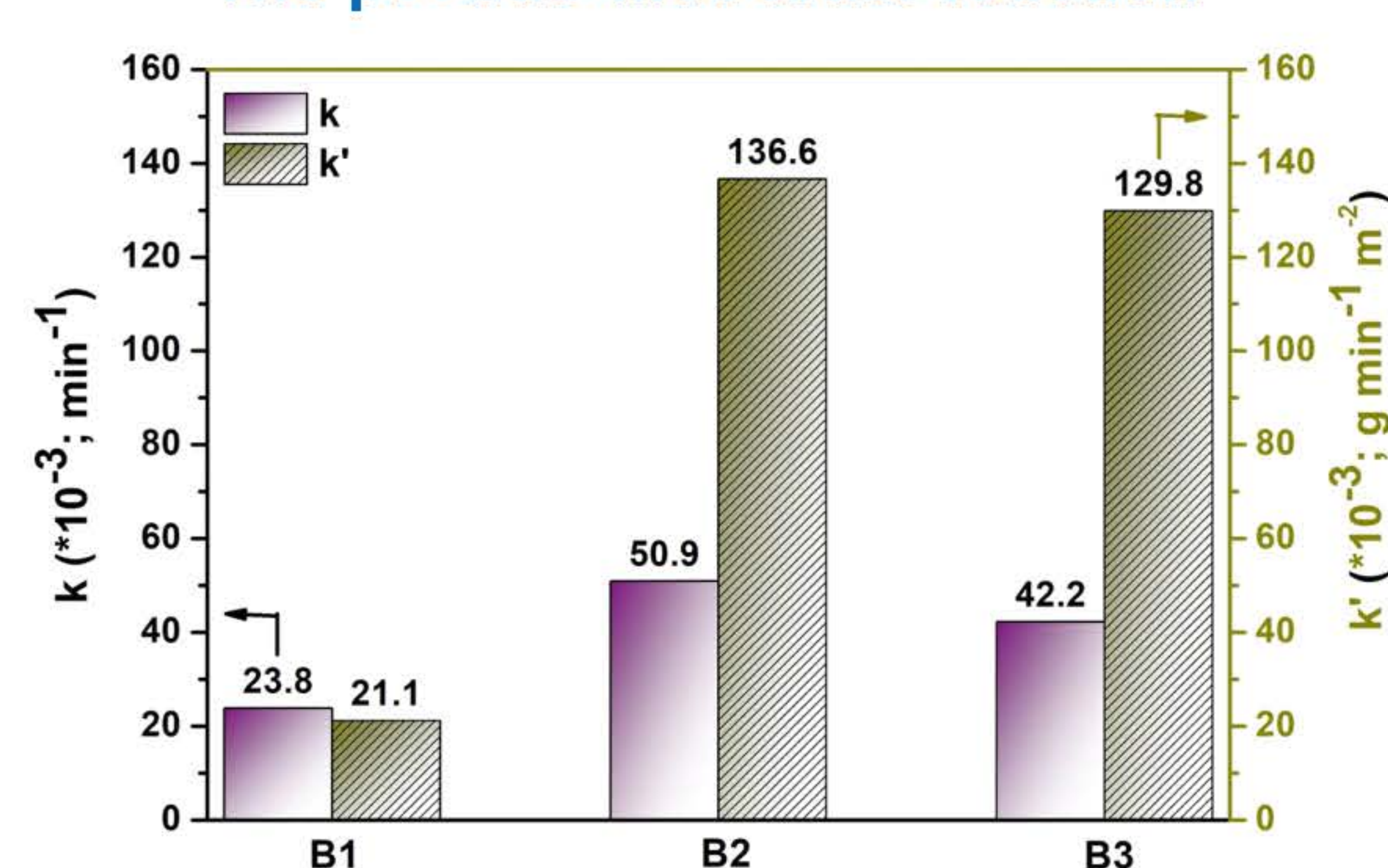
### XPS and EPR



### Rh B photodegradation

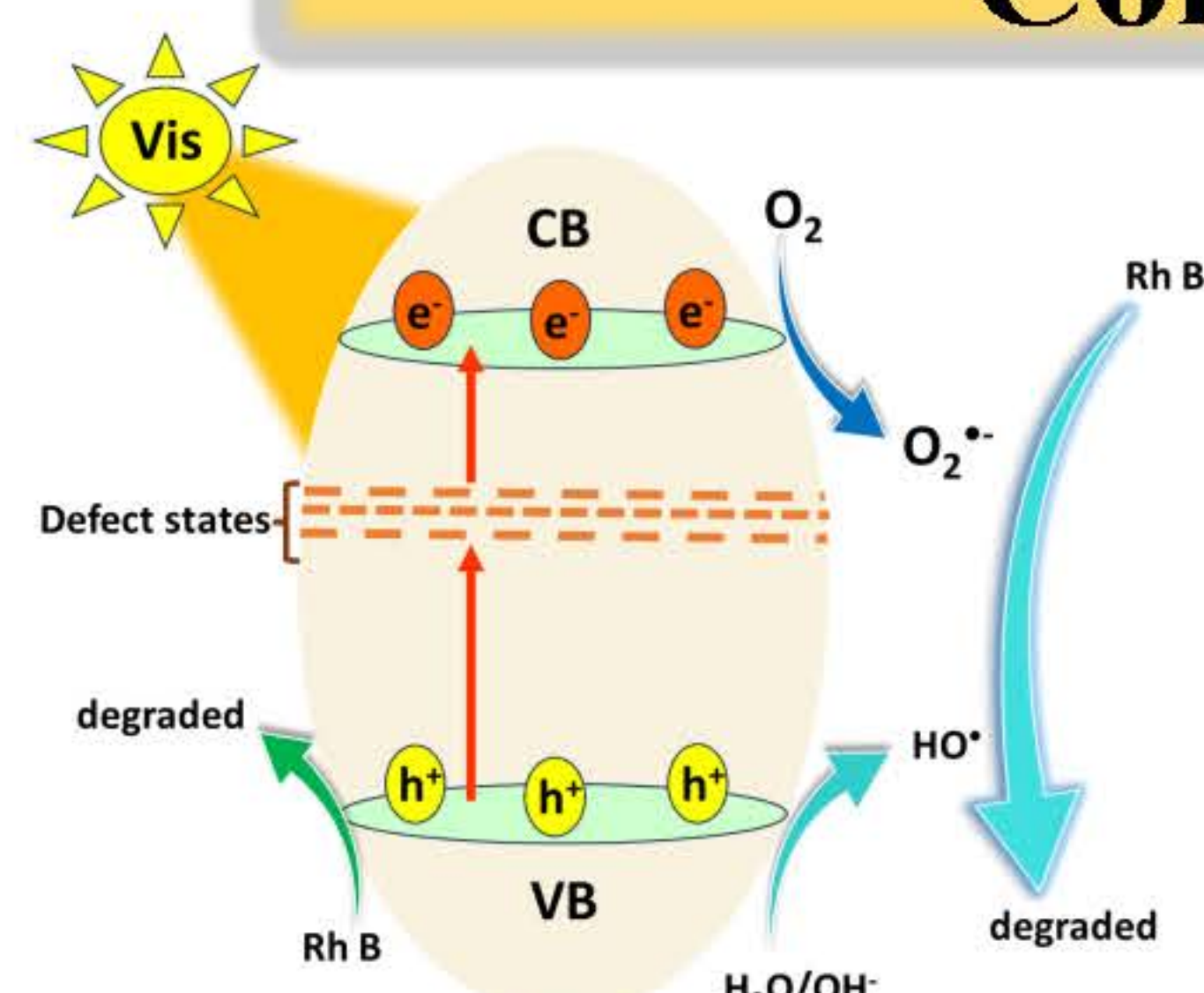


### The pseudo-first order reaction



- B2 display more oxygen vacancy than B3 and B1 respectively
- B2 has higher activity of rhodamine B photodegradation than B3 and B1 respectively

## Conclusion



- We successfully designed a soft chemical method to synthesize the BiOCl with plate-like morphology employing a co-precipitation at room temperature under acidic condition.
- The formation of oxygen vacancy exhibited excellent photocatalytic activity for the decomposition of rhodamine B under visible light.
- B2 exhibited the highest activity of rhodamine B photodegradation, due to more oxygen vacancy formation.

**Acknowledgements:** This research has received funding support from (i) Suranaree University of Technology (SUT) and (ii) the NSRF via the Program Management Unit for Human Resources & Institutional Development, Research and Innovation (PMU-B) [grant number B13F660067]





**BRAINPOWER**  
CONGRESS 2023

ร่วมกับสร้างและขับเคลื่อนงานวิจัยขั้นแนวหน้า  
สู่อุตสาหกรรมแห่งอนาคต



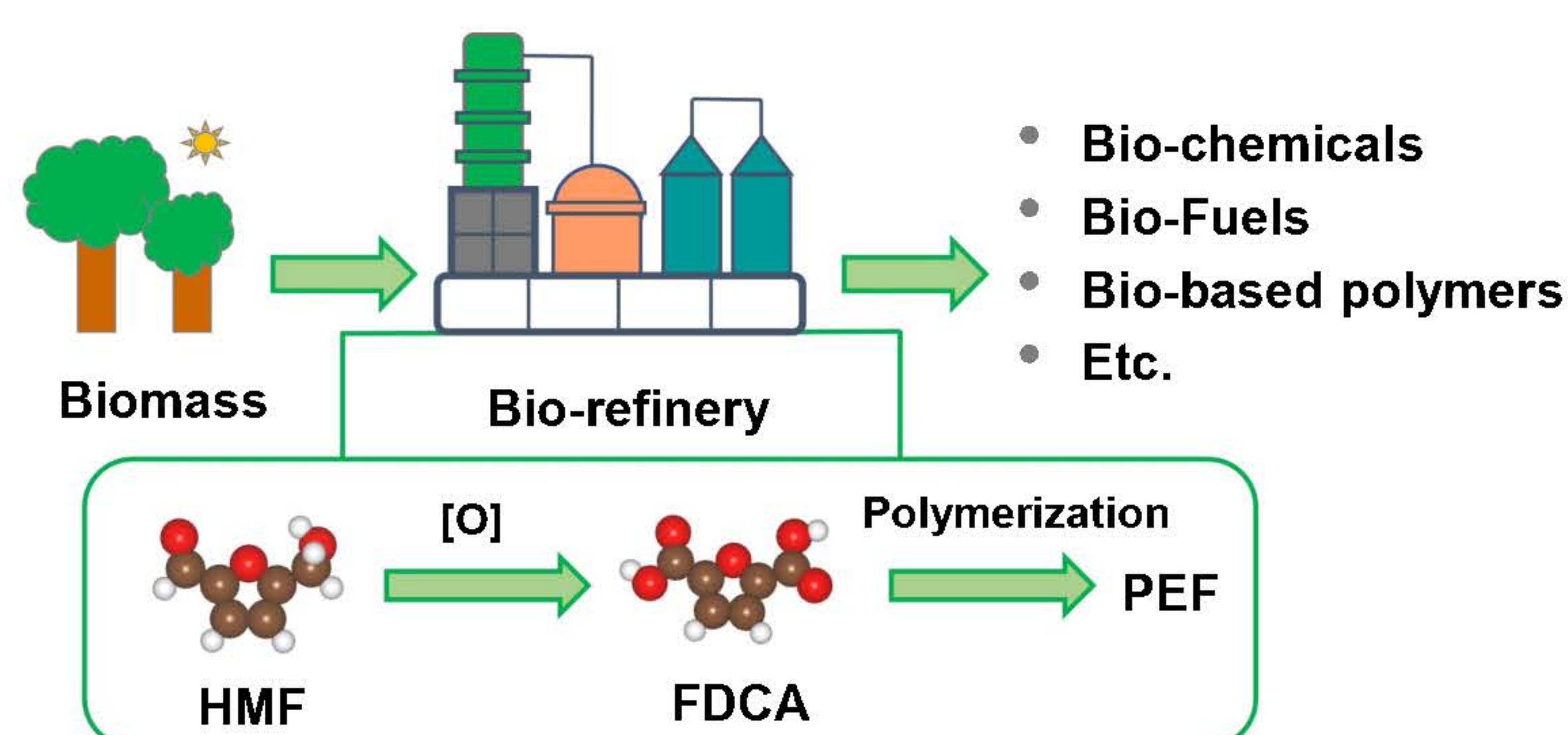
## Electrochemical oxidation of 5-hydroxymethylfurfural to 2,5-furandicarboxylic acid on Ni-based catalysts: DFT calculation

Bunrat Tharat<sup>1</sup>, Chattarika Sukpattanacharoen<sup>1</sup>, Anchalee Junkaew<sup>2</sup>, Suwit Suthirakun<sup>1,\*</sup>

<sup>1</sup> School of Chemistry, Institute of Science, Suranaree University of Technology, Nakhon Ratchasima 30000, Thailand

<sup>2</sup> National Nanotechnology Center (NANOTEC), National Science and Technology Development Agency, 111 Thailand Science Park, Pathum Thani 12120, Thailand

\* Corresponding author: suthirak@sut.ac.th



- FDCA is a monomer for producing polyethylene furanoate (PEF), the well-known bio-based polymers.

### Objective

This work presents the electrocatalytic activity of Fe-doped NiOOH in the oxidation of 5-hydroxymethylfurfural (HMF) to 2,5-furandicarboxylic acid (FDCA) using a first-principles approach based on density functional theory (DFT).

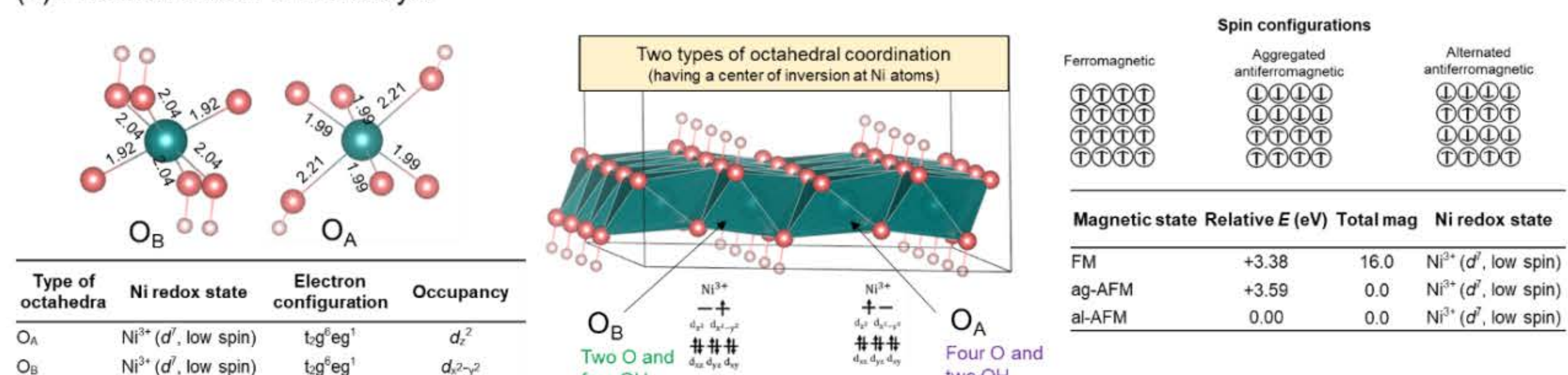
### Computational Details

- Periodic model calculations; VASP 6
- Spin-polarized PAW PBE+U-D3;  $U_{3d}(\text{Ni}) = 5.5$  eV,  $U_{3d}(\text{Fe}) = 3.5$  eV
- A vacuum gap; 20 Å
- 4x4 NiOOH(001) monolayer model; 3x3x1 k-points; 500 eV cutoff
- Energy and force convergence criterion;  $1 \times 10^{-6}$  eV and 0.01 eV/Å

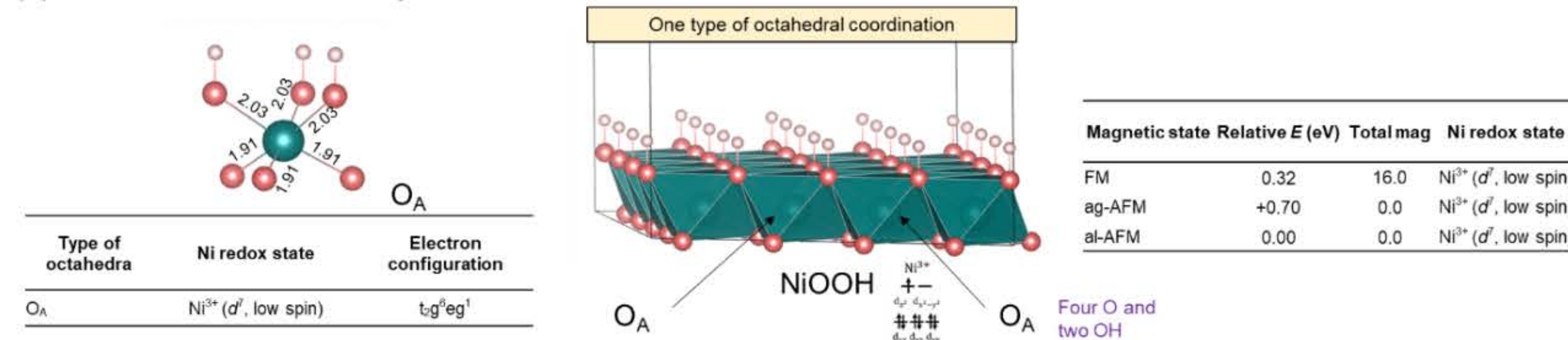
### Results

#### Structure and energetics of pristine NiOOH monolayer

(a) Pristine NiOOH-S monolayer

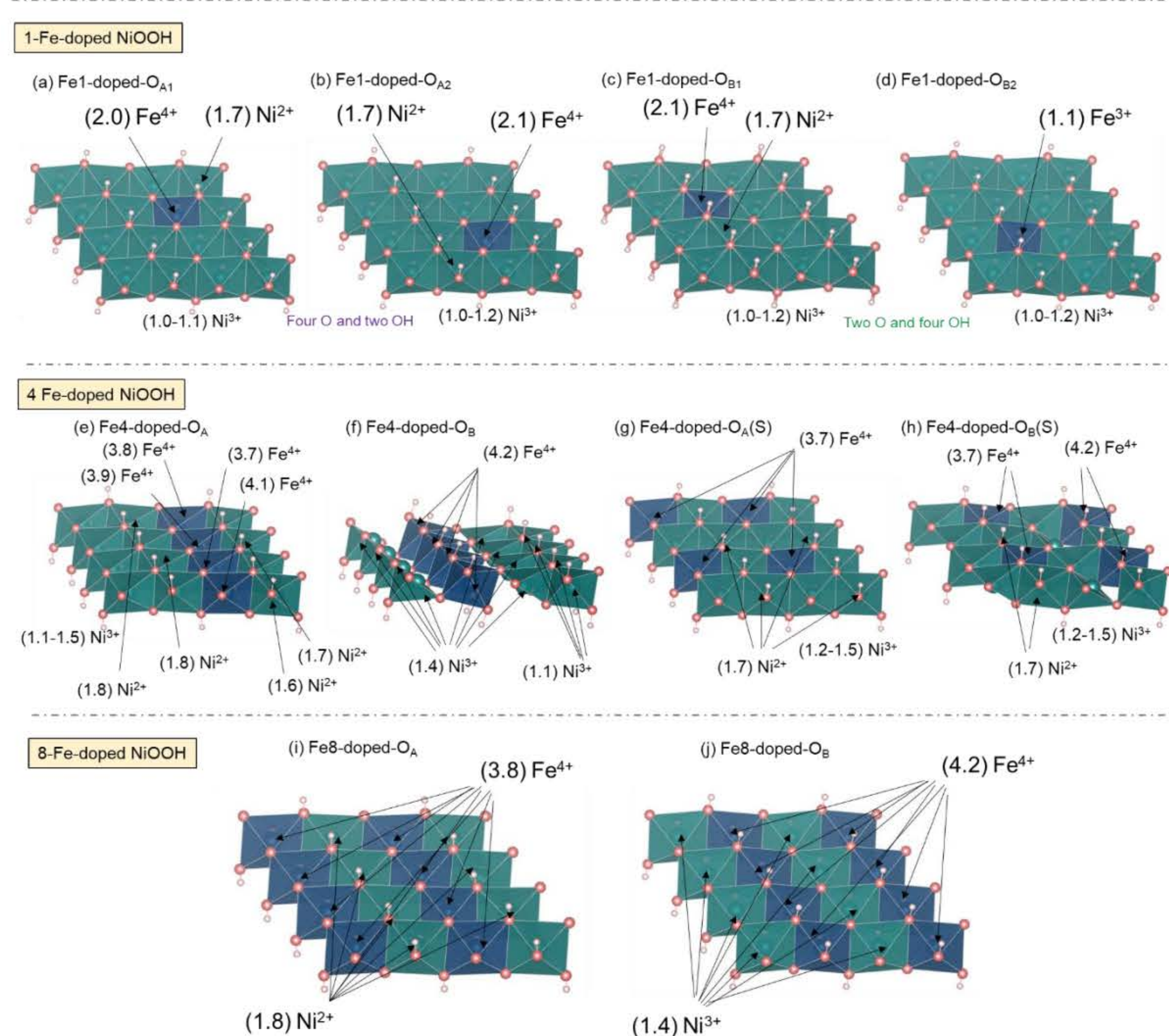


(b) Pristine NiOOH-U monolayer



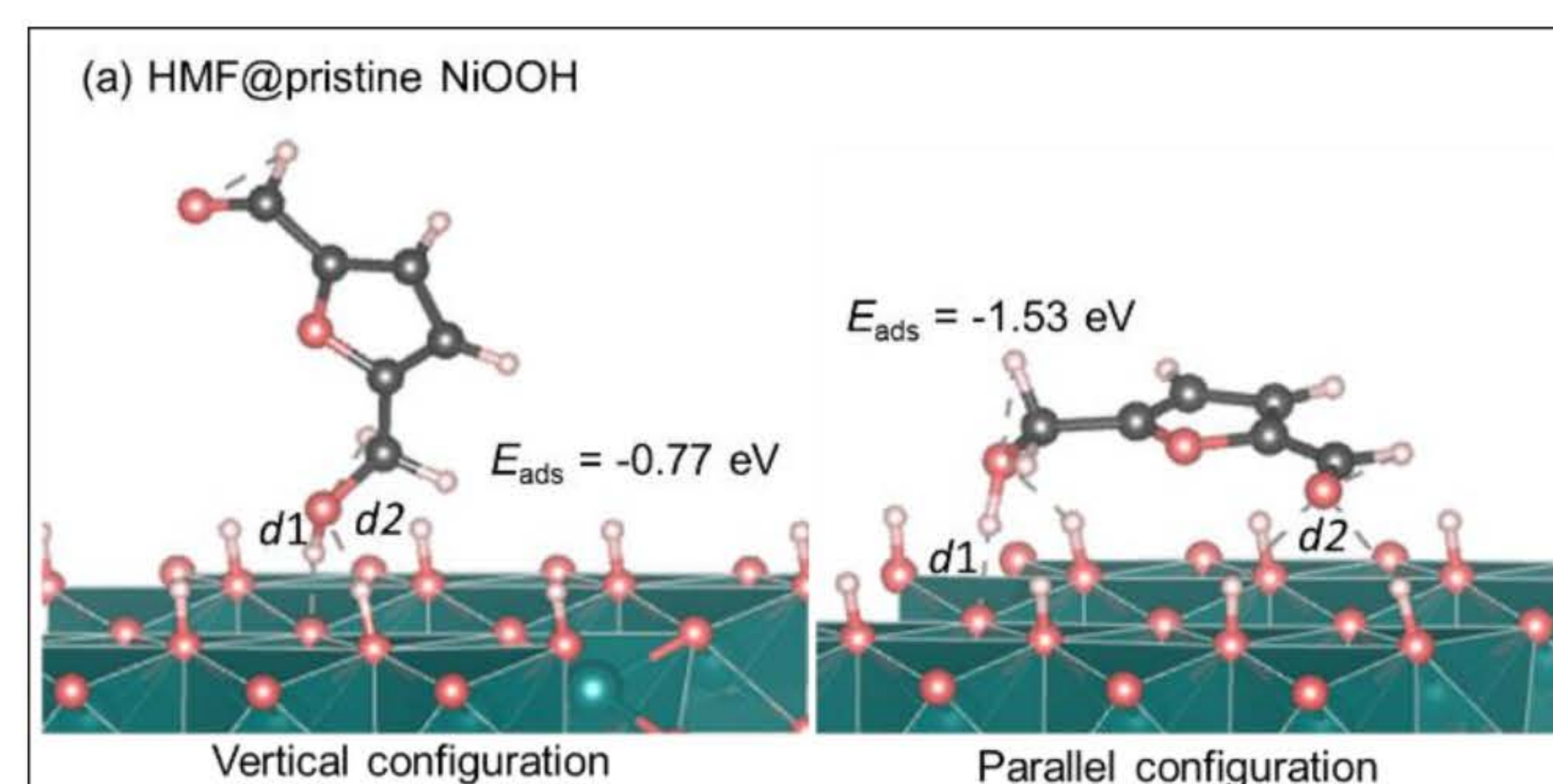
Optimized structures of (a) NiOOH-S and (b) NiOOH-U monolayer with two different types of H-distribution over the surface with the corresponding relative energies (eV) of different magnetic configurations.

#### Structure and energetics of Fe-doped NiOOH monolayer



Optimized structures of all possible Fe-doped NiOOH monolayers at octahedra type A ( $O_A$ ) and B ( $O_B$ ) with three different ratios of Ni and Fe atoms. Structures (a), (e), and (i) are the most stable structures for Fe-doped NiOOH (Fe concentrations; 6%, 25%, and 50%).

#### HMF Adsorption on pristine NiOOH monolayer



- The parallel adsorption configuration of HMF on the NiOOH monolayer is thermodynamically favorable compared to the vertical configuration.

### Conclusions

- The structure optimization shows the alternated antiferromagnetic (al-AFM) ordering has the most stability for the NiOOH-S and NiOOH-U monolayers.
- An energy comparison of octahedra revealed that Fe prefers to be in the  $O_A$  type than the  $O_B$  staggered structure was the most favorable.
- The parallel adsorption configuration of HMF on the NiOOH monolayer is thermodynamically favorable compared to the vertical configuration.

**Acknowledgments** This research has received funding support from (i) Suranaree University of Technology (SUT) and (ii) the NSRF via the Program Management Unit for Human Resources & Institutional Development, Research and Innovation (PMU-B) [grant number B13F660067]



## The influence of plastic pyrolysis oil on fuel lubricity and diesel engine performance

Anupap Pumpuang<sup>a,b</sup>, Ekarong Sukjit<sup>a</sup>, Niti Klinkaewa<sup>a</sup>

<sup>a</sup>School of mechanical engineering, Institute of engineering, Suranaree University of Technology, Nakhon Ratchasima, 30000, Thailand

<sup>b</sup>Institute of Research and Development, Suranaree University of Technology, Nakhon Ratchasima, 30000, Thailand

Email: [anupap.p@sut.ac.th](mailto:anupap.p@sut.ac.th)

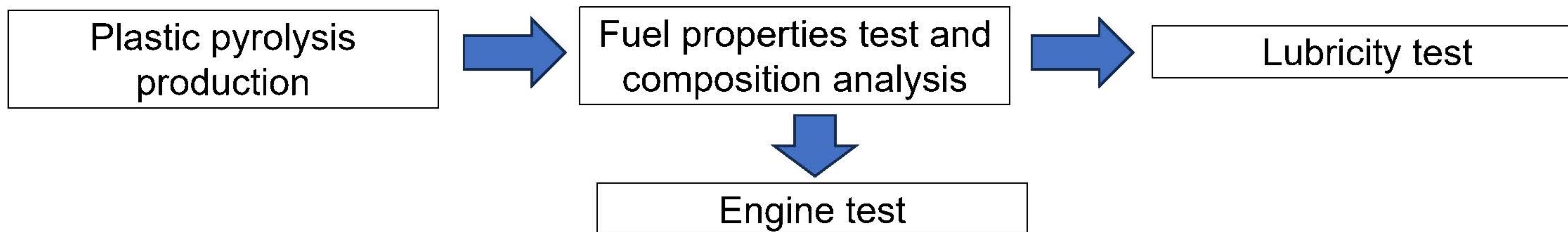
### Introduction

The pyrolysis-derived plastic oils exhibit comparable chemical and physical properties to conventional diesel fuel. Integrating plastic pyrolysis oils into a diesel engine can contribute to a reduction in the reliance on traditional diesel fuel derived from petroleum sources.

### Objective

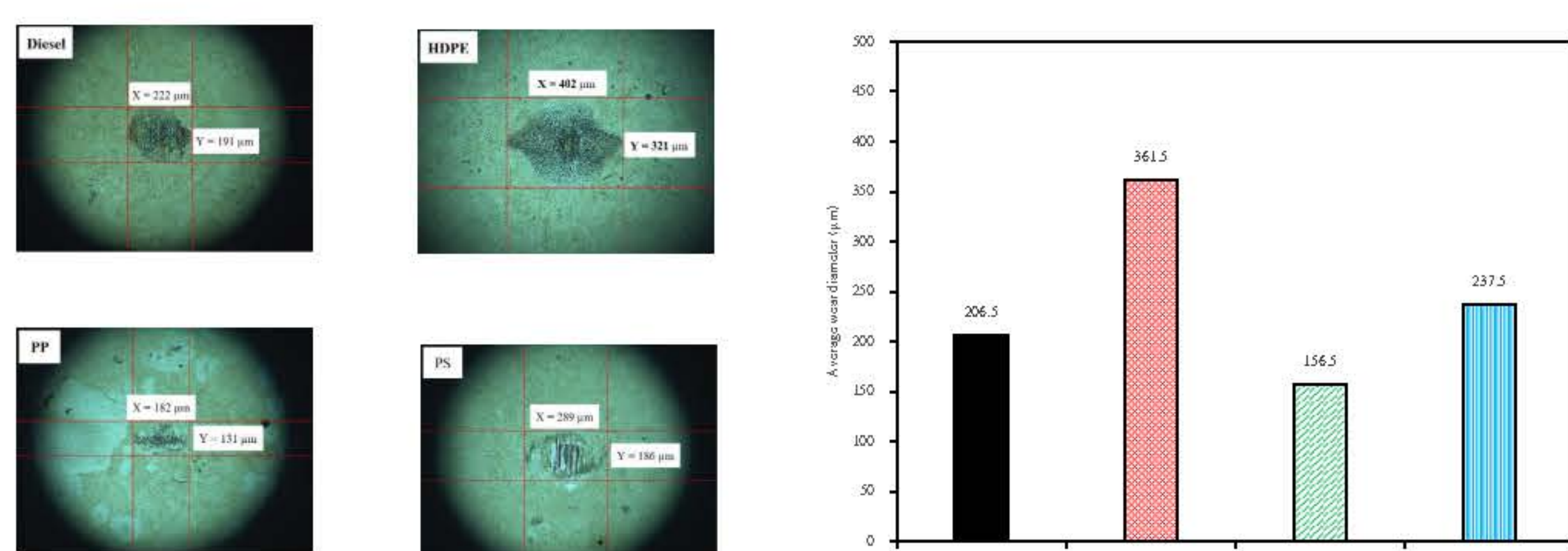
In this study using of three types of plastic pyrolysis oil which is the main plastic waste in Thailand, of High-density polyethylene (HDPE), Polypropylene (PP) and Polystyrene (PS) as compression ignition engine fuel were studied. Their three-chemical composition, chemical and physical fuel properties, fuel lubricity, engine performance, combustion characteristic and emission characteristic were investigated.

### Methodology



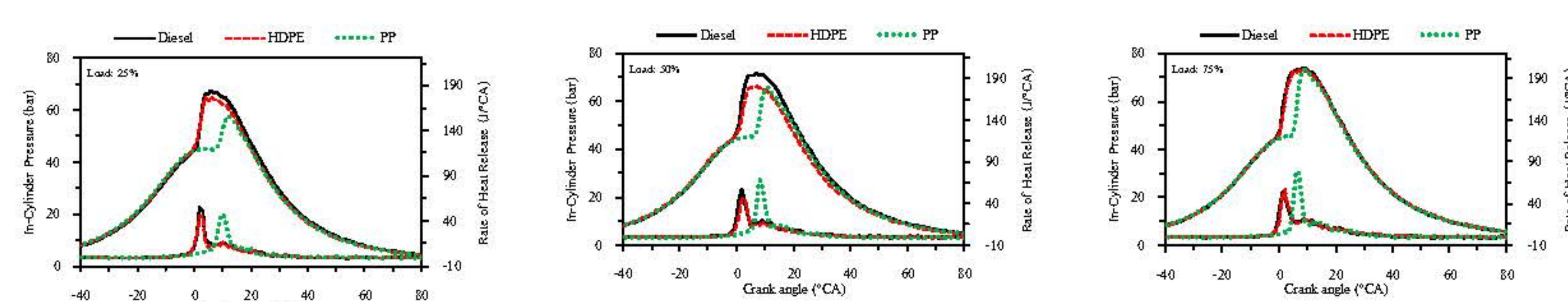
### Results & Discussion

#### Lubricity Test



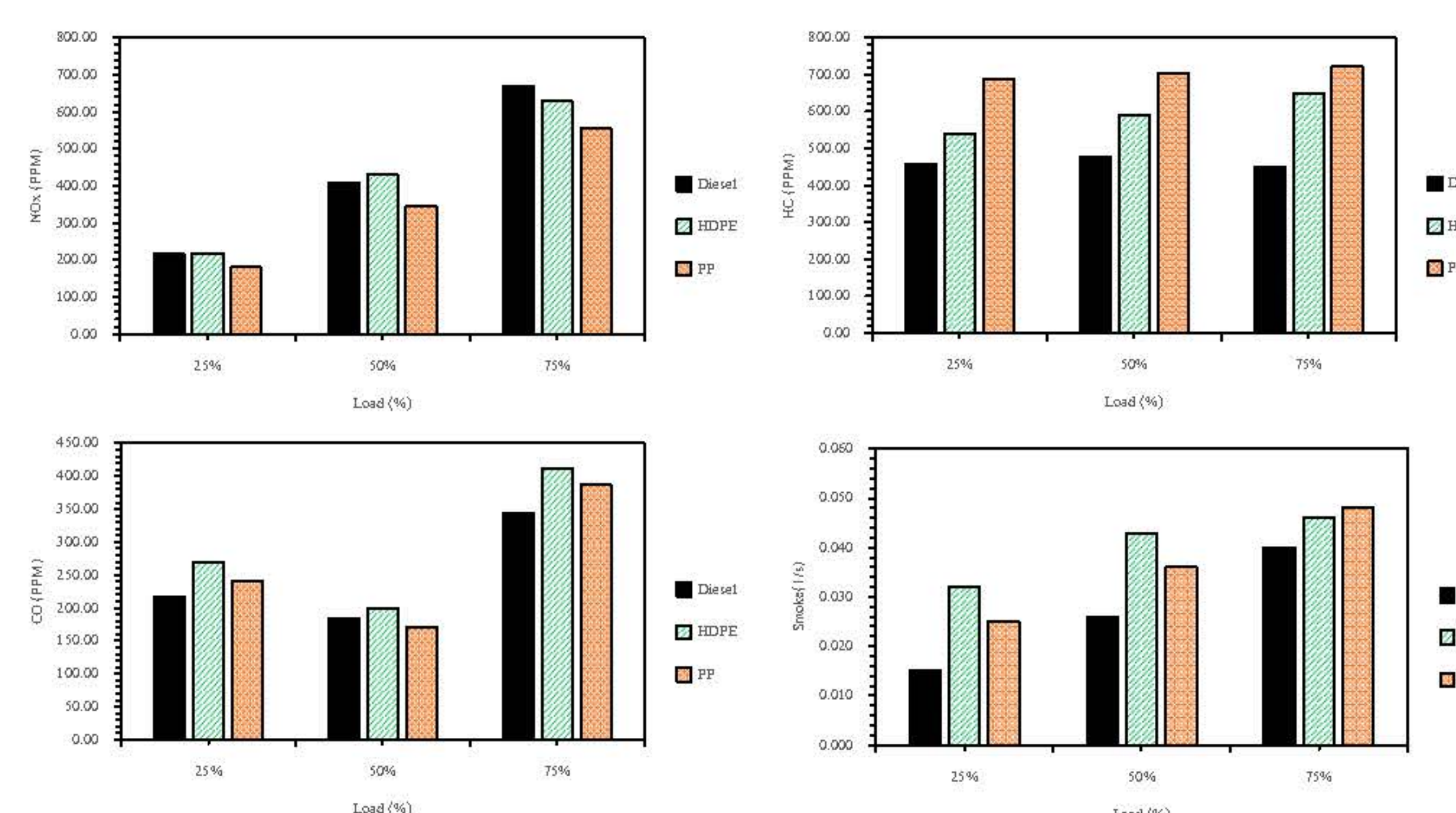
PP provide the best lubricity due to higher in kinematic viscosity and sulphur content result in thick film boundary formation. Diesel lubricity is the influenced by its 7% biodiesel content. Due to light component vaporized during HFRR test result in heavy components remain which provide better lubrication. HDPE provides worse lubricity due to lower in kinematic viscosity.

#### Combustion Characteristics



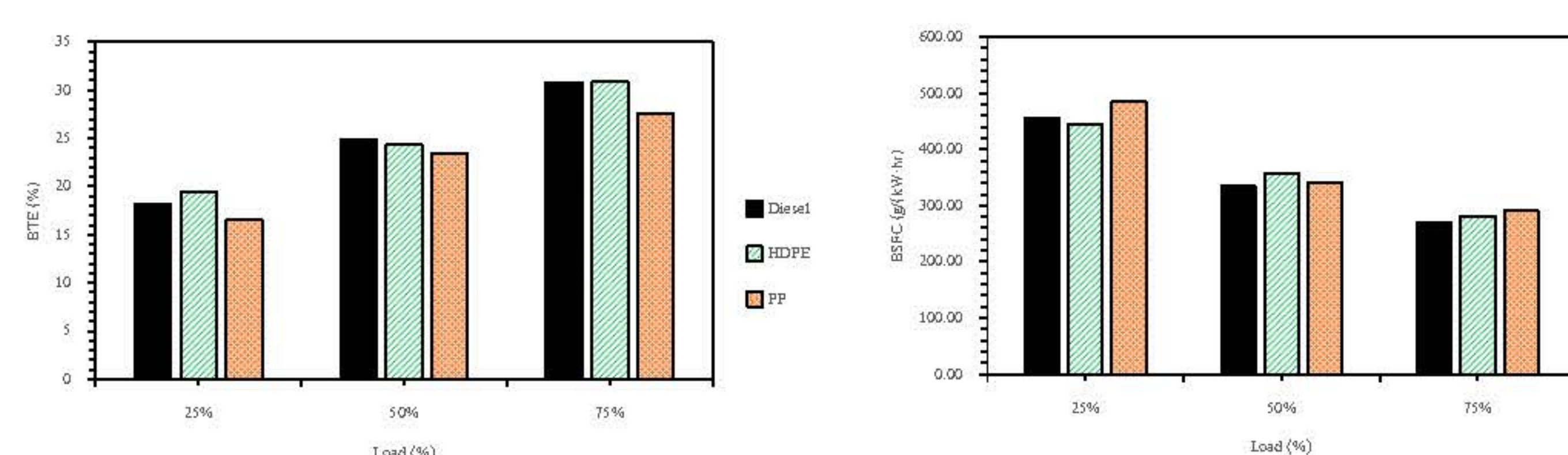
HDPE exhibits combustion characteristics similar to diesel, with slightly lower ICP and HRR attributed to its specific properties. In contrast, PP significantly delays combustion compared to diesel fuel, influenced by its lower oxygen content, higher viscosity, and lower density.

#### Emissions Characteristics



HDPE has no clearly trend in NOx. PP provides lower in NOx due to heat losses during combustion process. HC of both plastic pyrolysis oil higher than diesel fuel due to more fuel is supplied to the engine. CO of both plastic pyrolysis oil trend to higher than diesel fuel due to lower in combustion temperature. Smoke of both plastic pyrolysis oils higher than diesel fuel due to more fuel is supplied to the engine, higher in sulphur content and lower in oxygen content.

#### Engine Performance



Brake thermal efficiency of HDPE were similar to diesel fuel due to it's similar in fuel properties to diesel fuel while PP provide lower BTE than HDPE due to combustion retard occur during combustion process.

### Conclusion

- HDPE and PP can use as diesel engine fuel without any engine modification while PS cannot due to its composition.
- PP provide better lubricity than HDPE and PS.
- HDPE provide similar in engine performance and combustion characteristics while PP provides significantly difference in BTE and combustion characteristics
- Both plastic pyrolysis fuel provide difference in emission than diesel fuel due to their properties and composition.

### Acknowledgements

This research has received funding support from (i) Suranaree University of Technology (SUT) and (ii) the NSRF via the Program Management Unit for Human Resources & Institutional Development, Research and Innovation (PMU-B) [grant number B13F660067]





**BRAINPOWER**  
CONGRESS 2023

ร่วมกันสร้างและขับเคลื่อนงานวิจัยชั้นนำ  
สู่อุตสาหกรรมแห่งอนาคต



## Natural Rubber Latex-Modified Concrete with PET and Crumb Rubber Aggregate Replacements for Sustainable Rigid Pavements

Punvalai Choenklang<sup>a,c</sup>, Menglim Hoy<sup>b,c</sup>

<sup>a</sup>Institute of Research and Development, Suranaree University of Technology, Nakhon Ratchasima, 30000, Thailand

<sup>b</sup>School of Civil Engineering, Suranaree University of Technology, Nakhon Ratchasima, 30000, Thailand

<sup>c</sup>Center of Excellence in Innovation for Sustainable Infrastructure Development, Suranaree University of Technology, Nakhon Ratchasima 30000, Thailand

Email: [punvalai789@gmail.com](mailto:punvalai789@gmail.com)

### Introduction

There are ongoing research challenges for the addition of the blend of PET and crumb rubber in polymer-modified concretes, which aims to leverage the benefits of both materials. These materials cause environmental harm due to their slow decomposition and improper management. In this study, various percentage combinations of waste aggregates, such as PET and crumb rubber, were used to replace coarse and fine aggregates in natural rubber latex (NRL)-modified concrete. Engineering properties such as compressive and flexural strengths, modulus of elasticity, and toughness obtained from compressive- and flexural stress-strain curves were investigated. Scanning electron microscopy (SEM) analysis was performed to examine the microstructural properties and study the strength development of the studied concretes. This research helps repurpose waste materials and reduce the environmental footprint of concrete production.



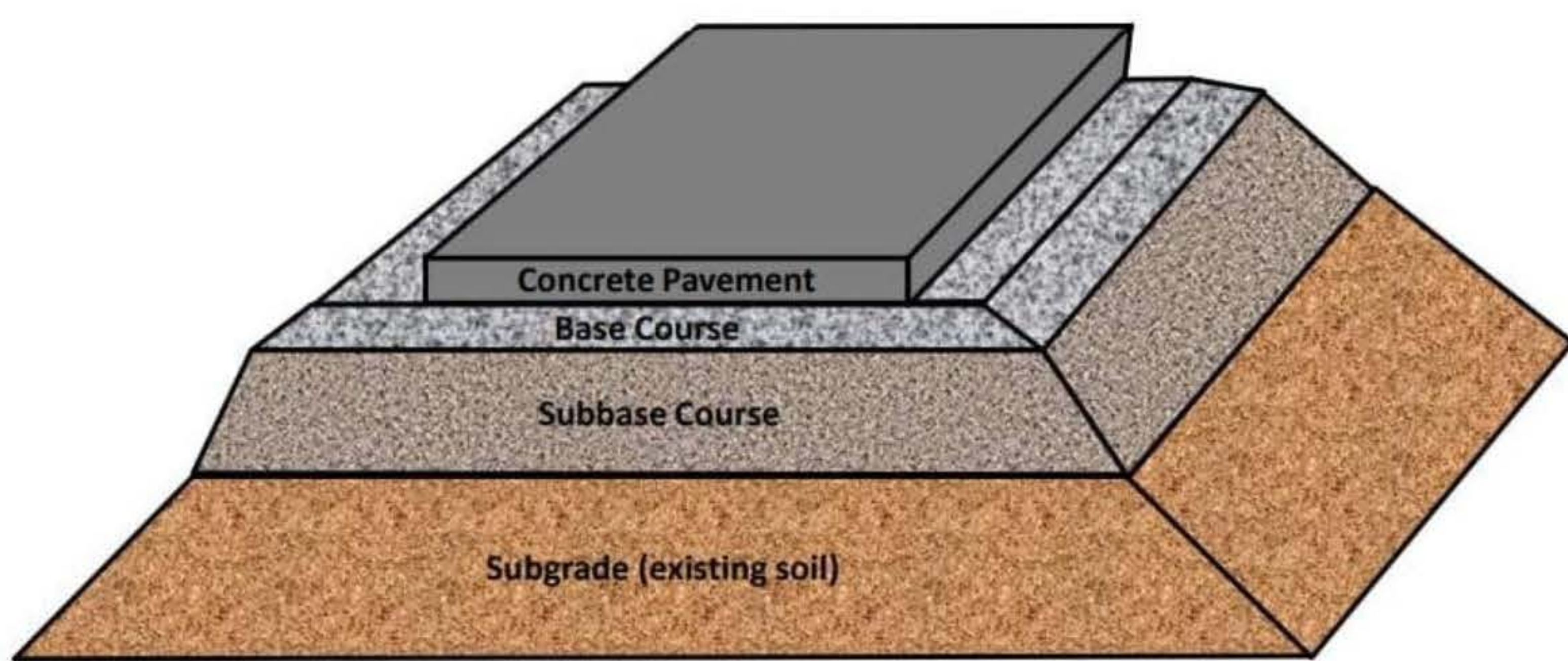
Recycled crumb Rubber



Recycled PET plastic



Natural Rubber Latex



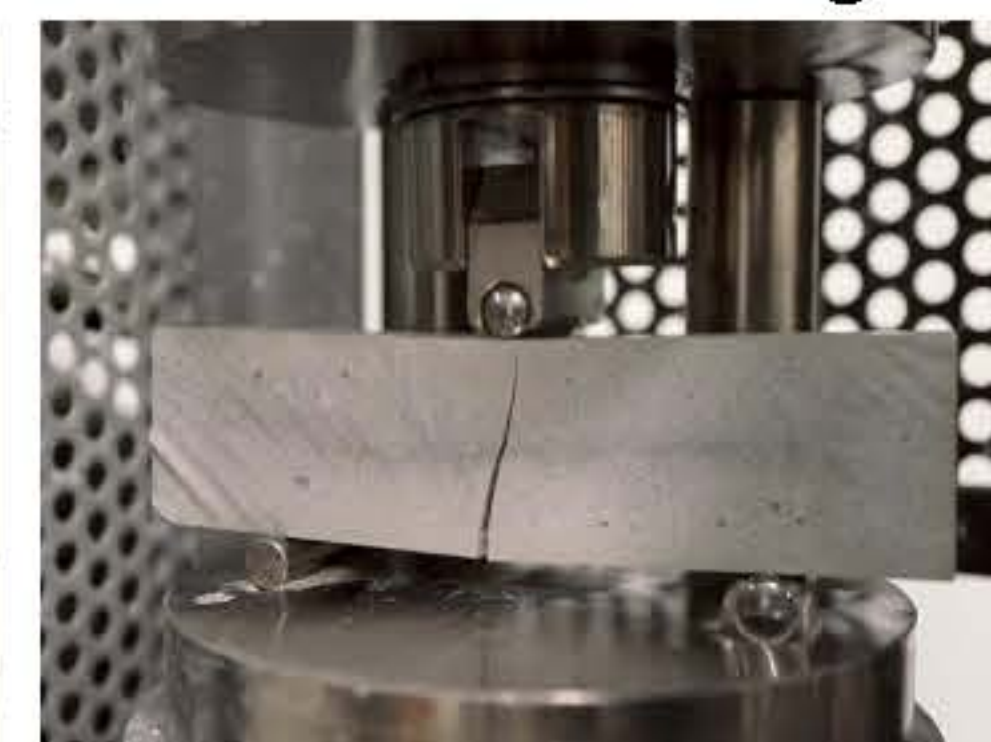
Sustainable Concrete Pavement

### Methods

#### 1. Basic properties and strength parameter of ultra-soft soil



Compressive Strength Test

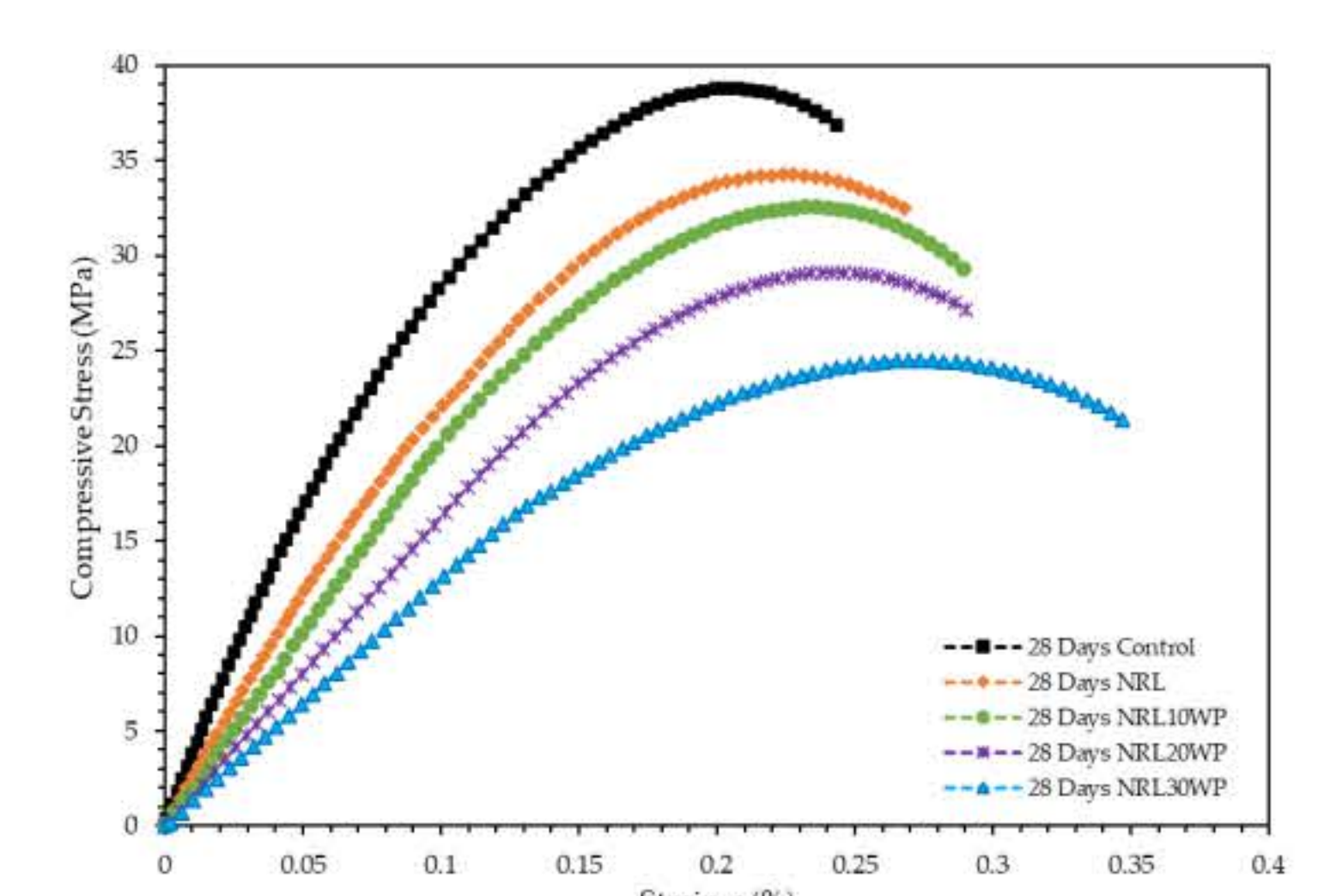
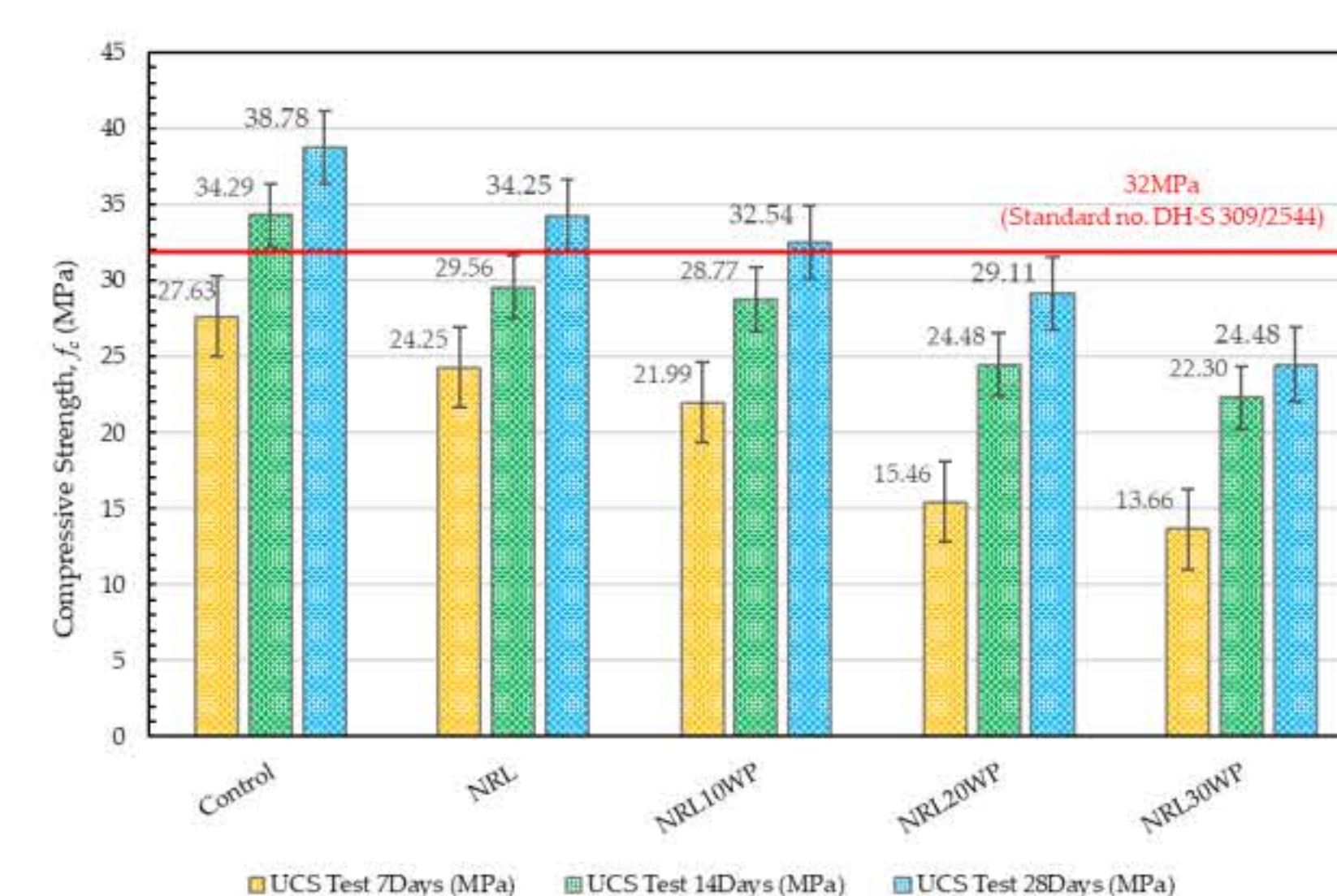


Flexural Strength Test

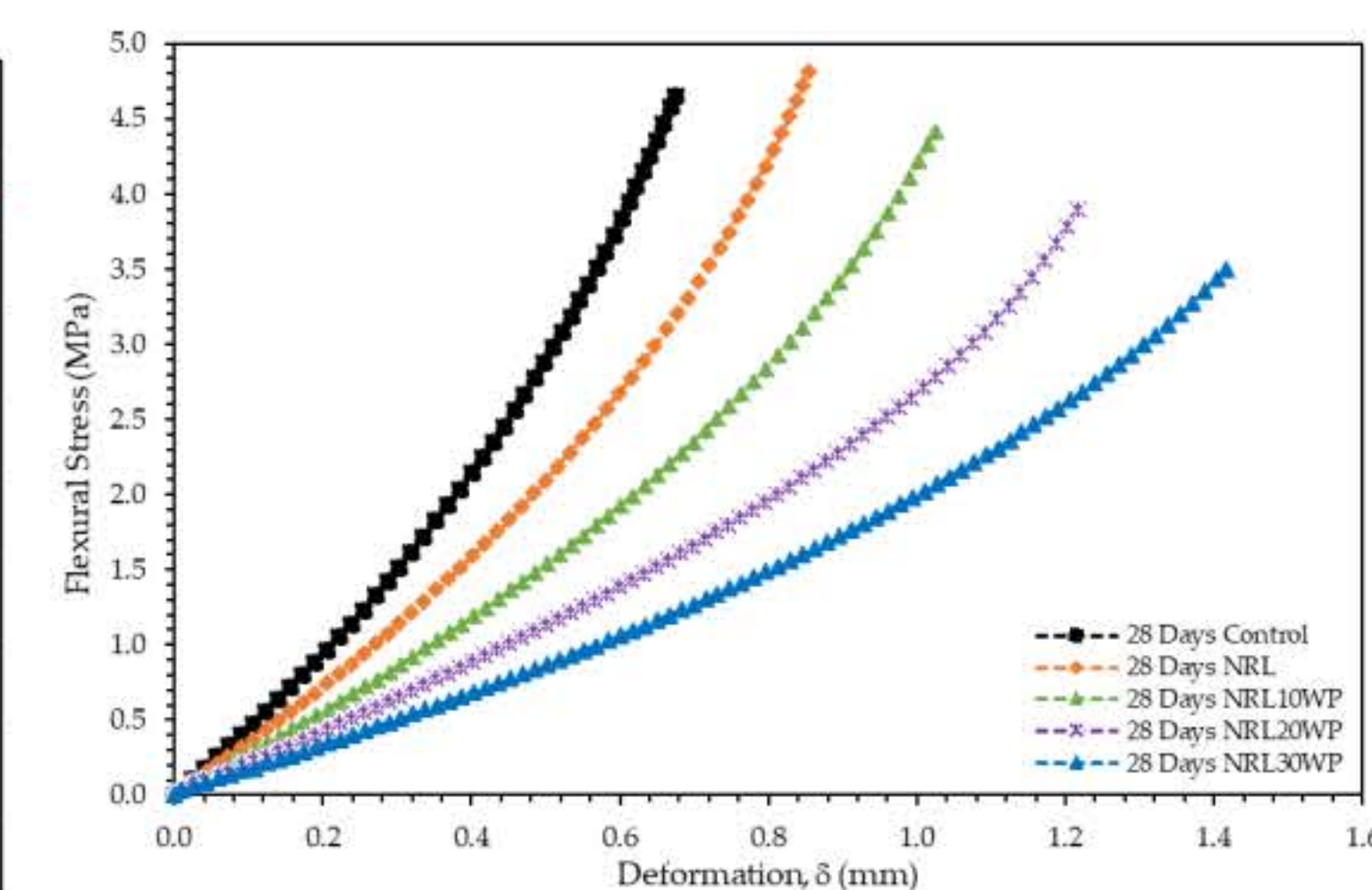
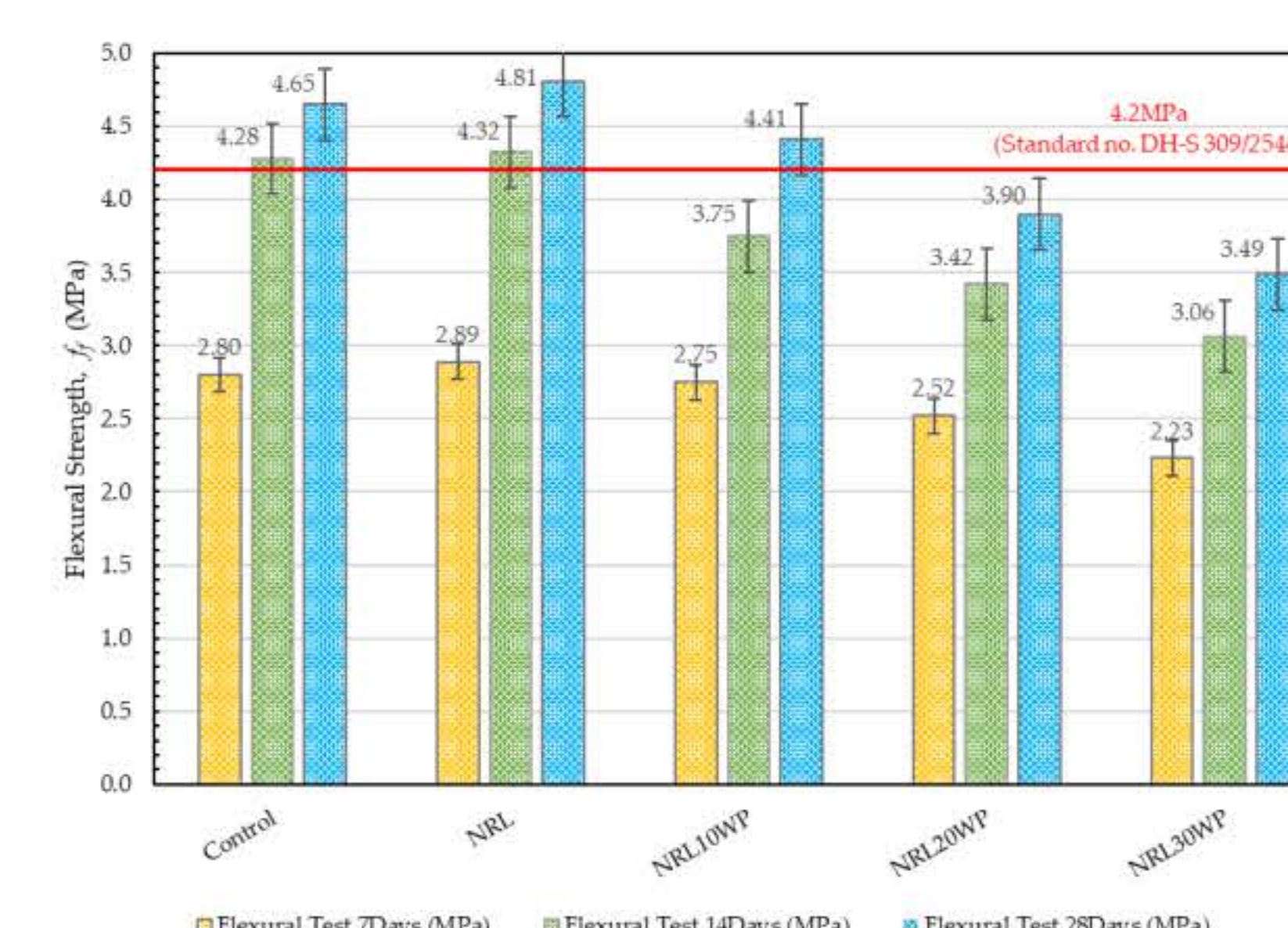


SEM Analysis

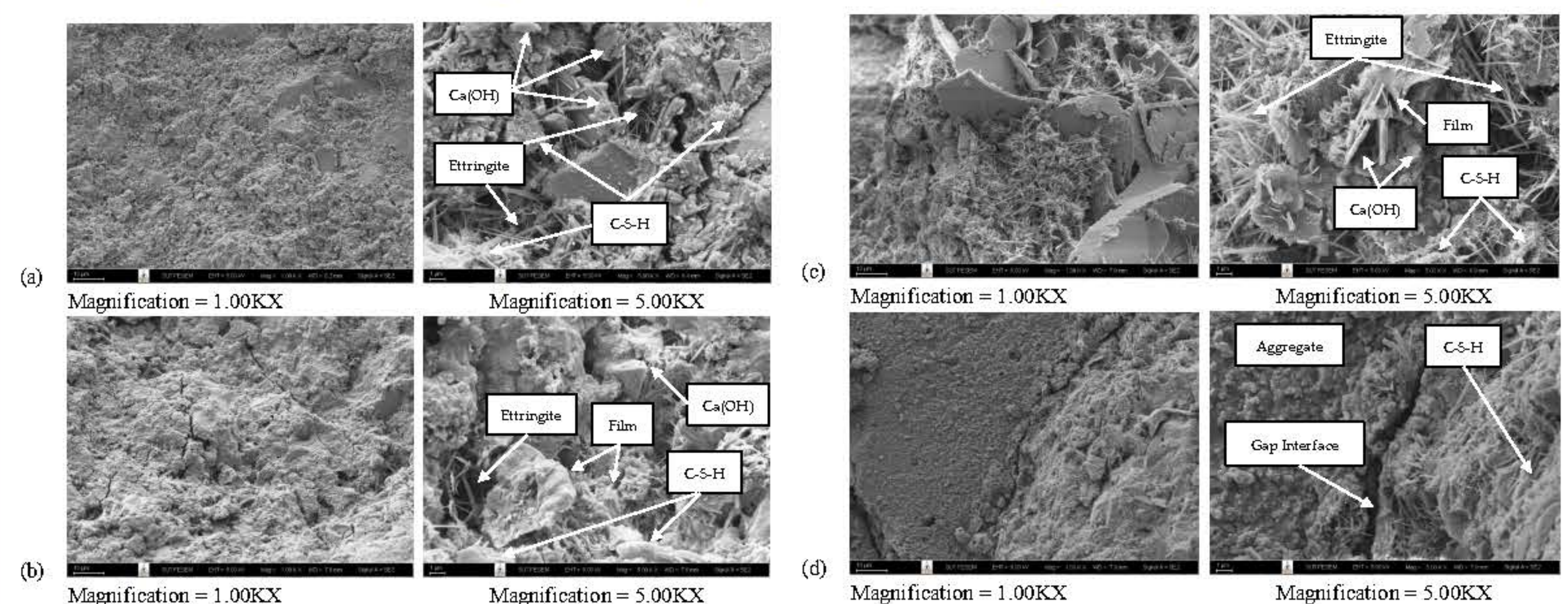
#### 2. Finite element analysis



Compressive Strength Development of Waste Polymer Concrete



Flexural Strength Development of Waste Polymer Concrete.



SEM image of: (a) Normal Concrete, (b) NRL-modified concrete, (c) NRL10WP, and (d) NRL30WP.

### Objective

The research focuses on leveraging the benefits of blending PET and crumb rubber in polymer-modified concretes. It aims to address the environmental issues associated with the disposal of used tires and PET plastics and to explore their use as sustainable construction materials.

### Conclusions

The research concludes that integrating waste PET and crumb rubber into concrete mixes is a sustainable practice and confirms that 10% of waste PET and crumb rubber aggregate replacement can be used in concrete mix for rigid pavement design. This incorporation has implications for the toughness and resistance to impact and dynamic loads of the concrete.

**Acknowledgements** : This research has received funding support from (i) Suranaree University of Technology (SUT) and (ii) the NSRF via the Program Management Unit for Human Resources & Institutional Development, Research and Innovation (PMU-B) [grant number B13F660067].